1986

Design Wind Speeds In Tropical Cyclone-prone Regions

Peter Nicholas Georgiou

CANADIAN THESES

THÈSES CANADIENNES

NOTICE

The quality of this microfiche is heavily dependent upon the quality of the original thesis submitted for microfilming. Every effort has been made to ensure the highest quality of reproduction possible.

If pages are missing, contact the university which granted the degree.

Some pages may have indistinct print especially if the original pages were typed with a poor typewriter ribbon or if the university sent us an inferior photocopy.

Previously copyrighted materials (journal articles, published tests, etc.) are not filmed.

Reproduction in full or in part of this film is governed by the Canadian Copyright Act, R.S.C. 1970, c. C-30.

AVIS

La qualité de cette microfiche dépend grandement de la qualité de la thèse soumise au microfilmage. Nous avons tout fait pour assurer une qualité supérieure de reproduction.

S'il manque des pages, veuillez communiquer avec l'université qui a conféré le grade.

La qualité d'impression de certaines pages peut laisser à désirer, surtout si les pages originales ont été dactylographiées à l'aide d'un ruban usé ou si l'université nous a fait parvenir une photocopie de qualité inférieure.

Les documents qui font déjà l'objet d'un droit d'auteur (articles de revue, examens publiés, etc.) ne sont pas microfilmés.

La reproduction, même partielle, de ce microfilm est soumise à la Loi canadienne sur le droit d'auteur, SRC 1970, c. C-30.

THIS DISSERTATION HAS BEEN MICROFILMED EXACTLY AS RECEIVED

LA THÈSE A ÉTÉ MICROFILMÉE TELLE QUE NOUS L'AVONS REÇUE

DESIGN WIND SPEEDS IN TROPICAL CYCLONE-PRONE REGIONS

by

PETER NICHOLAS GEORGIOU

Submitted in partial fulfillment
of the requirements for the degree

Doctor of Philosophy

Faculty of Graduate Studies
The University of Western Ontario
London, Ontario
September, 1985

ISBN 0-315-29510-4

ABSTRACT

Simulation methods have recently emerged as the most reliable, and in some cases, the only means available for predicting design wind speeds in tropical cyclone-prone regions of the world. Information on what wind speeds might occur and their relative risk is critical to the assessment of those areas most exposed to the hurricane hazard and to the design of structures to resist hurricane-force winds.

This thesis presents a refined simulation procedure. The windfield model is considerably more complex than those used in previous simulations. Wind speeds and directions are defined at three levels, (i) at the 700 mb height, where gradient balance is assumed to apply, (ii) at the 500 metre height, where surface friction and translation of the storm system itself combine to modify the circulation in a manner which, in the current simulation, is computed using a recently developed numerical hurricane boundary layer model, and (iii) at the surface or 10 metre height. Within the windfield model, the boundary layer variation of wind speed and direction and the influences on the three circulation levels when landfall is made are defined using data gathered in recently occurring tropical cyclones. The simulation also contains a new filling model taking into account the geographical variation of this phenomenon along the U.S. coastline.

The simulation windfield model is evaluated by comparing actual wind records obtained in recently occurring tropical cyclones with wind speeds and directions predicted by the model itself. The storms chosen for these comparisons include North Atlantic, Northwest Pacific and Australian tropical cyclones. The statistical representation of the tropical cyclone characteristic parameters required in the simulation is reviewed and in some cases new distributions have been proposed. The description of these climatological parameters has application in fields other than the prediction of design wind speeds.

The simulation procedure was applied to the Gulf and Atlantic Coasts of the United States to yield extreme wind speed estimates. The results show significant variation along the coastline and compare reasonably with two recent studies of U.S. hurricane design wind speeds.

Finally, the simulation procedure is extended to handle the increased risk sustained by line-like structures, such as transmission lines, and to be compatible with the methodology currently used in the calculation of structural response exceedances, basic to the prediction of wind-induced building response.

ACKNOWLEDGEMENTS

I would like to express my sincere gratitude to my supervisor, Dr. A.G. Davenport, for his unfailing enthusiasm, encouragement and counsel during this study. The opportunity to become involved in many exciting Wind Tunnel projects, to travel and participate in conferences, making many valuable friendships throughout the course of this thesis, was entirely due to his generous and thoughtful stewardship. Dr. B.J. Vickery provided valuable advice in the initial stages of the study. His continued interest throughout the course of my graduate work will always be deeply appreciated.

Many others in the Laboratory provided useful discussions, in particular Drs. D. Surry and N. Isyumov. The assistance of the entire BLWTL Staff and Library personnel is gratefully acknowledged. I was fortunate in having several extraordinarily bright and generous fellow graduate students, amongst them Roger Basu and Mike Mikitiuk, as friends during my studies. Their help and criticism was an important part of my education.

This thesis and my understanding of tropical cyclones and their behaviour was in large part made possible by the assistance of members of the Hurricane fraternity in Miami. Dr. C.J. Neumann provided the HURDAT data tape, Drs. R. Sheets and P.G. Black many enlightening explanations to a novice meteorologist, Dr. L.J. Shapiro the computer code to his numerical model and lastly, though most importantly, Mark Powell, for a multitude of tropical cyclone data, much constructive advice and for introducing me to the wonderul world of Miami and windsurfing. Their hospitality to the Australian from up North interested in hurricanes will always be greatly appreciated.

Initial funding for this work was provided by a grant from the U.S. Electric Power Research Institute, Palo Alto, California. The University of Western Ontario's Boundary Layer Wind Tunnel Laboratory kept me housed and fed thankfully for the remainder of this long odyssey.

Lastly, three people deserve the credit for inspiring and sustaining the work that this thesis represents, my parents, Nicholas and Amanda, and my wife Cathy. This thesis is as much yours as it is mine. Mum and Dad, your advice and guidance kept me unfailingly directed towards the finish line. Cathy, you got me there and managed to keep a normal household going, your own degrees finished and our marriage happy and thriving. This thesis is dedicated to you, my fantastic family.

TABLE OF CONTENTS

LIST OF TABLES

LIST OF FIGURES

CHAPTER 1

INTRODUCTION

Quantification of the risks imposed by tropical cyclones is of critical importance, offering the potential to greatly reduce the loss of human life and the damage caused by these storms. Within all countries affected, assessing the vulnerability of different regions to tropical cyclones is an important first step in any national disaster prevention plan involving land-use and zoning laws to control development in areas where the risk is high, in the definition of wind climate within the wind loading process, and finally, in the specification of design wind speeds for building codes setting out minimum structural safety standards.

Computer simulation methods predicting wind speeds in regions dominated by tropical cyclones have emerged as a powerful, reliable and currently the most frequently used tool in estimating long-term risk levels associated with these storms. A refined simulation procedure is presented in this thesis, incorporating windfield information gathered in a number of recently occurring storms and utilizing an improved statistical representation of the required simulation meteorological parameters. The simulation procedure is applied to the United States Gulf and Atlantic Coasts in addition to several problems of engineering design interest.

1.1 General

Tropical cyclones, or hurricanes and typhoons as they are known in some parts of the world, are the most devastating of all natural phenomena. Measured by their violence, duration and size of area affected, they are without equal in terms of the amount of destruction they can cause. The almost 100 tropical cyclones that occur world-wide every year cause an average 20,000 deaths and total economic damage exceeding $6 billion (Southern, 1979). Some of the most populated areas in the world are affected

by tropical cyclones including countries whose urban populations are doubling every 7 to 10 years. The potential for catastrophic loss of human life is enormous.

Tropical cyclones occur in all oceans of the world except the South Atlantic. Figure 1.1 illustrates world-wide areas of formation and typical track directions. In general they tend to be most frequent in late summer and early fall, when ocean temperatures and the air humidity and temperature near the surface are at their highest. The hazards imposed by tropical cyclones are threefold : high winds, river and local flooding resulting from intense and often persistent rainfall and storm surge, the rapid increase in sea-level along the coastline produced mainly by the action of winds driving the water ashore. Although the winds in tropical cyclones are strong, very gusty and may last for many hours, even days, at a particular site, it is often the subsequent inland flooding or coastal storm surge that produces the greatest damage. The tropical cyclone which struck Bangladesh on November 13, 1970 killed over 200,000 people (WMO, 1976), even though its minimum central pressure was only 950 millibars at the time. Its landfall however coincided with high tide and produced a storm surge estimated as high as 9 metres, the resulting cause of the terrible death toll. A single tropical cyclone can affect more than one nation during its lifetime. Hurricane David left a history of death and destruction as it moved through the Caribbean towards the United States, leaving 1000 dead and over 100,000 homeless from Dominica to Hispaniola and a damage total over $1 billion in September 1979 (Hebert, 1980).

Tropical cyclones were already well-known to inhabitants of the Western Hemisphere before news of them spread to Europe with the expeditions of Columbus. In the "New World", as was the experience in the Far East, they were to play an important role in history in succeeding years. The Spanish domination of Cuba came about when a hurricane destroyed a Dutch fleet of 36 ships in Havana under the command of Holland's Admiral Jol on September 11, 1640. Twenty-six years later the French were able to acquire Guadeloupe when an English fleet was destroyed there on August 14-15, 1666 (Sugg, 1968). An attack on the lower Carolina settlements by a Spanish Armada was foiled by a hurricane on September 4-5, 1686 (Ludlum, 1963).

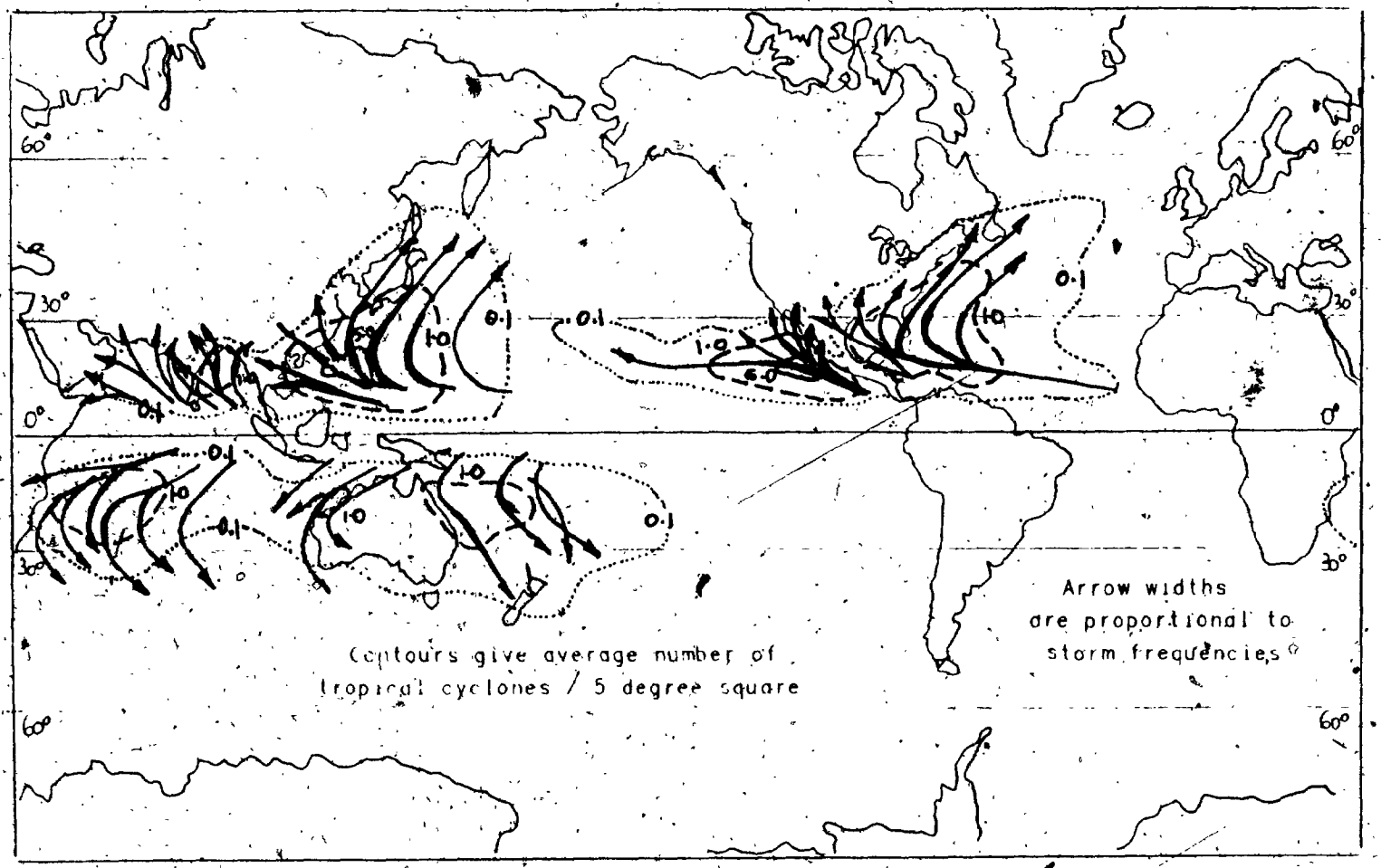

FIGURE 1.1 World-wide Areas of Tropical Cyclone Occurrence and Typical Tracks (Crutcher and Quayle, 1974)

The word "hurricane" itself appears to have originated from the name "Huracan", attributed to an ancient Central American native group, the Tainos, meaning "God of Evil" (Anthes, 1982). The terminology used within this thesis regarding the classification of tropical cyclones by intensity follows that established by the United States National Hurricane Center, Miami, Florida, and is shown in Table 1.1. The word "storm" by itself is used herein as a generic term and is synonymous with tropical cyclone. A classification commonly used to relate hurricane intensity to damage potential is the Saffir/Simpson Hurricane Intensity Scale. This descriptive scale, ranging from Category Number 1 through 5, is given in Table 1.2. The terms "major" hurricane and "great" hurricane found in various references are comparable to Category 3, 4 or 5 storms on the Saffir/Simpson Scale.

The United States has been fortunate relative to many tropical cyclone-prone countries in that the loss of life from these storms has shown a steady decrease throughout the whole of this century. This can be attributed to improved forecasts and timely warnings made possible through the use of radar and satellite technology, accompanied by better local planning and construction practices. At the same time, the vulnerability of hurricane-prone areas in the United States, as represented by the economic losses resulting from tropical cyclones, has increased dramatically (Sheets, 1980) as shown in Figure 1.2. A number of factors are contributing to this increased risk, the chief one being the explosive population increases occurring along Gulf Coast and lower Atlantic Coast States in recent years. In the 20 years to 1977 the populations of the Houston area (Harris County) and Miami area (Dade County) had risen from 750,000 to 1,750,000 and 500,000 to 1,300,000 respectively (Simpson and Riehl, 1981). This trend has continued unabated in the 1980's, spurred on by phenomenal economic growth, and supported by the growing number of elderly people seeking retirement in the "sunshine" states. In 1982-1983 Texas alone accounted for 22 percent of the total nation's housing starts (Naisbitt, 1984). The geographical distribution of these population increases, illustrated in Figure 1.3, shows that the greatest increases have occurred in the most vulnerable locations, beach and coastal subdivisions. Other factors adding to the vulnerability of the United States to tropical cyclones include huge increases in the number of mobile homes built mostly in warmer climates (i.e. hurricane-prone areas), escalating costs of

TABLE 1.1
CLASSIFICATION OF METEOROLOGICAL SYSTEMS

Tropical Cyclone: a non-frontal low pressure synoptic-scale system developing over tropical or sub-tropical waters having definite organized circulation, subdivided in terms of intensity into :

Tropical Depression	- Vms ≤ 17 m/s
Tropical Storm	- 17 m/s < Vms ≤ 24 m/s
Severe Tropical Storm	- 25 m/s ≤ Vms < 33 m/s
Hurricane	- Vms ≥ 33 m/s

Vms = maximum sustained (1-minute), surface (10-metre) wind speed.

TABLE 1.2
SAFFIR/SIMPSON HURRICANE INTENSITY SCALE

Scale Category No.	Central Pressure (mbar)	Wind Speed (m/s)	Storm Surge (m)	Damage
1	≥980	33 - 42	1.25 - 1.50	Minimal
2	965 - 979	43 - 49	1.75 - 2.50	Moderate
3	945 - 964	50 - 58	2.75 - 3.75	Extensive
4	920 - 944	59 - 69	4.00 - 5.50	Extreme
5	≤ 919	≥ 70	≥ 5.75	Catastrophic

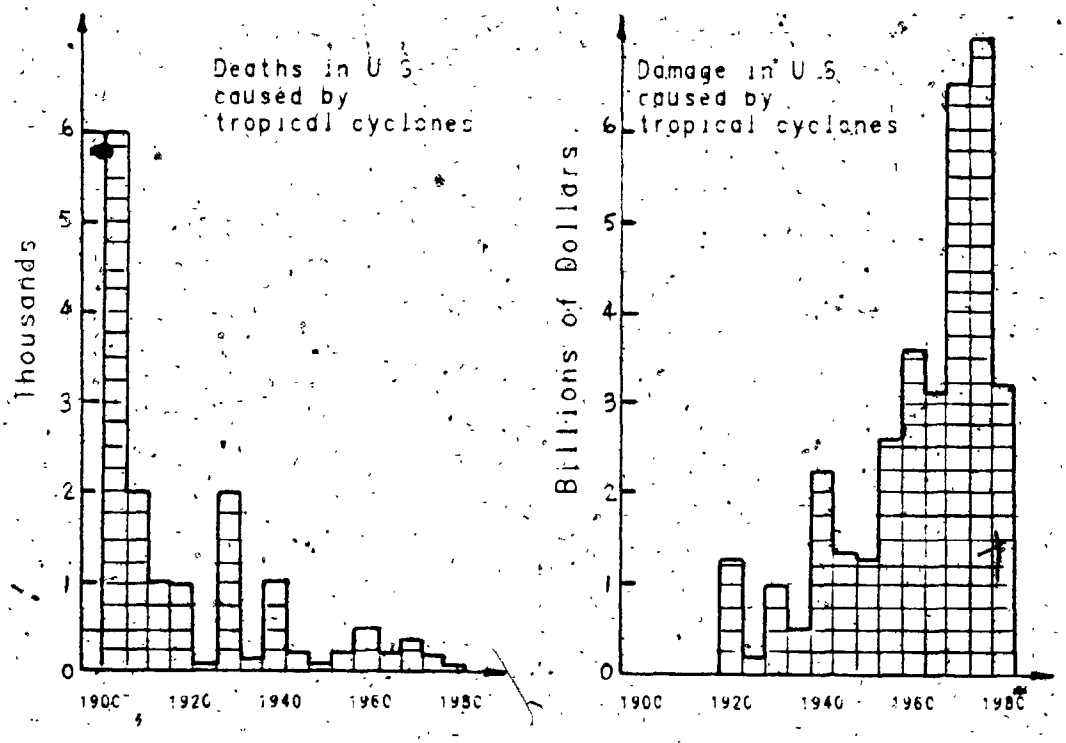

FIGURE 1.2 **United States Damages and Deaths in 5-Year Periods Caused by Tropical Cyclones**

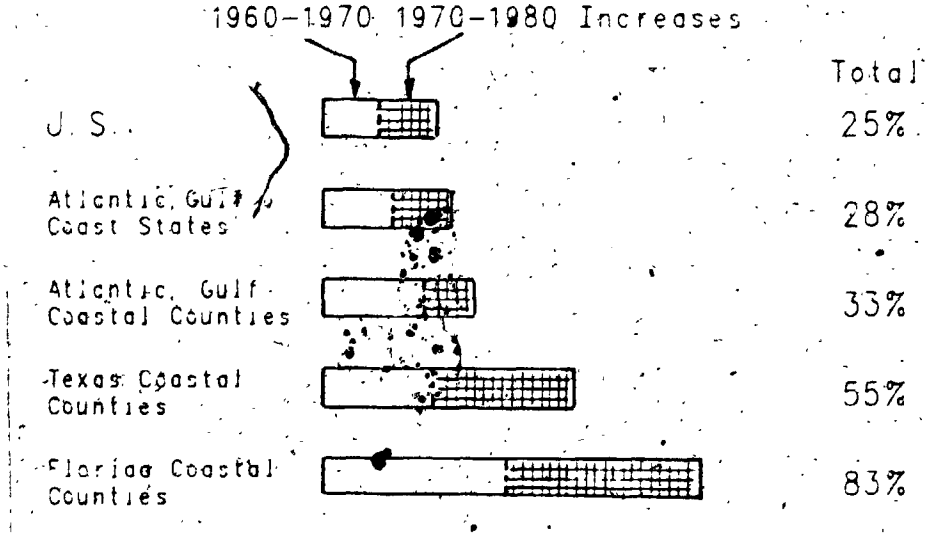

FIGURE 1.3 **United States Population Trends 1960-1970-1980**

building material and labour which have consistently outpaced the inflation rate, uneven regional enforcement of building codes, inadequacy of evacuation routes and places of refuge, and finally, a complacent public.

This increased vulnerability was highlighted in a report issued by the Southwest Florida Regional Planning Council (SFRPC, 1982), which estimated that the impact sustained by the six counties in the Southwest Florida Region, if struck by a major hurricane, would range from $3 to $5 billion. Such figures are supported by experiences with recent tropical cyclones which have affected the United States. Hurricane Alicia made landfall at the southwest tip of Galveston Island before moving northwards passed Houston on August 18, 1983. Alicia was a medium-sized hurricane which reached only minimal Category 3 status on the Saffir-Simpson Scale. Alicia's track however coincided with much of the infrastructure in the Galveston-Houston corridor. As a result, Alicia became the third most costly hurricane in United States history after Hurricanes Frederic (1979) and Agnes (1972), whose damage had resulted mostly from abnormal flooding in many far-inland areas. Damage estimates for Alicia are $2 billion (Savage et al, 1984). If Alicia had been as intense a storm as was Hurricane Frederic, the damage total could well have exceeded a staggering $5-6 billion.

The design of buildings to withstand tropical cyclone winds clearly occupies an important position in the wind engineering community, particularly when wind tunnels are utilized in the estimation of wind-induced structural response. Figure 1.4 adapted from Surry and Davenport (1979) depicts the standard sequence involved in estimating a building's response to the wind. The "wind loading chain" begins with an evaluation of the local wind climate at the site. Wind tunnels have proved a valuable aid in the computations involved in subsequent "links". Final predictions of a given wind-induced response for a structure located at a particular site represent a synthesis of the results obtained from all links. Also in Figure 1.4 are shown estimates of the uncertainty expected in the individual predictions associated with each link of the wind loading chain. Two points are immediately apparent. Firstly, the use of wind tunnel tests to compute the dynamic behaviour of a structure in a given terrain can significantly increase the reliability of the final predictions. More importantly, it can be seen that

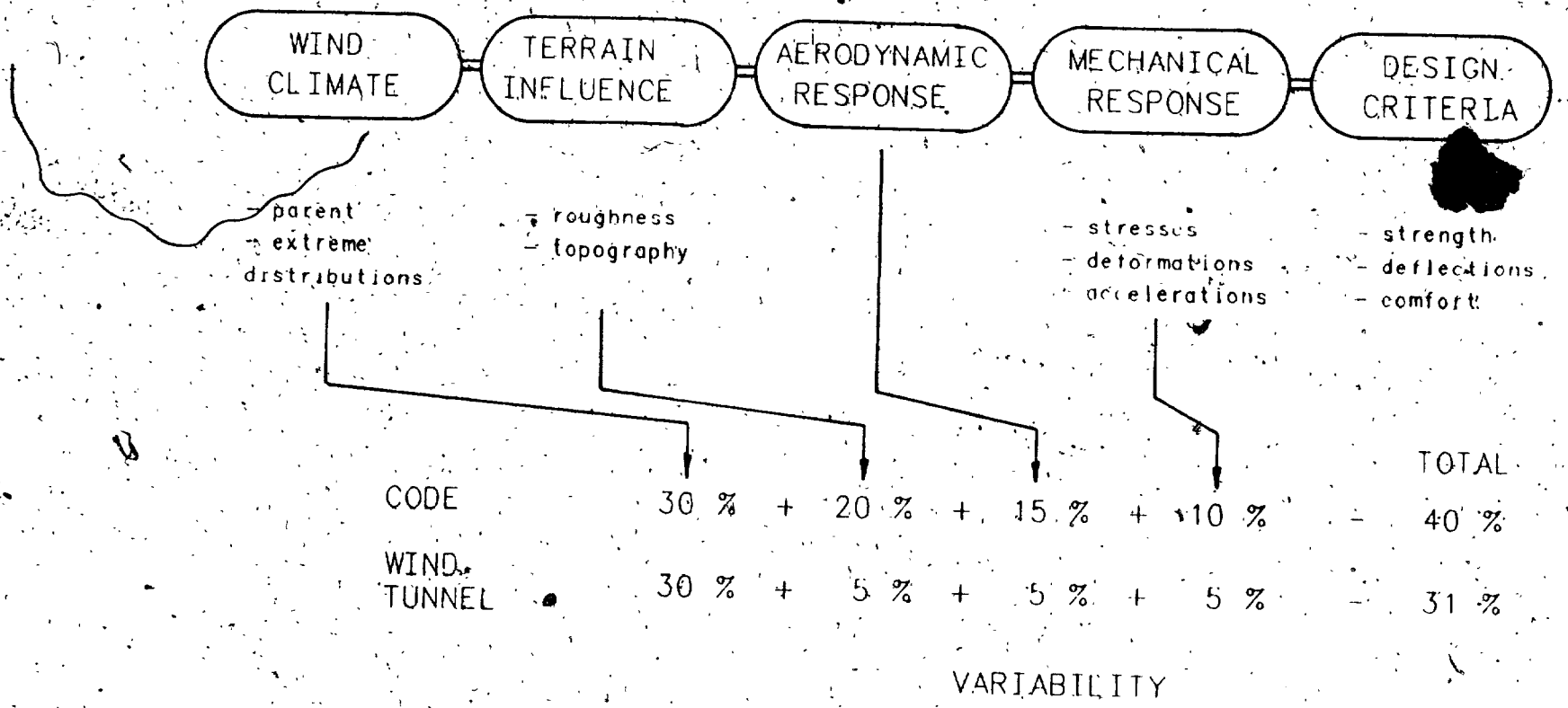

FIGURE 1.4 The "Wind Loading Chain"

uncertainties in the definition of the wind climate then become the major contributor to the overall uncertainties in the final predictions. Greater uncertainty is expected, not surprisingly, for those structures located in areas affected by tropical cyclones. It is thus evident that expensive and elaborate wind tunnel investigations should be accompanied by equally strenuous efforts to evaluate the wind climate as accurately as possible.

1.2 The Role of Wind Climate in Determining Design Wind Speeds for Engineering Structures

The prediction of full-scale wind-induced effects for design purposes begins with the definition of the local characteristics of the wind climate. This cannot be done in a deterministic sense as wind speed is a statistical variable subject to random fluctuations. Hence a locality's wind climate is usually described in a probabilistic format through the probability density function of mean wind speed and direction, $p(V,\theta)$, and the extreme-value distribution of maximum mean wind speed, $F(V)$.

The former, known as the "parent" distribution, identifies the continuous variation of wind speed and direction at a site, typically on an hourly basis. It is used in determining comfort, serviceability and fatigue-related criteria for wind-induced effects, evaluating ventilation and wind energy potential at a particular site and in combination with wind tunnel predictions of building response versus wind speed and direction. The latter, referred to as the distribution of the "extremes", defines the occurrence of the strongest (and most rare) winds at the site, regardless of direction and normally on an annual basis. Design wind speeds found in building codes governing the overall structural loads for a building are derived from the extreme-value distribution. The theoretical relationships connecting extremes with the parent distribution from which they are drawn were developed by Fisher and Tippett (1926) and Gumbel (1958), who showed that all parent distributions converge asymptotically to one of three extreme forms, the Fisher-Tippett Type I, II and III distributions.

Figure 1.5 shows an example of the parent and extreme-value distributions for New York City based on upper-level wind speed and direction data obtained from J.F. Kennedy International Airport and Mitchell U.S. Air Force Base (Hampstead) for the period 1950-1975. The parent distribution indicates that relatively common winds (with a frequency of exceedance greater than 10-100 per annum) are equally likely for southwesterly to northwesterly directions. Stronger winds (exceedance frequency less than once per annum) are most likely from the south. Two Type I extreme-value distributions are shown, one obtained by fitting the actual set of annual maximum hourly wind speeds recorded in the 1950-1975 period, the second derived from the parent distribution using extreme-value theory. The agreement between the two extreme-value curves is seen to be good.

If the available record of annual maxima is long enough, the extremes may be calculated directly using the traditional "Gumbel" approach, in much the same way that design flood levels are estimated for bridge and embankment elevations, design wave heights for offshore structural loading and many other common engineering problems. These methods rely upon the accumulation of a long enough record of annual or monthly extreme observations which are ranked in ascending order, assigning a cumulative probability value to each, equal to $m/(N+1)$ for the m'th extreme in a set of N. An appropriate extreme-value distribution is then chosen to model the data using any one of a number of standard fitting techniques, e.g. the Gumbel method, the Leiblien method.

The accuracy of any local wind climate model, especially the extremes, depends upon the length, reliability and homogeneity of wind data at the particular site. Data reliability is linked to the type of instrumentation, its adequate calibration and maintenance, and the proper location of wind-measuring sensors to ensure, for example, that no nearby obstructions induce local flow effects. Homogeneity of the data is ensured if standard averaging times, measuring heights and similar exposure conditions are maintained over the life of the wind record in question.

A further condition necessary for homogeneity to be satisfied is that the wind data should be drawn from a climatological series belonging to a single

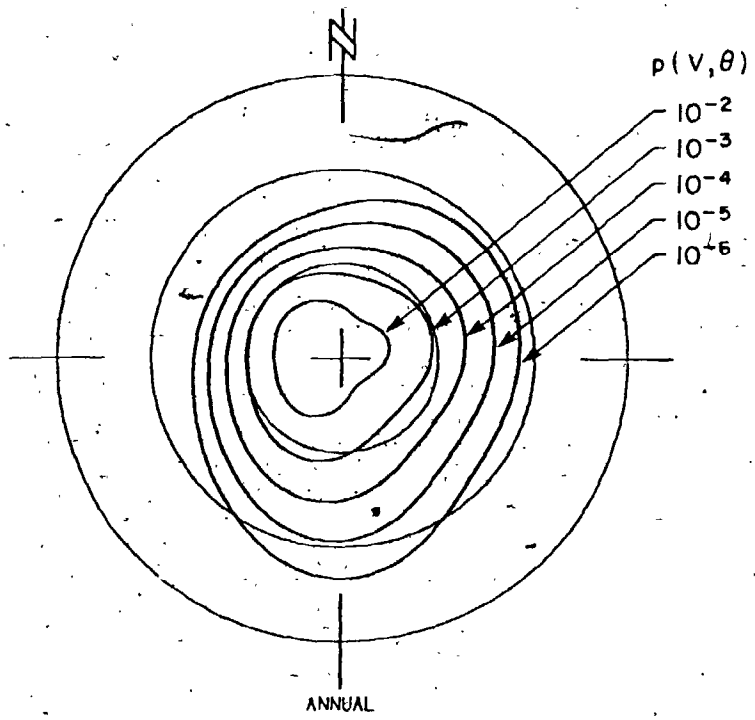

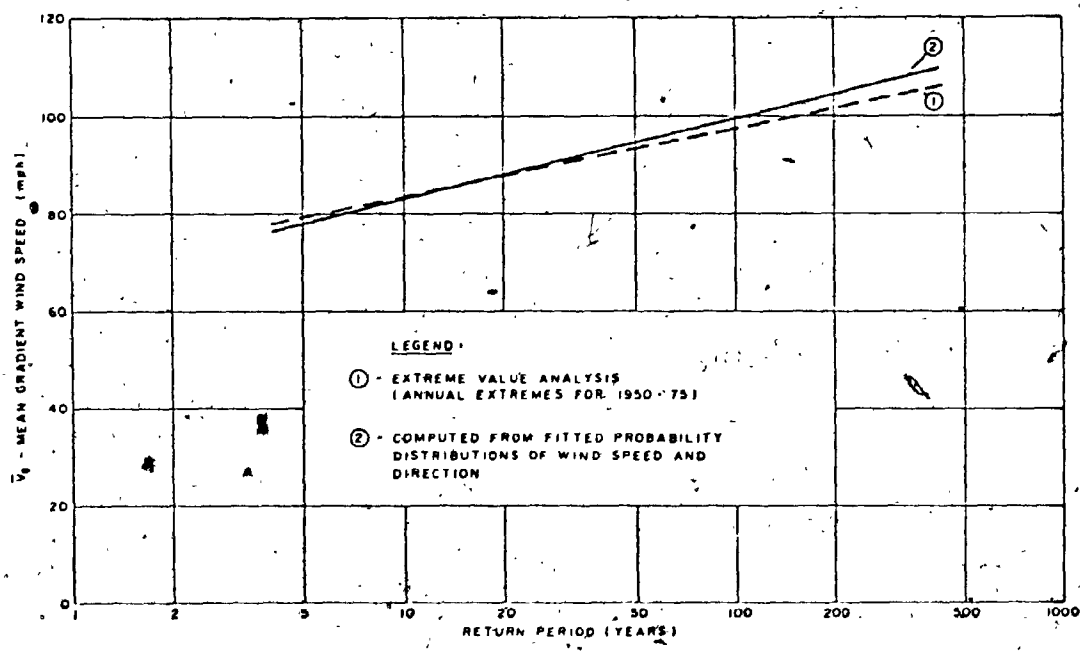

FIGURE 1.5 Parent and Extreme-Value Distributions of Gradient Height Wind Speed for New York City, New York

population, i.e. a single meteorological phenomenon. When more than one meteorological system affects the wind regime at a particular site the resulting wind climate is said to be "mixed". In such cases a combination of extra-tropical extensive pressure systems, thunderstorms, tropical cyclones and/or tornadoes may be contributing to the collection of recorded annual extremes. In practice only two distinct weather systems are usually present, e.g. thunderstorms and tropical cyclones, and one of the storm types invariably contributes more of the higher wind speed maxima to the distribution of the extremes than the other.

The uncertainties involved in estimating extreme winds in such "mixed" climates were first recognized by Thom (1968), who recommended characterizing the wind climate at such sites using separate distributions to define the extremes for each storm type, recombining them later taking into account their relative probability of occurrence at the site of interest. This approach was dealt with in greater detail by Gomes and Vickery (1977-78) who showed that when the extremes were not separated and treated as if from different populations, extreme-value distributions fitted to the mixed data invariably underestimated wind speeds at higher return periods. This was particularly so for sites affected by rare but intense tropical cyclones which dominated the "tail" of the extreme-value distribution but did not contribute strongly to its "body".

After separation, analysis of each meteorological phenomenon can then proceed using the method best suited to that data set. More importantly, the extremes can then be predicted from the parent distribution, greatly expanding the data base, or conversely, permitting the use of shorter records. Computational methods for estimating extremes from their parent distribution have been developed by Davenport (1967) and Gomes and Vickery (1976). These techniques have been shown to give reliable estimates when the wind climate is said to be "well-behaved", which implies that the meteorological systems affecting the site should be relatively slow-moving, spatially large and exhibit a relatively high annual frequency of occurrence. Locations whose meteorology is dominated by thunderstorms and/or extra-tropical extensive pressure systems have well-behaved wind climates. In these circumstances reliable estimates of the extremes can be made if a record

length of 10 to 20 years of continuous mean hourly wind speed data is available.

For a variety of reasons discussed in the following section climates dominated by tropical cyclones are not well-behaved and the prediction of extreme wind speeds for design purposes using the normal statistical approaches outlined above can lead to considerable uncertainties.

1.3 Limitations of Tropical Cyclone Wind Data

Special problems are encountered when dealing with tropical cyclones which can make the prediction of extremes highly misleading. These include :

(i) Infrequent Occurrence Rate : compared with the synoptic-scale depressions of temperate latitudes, tropical cyclones are relatively small, usually having a diameter of only a few hundred kilometres, with the highest winds commonly occurring within one hundred kilometres of the storm centre. For affected areas in the United States the frequency of occurrence of hurricane-intensity wind speeds at any particular locality is much less than once per annum. They therefore constitute a relatively rare meteorological event.

(ii) Continuity and Homogeneity of Record : alterations to instrumentation and the inevitable relocation of anemometers in response to changes in the urban environment are typical problems found at most recording stations. In the case of tropical cyclones the resulting loss of uniformity of the record exacerbates the problem of the low frequency of measurements . An example of note is the remarkable record of tropical cyclone wind speeds and directions that has been kept at the Royal Observatory, Hong Kong, since 1884. The encroachment of tall buildings however has seriously affected the uniformity of the record. For example, in the period 1948-1975 the mean wind speed equalled or exceeded 22 knots for more than 100 hours in every year prior to 1958 but in only one year during the subsequent 17-year period (Chin and Leong, 1978).

(iii) Vulnerability of Surface Instruments to Damage : due to the large amounts of flying debris and frequent power failures common in tropical cyclone conditions, especially the more severe cases, anemometers are often damaged, typically with no indication of whether the highest wind speeds were recorded or not. Examples of the frailty of surface measuring instruments in the face of hurricanes abound. Of the total number of recording stations operating in the Galveston-Houston area when Hurricane Alicia made landfall in August 1983, about a third only were unaffected by power failure or equipment breakdown terminating either the record of wind speed or direction (Savage et al, 1984). These were sufficient however to make Alicia one of the best-ever documented landfalling hurricanes in the North Atlantic. In many cases no record of the maximum winds accompanying a storm is available. Two localities, Aransas Pass and Refugio, exposed to the highest winds when Hurricane Celia made landfall near Corpus Christi, Texas on August 3, 1970, both had their anemometers "blown away" at gust speeds in excess of 60 m/sec with observers present estimating that gusts later reached as high as 80 m/sec (Orton and Condon, 1971). The most damaging tropical cyclone ever to hit the Australian coastline was Cyclone Tracy, which devastated the northern city of Darwin on December 25, 1974. The only operating meteorological station in the area lay in the path of the eye of the storm. The station's anemometer was struck by debris and ceased to function shortly before the eye arrived. The record showed the wind gusting up to 60 m/sec prior to failure but verbal reports and observations indicate wind speeds increasing after that point to perhaps over 70 m/sec (Walker, 1975).

(iv) Interpretation of Data Records : even when good "clean" records of wind speed and direction are obtained during the passage of a tropical cyclone, significant obstacles arise in interpreting these records. Some means is usually required to adjust the speeds to a common reference height, which means not only being able to account for the effects of local terrain and topography, but knowing fairly accurately what the variation of wind speed with height is under tropical cyclone conditions. Rapid and significant changes take place to tropical cyclone surface wind speeds when landfall is made, which is normally the situation experienced by most recording stations. Another formidable problem in interpreting available records arises from mesoscale variations in the tropical cyclone windfield due to the presence of

spiral rainbands, in which wind speeds close to the surface are often temporarily increased due to enhanced vertical momentum transfer. Not only are speeds affected but also the wind direction in these regions exhibits much greater local variation than in other parts of the storm. This often makes it difficult to correlate wind records from different weather stations during the same tropical cyclone event, even though the stations may only be separated by several kilometres.

Once again the Hurricane Alicia experience serves to highlight some of these problems. Of the surface records which were unaffected by power failure or instrument damage, most required substantial correction factors to account for the surrounding topography. Stations at several sites required multiple correction factors due to the change in wind direction occurring during Alicia's passage. Because of the extensive damage done to high-rise buildings in the downtown Houston area a great deal of interest centred on estimating wind speeds in that area. However the two closest stations were both located in the vicinity of nearby obstructions which made these records virtually unusable. In contrast, the wind record obtained at the National Weather Service Office in Alvin can be considered to be a "clean" one. The surrounding terrain is fairly flat and open and the anemometer is located on a 10-metre high mast. The site lay just to the east of Alicia's track and would have presumably registered the maximum winds surrounding Alicia as it approached from the south. Maximum mean wind speeds recorded however were under 30 m/sec. Considering the damage caused several hours later in the downtown Houston area with implied mean wind speeds over 40 m/sec it is difficult to correlate the Alvin record with the general intensity of the storm. Examination of radar composites however at the time when the maximum winds were being recorded in Alvin reveals that the eye of the storm was particularly ill-formed in the quadrant covering the Alvin area, hence accounting for the benign wind speeds. Had the radar composites not been available, as would have been the case a decade ago, it would have been extremely difficult to relate the Alvin wind record to others made during Alicia's passage or with wind speed estimates based on the observed damage in surrounding areas.

These observations illustrate the difficulties encountered in analyzing wind records obtained during tropical cyclone occurrences. Two recent reports by Powell, Marks and Black (1984) and Marshall (1984) analyzing Hurricane Alicia's windfield and determining fastest-mile wind speeds in the landfall region respectively indicate the efforts that were required to document just one single hurricane's surface wind speeds and transform them into standard conditions suitable for the evaluation of structural performance and design. It is clear that measurements of wind speed maxima made during previous hurricane occurrences have not been subject to the same degree of scrutiny as those recorded in Alicia. This unreliability associated with the historical data base of tropical cyclone extreme wind speeds coupled with the infrequent occurrence of the storms themselves at specific locations makes the reconstruction of the wind climate arising from tropical cyclones using measured wind speed data extremely difficult and the prediction of extremes for design purposes equally doubtful.

1.4 The Monte-Carlo Simulation Method for Predicting Tropical Cyclone Design Wind Speeds

An alternative methodology suitable for the prediction of design wind speeds associated with tropical cyclones involves a Monte-Carlo approach, so-named because of the statistical procedure employed in the computations. First suggested by Russell (1971), succeeding developments of this approach have been used by Russell and Schueller (1974), Tryggvason, Surry and Davenport (1976), Batts et al (1980) and Georgiou, Davenport and Vickery (1983) in studies in the U.S.A., Davenport, Georgiou and Surry (1985) for the Caribbean, Martin (1974), Gomes and Vickery (1976) and Tryggvason (1979) in studies in Australia, and Davenport et al (1984) for the Hong Kong region. In essence, this method seeks to create a time history of the winds experienced at any given locality due to tropical cyclone events. The resulting computer-simulated wind speeds are then used to provide estimates of extreme winds, directional characteristics etc., over what are effectively long periods of time. The simulation approach to the prediction of tropical cyclone wind speeds is made possible because of the following two observations :

(1) Wind speeds and directions in a tropical cyclone can be fairly accurately predicted from a knowledge of a limited number of characteristic storm parameters. These include the central pressure difference, radius of maximum winds, translation speed and variables which define the geographical distribution of the storms, their directions of movement and finally their occurrence rate in time. It may be somewhat surprising that although large variations are often observed in the detailed features of individual storms, the basic structure and energetics of all tropical cyclones are similar.

(2) Historical records of these same characteristic parameters exist which are not prone to the sampling and interpretation problems that affect wind records. This is primarily because these parameters vary gradually for any particular tropical cyclone with time periods of the order of an hour or more. In the case of North Atlantic tropical cyclones, the data base extends back to 1886, a record length of almost 100 years. Similar records documenting the tracks and intensities of all known tropical cyclones exist for the Northwest Pacific and Australian regions. The length of these records and the reliability of the data itself allows the use of normal statistical methods to obtain a probabilistic representation of these parameters at any particular location of interest. All historical tropical cyclones can be included in the analysis, not just those reaching hurricane intensity, thereby increasing the data base, and consequently, the reliability of the analysis.

These two notions form the basis of the simulation method, as shown in flow chart form in Figure 1.6. At any particular location, the historical data records are analyzed to produce a statistical representation of the tropical cyclone parameters required by the windfield model used in the simulation. Tropical cyclones are then computer-generated, moved past the site of interest within some specified distance and the wind speeds and directions at the site recorded. The storms created during the simulation bear the same characteristics as those that were determined at the site from the historical records. The simulation can be run over virtually any length of time (i.e. over thousands of years). The resulting time history of winds is then analyzed to

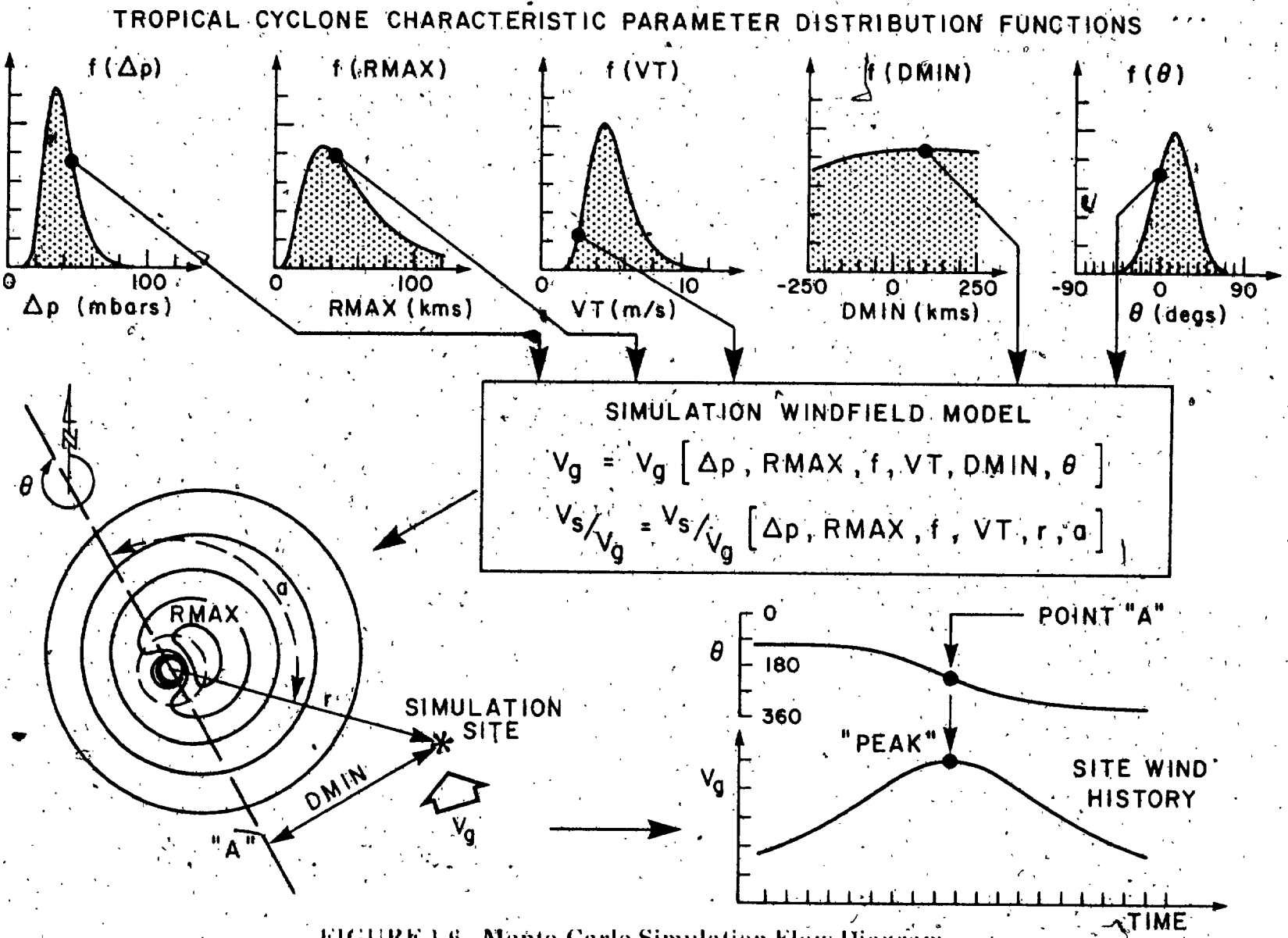

FIGURE 1.6 Monte-Carlo Simulation Flow Diagram

yield predictions of extreme wind speeds etc. The success of the method depends upon two factors:

(a) the reliability of the windfield model used in the simulation to predict wind speeds and directions, and

(b) the accuracy of the statistical representation of the tropical cyclone characteristic parameters required by the above-mentioned windfield model.

The simulation method is thus the logical extension of an approach used in a number of hurricane risk studies (Gilman and Myers, 1961; Simpson and Lawrence, 1971; Myers, 1975; Schwerdt, Ho and Watkins, 1979) relating hurricane hazard to the climatological characteristics of these storms, their frequency of occurrence, preferred track directions, likely intensity etc. Figure 1.7 taken from Simpson and Lawrence (1971) shows the relative frequency of occurrence that a hurricane or great hurricane will occur in any one year along affected U.S. coastal segments.

The simulation method is amenable to applications in a number of directions. The procedure can be applied repetitively throughout a region to yield a hazard map of tropical cyclone extreme wind speeds, as is done in Chapter 6 for U.S. hurricane-prone regions. The wind speeds and directions generated during a simulation can be used to make storm surge predictions or can be combined with wind tunnel test results to yield estimates of building structural response. Another example of an application of the method is shown in Figure 1.8 taken from Friedman (1977). A relatively simple [redacted] model was used in conjunction with information on the number and location of people and buildings exposed to the hurricane hazard in a simulation procedure which yielded estimates of a catastrophe index for the loss potential along the U.S. coastline resulting from a major hurricane experience. The flexibility of the simulation method is thus capable of providing answers to many questions raised in section 1.1 regarding the magnitude of the risk imposed by tropical cyclones.

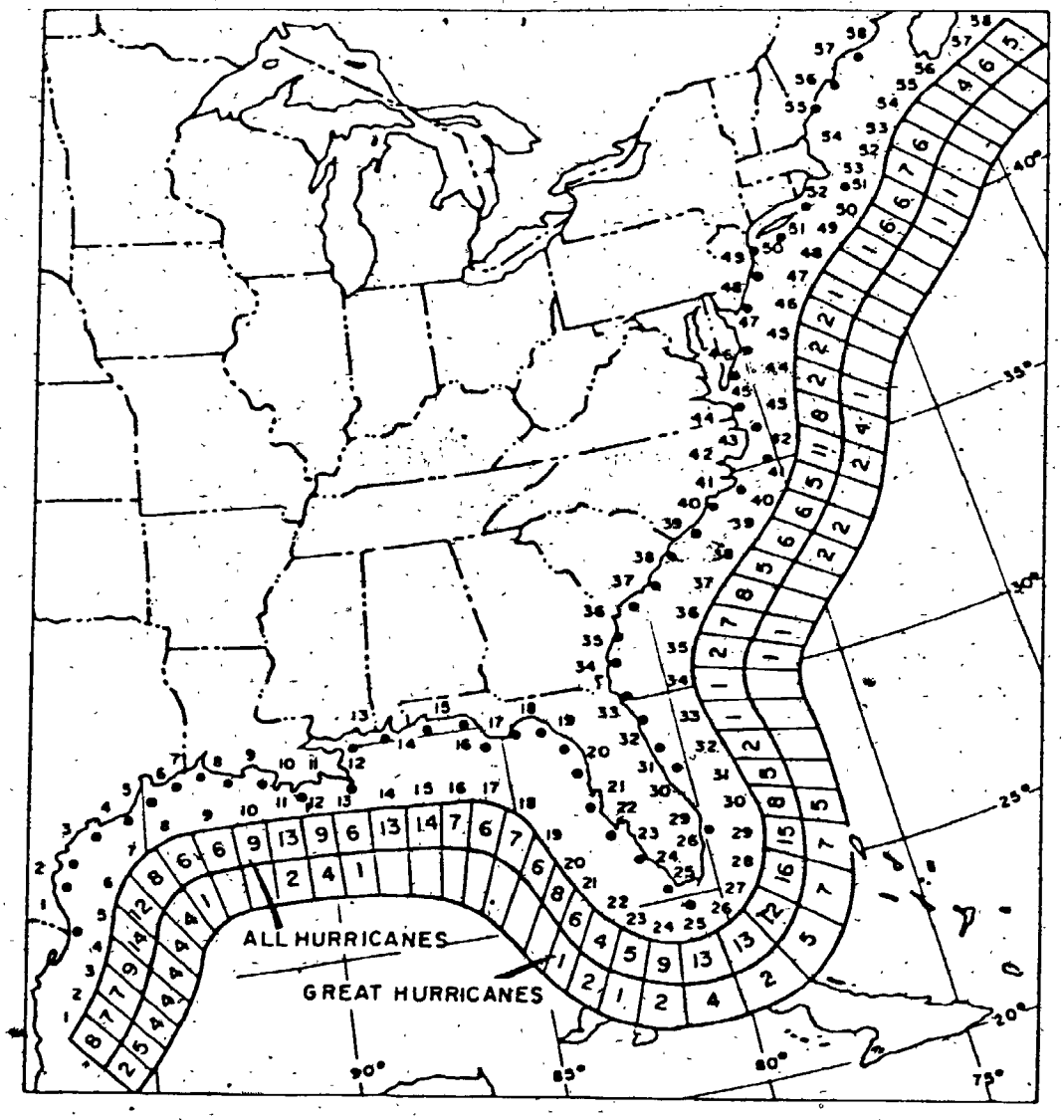

FIGURE 1.7 Relative Frequency of Occurrence of Hurricane or Great Hurricane Along U.S. Coastal Segments

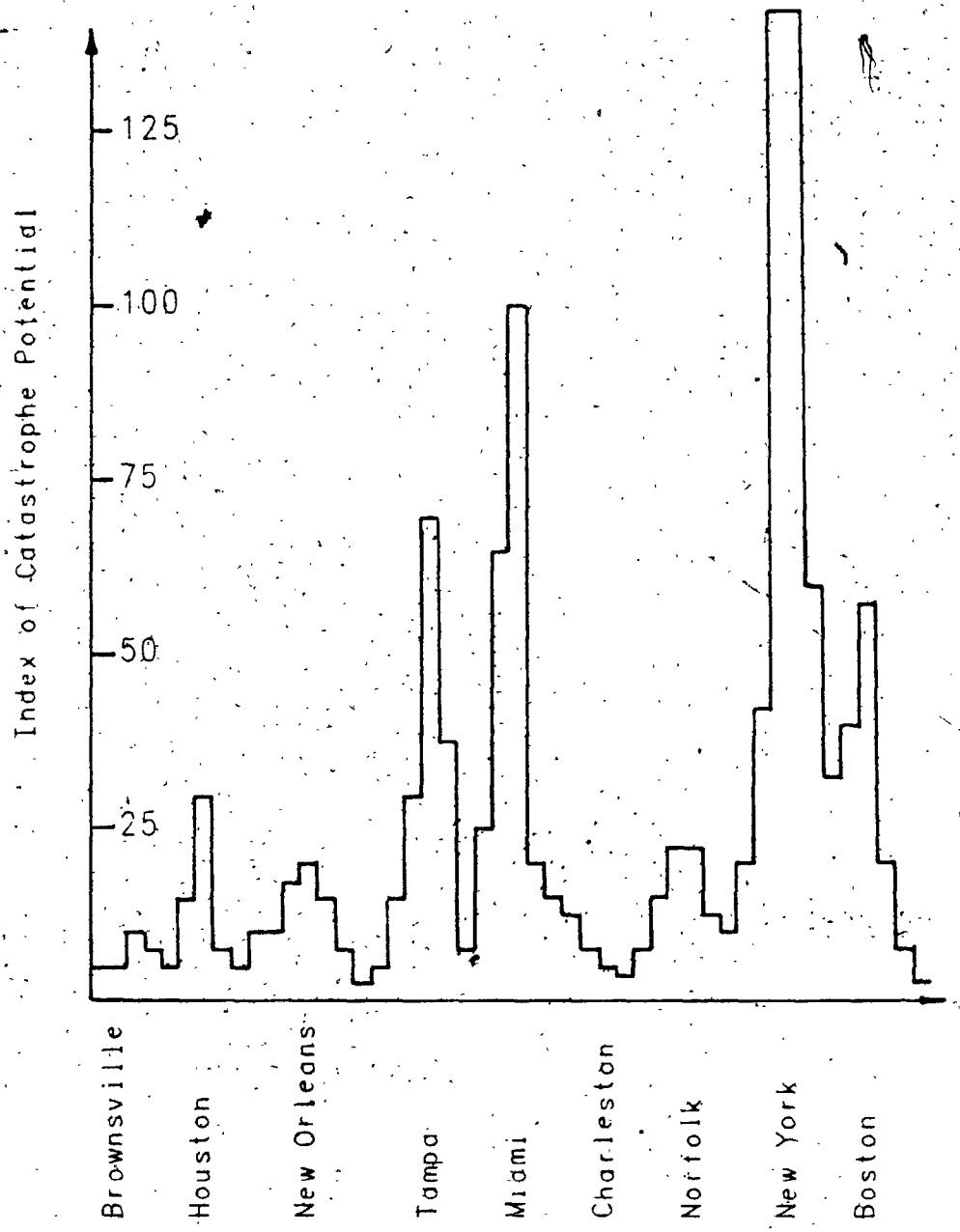

FIGURE 1.8 Catastrophe Potential Index for Major Hurricane Occurrence Around U.S. Coastline

Simulation procedures developed over the past decade have each had their own individual focus of interest. Those adapted for United States hurricane-prone regions normally predict fastest-mile, surface (10 metre) height wind speeds while those being applied to Australia's tropical cyclone regions require the estimation of 3-second gust speeds at the surface. On the other hand simulation procedures are now being routinely used in conjunction with wind tunnel test programs for building structural response. In this case the specification of mean speeds at gradient height is usually required. Most simulations make some allowance for the decay of tropical cyclones once they have made landfall and possibly allow for a variety of terrain roughnesses to adjust surface speeds over land. Few estimate wind speeds at intermediate heights between the surface and say 500 metres above ground-level. Some procedures concerned only with the application of the Monte-Carlo approach to predict extreme wind speeds do not specify wind directions in the windfield model. A similar diversity is found amongst simulations in the statistical distributions used to fit the windfield model characteristic parameters. There is thus a substantial variation in both the content and complexity of simulation procedures currently in use.

Simulations quite naturally have relied upon information obtained from the meteorological community in the formulation of windfield models. Some of the basic assumptions common to many models however have been based on data obtained more than a decade ago and not subject to the standard forms of expression required for wind engineering applications, e.g. mean or sustained wind speeds reported with no accompanying averaging time supplied, surface wind speeds recorded without corrections for the height and exposure involved.

Meanwhile, meteorological understanding of the structure of tropical cyclones has advanced greatly in recent years with the availability of flight-level observations and radar data obtained by N.O.A.A. P-3 Aircraft. This has been accompanied by equally exciting strides in the theoretical area involving computer models of tropical cyclones which are able to simulate hurricanes with asymmetric windfields, latent heating and realistic rainband and convective cluster features. An area which is currently receiving special

attention is the structure of the low-level windfield of tropical cyclones and the behaviour of landfalling storms.

The Hurricane Landfall Program run by the Hurricane Research Division of the Atmospheric and Oceanic Meteorological Laboratory, Miami, has been of immense value in this respect. H.R.D. "chase" teams, which record data from nearby radar stations, collect post-storm measurements and afterwards assimilate this data with aircraft observations, were first used during the occurrence of Hurricane Frederic in 1979. They were responsible in great part for most of the data gathered in Hurricane Alicia in 1983. These two storms have become the best-documented landfalling storms in the United States region, surpassing all others in terms of both quantity and quality of data.

In addition to the extensive amount of meteorological data obtained, the Hurricane Alicia experience became unique for another reason. At the time of Alicia's passage inland in August 1983, the tallest downtown Houston building, the Allied Bank Plaza, a 71-storey structural steel office tower, had accelerometers mounted at its top floor as part of a program monitoring the dynamic response of the building. Despite the extreme hazard evident at the time, personnel from the consulting structural engineering firm responsible for the project (Skidmore, Owings and Merrill) were able to reach the top of the building and operate the accelerometer manually. An acceleration record was obtained lasting some 90 minutes just prior to the peak of Alicia's influence on the downtown Houston area. This record is a unique one, providing for the very first time evidence of the dynamic response of a very tall structure during an extreme wind event. Coincidentally, the building had been subject to a detailed wind tunnel test investigating its dynamic characteristics. Hence with the large body of meteorological data measured during the storm's passage inland, it was possible to compare the actual accelerations recorded with those predicted by combining the wind tunnel response analysis with the reconstructed wind history experienced at the building site.

A second source of invaluable information became available throughout the course of this thesis as a result of a wind tunnel study of another structure

located in a tropical cyclone-prone area, namely the new HongkongBank headquarters in Hong Kong. In support of the wind climate component of this project records of wind speed and direction obtained during the passage of typhoons in the period 1953-1983 were acquired from various meteorological stations in the area. One of these, Waglan Island, stood out because of its relatively good exposure and long fetch of winds over water in most directions. To take advantage of this unique collection of wind records a detailed topographic wind tunnel test was conducted for Waglan Island to account for the aerodynamic influence of the island's shape on wind speeds at the anemometer location.

These developments thus created a unique opportunity to produce an updated simulation windfield model incorporating the growing body of meteorological information compiled in the last decade and at the same time to assess the revised model using the unique data gathered in recent storm occurrences.

1.5 Contribution of Current Study

The current study comprised four broad aims :

(1) In view of the importance of the simulation method to the prediction of long-term risk levels associated with tropical cyclones the whole procedure was re-examined and a revised, refined procedure formulated. This involved two separate efforts. Firstly, an updated windfield model was produced in accord with currently accepted meteorological notions and, secondly, the statistical representation of the tropical cyclone windfield characteristic parameters was improved through a detailed investigation of the most suitable probability distributions fitting them.

(2) Data obtained from a number of tropical cyclones were analyzed for the purpose of providing an independent assessment of the proposed simulation windfield model. The comparisons of actual wind records with model-predicted wind speeds and directions centred mainly on recently occurring storms, including North Atlantic tropical cyclones,

Northwest Pacific typhoons and North Australian cyclones. These case studies included the Hurricane Alicia event and Allied Bank acceleration record investigation and the analysis of records obtained from the Waglan Island anemometer station in Hong Kong.

(3) The simulation model was applied to the Gulf and Atlantic Coasts of the United States to yield hazard maps of hurricane extreme wind speeds at upper-level and surface heights. The variation of the risk imposed by these storms with distance inland was also investigated.

(4) Finally, two novel applications of the revised simulation model were made. The question of risk was extended to investigate "line-like" structures such as transmission lines located in various coastal regions of the United States. Secondly, a modified approach was developed to calculate structural response exceedances where the climate input is the simulation-predicted parent distribution of wind speed and direction, whose stationarity characteristics do not satisfy the normal requirements found in "well-behaved" wind climates.

A general description of tropical cyclones is given in Chapter 2, focussing on those features relevent to the formulation of the proposed windfield model. As many as possible of the most recent meteorological studies in this field, both data-related and theoretical, are included. In Chapter 3 this information is synthesized into a complete windfield model, including the specification of the circulation both within and above the tropical cyclone boundary layer, and the way in which the windfield is affected once landfall is made. Chapter 4 presents the assessment of the windfield model using actual measured data.

Chapter 5 is devoted to the improved statistical representation of the tropical cyclone parameters required in the simulation windfield model. Chapter 6 presents the application of the simulation procedure to hurricane-prone areas of the United States to yield hazard maps of tropical cyclone extreme wind speeds. In Chapter 7 the results of the extension to examine the risk to "line-like" structures are given as well as the modified exceedance approach suggested for use in tropical cyclone structural response predictions. Potential applications of the simulation and possible refinements to both the

simulation windfield model and the representation of the tropical cyclone characteristic parameters are discussed in Chapter 8.

CHAPTER 2

METEOROLOGICAL CHARACTERISTICS PERTINENT TO THE DETERMINATION OF TROPICAL CYCLONE WIND SPEEDS

The description of the tropical cyclone windfield which follows lays the foundations for the simulation windfield model proposed in this thesis. This model differs appreciably from others utilized in previous simulation procedures. Attention is focused on the steady-state structure of mature tropical cyclones. For such storms variations in the windfield take place over time periods of an hour or more. Emphasis is placed on the lower levels of the storm circulation, which are of the greatest engineering interest. A concluding section summarizes those characteristics of the tropical cyclone windfield which are deemed important for the simulation procedure to adequately and accurately represent the effect of these storms and their resulting risk potential.

2.1 Early Studies

Understanding of the three-dimensional structure of tropical cyclones has kept pace with the introduction of ever-more sophisticated observational techniques. Initially, studies were restricted to surface wind and pressure measurements. Upper air data became available with the establishment of the global radiosonde network in 1936. Aircraft reconnaissance flights into hurricanes began in 1943. A continuous U.S. coastal radar network became operational in 1955. The latest technological leap forward occurred in 1960 when TIROS I launched the era of the weather-satellite.

Quantitative data documenting the pressure characteristics and cyclonic flow around tropical cyclones can be found in a number of early studies (Hall, 1917; Cline, 1926; Deppermann, 1947). Hughes (1952) presented data from a number of aircraft flights into Northwest Pacific tropical cyclones. The most significant outcome of this study was a combined pattern of total wind speed at the 1000 foot level, displayed in Figure 2.1. This showed a concentric windfield with a definite wind maximum located in the right-rear quadrant of

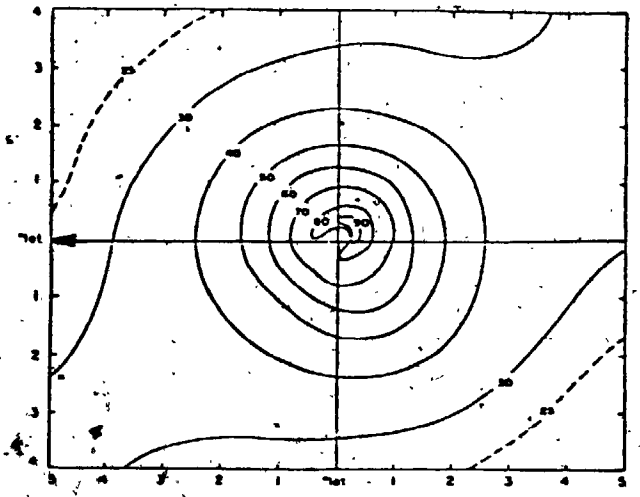

Total Wind Speed in Knots

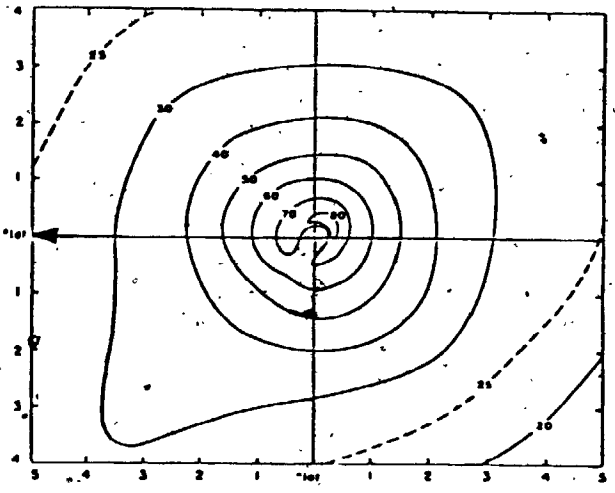

Tangential Velocity in Knots

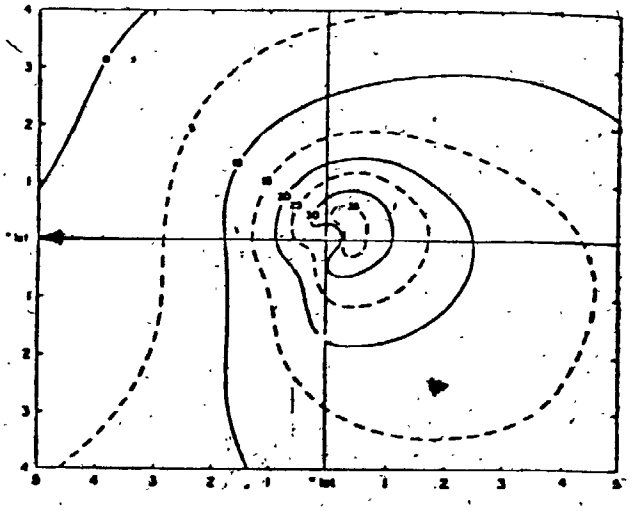

Radial Velocity in Knots

FIGURE 2.1 Hughes (1952) Wind-Speed Flight-Level Composite Data (Arrow Shows Direction of Storm Motion)

the storm. Hughes' composite windfield was widely quoted in subsequent studies and had a lasting effect on the perception of tropical cyclone wind structure. It influenced the choice of a representative windfield for so-called design hurricanes in many studies examining risk considerations (NHRP Staff, 1957; Graham and Nunn, 1959; Gilman and Myers, 1961).

Tropical cyclone research moved into high gear with the inception of the National Hurricane Research Project (NHRP), Miami, Florida, established in 1956, particularly with the commencement of regular aircraft reconnaissance of the high energy core of tropical cyclones. The first comprehensive storm analysis made possible by these flights was with Hurricane Carrie in September 1957 (NHRP Staff, 1958). Synoptic analysis of Carrie's structure at the 11,000 foot and 14,000 foot levels identified horizontally symmetric pressure and temperature distributions around the storm centre as opposed to a distinctly asymmetric windfield distribution. Analysis of subsequent hurricanes revealed that horizontal symmetry of the pressure and temperature fields extended to the vertical direction as well (LaSeur and Hawkins, 1963; Hawkins and Rubsam, 1968; Hawkins and Imbembo, 1976). Figure 2.2 shows vertical cross-sections of the highly symmetric pressure and temperature fields computed from flight data through Hurricane Inez, 1966. Both pressure and temperature distributions have their strongest gradients in the eyewall region. Wind speed contours and streamlines at the 750 mb level of Inez are shown in Figure 2.3. While the horizontal windfield displays some asymmetry, the almost circular streamlines indicate that at this height the tangential component of wind speed must have been close to gradient balance, i.e. the pressure gradient force equalling the oppositely directed centrifugal plus Coriolis forces.

Data from numerous tropical storms and hurricanes established (i) the symmetric distribution of pressure around the storm eye, (ii) the bias toward stronger winds on the right-hand side of the storm and (iii) the roughly circular streamline pattern at about the 3 kilometre height, as standard features of the tropical cyclone circulation. Hawkins (1962) combined flight data from mature storms to develop a vertical cross-section of wind speed extending down to the 1500 foot level, shown in Figure 2.4. Very little vertical shear was found in the wind from the 1500 foot level to about the

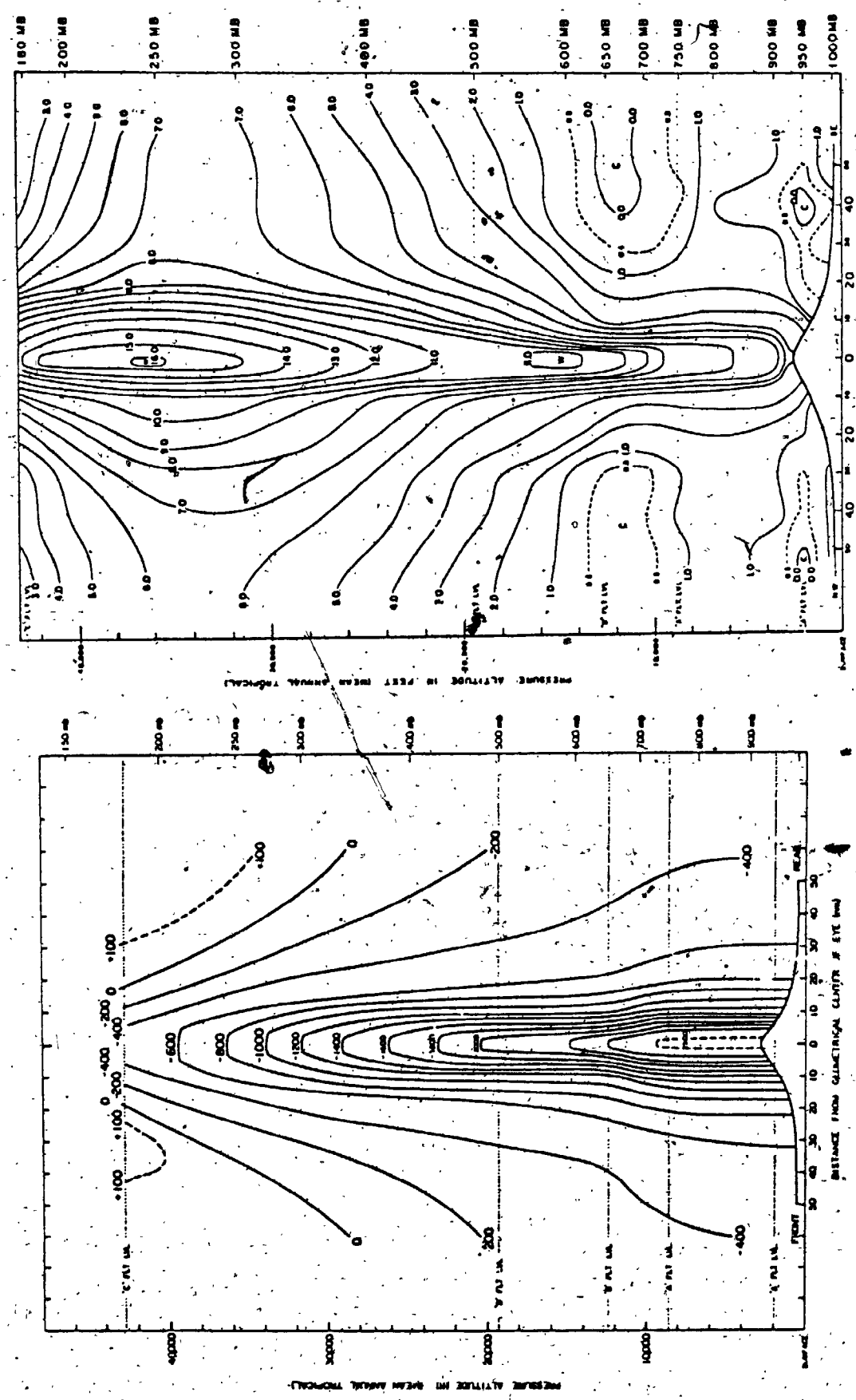

FIGURE 2.2 Vertical Cross-Sections of D-Values (ft) and Temperature (°C) for Hurricane Inez, September 28 1966

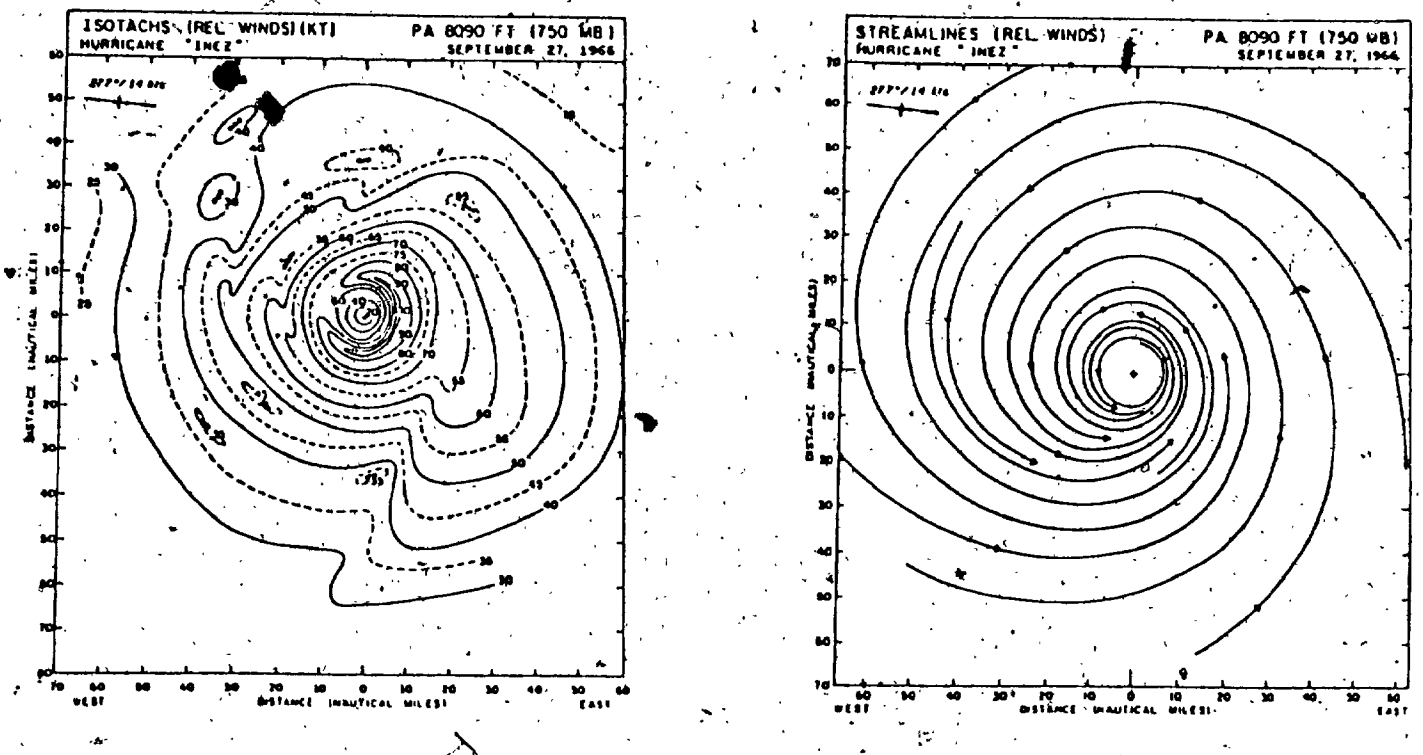

FIGURE 2.3 Wind Speeds and Streamlines Relative to the Storm Centre at the 750mb Level for Hurricane Inez, September 28 1966

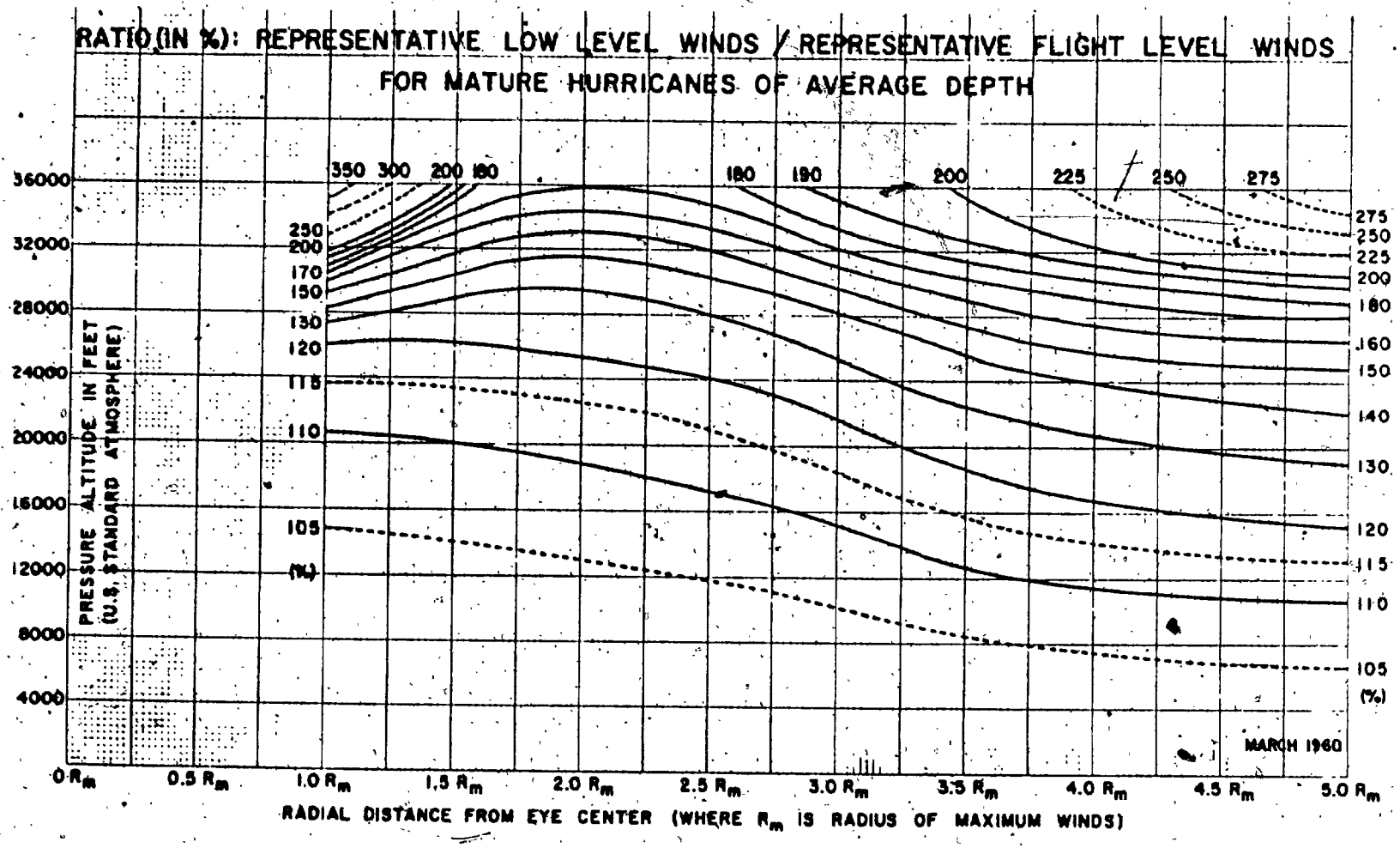

FIGURE 2.4 Hawkins (1962) Representative Vertical Cross-Section of Radial Wind Speed Profiles

700 mb level. Riehl (1963), Colon (1963) and Miller (1967) examined aircraft data and fitted observed radial wind profiles with a modified Rankine combined vortex of the form :

$$V(r) = \left(\frac{r}{RMAX}\right)^m \cdot V_{max} \qquad r \le RMAX \qquad E2-1a$$

$$= \left(\frac{RMAX}{r}\right)^n \cdot V_{max} \qquad r \ge RMAX \qquad E2-1b$$

r = radial distance from storm centre
$RMAX$ = radial location of maximum wind speed, $Vmax$
m,n = positive constants

This representation was first suggested by Depperman (1947). The inner exponent "m" was generally found to lie close to 1.0, although the range of actual observed values was wide, from less than 0.5 to 2.0 (Gray, 1981). Riehl found the outer exponent "n" to be approximately 0.5. Colon found values of "n" ranging from 0.2 to 0.6. These and other studies found "n" to be typically 0.5 with a standard deviation of $\pm$ 0.3 (Gray, 1981).

The first attempt to formulate a pressure profile to relate the windfield to the pressure field was made by Schloemer (1954). His analysis of nine Florida hurricanes led to an exponential pressure distribution of the form :

$$\frac{p(r) - Pc}{Pn - Pc} = exp\left\{-\frac{RMAX}{r}\right\} \qquad E2-2a$$

$p(r)$ = pressure, at distance r from storm centre
Pc = central pressure, at the storm centre
Pn = periphery pressure, at the circulation extremity
$RMAX$ = radius of maximum winds
ΔP = $(Pc-Pn)$, the central pressure difference

Graham and Hudson (1960) suggested a modified form of the Schloemer equation :

$$\frac{p(r) - Pc}{Pn - Pc} = exp\left[-\left(\frac{RMAX}{r}\right)^{B}\right] \qquad E2-2b$$

B = pressure profile exponent

This was found to produce a better fit to observed hurricane pressure profiles in the outer parts of the storm circulation. Differentiation of E2-2b shows that increasing the value of B increases the "peakiness" of the wind profile near the radius of maximum winds. Schwerdt, Ho, and Watkins (1979) examined 10 alternative pressure profile formulae and found that the Schloemer exponential form gave the base overall fit, especially for the more intense storms.

Holland (1980) examined three Australian and nine Florida hurricanes and found that the modified exponential form in E2-2b gave a superior fit to the observed radial pressure profiles and that the Schloemer profile ($B = 1.0$) consistently underestimated the radial pressure gradient in the eyewall region. It was suggested that a theoretically admissable range of values for B is 1.0 to 2.5. In attempting to derive a climatological value for the pressure profile exponent, B, Holland deduced a consistent increase in B with decreasing central pressure. This implies that the tropical cyclone windfield becomes more "peaked" with increasing storm intensity.

The strong relationship in tropical cyclones between the circulation maximum wind speed, V_{max}, and the minimum central pressure, Pc, had long been observed. The inference that winds in the vicinity of the eyewall were in almost cyclostrophic balance (pressure gradient force equal to the centrifugal force) and the form of the pressure profile in equation E2-2a indicated that they should be related by a functional relationship of the form:

$$V_{max} = C\left|Pn - Pc\right|^{n} \qquad E2-3$$

C, n = constants

Over the years a number of such minimum pressure-maximum wind equations were developed (Takehashi, 1939; Fletcher, 1955; Myers, 1957). The variability of ship observations, anemometers being put out of action and a general lack of attention in applying corrections to land records to account for terrain and topography conditions contributed to a wide scatter of the wind speed measurements used to define these relationships. Perhaps the two most reliabile developed were those of Kraft (1961) and Atkinson and Holliday (1975) for the North Atlantic and Northwest Pacific regions respectively :

Kraft

$$V_{max} = 7.20 [Pn - Pc]^{0.5} \qquad E2-4a$$

Atkinson-Holliday

$$= 3.45 [Pn - Pc]^{0.644} \qquad E2-4b$$

Vmax in m/sec, *Pn* and *Pc* in millibars.

To simplify operational use of these equations the periphery pressure, *Pn*, was assigned average values equal to 1013 and 1010 mb for the North Atlantic and Northwest Pacific regions respectively. Holliday (1969) showed that Kraft's relation predicted maximum "sustained" (1-minute average) surface speeds with a standard deviation of ± 4.0 m/sec for hurricanes with a range of minimum pressures from 990 to 930 mb. The comparable figure for the Atkinson-Holliday relationship is ± 4.5 m/sec.

The cyclostrophic relationship in E2-3 was extended to include the Coriolis force and hence obtain expressions for the windfield in the form of a gradient balance. Graham and Nunn (1959) defined the maximum wind speed in tropical cyclones by :

$$V_{max} = 5.61 [Pn - Pc]^{0.5} - f.RMAX \qquad E2-5$$

f = Coriolis parameter

In subsequent studies, the constant preceding the central pressure difference term in E2-5 was adjusted to take into account the variation of air density with latitude (Schwerdt, Ho and Watkins, 1979). Early studies approached the problem of windfield asymmetry due to storm motion by defining a symmetric circulation based on formulae such as E2-4a,b or E2-5 and superimposing a right-left asymmetry by adding to the windfield a speed component equal to :

$$V_{add} = C \cdot VT^n \cdot \cos\beta \qquad E2-6$$

V_{add} = additional wind speed due to storm motion
VT = translation speed of storm
β = trigonometric angle (i.e. 0° = East, 90° = North etc. assuming northwards storm motion)
C, n = positive constants

Graham and Nunn (1959) used $C=0.5$. Graham and Hudson (1960) found values of C ranging from 0.25 to 1.0 for $n=1.0$. Schwerdt, Ho and Watkins (1979) gave $C=0.60$ and $n=0.63$, implying that the storm translation speed played a relatively more important role for slower moving storms. Jelesnianski (1967) used an additive term that was a function of radius :

$$V_{add} = \left| \frac{r^2}{r^2 + RMAX^2} \right| \cdot VT \cdot \cos\beta \qquad E2-7$$

Early studies specified the wind direction in terms of the inflow angle, defined as the deviation of a given trajectory from a local tangent to a circle located around the storm centre. Graham and Nunn (1959) suggested a value of inflow angle equal to 20° at the radius of maximum winds, $RMAX$, increasing to 25° at $1.2RMAX$, and constant further out. Malkus and Riehl (1960) assumed a constant inflow angle from a distance of 100 km out from the centre, decreasing linearly to 0° at the eyewall. This constant value was varied from 20° to 25° for moderate to intense hurricanes respectively. Schwerdt, Ho and Watkins (1979) developed a nomogram of inflow angles based on Jelesnianski's (1967) surface wind analysis. The magnitude and

location of the maximum inflow angle were both shown to increase with storm intensity. Further out in the storm circulation the inflow angle was assumed to decrease rather than remain constant.

The balance of forces governing the tropical cyclone windfield distribution was examined by Riehl and Malkus (1961) and Gray (1963). Gray used flight data from a number of storms to calculate the magnitude of the excess of pressure gradient over the centrifugal and Coriolis accelerations. Figure 2.5 shows the values computed for Hurricane Daisy (1958), indicating a positive imbalance on the right-hand side of the storm and a negative imbalance on the left-hand side. A composite 10-level analysis combining data from a number of storms showed that the imbalance was only partially reduced when the translation speed was removed from the total wind speed vectors, more so outside the radius of maximum winds. Gray's data also showed that the asymmetry in wind speeds between the right and left sides of the storm circulation at intermediate levels (700 mb) could be reasonably computed using Blaton's formula, i.e. substituting an adjusted radius of curvature for the wind flow using the following equation :

$$\text{adjusted curvature} \qquad r_t = \frac{r}{1 \pm \frac{VT}{V}\sin\alpha} \qquad E2-8$$

r = distance from storm centre
V = actual wind speed
VT = translation speed of the storm
α = angle, clockwise positive from translation direction

In defining the salient characteristics of the tropical cyclone windfield these early studies often contradicted each other. While Gray's (1963) study indicated that the eyewall region was in neither gradient nor thermal balance, individual case studies, e.g. Hawkins and Imbembo (1976), seemed to suggest the opposite. Questions were raised about the value of case studies versus composite data studies, effects of precipitation on Doppler wind measurements, the relation of aircraft winds to surface station winds etc. Recent studies have tackled these problems and in the interim, aircraft instrumentation technology has been improved. Before proceeding to these

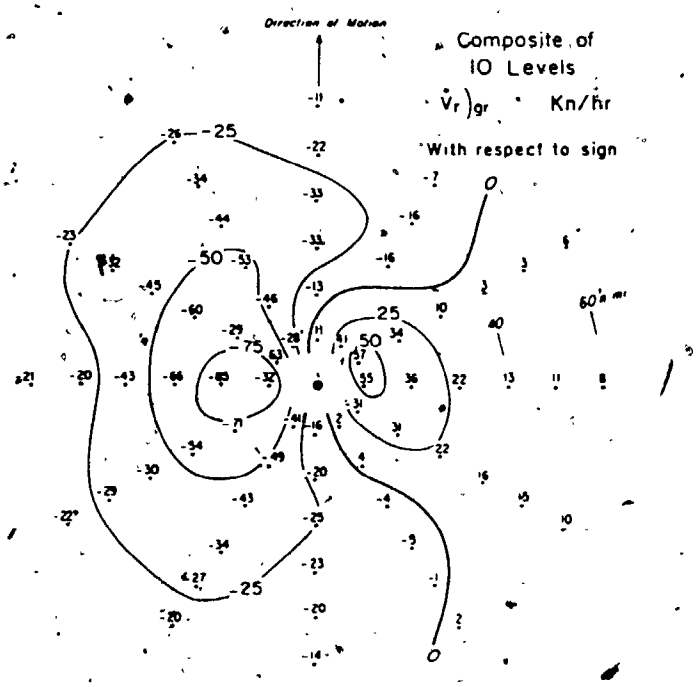

FIGURE 2.5 Excess of Pressure Gradient over Coriolis and Centrifugal Accelerations for Hurricane Daisy, 1958

however, the applicability of the gradient balance assumption and the balance of forces generally are investigated.

2.2 Scale Analysis of the Tropical Cyclone Boundary Layer Equations of Motion

To help clarify the arguments discussed in the preceding section, an analysis of the boundary layer equations of motion is made to establish the order of magnitude of the constituent terms and hence to identify their importance within the circulation. The tropical cyclone boundary layer radial and tangential momentum equations in a cylindrical co-ordinate system (r,θ,z) whose origin is located at the centre of a stationary storm are :

I - Radial E2-9

$$\underset{1}{\frac{\partial u}{\partial t}} + \underset{2}{u\frac{\partial u}{\partial r}} + \underset{3}{\frac{v}{r}\frac{\partial u}{\partial \theta}} + \underset{4}{w\frac{\partial u}{\partial z}} - \underset{5}{fv} - \underset{6}{\frac{v^2}{r}} = \underset{7}{-\frac{1}{\rho}\frac{\partial p}{\partial r}} + \underset{8}{\frac{1}{\rho}\frac{\partial \tau_{rz}}{\partial z}} + \underset{9}{F_r}$$

II - Tangential E2-10

$$\underset{1}{\frac{\partial v}{\partial t}} + \underset{2}{u\frac{\partial v}{\partial r}} + \underset{3}{\frac{v}{r}\frac{\partial v}{\partial \theta}} + \underset{4}{w\frac{\partial v}{\partial z}} + \underset{5}{fu} + \underset{6}{\frac{uv}{r}} = \underset{7}{-\frac{1}{\rho r}\frac{\partial p}{\partial \theta}} + \underset{8}{\frac{1}{\rho}\frac{\partial \tau_{\theta z}}{\partial z}} + \underset{9}{F_\theta}$$

u,v,w = radial, tangential and vertical velocity components.
p = pressure
f = Coriolis parameter
ρ = air density
τij = turbulent mixing shear stresses

$$F_r = \frac{1}{\rho}\left[\frac{\partial \tau_{rr}}{\partial r} + \frac{1}{r}\frac{\partial \tau_{r\theta}}{\partial \theta} + \frac{\tau_{rr} - \tau_{r\theta}}{r}\right] \qquad F_\theta = \frac{1}{\rho}\left[\frac{\partial \tau_{rz}}{\partial r} + \frac{1}{r}\frac{\partial \tau_{\theta z}}{\partial \theta} + 2\frac{\tau_{r\theta}}{r}\right]$$

Individual terms are identified by numbers, e.g. E2-9(1) is the local acceleration term in the radial component equation. To identify the relative importance of each of the terms, approximate values were assigned to each variable consistent with actual tropical cyclone observations. This was done for two regions of interest in the storm - (a) in the vicinity of the radius of maximum winds and (b) the outer part of the storm (at about 5 times the radius of maximum winds). These regions are referred to respectively as the eyewall and outer regions. Table 2.1 lists the values of each of the variables estimated. They are representative of a mature tropical cyclone. Since the intention of this exercise was to indicate the relative importance of each term in the momentum equations, the accuracy of the numerical computations is of an order of magnitude only.

Table 2.2 shows the magnitudes computed for each of the terms. It was assumed that the storm was in a steady-state. Therefore time derivatives and azimuthal derivatives were set to zero. Inspecting the results for the eyewall region first, it can be seen that the balance of forces in the radial component is completely dominated by terms E2-9(6) and (7), the centrifugal accelerations of the tangential wind and the radial pressure gradient. The force balance suggested in the tangential component equation involves 5 terms whose magnitudes are comparable but relatively small compared to the two dominant terms in the radial component equation. This suggests that at the radius of maximum winds the balance of forces is almost cyclostrophic for the tangential component. The radial component of wind speed is very much smaller anyhow. These observations support the gradient balance assumption in the eyewall region. If the Coriolis force term is included, this allows winds near the radius of maximum winds to be estimated by the gradient balance equation:

$$\frac{1}{\rho}\frac{\partial p}{\partial r} \simeq fv + \frac{v^2}{r} \qquad E2-11a$$

$$u << v \qquad E2-11b$$

The balance of forces in the outer region for both radial and tangential components is more complex. Although the radial pressure gradient term,

TABLE 2.1
BOUNDARY LAYER SCALE ANALYSIS VARIABLE REPRESENTATIVE VALUES

Variable		EYEWALL Region	OUTER Region
R	m	50,000	250,000
u	m/sec	1.0	15.0
v	"	50.0	30.0
w	"	0.25	0.1
p	mb	25.0	50.0

	z	=	1000.0 m
common	f	=	0.00005
to both	ρ	=	1.00 kg/m^3
regions	Cd	=	0.002
	K	=	50,000.0 m^2/sec

TABLE 2.2
COMPUTED MAGNITUDES FOR TROPICAL CYCLONE BOUNDARY LAYER CONSTITUENT TERMS

Term No.	EYEWALL Region		OUTER Region	
	Radial E2-9	Tangential E2-10	Radial E2-9	Tangential E2-10
1	-	-	-	-
2	0.2	1.0*	1.0*	1.8*
3	-	-	-	-
4	0.1	2.5*	0.25	0.5*
5	2.5*	0.05	1.5*	0.8*
6	50.0**	1.0*	3.5*	1.8*
7	50.0**	-	20.0**	-
8	0.1	3.0*	1.0*	1.5*
9	1.0	1.0*	0.025	0.025

** major dominant term

* minor dominant term

E2-10(7), is larger than the others, it is not simply balanced by the Coriolis and centrifugal accelerations. Advective acceleration and frictional drag terms are appreciable in both radial and tangential component equations. This upsets the gradient balance, with the result that the flow experiences a net acceleration inwards and produces boundary layer inflow, as is in fact observed. Within the boundary layer away from the eyewall it would appear that no simple relationship exists to predict wind speed magnitudes nor estimate inflow angles.

2.3. Composite Data Studies

By the 1970's, well over 10 years of rawinsonde data and aircraft observations had been accumulated in the North Atlantic, Northwest Pacific and Australian Pacific regions. The coverage of wind speed, wind direction, surface pressure etc. data then became sufficient to obtain a picture of a "composite" tropical cyclone. This approach began and remains centred amongst researchers working under Professor W.M. Gray at Colorado State University. Composite rawinsonde data banks have been screened and processed for the period 1961-1974 for the North Atlantic, the period 1961-1970 for the Northwest Pacific area and the period 1961-1970 for the Australian Pacific area. The first two data sets contain more than 10000 and 15000 individual rawinsonde soundings respectively.

In the "compositing" technique, data from a large number of storms are overlapped to reveal the structure of an "average" or "composite" tropical cyclone. With a large enough data base, it is possible to subdivide the data to analyze different storm types, e.g. tropical storms, hurricanes. It is also possible to classify the data by grouping storms in terms of one parameter, e.g. intensity or latitude, and then observing the variation of other characteristic parameters within each group. Individual variability and asymmetries in storm structure tend naturally to be smoothed out by the compositing approach. Asymmetries however which are a consistent feature of the tropical cyclone structure are preserved.

The first major compositing study was the aircraft data analysis of Shea and Gray (1973), based on observations from approximately 100 NHRP flight missions into 21 hurricanes during the period 1957-1969. Figure 2.6 shows plan views of composite D-values and actual and relative tangential winds at the 900 and 750 mb levels. The pressure field around the tropical cyclone eye is very symmetric. The actual tangential winds show a significant bias towards higher winds on the right-hand side of the circulation. The relative tangential winds are obtained by subtracting the translation speed of the storm from the actual winds. It can be seen that a large amount of the asymmetry is thereby removed. Computations were made along radial legs to calculate the magnitude of the pressure gradient force *(Pgf)*, Coriolis force *(Cof)* and centrifugal acceleration force *(Cef)*. These were averaged azimuthally and the ratio $(Cof+Cef)/Pgf$ determined. A ratio of unity would indicate gradient balance in the windfield at the particular height examined. Figure 2.7 shows the values computed for the composite 900 and 750 mb height data. A significant divergence from gradient balance is evident. At the 900 mb height wind speeds near the radius of maximum winds are 20-30% higher than those that would have been obtained assuming gradient balance. Willoughby (1980) has argued that the super-gradient winds indicated in Shea and Gray's data could have arisen as a result of the computation procedure, if the tangential wind was the sum of a symmetric component in gradient balance and an asymmetric component that was a function of radial distance in the storm. Averaging with respect to the radius of maximum winds but not the storm centre would then produce super-gradient winds at the apparent composite radius of maximum winds even though the azimuthal average was close to being in gradient balance. Anthes (1982) showed that the azimuthal averaging of a number of radial profiles of balanced tangential wind resulted in sub-gradient average wind profiles.

The large departure from gradient balance reported in Shea and Gray's study was not observed in a more recent composite study. In an analysis of 700 mb U.S.A.F. reconnaissance aircraft data for 25 Northwest Pacific tropical cyclones, Dunnavan (1983) showed that the gradient balance wind equation gave a superior fit to the observed winds measured in over 1000 radial flight legs through the storms, at distances ranging from 50 to 200 km from the storm centre.

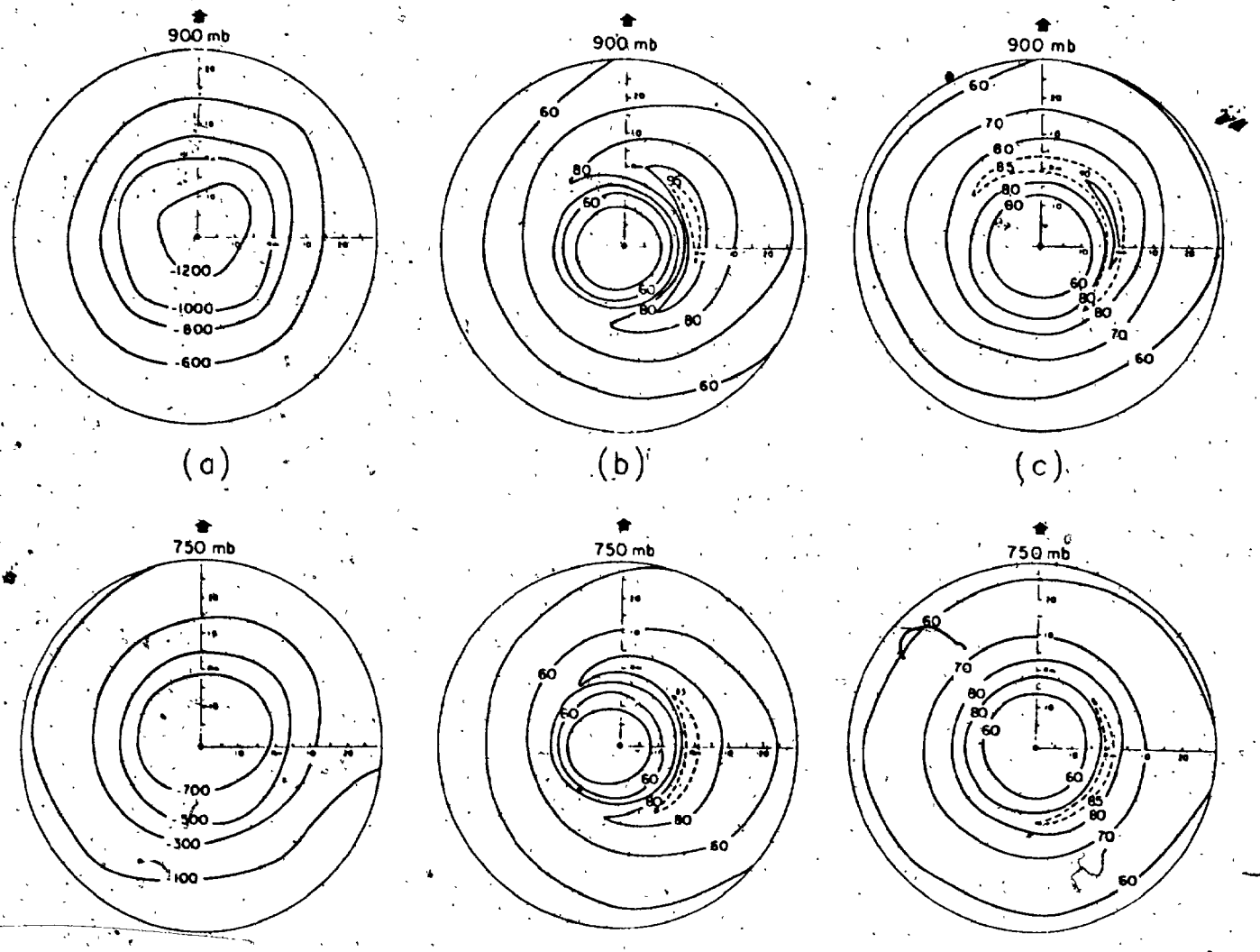

FIGURE 2.6 Composited Data (a) D-Values (b) Actual and (c) Relative Windfields at the 900 and 750 mb Levels (Shea and Gray, 1973)

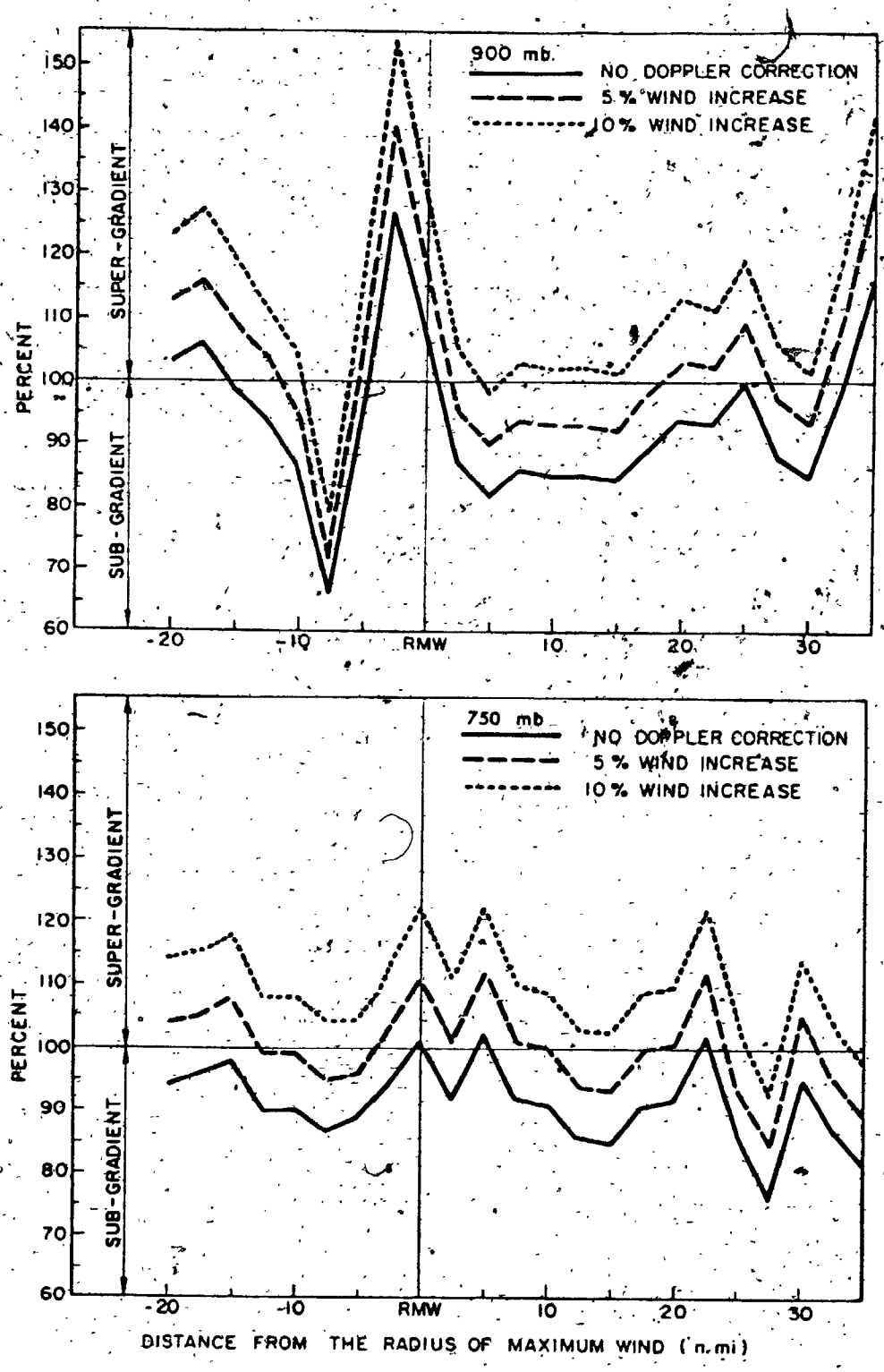

FIGURE 2.7. Composited Data Ratio of Actual Acceleration to Gradient Balance Acceleration (Shea and Gray, 1973)

The compositing of rawinsonde data yielded equally valuable information about the structure and energetics of tropical cyclones. Figure 2.8 shows vertical cross-sections of the azimuthally-averaged tangential windfield for composite North Atlantic and Northwest Pacific storms through various stages of development (McBride, 1981). For fully developed tropical cyclones it can be seen that the tangential wind has a maximum at or just above the 900 mb level, corresponding to a height above the earth's surface of 500-1000 metres.

George and Gray (1976), Frank (1977) and Frank and Gray (1980) investigated the horizontal asymmetry in the tropical cyclone windfield. Figure 2.9 gives north-south and east-west vertical cross-sections of the tangential windfield for a composite Northwest Pacific tropical cyclone, showing stronger tangential winds to the right of the storm's direction of motion. Nunez and Gray (1977) presented composite analyses of the inflow angles for mean-steady-state hurricanes and typhoons, shown in Figure 2.10. The inflow angle is, as expected, greatest at the surface. The inflow becomes almost negligible above the 800 mb level (1500 metre height). For the two composite storms inflow angles are greatest in the right and front quadrants.

Merrill (1984) compared the structure and energetics of large and small tropical cyclones. This composite analysis included the computation of the relative angular momentum (RAM) and intergrated surface friction losses (SFL) for five mutually exclusive North Atlantic storm groups : small to medium tropical storms, large tropical storms, small hurricanes and large hurricanes located north and south of the 25 degree latitude. The RAM and SFL values, shown in Figure 2.11, clearly indicate that the angular momentum and surface loss processes within tropical cyclones are much more strongly related to size than to intensity. A number of previous simulations have restricted themselves to modelling only the behaviour and characteristics of hurricanes. Merrill's findings support the inclusion of tropical storms as well as hurricanes in the simulation of the tropical cyclone wind history at any particular site. The exclusion of tropical storms not only limits the amount of available data unnecessarily but would appear to be in conflict with the physical processes underlying the wind climate itself.

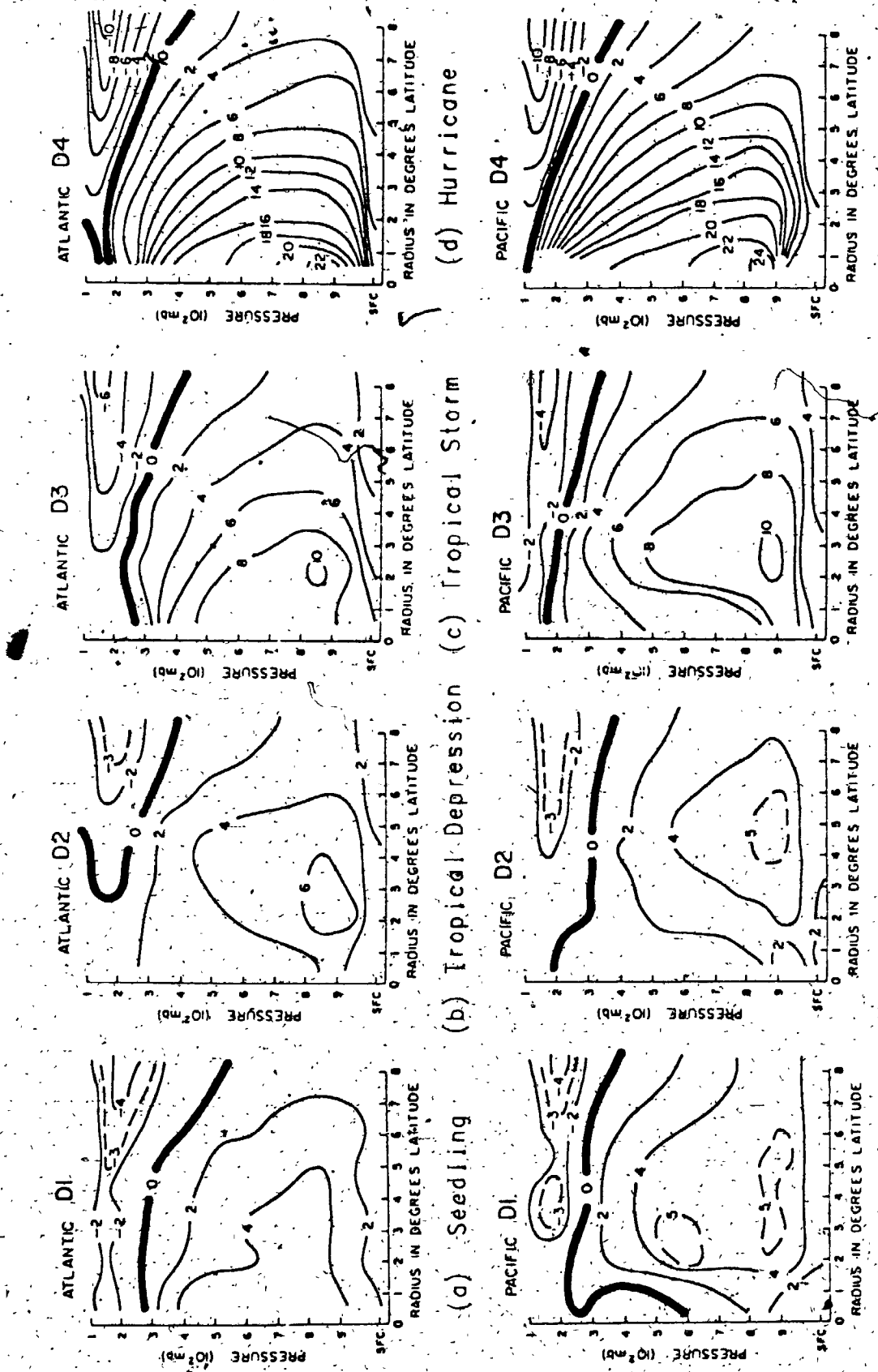

FIGURE 2.8 Vertical Cross-Sections of Composite North Atlantic and Northwest Pacific Tropical Cyclones During Various Stages of Development (McBride, 1981)

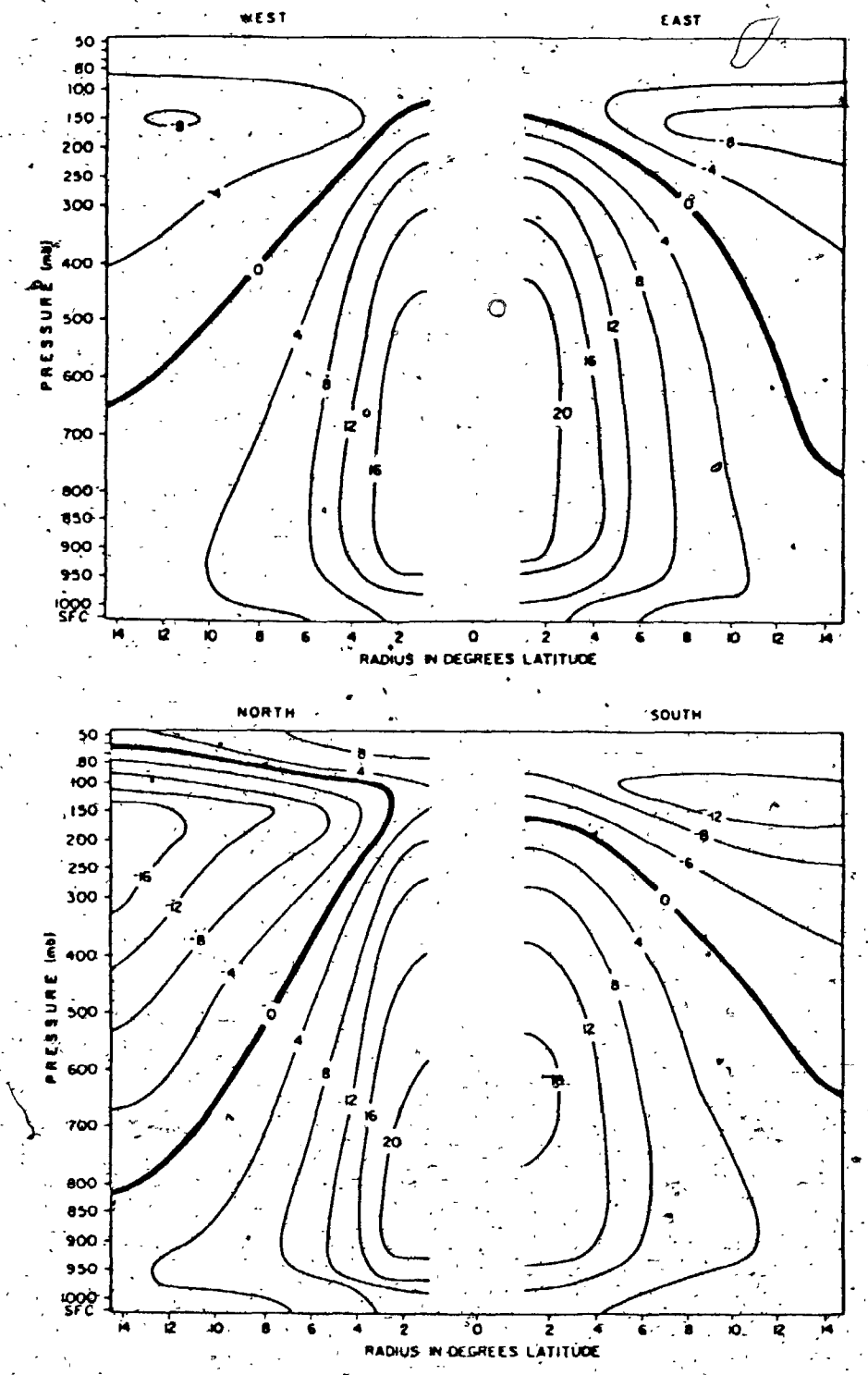

FIGURE 2.9 Vertical Cross-Sections Through Composite Northwest Pacific Typhoons (Frank, 1977)

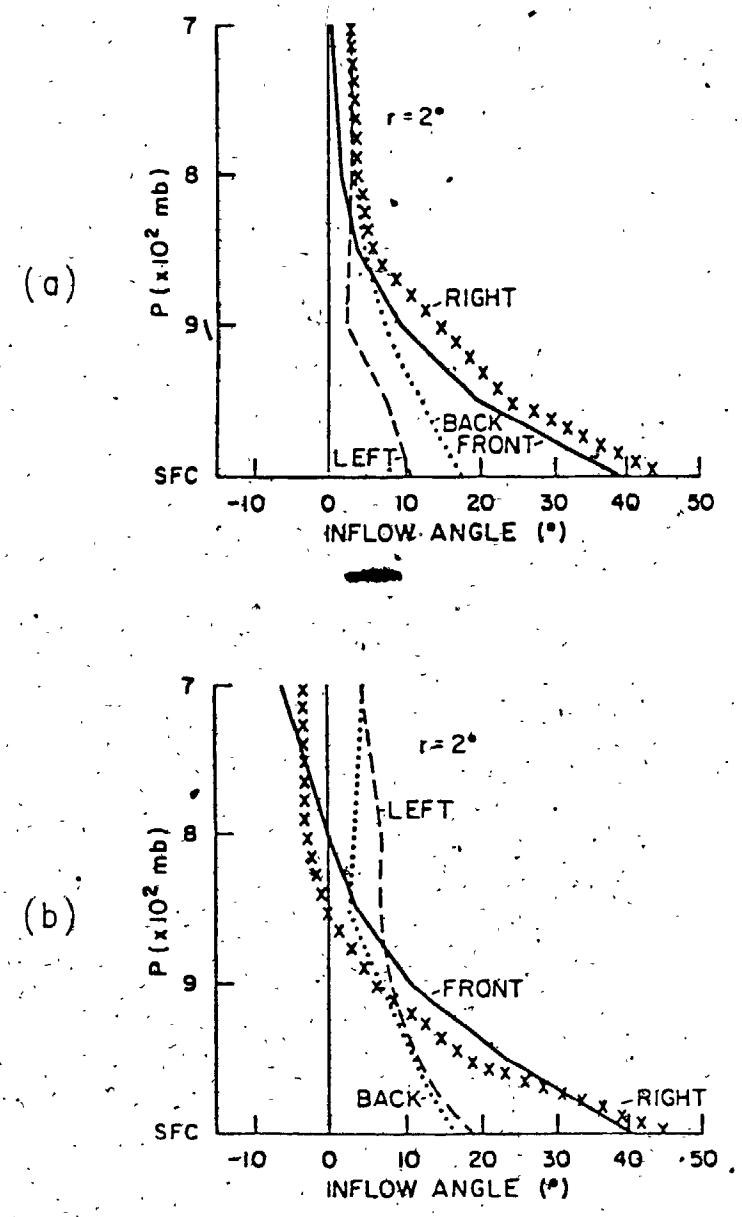

FIGURE 2.10 Composite Inflow Angles for Mean Steady-State (a) Hurricane and (b) Typhoon (Nunez and Gray, 1977)

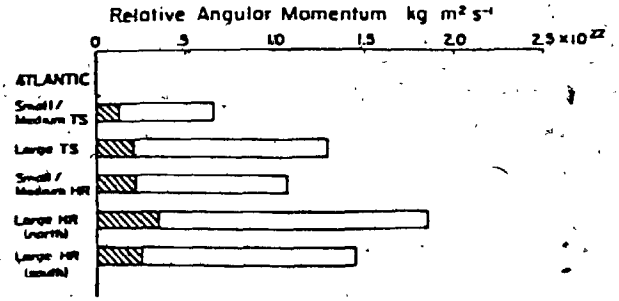

Integrated relative angular momentum (RAM) from 0 to 4° latitude radius and from 950 to 100 mb for Atlantic tropical cyclone composites. The shaded area is the estimated RAM for the 0–2° region using the fitted modified Rankine vortex approximation described in the text.

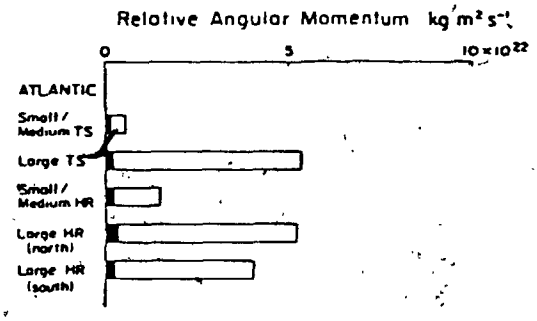

As above but from 0 to 8° radius. The black area is the estimated RAM from 0 to 2° latitude radius.

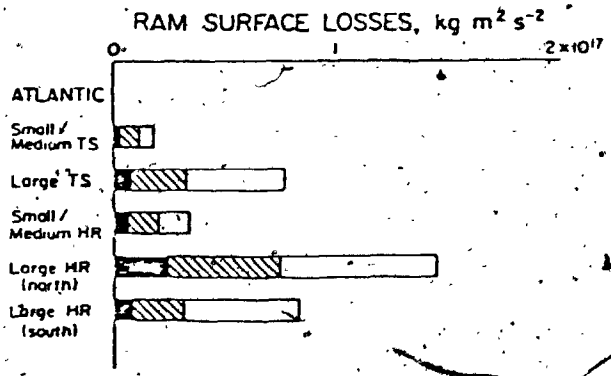

Integrated surface sink of cyclone RAM from 0 to 8° latitude radius for Atlantic tropical cyclone composites, showing surface losses within 2° latitude radius of the center (black), from 2 to 4° (hatched), and 4 to 8° (unshaded).

FIGURE 2.11 Integrated Relative Angular Momentum and Surface Friction Losses for North Atlantic Composite Tropical Cyclones (Merrill, 1984)

The very success of the composite technique in obtaining meaningful average characteristics of tropical cyclones provides strong support for the ultimate success of the Monte-Carlo simulation method used to determine extreme winds associated with these storms. Composite studies have provided strong evidence that the basic structure and energetics of all tropical cyclones are similar despite the obvious differences between individual storms.

2.4 Numerical Models

Numerical modelling of tropical cyclones has progressed significantly from the first attempts of Kasahara (1961) and Syono (1962) to today's sophisticated three-dimensional models used both operationally and for research purposes to improve the understanding of tropical cyclones. An excellent summary of the development of tropical cyclone numerical models can be found in Anthes (1982).

The first simulations which produced the evolution of a circulation resembling a typical tropical cyclone were reported by Ooyama (1967, 1969) and Yamasaki (1968a,b). In addition to the realistic behaviour of the winds, Ooyama's model hurricane had many properties found in typical hurricanes, comparable rainfall rates and similar kinetic energy components. These similarities gave credibility to the model and paved the way for future development and improvements. With this initial model Ooyama was able to demonstrate the sensitivity of tropical cyclones to changes in sea-surface temperature, to varying frictional constraints and different initial conditions inducing storm intensification. For example, when the exchange coefficient in the model was set to zero (equivalent to cutting off the supply of latent heat through evaporation, as would occur at landfall) Ooyama's model hurricane would quickly decay.

Improvements to numerical models were soon introduced. Ooyama's three-level model assumed that the windfield was in a balanced state with respect to the pressure field. Later models did not make this assumption but utilized the so-called "primitive" equations of motion and with greater

computer power being made available increased the number of vertical levels used. These initial models were all two-dimensional and hence symmetric about the storm centre. To reproduce the asymmetry normally found in tropical cyclones and to investigate the interaction of a storm with its environmental flow, it was necessary to develop three-dimensional models. The first of these, reported by Anthes (1971), was able to produce realistic asymmetries in the outflow layer and spiral rainbands. Three-dimensional models were used to investigate the effect of the variation of Coriolis parameter (Madala and Piacsek, 1975; Anthes and Hoke, 1975) and the influence of various types of steering current on the motion of a mature tropical cylone (Jones, 1977). The three-dimensional model used by Anthes and Chang (1978) to investigate the hurricane's response to changes in sea surface temperature contained a parameterization of the boundary layer consisting of surface and mixed layers whose fluxes were specified according to Monin-Obukhov surface similarity theory. Flow in the boundary layer was found to be typically sub-gradient due to surface friction. Maximum wind speeds were located just above the top of the boundary layer, which varied between 400 and 700 metres above sea-level. There were nearly uniform cross-isobaric inflow angles of 20 to 25 degrees at the surface.

Tuleya and Kurihara (1978), Moss and Jones (1978) and Tuleya, Bender and Kurihara (1984) utilized three-dimensional asymmetric models to investigate the change to tropical cyclone structure experienced at landfall. The cut-off of evaporation over land was shown to cause adiabatic cooling in the surface inflow layer which soon became drier and produced a weakening of the storm. Increased surface friction over land produced a reduction of surface winds only. All three models exhibited somewhat complex changes in the windfield at landfall. While the tangential wind component typically decreased over land, the radial component was often seen to increase. Enhanced boundary layer inflow was detected in the right front quadrant of the storm. Some of these features are reproduced in Figure 2.12 showing an example landfall simulation from the Tuleya-Bender-Kurihara model.

Willoughby (1979) and Shapiro and Willoughby (1982) developed a balanced vortex model based on Eliassen's (1951) forced secondary circulation model. A scale analysis similar to that performed in section 2.2 showed that if

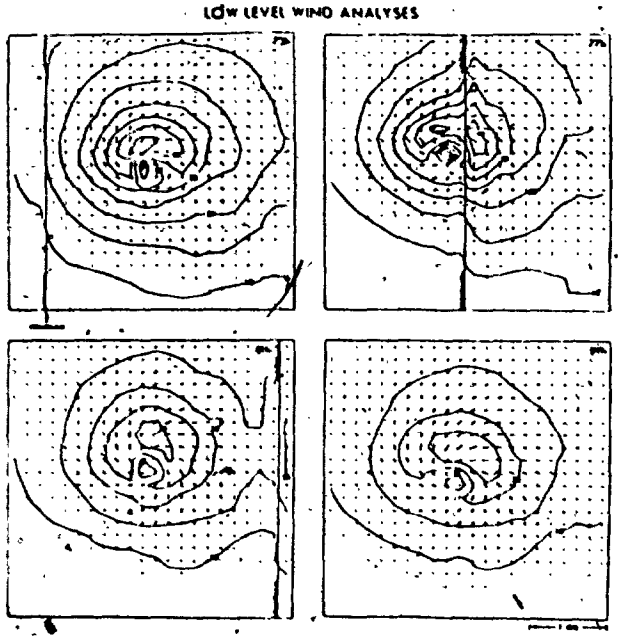

Low level (σ = 0.992) wind analyses for the basic landfall experiment, L298, for 73, 81 and 89 h. The center of the storm as defined by the surface pressure field is indicated by the hurricane or tropical storm symbol. Isotachs (m s^{-1}) and vectors indicate wind magnitude and direction, respectively. Land is to the west of the indicated coastline.

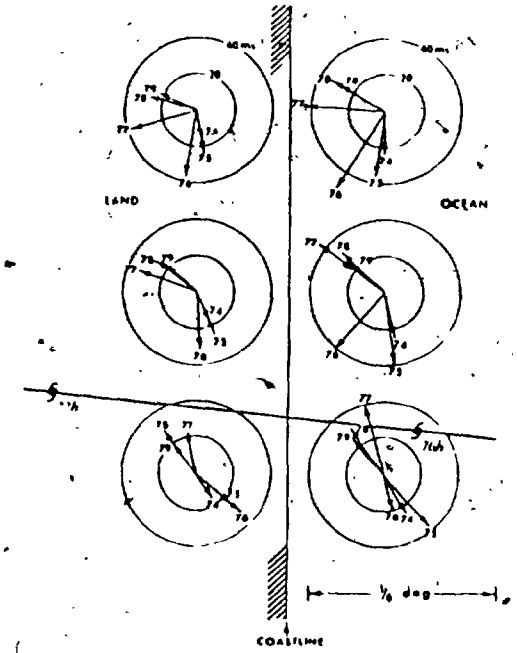

Hourly low level (σ = 0.992) wind vectors at six grid points near the point of storm landfall for experiment L298 for the period 74–79 h. Storm track and 76 h and 77 h storm positions are also indicated. Land is to the west of the indicated coastline.

FIGURE 2.12 Landfall Simulation with Tuleya-Bender-Kurihara 1984 Numerical Model

the asymmetric components of the tangential and radial motions were small compared to the symmetric parts, the tangential flow would be in hydrostatic and gradient balance. The model indicated a tangential wind speed maximum just inside of the radius of maximum winds leading to a contraction of the wind maximum as the vortex intensified. The model thus predicted storm intensification through both angular momentum convergence and contraction of the radius of maximum winds, consistent with the more and more commonly observed phenomenon of the replacement of a pre-existing inner eyewall by an outer concentric eyewall in recently occurring tropical cyclones.

The numerical model of Shapiro (1983) forms the basis of the inflow layer windfield model chosen for the current simulation. This model analyzes the effects of storm translation on the tropical cyclone boundary layer windfield. As in Chow (1971), the momentum equations are solved for a slab boundary layer of constant depth translating under a symmetric pressure distribution. The co-ordinate system translates with the storm. Using the same notation as section 2.2, the momentum equations solved are:

Radial E2-12a

$$u\frac{\partial u}{\partial r} - \frac{v^2}{r} - fv + \frac{v}{r}\frac{\partial u}{\partial \theta} + \frac{1}{\rho}\frac{\partial u}{\partial r} - K\left|\nabla^2 u - \frac{u}{r^2} + \frac{2}{r^2}\frac{\partial v}{\partial \theta}\right| + F_d(u,VT) = 0$$

Tangential E2-12b

$$u\left(\frac{\partial v}{\partial r} + \frac{v}{r}\right) + fu + \frac{v}{r}\frac{\partial v}{\partial \theta} - K\left|\nabla^2 v - \frac{v}{r^2} + \frac{2}{r^2}\frac{\partial u}{\partial \theta}\right| + F_d(v,VT) = 0$$

K = eddy diffusion
VT = translation speed of storm
$Fd((u,v),VT)$ = frictional drag induced by surface

The particular formulation of the advective and diffusive terms is due to Batchelor (1967). Whereas Myers and Malkin (1961) in their theoretical study of the same phenomenon used an empirically determined frictional drag term with almost equal tangential and normal components, Shapiro assumed

that the frictional drag term, Fd, acted parallel to the total wind $(V + VT)$ and had a quadratic form given by :

$$F_d(V,VT) = \frac{Cd}{H}(V+VT)\,|(V+VT)| \qquad E2-13$$

V = total wind speed relative to storm centre, $\sqrt{(u^2+v^2)}$
VT = storm translation speed
H = depth of the boundary layer

The drag coefficient, Cd, was assumed to be linear :

$$C_d = \left| a + b\,(V+VT) \right| x\,10^{-3} \qquad E2-14$$

$a = 1.1$ and $b = 0.04$, VT in m/sec.

Shapiro's model showed that the boundary layer windfield asymmetry produced by storm translation was not a simple local response to surface drag, but resulted from the asymmetrical distribution of friction drag induced by storm motion. Radial advection carrying momentum into the storm centre from the peripheries played an important role. This agrees with the results of the scale analysis performed in section 2.2. When the total wind was broken up into tangential and radial components it was found that the tangential component was sub-gradient outside the radius of maximum winds and slightly super-gradient at and just inside of the radius of maximum winds. Most importantly, a front to rear asymmetry was induced by the action of storm translation on the windfield even after the storm speed was subtracted from the total windfield. In general, for storms moving with average translation speeds, inflow and maximum winds were found to lie ahead of the storm circulation, in the left-front quadrant relative to the moving centre and in the right-front quadrant relative to the earth's surface. An example is shown in Figure 2.13.

A number of recent models (DeMaria and Schubert, 1984; Willoughby, Jin, Lord and Piotrowicz, 1984) have indicated similar features in the tropical

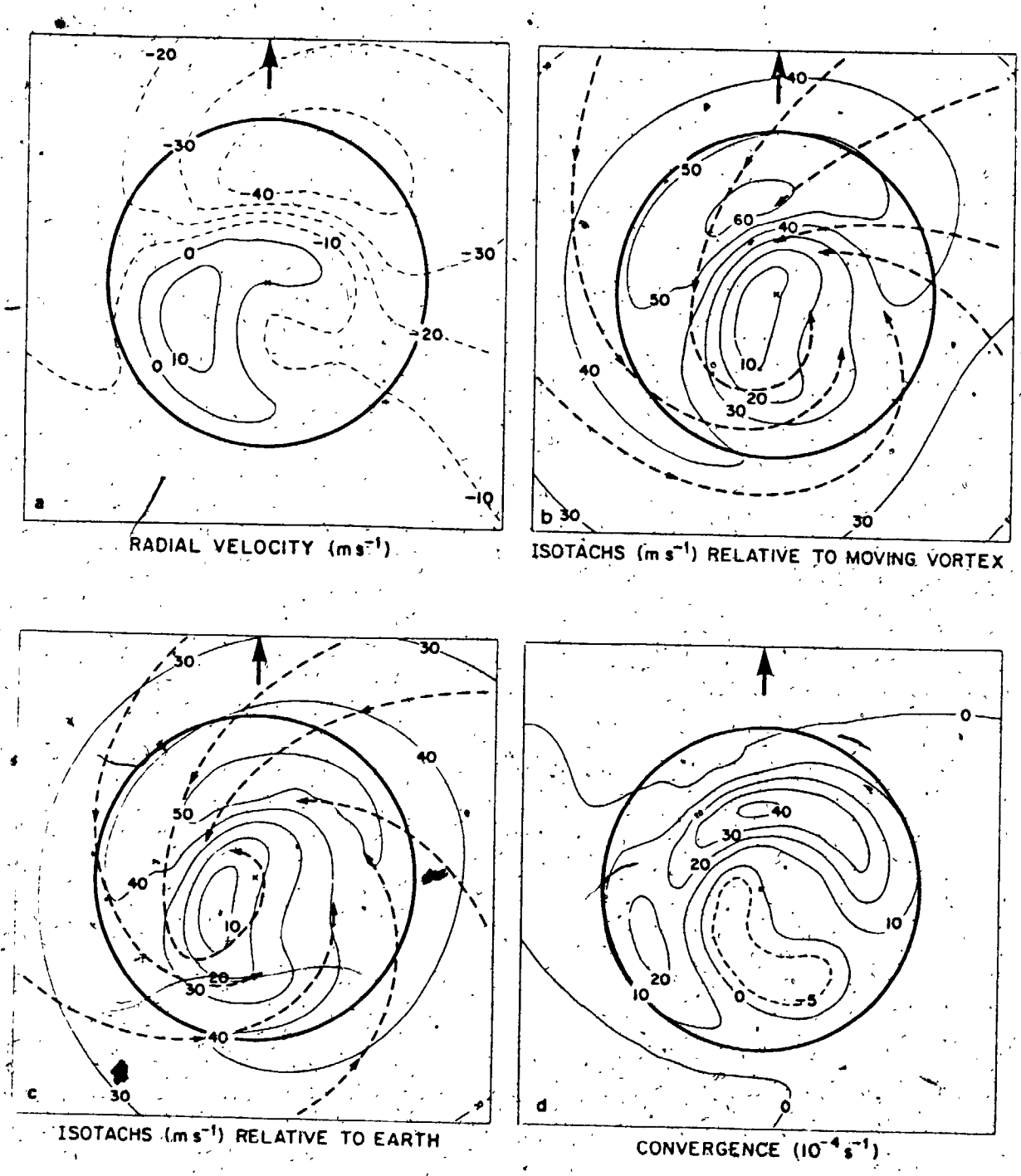

FIGURE 2.13 Shapiro (1983) Numerical Model Windfield for a Storm Moving with a Translation Speed of 10 m/sec

cyclone boundary layer of a moving storm, in particular the location of the maximum inflow and maximum wind speed contours. It will be shown in section 2.7 that these features are supported by recent observations of boundary layer asymmetries in moving tropical cyclones.

2.5 The Tropical Cyclone Boundary Layer and Surface Layer Similarity Theory

Analysis of the tropical cyclone boundary layer was held back initially by lack of data. Interest soon heightened with the necessity imposed by the needs of researchers developing numerical models and by the needs of those involved in the STORMFURY project. Early knowledge of the tropical cyclone boundary layer was based upon indirect methods of analysis. Surface fluxes were computed from bulk heat and momentum budgets (Riehl and Malkus, 1961; Miller, 1964; Hawkins and Rubsam, 1968; Hawkins and Imbembo, 1976). The accuracy of these methods typically relied upon a partially subjective analysis of usually incomplete aircraft data.

The first multi-level hurricane vertical profile data were obtained from Brookhaven National Laboratory (Singer, Nagle and Brown, 1961; Cohen and Spar, 1963), Tokyo Tower (Shiotani, 1975) and North West Cape Tower (Wilson, 1977). The Brookhaven and Tokyo Tower data conformed reasonably well to logarithmic profiles. These yielded values of surface roughness, Zo, ranging from 1.21 to 2.07 metres, and friction velocity, $u*$, ranging from 1.46 to 2.16 m/sec. They were however over-land profiles and only one case involved wind speeds in excess of 25 m/sec. The first over-water profile data were obtained from Hurricanes Caroline and Eloise (1975). Some doubts must be placed on the representativeness of the two profiles obtained from these storms. At the time the data were measured, Eloise's circulation was strongly affected by nearby islands and the Caroline profile was obtained some 100 km out from the storm centre.

Using these profiles, the Brookhaven and Tokyo tower measurements, N.O.A.A. data buoy observations and other data obtained from previous research studies, Bates (1977) constructed two normalized vertical wind

profiles for over-water and over-land conditions. These are shown in Figure 2.14. The wind speed was assumed to be constant between the 150 and 350 metre levels, the maximum wind was located at approximately the 1000 metre height and the ratio of surface to 150-350 metre wind speed was 0.72 and 0.40 for over-water and over-land conditions respectively. Comparison with the land data that had been used to develop the Kraft and Atkinson-Holliday relations, given in section 2.2, indicated that the Bates profiles underestimated surface speeds, probably as a result of the low wind speeds from which the profiles had been constructed. There was thus a suggestion that the greater the wind speed or alternatively the closer to the eyewall, the less the vertical wind shear in the boundary layer.

A number of other hurricane vertical wind profiles have since been obtained, the majority of which were gathered at the periphery of the respective storms. The data of Wilson (1977) are the only exception. A composite diagram of available over-water profiles compiled by Black and Adams (1983) is shown in Figure 2.15. The profiles have all been normalized with respect to the 500 metre height wind speed. All wind profiles have maxima at heights between 700 and 1500 metres above sea-level. Secondary low-level wind maxima are indicated in two of the profiles at the 150 and 60 metre levels for the Hurricane Eloise (1975) data and Wilson's (1977) composite profile respectively.

Moss and Rosenthal (1975) applied Deardorff's (1972) planetary boundary layer parameterization scheme to compute surface exchange coefficients for Hurricanes Daisy (1958) and Inez (1966). Drag coefficients computed using this similarity-based approach compared favourably with those determined from bulk studies (Riehl and Malkus, 1961; Hawkins and Imbembo, 1976). Moss (1978) used the 1975 Hurricane Eloise and Caroline data to confirm the success of similarity theory-predicted surface fluxes. The momentum flux profile obtained from the Hurricane Eloise data indicated a surface stress within 3% of that estimated using the Deardorff scheme, and showed that the height where the stress vanished was at approximately the 500 metre level. Deardorff's (1972) parameterization defined the top of the planetary boundary layer as the height above which shear-generated turbulence becomes negligible. Moss and Rosenthal (1975) and Moss (1978) showed that this

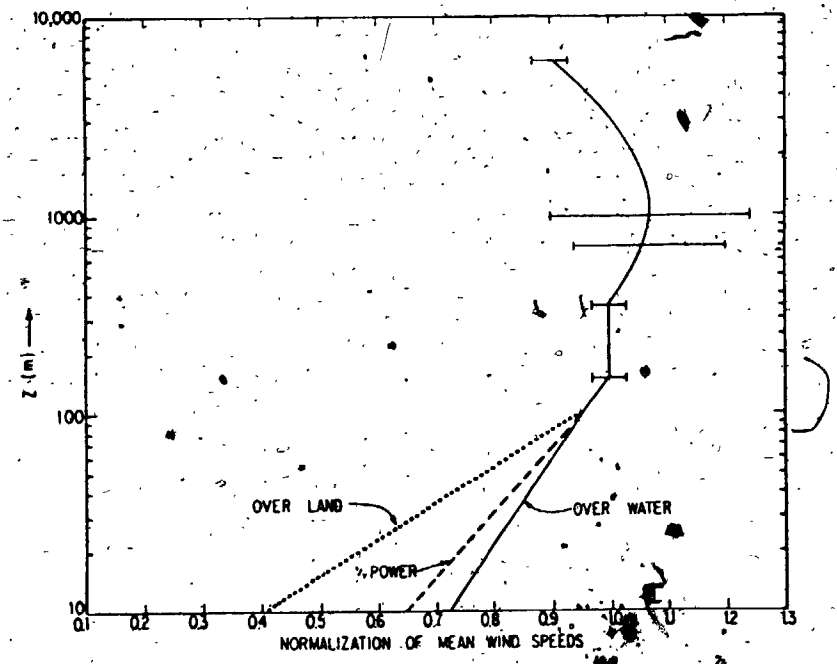

FIGURE 2.14 Normalized Profile of Variation of Mean Wind Speed with Height in Tropical Cyclones (Bates, 1977)

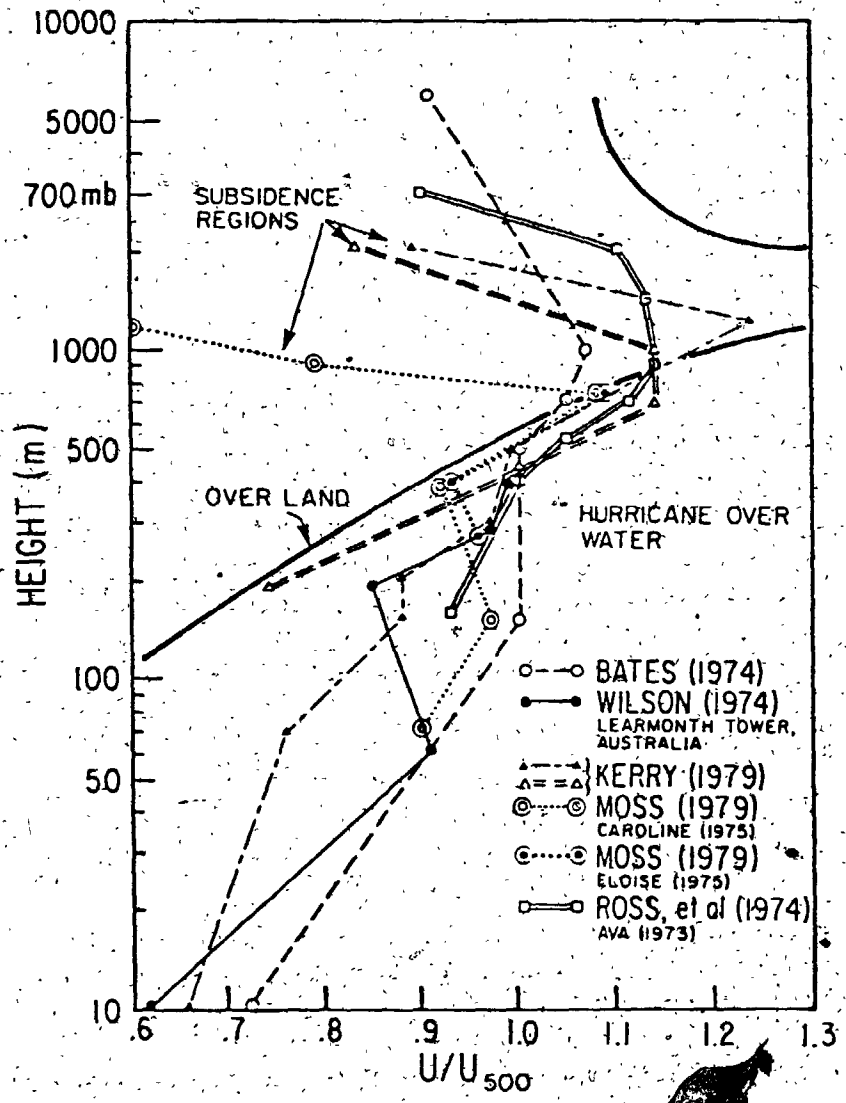

FIGURE 2.15 Combined Over-Water Boundary Layer Profiles (Black and Adams, 1983)

height coincided in the case of tropical cyclones with the lifting condensation level in cloud-rain areas and the lowest inversion height for clear areas. Figure 2.16 shows the depth of the boundary layer computed for Hurricanes Daisy and Inez using this definition. It can be seen that the depth increases with increasing distance away from the storm centre.

In surface layer similarity theory the non-dimensional vertical gradient of wind speed is a universal function of the stability parameter, z/L (z = height above the ground, L = Monin-Obukhov length). The non-dimensional gradient can then be integrated with respect to height to obtain a vertical wind profile, $u(z)$, which has a logarithmic form :

$$u(z) = \frac{u_*}{k}\left[ln\left(\frac{z}{z_o}\right) + \Psi_m\right] \qquad E2-15$$

k = 0.4, the von Karman constant

Ψ_m = stability function, a function of (z/L)

A number of different models were developed to apply similarity theory to tropical cyclones. They differed primarily in the way that the roughness length and the stability parameter were determined. The stability condition was typically specified using a bulk Richardson Number which required as input the height, wind speed and virtual potential temperature at the top of the boundary layer and the air-sea virtual potential temperature difference at the surface (assumed to be about the 10-20 metre level). It was thus possible to test similarity-based predictions by substituting flight-level data for the required boundary layer height data and N.O.A.A. data buoy measurements for the required surface temperature data. The same data buoys could then be used to compare predicted surface wind speeds etc. with measured ones. This was done by Powell (1979), using data obtained from aircraft, N.O.A.A. data buoys and ships during the passage of Hurricanes Eloise (1975), Caroline (1975) and Anita (1977). Four diagnostic boundary layer models were evaluated along with the Bates (1977) normalized boundary layer over-water profile and the so-called "0.8 rule". According to this rule, in the absence of alternative meteorological data, the ratio of surface (10 metre) to low-level

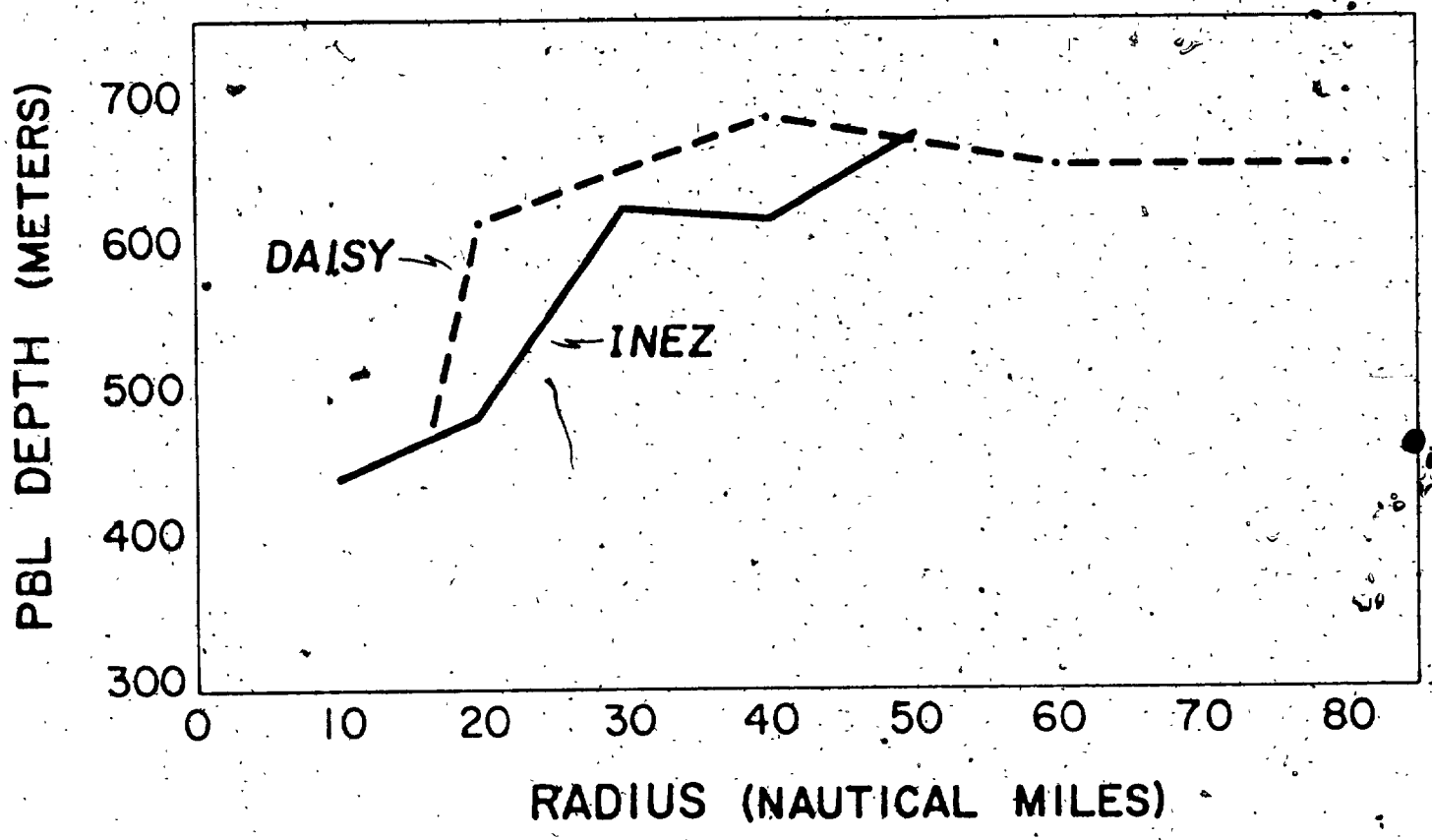

FIGURE 2.16 PBL Depth Versus Radial Distance from the Eye for Hurricanes Daisy (1958) and Inez (1966) (Moss and Rosenthal, 1977)

(500 metre) flight winds is assumed to equal 0.8. The results of the comparisons are shown in Figure 2.17. Three of the similarity models (Cardone, 1969; Moss-Rosenthal, 1977; Powell, 1978) and the 0.8 rule were shown to estimate 10 metre height wind speeds to within 10% accuracy. The fourth similarity model and the Bates profile appeared to consistently underestimate the surface speeds.

A modified form of Powell's (1978) surface similarity boundary layer model is currently being used at the National Hurricane Center as the standard method for converting aircraft winds to surface winds. Comparisons of predicted surface winds with measured ones in recent hurricanes have confirmed the reliability of the method and the suitability of the logarithmic profile for over-water profiles in tropical cyclones, particularly in the lowest several hundred metres.

Drag coefficients, values of friction velocity and roughness lengths obtained in Powell's study are shown in Figures 2.18 to 2.20. Values of u_* ranged from 0.1 m/sec in the centre of the eye to 2.5 m/sec in the region of maximum winds. These values are similar to data obtained from the Brookhaven and Tokyo Tower land profiles. In the same regions, values of Zo ranged from less than 1 millimetre to just over 25 millimetres respectively. These are at least one order of magnitude less than roughness lengths obtained from the land tower data cited above.

Large negative values of the Monin-Obukhov length were present in almost all of Powell's comparisons except for a single small positive value determined inside the eye of Hurricane Anita on September 2, 1977. Over a large portion of the tropical cyclone windfield, the boundary layer stability is thus predominantly neutral to slightly unstable and may account for the success of the simple "0.8 rule" in predicting surface speeds from low-level aircraft winds. Uniform surface to upper-level wind speed ratios have been found in other studies. Composited data examined by Frank (1977) and Frank and Gray (1977) showed averaged ratios of surface wind to the 900 mb and 850 mb wind of 0.8 and 0.75 respectively. Black and Adams (1983) suggested that surface winds should average 70-80% of the 700 mb or 1500 foot flight-level

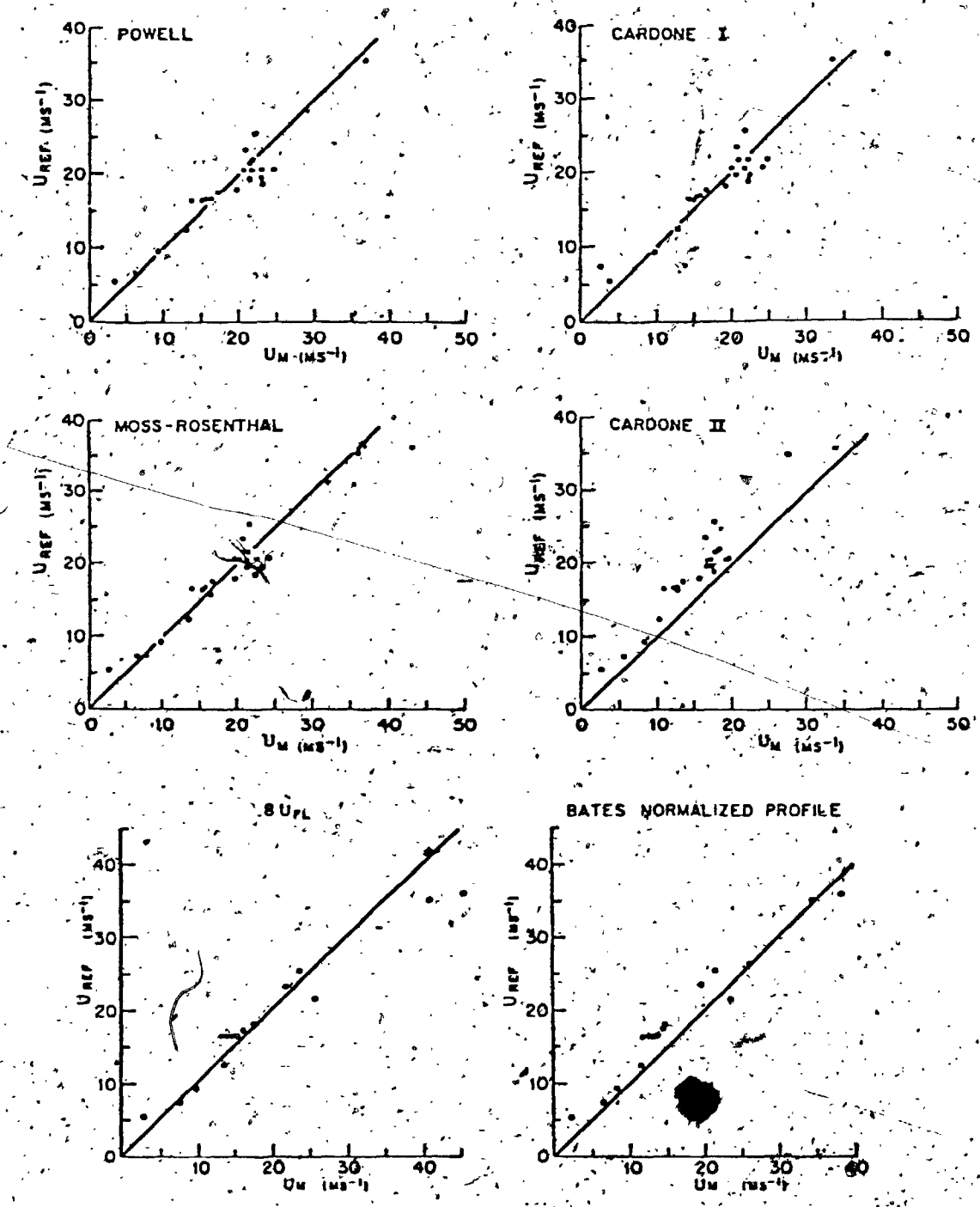

FIGURE 2.17 Comparison of Similarity Theory-Predicted Speeds (Um) with Measured Speeds (Uref) (Powell, 1977)

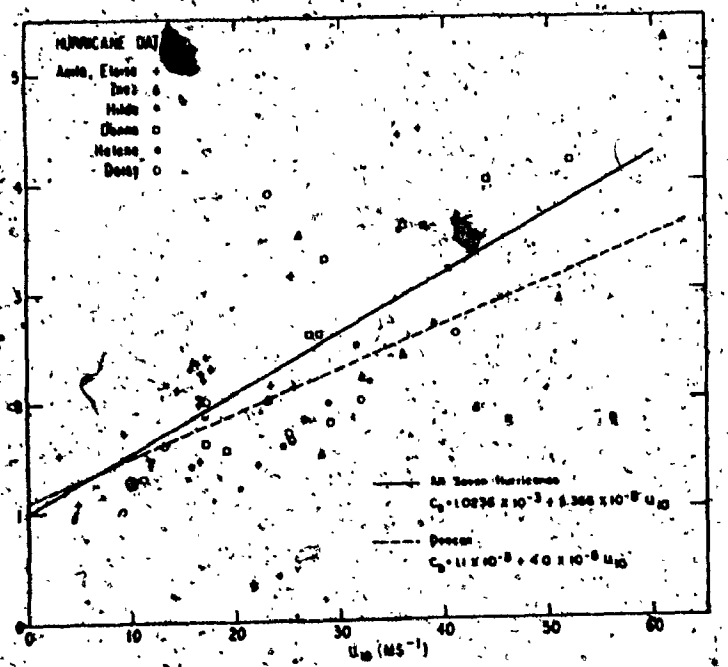

FIGURE 2.18 10 Metre Height Neutral Drag Coefficient from : Several Studies (Powell, 1977)

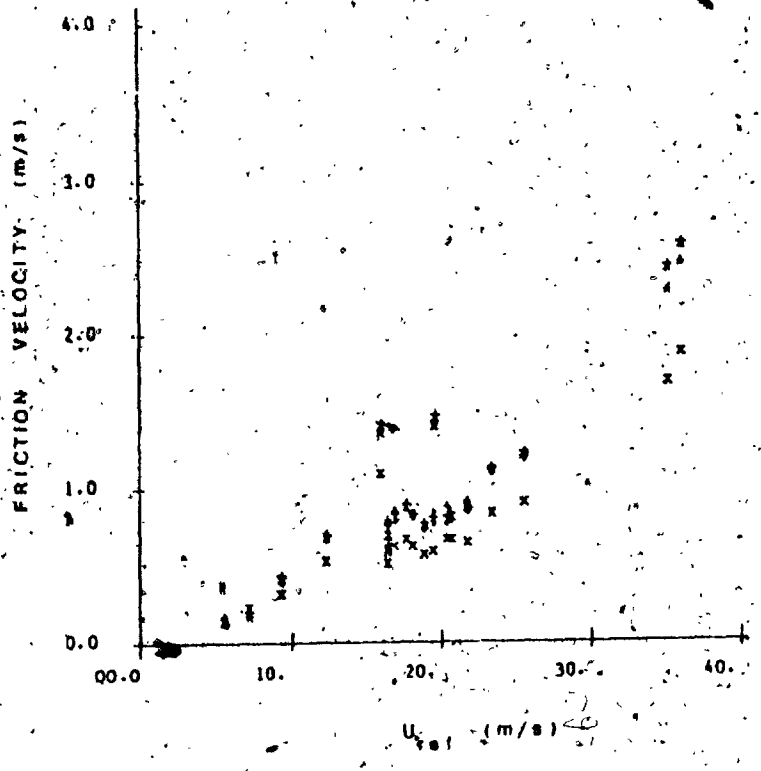

FIGURE 2.19 Computed Values of Friction Velocity Versus Measured Surface Speed (Powell, 1977)

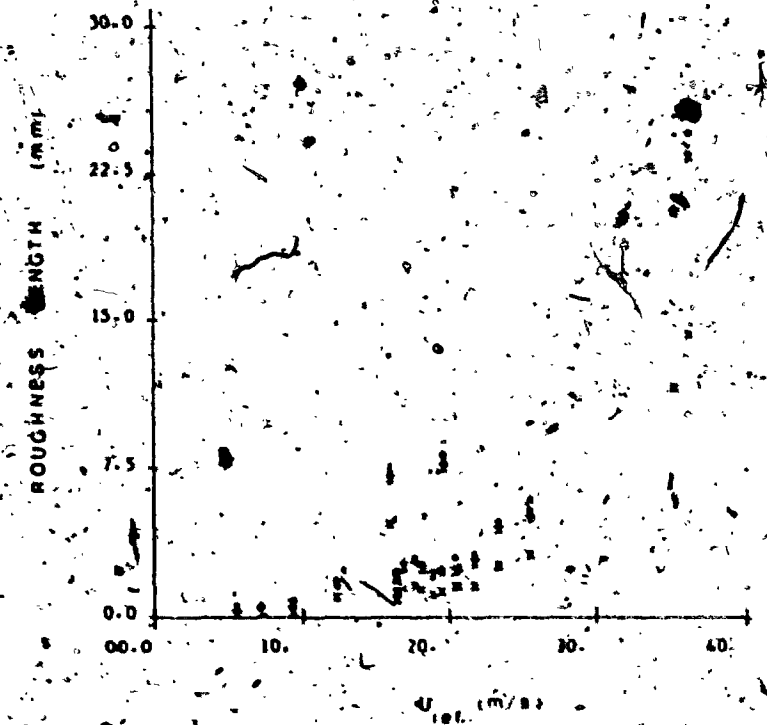

FIGURE 2.20 Computed Values of Roughness Length Versus Measured Surface Speed (Powell, 1977)

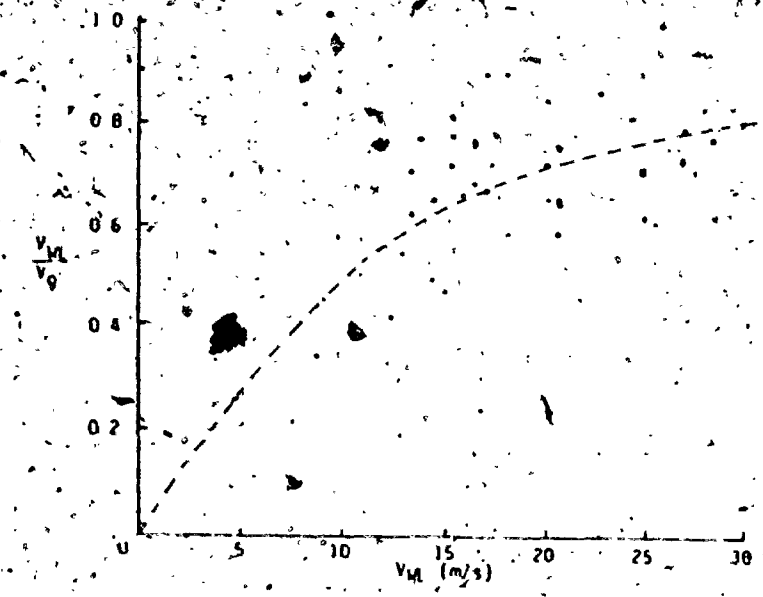

FIGURE 2.21 Ratio of Waglan Island Anemometer to Upper Level Typhoon Wind Speeds (Choi, 1983)

wind. Using data obtained in recent hurricanes, Powell (1984) suggests a value of 0.75 for the average ratio of surface to 500 metre height wind speed.

Two locations where different ratios have been found are the eyewall (higher ratios) and the right-rear quadrant of the storm (lower ratios). Choi (1983) compared typhoon winds measured at the Waglan Island anemometer station (elevation 75 metres) with upper-level measurements made at the nearby King's Park station. Figure 2.21 taken from this study shows the ratio of Waglan speeds to upper-level speeds in the range 0.6 to 1.0 for wind speeds higher than 15 m/sec. The ratio monotonically increases with wind speed. On the assumption that the higher wind speeds were measured at distances closer in to the respective storm centres, this data agrees extremely well with the previous ratios discussed, and accounts for the observed tendency to underestimate wind speeds using the Bates (1977) profile.

Lower ratios occur in the right-rear quadrant of tropical cyclones as a result of the upwelling of colder water to the surface after the passage of the storm. This phenomenon, illustrated in Figure 2.22, has been documented by Black (1983). Higher winds on the right-hand side of the storm produce the observed "cold wake" behind a moving storm, with the result that the normal air-sea temperature difference may actually reverse sign, producing positive bulk Richardson numbers, and hence a stable boundary layer. Under these conditions the ratio of surface to upper-level winds may drop below the 0.6 level.

2.6 Behaviour of Landfalling Tropical Cyclones

Tropical cyclones weaken substantially once they make landfall and move inland. Miller's (1963) study of the landfall of Hurricane Donna (1960) showed that the removal of the underlying oceanic heat source and not the increase in surface friction produced this "filling". Over land, inflow trajectories assume paths that are nearly moist adiabatic, weaken the radial temperature gradient, and cause warm air in the cyclonic core to spread out. The resulting decrease in azimuthal pressure gradients inhibits the production of kinetic energy, even though the storm mass flow remains

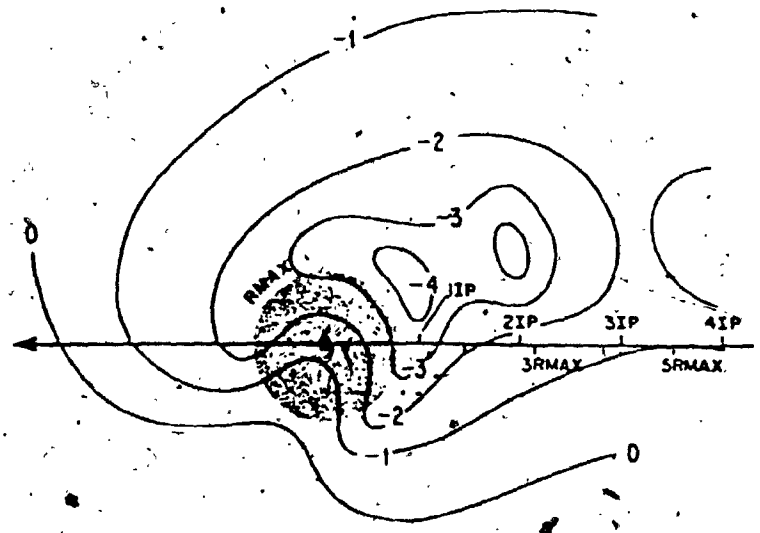

SST CHANGE - SLOW MOVING STORM, LARGE RMAX

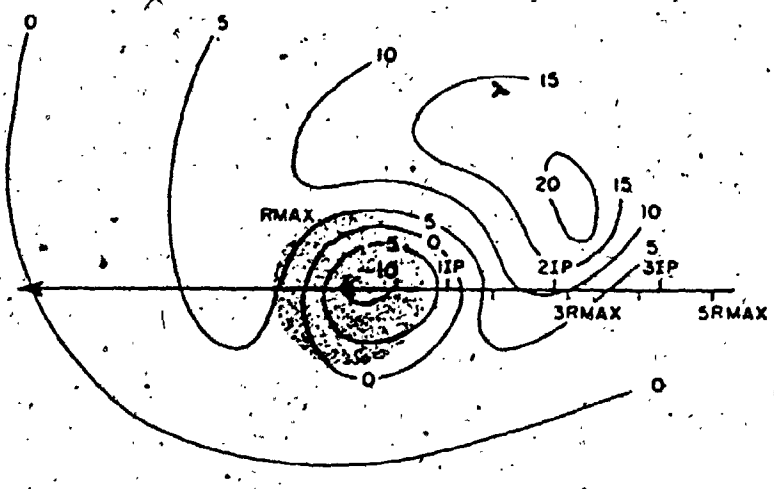

MLD CHANGE - SLOW MOVING STORM, LARGE RMAX

FIGURE 2.22 Sea-Surface Temperature (°C) and Mixed Layer Depth (m) Changes for a Large, Slow Moving Storm. Shaded Area Indicates Region Inside RMAX (Black, 1983)

constant for at least several hours after landfall. These actions, in particular the rise in central pressure, weaken the whole storm circulation.

In addition to this overall weakening, an immediate decrease is observed in surface speeds for over-land wind trajectories even before the eye has made landfall. This is brought about by the change in surface roughness over land which may increase by up to two or more magnitudes. These two processes, the storm weakening due to pressure gradient degradation and the frictionally-induced decrease in surface speeds, take place more or less independently during the first few hours after landfall is made. Thus upper-level winds are substantially affected initially by the change in central pressure only, and not by the reduction in surface winds. Because of this, it is possible to view the changes to the windfield of a landfalling storm as a reduction at all levels due to the rise in central pressure and a separate decrease in the speeds at the surface. The intermediate boundary layer then adjusts to the speeds at the upper and lower ends.

Figure 2.23 shows the rise in central pressure and accompanying drop in maximum wind experienced after Hurricane Alicia made landfall near Galveston, Texas, in August 1983. The close relationship between the two variables indicates the suitability of accounting for the effects of filling through the reduction of the central pressure difference of the storm. Malkin (1959) analyzed central pressure time traces of 13 landfalling hurricanes and determined an average filling curve, suggesting that the filling rate was dependent on the ratio of land to water in the underlying surface. Schwerdt, Ho and Watkins (1979) examined 16 landfalling tropical cyclones and subdivided the storms into three categories A, B and C, corresponding to their landfall locations along the Gulf Coast, Florida Peninsula and Atlantic Coast respectively. Figure 2.24 shows that these sub-groups did exhibit distinct filling rates. Category B storms, with more of their circulation over water while landfall was taking place, had the slowest rates. Category A storms filled the fastest.

Myers (1954) investigated the ratio of surface to upper-level winds using a considerable data base of surface wind and pressure records obtained from anemometer stations located within and surrounding Lake Okeechobee,

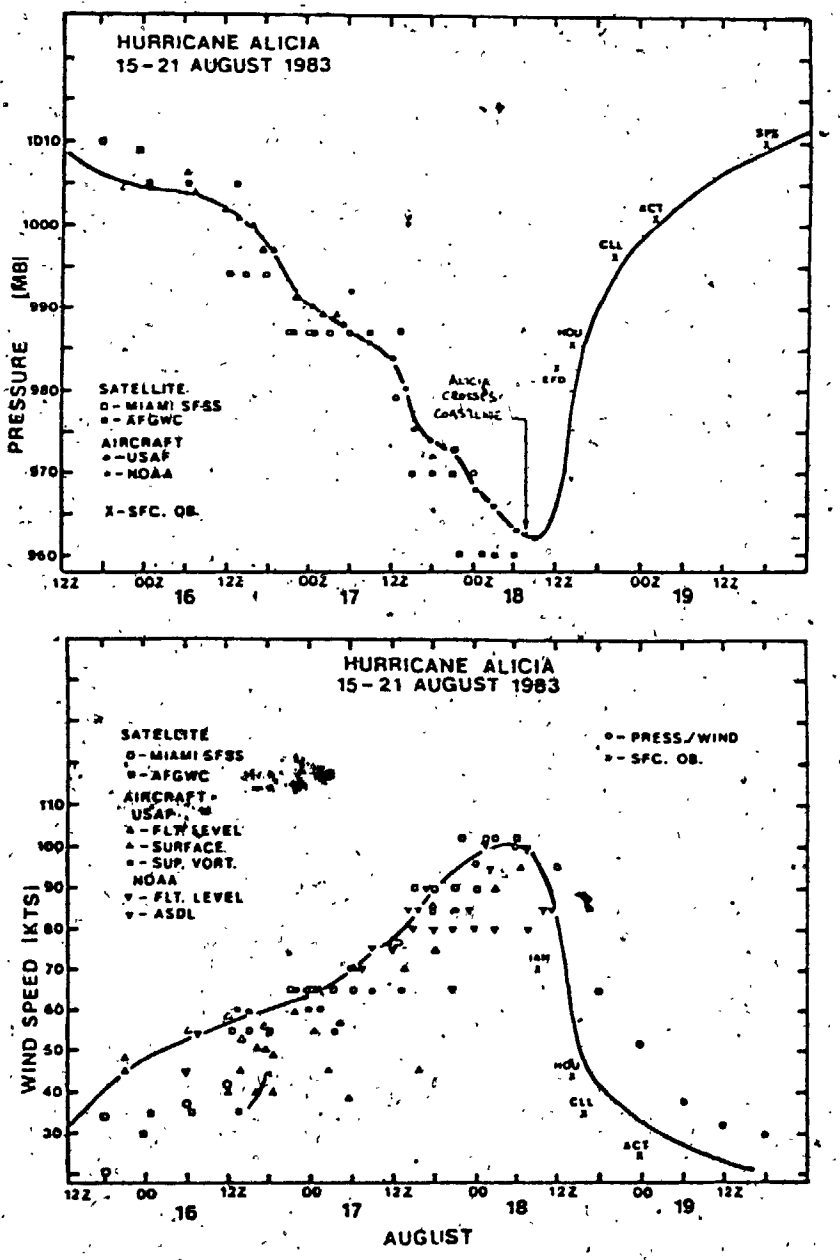

FIGURE 2.23 Central Pressure and Maximum Wind Speed History for Hurricane Alicia, August 15-20 1983

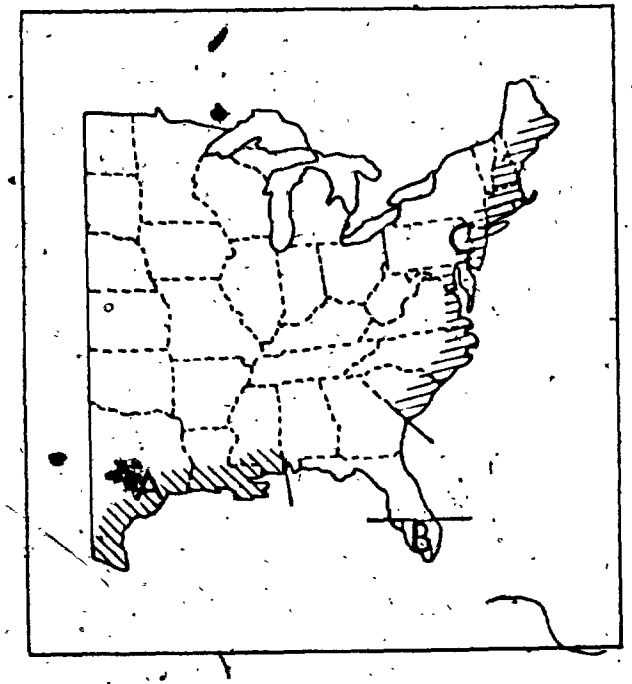

$$\sqrt{\frac{\Delta p\,(t)}{\Delta p\,(t=0)}}$$

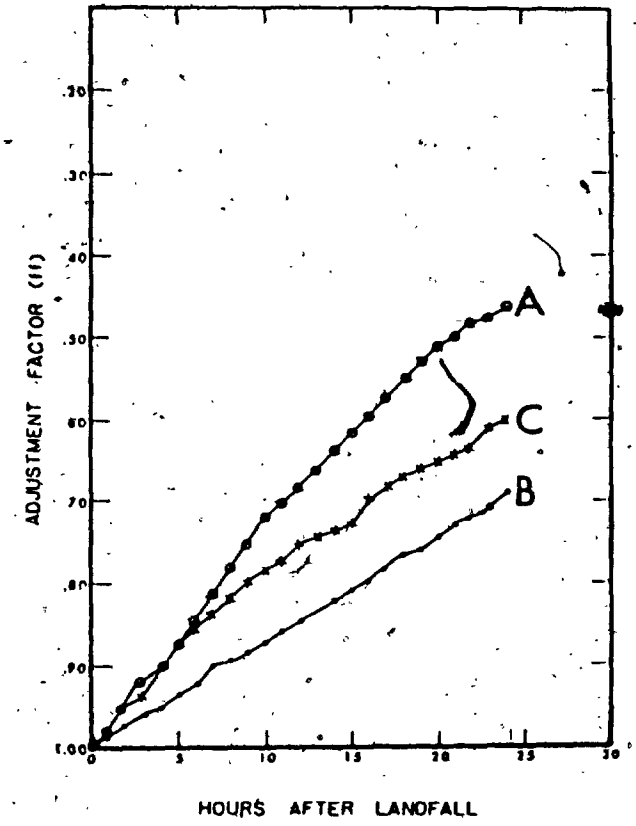

FIGURE 2.24 Filling Factors Obtained by Schwerdt, Ho and Watkins (1979)

Florida. Wind speed profiles measured for over-water, off-water (water to land) and off-land (land to water) conditions were compared to the theoretically calculated gradient and cyclostrophic winds computed from the pressure field. This and other data were combined to determine a standard reduction curve for the ratio of the 10-minute average over-water surface wind to the gradient wind speed. This is shown in Figure 2.25. Reduction factors were calculated for land stations for both off-water and off-land wind flow. These are depicted in Figure 2.26 and show off-water ratios independent of wind speed and equal to 0.89. Off-land ratios showed a strong dependence on wind speed. These surface reduction factors became widely adopted and indeed have remained so to the present time (Graham and Nunn, 1959; Graham and Hudson, 1960; Schwerdt, Ho and Watkins, 1979). Recently some doubts have been raised regarding the influence of topography on the original anemometer data, which were obtained at the top of levees on the shoreline of the lake.

Abrupt changes take place within the boundary layer of a landfalling tropical cyclone. In addition to sustaining a sudden reduction in speeds at the surface, winds in the boundary layer are influenced by the physical effect of the land mass on the low-level storm inflow. The pressure contours in front of a storm approaching land become somewhat compressed and produce a convergence typically in the right-front quadrant of the storm. In this location precipitation is usually extremely heavy and tornadogenesis is highly likely.

Figure 2.27 taken from Novlan and Gray (1973) shows the preferred location of tornado formation for landfalling storms relative to the storm centre and the distribution characteristics of the distance inland of tornado-spawning storms. Almost all tornadoes form in the right-front quadrant of the storm. Figure 2.28, compiled by Black and Adams (1883), shows a number of boundary layer profiles obtained from land stations, either through rawinsonde measurements (Novlan, 1971), or from tower data (Shiotani, 1975; Bates, 1977; Sethuraman, 1978). Very much larger shears both above and below the 500 metre level are evident compared to the over-water profiles shown in Figure 2.15. The surface layer appears to become decoupled from the upper parts of the boundary layer. Sustained winds over land are

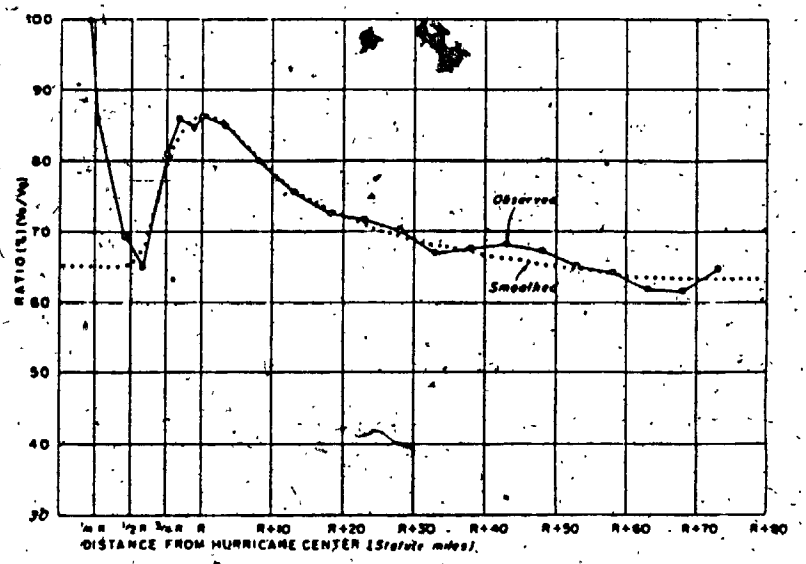

FIGURE 2.25 Ratio of 10-Minute Average Over-Water to Gradient Wind Speed (Myers, 1954)

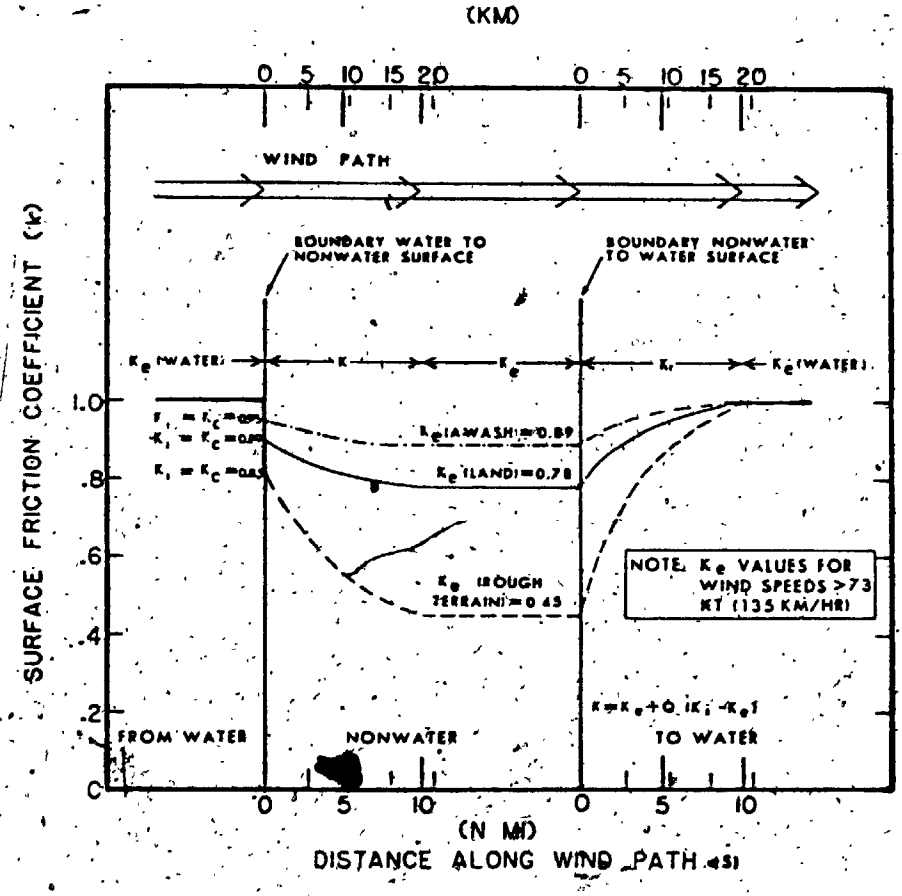

FIGURE 2.26 Ratio of Over-Land to Over-Water 10 Metre Wind Speed (Schwerdt, Ho and Watkins, 1979)

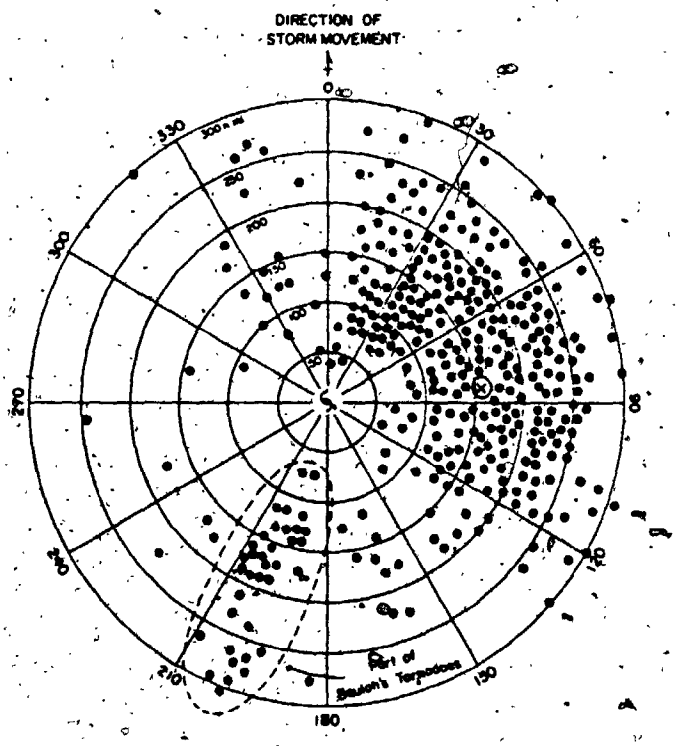

FIGURE 2.27 Plan View of 373 U.S. Tornadoes Associated with Hurricanes (1948-72) with Respect to the Direction of Storm Motion. The Symbol · is the Centroid of all Tornadoes (Novlan and Gray, 1974)

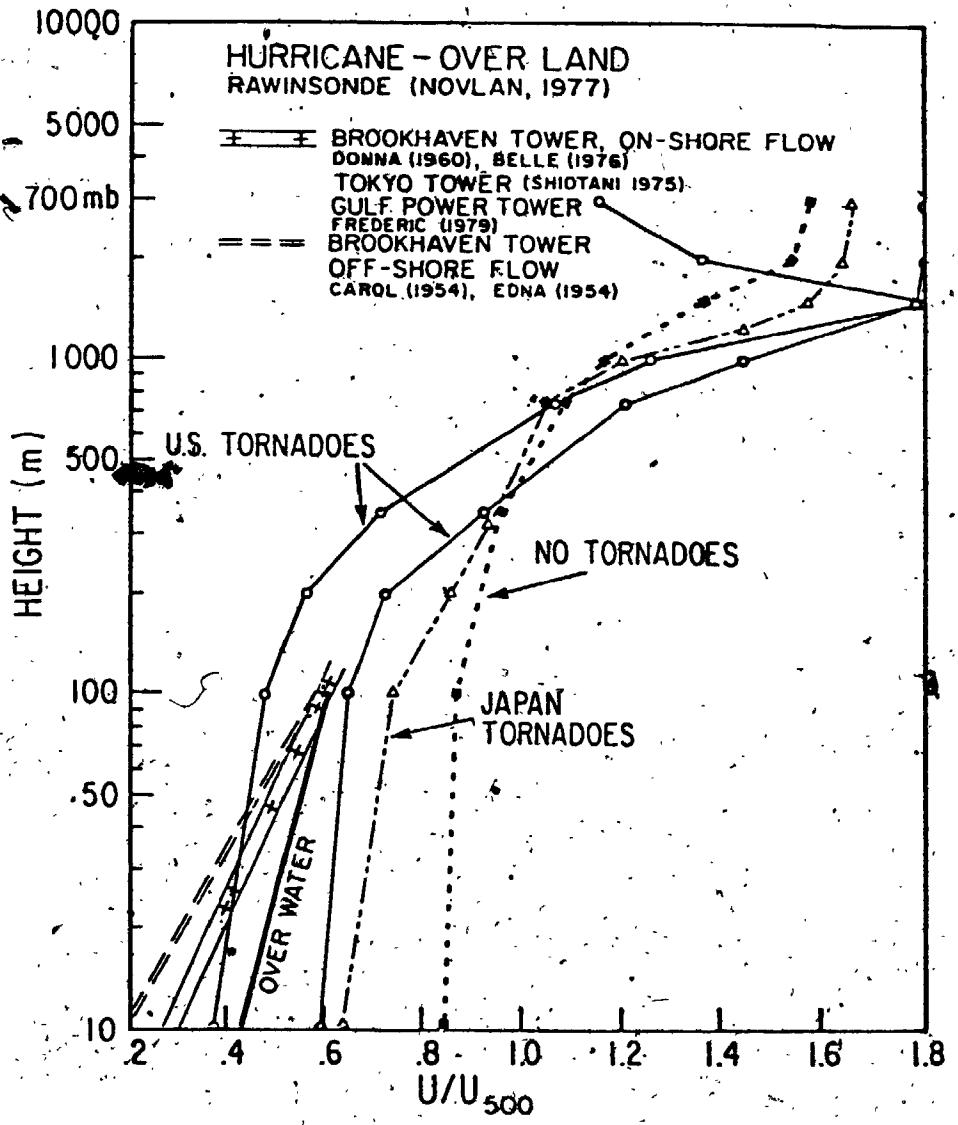

FIGURE 2.28 Combined Over-Land Boundary Layer Profiles (Black and Adams, 1983)

considerably weaker than over the sea for the same normalized 500 metre height wind speed. Wind maxima for the land profiles appear to be at around the 700 mb height, somewhat higher than the wind maxima indicated in the over-water profiles. More importantly, the over-land profiles show a continuing correlation between surface winds and 500 metre height winds, whereas the relationship to 700 mb winds becomes quite variable. Although the profiles are few in number they do suggest that vertical wind shear in the boundary layer is less near the eyewall than at the storm's periphery.

2.7 Selected Recent Studies

The primary reason for separating the studies now discussed is their resolution of several problems which plagued earlier studies. In the late 1970's reconnaissance aircraft which flew into hurricanes were equipped with quantitative plan position indicators and range height indicators coupled with inertial navigation systems, thereby clearing up many of the instrument problems affecting measured flight-level winds in early years. Recent studies examining surface wind records have attempted to properly account not only for the averaging times of wind speeds but for the effects of the local terrain and topography on the measurements. Recent studies have also sought to resolve the difficulties in comparing anemometer data, representing a fixed point sample in a tangential sense relative to the storm centre, and flight-level data, representing a moving sample typically in a radial direction relative to the storm centre and dependent upon the particular aircraft's own speed. Aircraft data are best suited to estimating flight-level winds with 10 to 30-second averaging periods. For an average storm translation speed of 5 m/sec, this would correspond to a sustained (1-minute average) speed measured at the surface for wind speeds ranging from 20 to 50 m/sec (Black and Adams, 1983). The studies selected in this section all pertain to hurricanes occurring since Anita (1977). They have been chosen because they shed light on one or other of the major points of interest in this thesis, including the applicability of the gradient balance assumption, the extent of the inflow layer and its relationship to the tropical cyclone boundary layer and changes to the windfield once landfall is made.

Willoughby (1979) and Sheets (1981) examined Hurricane Anita's (1977) windfield at the 700 mb (3 km) height. At the time when Anita was in a mature, steady-state, Willoughby found that (a) the most intense ascent occurred just inside the radius of maximum winds and (b) the azimuthally-averaged tangential windfield was in gradient balance, as can be seen in Figure 2.29. Sheets found the same for the period when Anita was a well-organized, intense hurricane, but found the windfield to be outoof balance during Anita's formative and dissipative stages.

Willoughby, Clos and Shoreibah (1982) showed that the wind speeds computed using the gradient balance assumption coincided almost exactly with the observed speeds in the eyewall of Hurricane Allen on August 8, 1980. Figure 2.30 shows relative wind isotachs and streamlines for Hurricane Allen reconstructed by Jorgensen (1984). The eyewall was in both gradient and thermal balance. The eyewall was found to slope outwards with height and maximum vertical motion within the eye was located inside of the radius of maximum winds. In Hurricane Allen and Hurricanes Anita (1977), Frederic and David (1979), Jorgensen found strong two-dimensionality (in the radial direction) in the circulation, i.e. consistent windfield features in azimuthally-averaged windfield cross-sections.

Frank (1984) studied flight-level data obtained while Hurricane Frederic (1979) was over the Gulf of Mexico. Figure 2.31 shows Frederic's windfield at the 560 metre level. The wind maximum is in the right-front quadrant of the storm. When the storm's motion is subtracted, the windfield is nearly symmetrical in a left-right sense but exhibits a front-back asymmetry, with the winds ahead of the storm exceeding those in the rear. Frank found that the total wind speeds were, on average 1 m/sec greater than the tangential winds out to approximately 150 km from the storm centre. Also, wind speeds at the 1600 metre level were slightly stronger than at the 500 metre level at all radii. The relative radial windfield, also shown in Figure 2.31, indicated greatest inflow in the right-front quadrant. Frank found the asymmetries in the radial windfield comparable at the surface, 560 metre and 1600 metre levels. Analysis showed that the inflow layer became deeper with increasing distance away from the eyewall. In the vicinity of the eyewall, the depth of the inflow layer was approximately 500 to 600 metres, coincident with the top

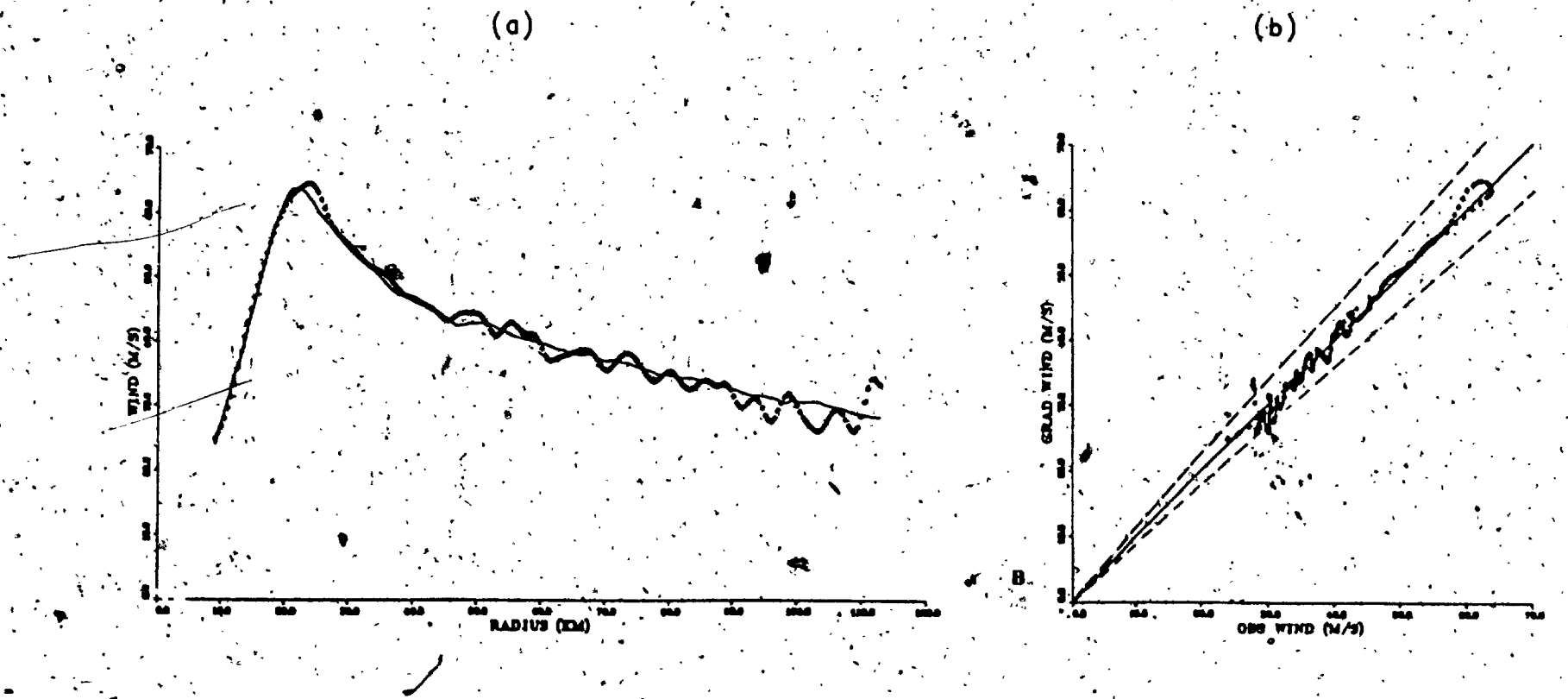

FIGURE 2.29 Comparison of Observed Tangential Wind with Gradient Balance Wind Speed for Hurricane Anita (1977), (a) Solid Curve is Observed Wind, Crosses the Gradient Balance Wind and (b) Scatter Diagram for Same Quantities (Willoughby, 1979)

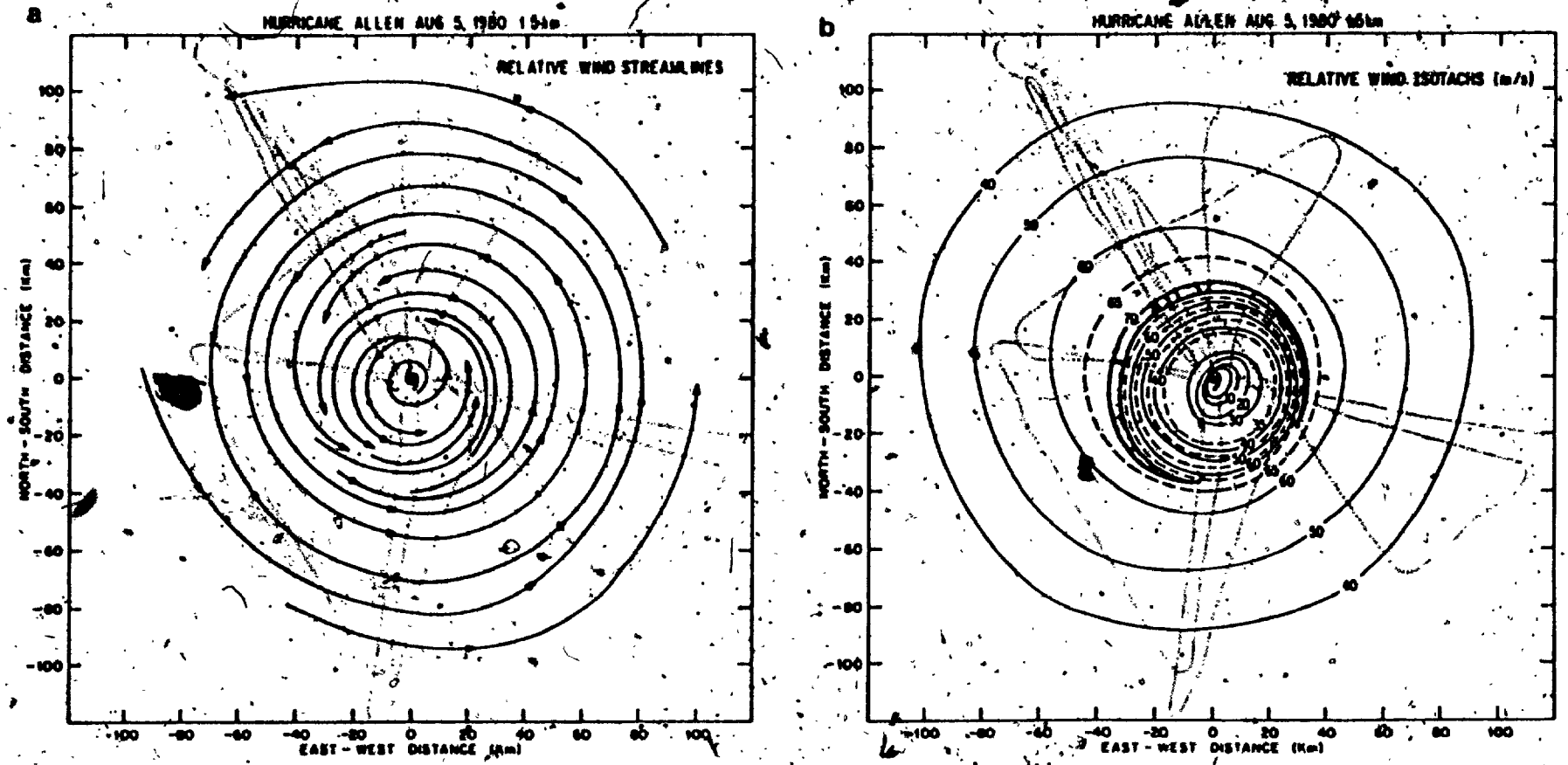

FIGURE 2.30 Low-Level (a) Streamline and (b) Isotach Analysis for Hurricane Allen on August 5 1980. Dotted Lines Show Flight Legs Relative to Storm Centre

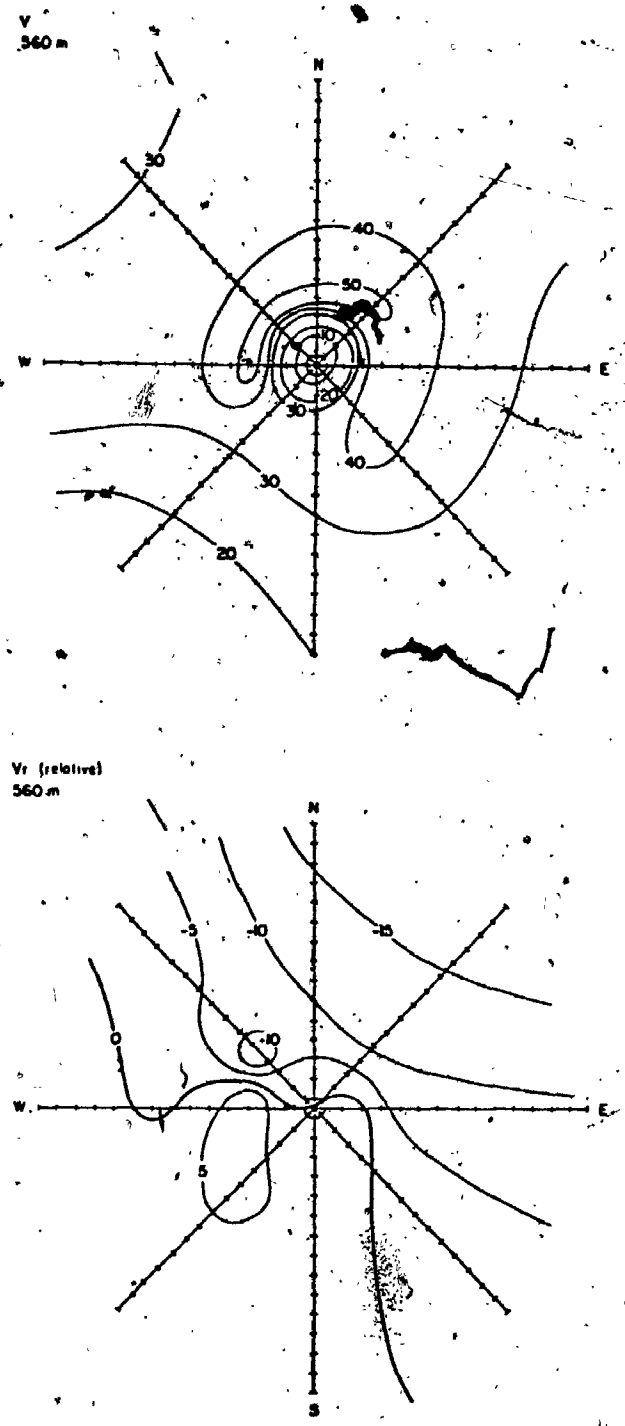

FIGURE 2.31 (a) Total Wind Speeds in Stationary Co-ordinates and (b) Radial Wind Speeds Relative to Storm Centre, at the 560 Metre Level for Hurricane Frederic, September 12 1979. (Radial Marks are at 10 km Intervals)

of the strongly turbulent friction layer. The Frederic data was shown to support the concept of a balanced, frictionally-driven inflow layer.

Similar features were reported in the analysis of Hurricanes David (1979) and Gert (1981) by Willoughby, Marks and Feinberg (1984). Figure 2.32 shows horizontal cross-sections of wind speed and inflow angle for these two storms at the 850 mb level. The tendency for the wind maximum to occur in the front and to the right of the storm is shown in both cases.

The landfall behaviour of Hurricanes Frederic (1979) and Alicia (1983) was the subject of two intensive studies by Powell (1982) and Powell, Marks and Black (1984) respectively. In both cases several distinctive features were present. Figure 2.33 shows the surface windfields for the storms at the time of landfall. A sharp discontinuity in isotachs and an immediate reduction in wind speed magnitude at the coastline is evident. In Frederic the mean over-land to over-water ratio was 0.8 to the right and left of the landfall position, i.e. for both off-water and off-land trajectories. Maximum inflow angles were found to move from the right-rear quadrant to the right-front quadrant at landfall, while the wind maximum remained in the right-front quadrant. In comparing flight-level winds with surface data at the time of Frederic's landfall, Powell found that while surface winds showed an immediate decrease over land, the winds at 500 metres did not differ appreciably. The vertical wind shear was found to be much greater over land than over water, even at 8 hours after landfall had been made. The same features were observed to take place in Alicia. For both storms average values were computed for (a) the ratio of over-water surface to flight-level winds, (b) the ratio of surface over-land to over-water winds and (c) over-land gust factors based on the ratio of 2 to 3-second gust to 10-minute mean surface winds. These were found to be (a) 0.71 and 0.77, (b) 0.81 and 0.74 and (c) 1.4 and 1.6, for Hurricanes Frederic and Alicia respectively.

Hurricane Debby (1982) was the first storm where vertical profiles were obtained using the new airborne-Doppler radar (Powell and Black, 1984). In Debby and Hurricane Tico (1983), observations indicated that the boundary layer on the inside of rainbands was more mixed and deeper than on the outside. Profiles measured in Debby showed the height of the wind maximum

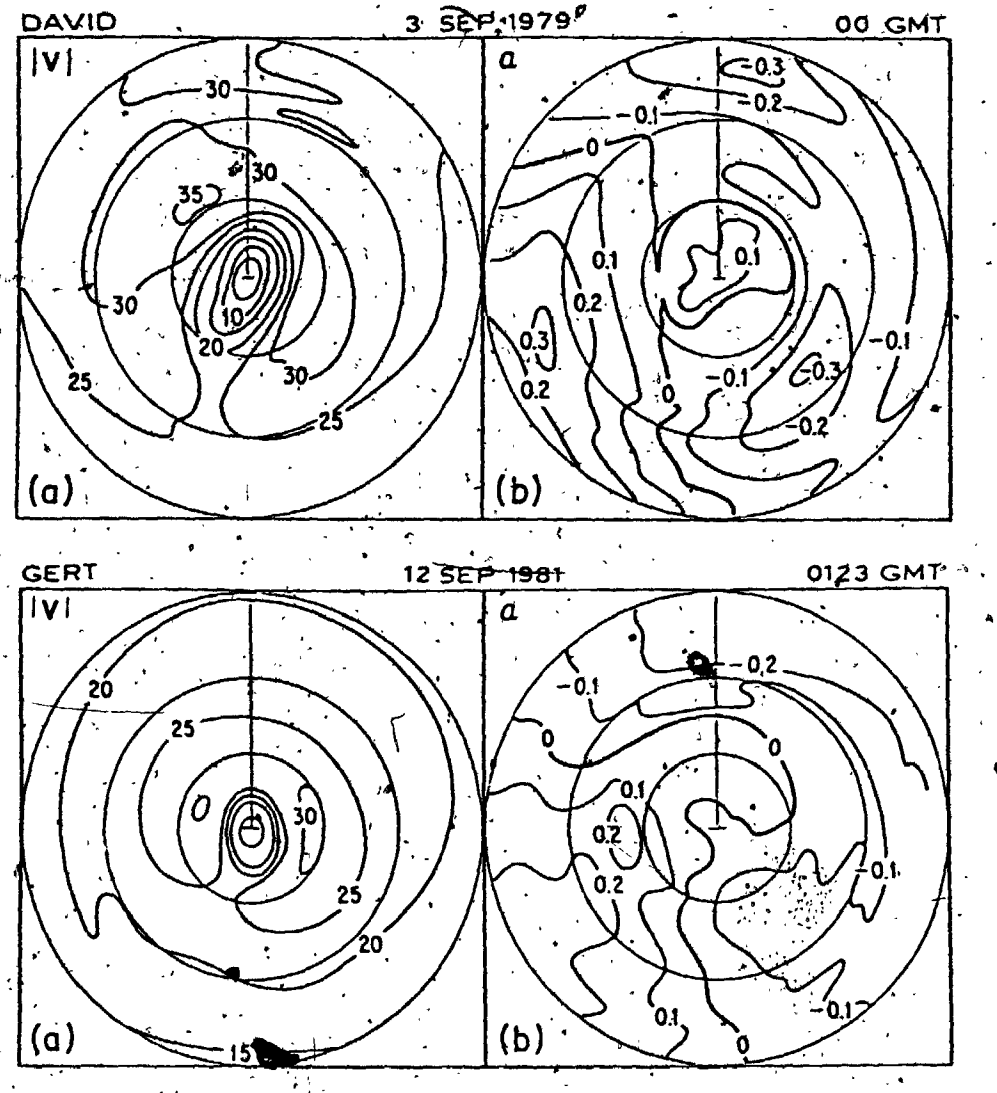

FIGURE 2.32 850 mb Level Total Wind Speed, V, and Inflow Angle, α, for Hurricanes David (September 3 1979) and Gert (September 12 1981). (Storm Motion is Indicated by Arrows)

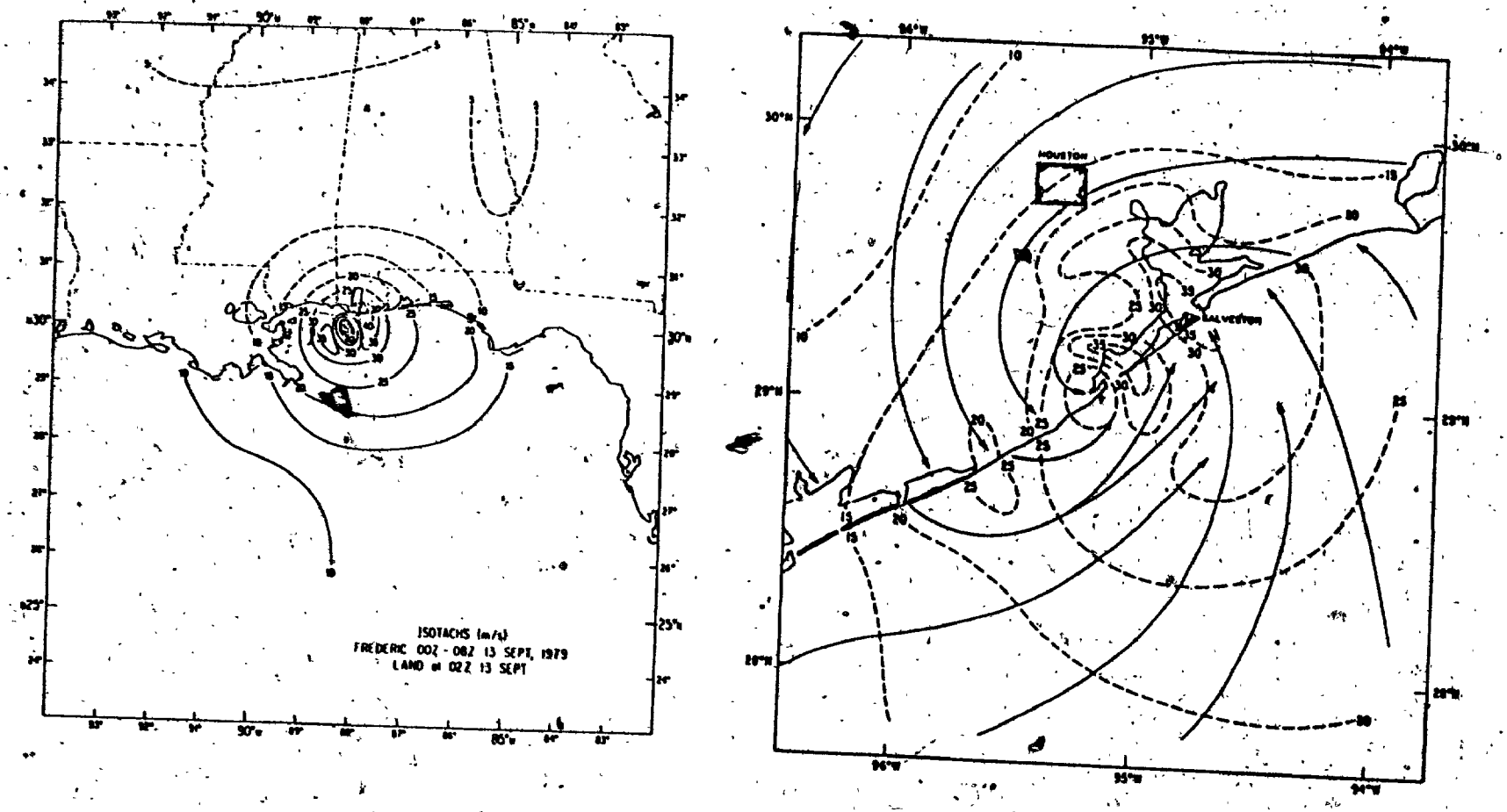

FIGURE 2.33 Landfall Isotach Analysis (m/sec) for Hurricanes Frederic (1979) and Alicia (1983)

within the same rainband to increase with decreasing distance from the storm centre.

2.8 Summary

(i) Tropical Cyclone Over-Water Windfield :

The data suggest that within the area of interest to this study three distinct regions with different circulation patterns exist within the tropical cyclone : (a) a region where the windfield is in gradient balance, (b) an inflow region which the circulation reflects the influence of surface friction and (c) the surface, corresponding to the lowest few tens of metres from the ground.

The gradient balance region begins essentially at the top of the circulation inflow layer. Its existence at about the 700 mb level (3 km) is supported by an impressive number of individual tropical cyclone case studies, especially for more mature storms, by the scale analysis performed in section 2.2 and Dunnavan's (1983) flight-level data composite study. Above the 700 mb level the windfield revolves around the storm centre like a giant carousel. In this region the effect of storm translation can be assumed to introduce a predominantly right-left asymmetry in the windfield, as indicated by Shea and Gray's (1972) composite study.

Within the inflow layer the scale analysis in section 2.2 shows that while gradient balance is still applicable to stationary storms near the eyewall, other acceleration terms are involved in the balance of forces further out in the circulation. Recent observations and numerical models of moving storms show that an asymmetry is introduced which produces maximum inflow and the highest wind speeds in the right-front quadrant of the storm. These observations support Shapiro's (1983) boundary layer windfield model and disagree with Hughes (1952) aircraft composite windfield. A distinction exists between the inflow layer and boundary layer, if the latter is defined by the extent of predominantly mechanically-generated turbulence within the flow. The depth of these two layers appears to coincide near the eyewall, although the intense vertical motion in this region makes their identificaton

difficult. Away from the eyewall the inflow region becomes deeper than the boundary layer. Thus, two sub-regions can be identified within the inflow layer, separated by the top of the mechanically-dominated boundary layer which lies at about the 500 metre level. Above this level very little shear exists in the wind profile. The circulation appears to move as a coherent slab around the storm centre. Below this level recent aircraft and ocean buoy data suggest that the vertical profile of wind speed follows a logarithmic profile commensurate with a neutral or slightly unstable boundary layer.

At the surface (10 metre level) the windfield appears to be well correlated with the 500 metre level circulation. Comparison of simultaneously recorded buoy winds with low-level aircraft winds indicate uniform surface to flight-level ratios of about 75-80%. Data suggest that this ratio may be somewhat higher approaching the eyewall and lower further out in the storm circulation. The location of the wind maximum remains in the right-front quadrant with the only significant change being increased inflow angles at all radii. This disagrees with surface windfield models such as found in Schwerdt, Ho and Watkins (1979) which indicate maximum winds in the right-rear quadrant of moving storms. Wind speeds above the surface can be adequately described using the logarithmic profile, for which appropriate values of $u*$ and Zo can be obtained from recent studies (e.g. Powell, 1982).

(ii) Windfield Evolution After Landfall :

Anticipating that the greatest interest lies in locations reasonably close to the coastline, the changes brought about by the occurrence of landfall can be treated as being additive. The whole circulation is gradually weakened by the increase in central pressure after landfall is made. This takes place gradually, as opposed to the immediate reduction in speeds at the surface. The filling rate is a function of geographical location. Thus, the reduction of the 700 mb and 500 metre level winds over land is due initially only to the rise in central pressure. This also reduces surface winds which are additionally weakened due to frictional retardation. The shear in the vertical profile over land between the surface and 500 metre level is thus greater than over water. Inflow angles over land would appear to increase by 10 to 20 degrees from their over-water equivalents.

Rainfall activity and tornadogenesis indicate that as a tropical cyclone makes landfall the windfield in front of the storm over land experiences increased inflow, accompanied by intense rainfall activity. Thus winds throughout the boundary layer may not decrease in direct proportion to their surface counterparts. Recent landfalling storms have shown evidence of a low-level maximum in vertical boundary layer profiles over land at the time of landfall.

Windfield models adopted in previous simulation procedures have mostly utilized data and wind speed relationships described in section 2.1. To date none have attempted to differentiate the circulations into the various regions and accompanying windfield maxima and inflow characteristics described above. The windfield model proposed in Chapter 3 attempts to include all of the critical features of the tropical cyclone circulation discussed in this last summary section.

CHAPTER 3

PROPOSED TROPICAL CYCLONE WINDFIELD MODEL

3.1 Objectives and Constraints of the Simulation Windfield Model

The choice of windfield model for a particular simulation procedure depends upon the use to which it will be put. Some simulations seek only to estimate extreme winds at a particular site, regardless of direction. In these cases even empirical relationships such as those discussed in section 2.1 will suffice. The current simulation procedure however was developed with the capability of computing building response estimates in mind. This requires the specification of both wind speed and wind direction in the windfield model. Because many of the structures that the simulation was intended to study are high-rise (over 300 metres), the windfield model developed in the current simulation had to specify the vertical wind velocity profile throughout the tropical cyclone boundary layer. One of the aims of this study was to identify the inland extent of the hurricane risk along the U.S. Gulf and Atlantic coastline. Therefore the windfield model also had to be adjustable at all levels once a storm made landfall.

A simulation designed to produce extreme wind speed estimates usually needs to generate over one thousand storms for statistically reliable results. When directional information is required, as in the case of structural dynamic response estimates, the number of simulated storms increases by an order of magnitude. So, for example, some of the numerical models described in section 2.4 which simulate tropical cyclone landfall (e.g. Tuleya, Bender and Kurihara, 1984) would be unsuitable for a Monte-Carlo simulation because they typically require as much computer time to evolve the windfield of a single storm as a normal hurricane simulation of the type developed in this study takes to generate one thousand storms. Hence physical constraints imposed by limited computer time dictate a maximum level of complexity for the simulation model.

On the other hand a simulation windfield model should be realistic if the Monte-Carlo approach to the estimation of tropical cyclone design wind speeds is to have any legitimacy. The need to adequately reproduce the impact of tropical cyclone winds at any particular site dictates a minimum level of complexity for the simulation windfield model. The summary section in Chapter 2 sought to establish those features of the tropical cyclone windfield which should if possible be reproduced. These include the proper location of the maximum winds within the inflow layer, a realistic boundary layer profile and the adequate representation of changes to the windfield once landfall is made. A compromise between the above constraints led to the choice of windfield model developed in the current simulation.

3.2 Over-Water Gradient Balance Windfield

The simulation windfield model assumes that the gradient balance assumption (E2-11a) can be used to define mean wind speeds at the 700 mb level in tropical cyclones. The effect of storm translation is accounted for by using Blaton's formula (E2-8). The wind speed magnitude at the 700 mb level is thus given by :

$$\frac{1}{\rho}\frac{\partial p}{\partial r} = \frac{V_{gb}^2}{r}\left|1 - \frac{VT}{V_{gb}}\sin\alpha\right| + f.V_{gb} \qquad E3-1$$

Vgb = mean gradient balance wind speed at (r,α)
r = radial distance from storm centre
α = angle, clockwise positive from translation direction
p = pressure, at distance r
VT = storm translation speed
f = Coriolis parameter
ρ = air density

The direction of the mean gradient balance wind speed is given by :

$$\theta gb = \theta + a + \beta \qquad E3-2$$

θgb = wind direction corresponding to Vgb
θ = storm approach angle, clockwise positive from North
β = 90° in the Northern Hemisphere (270° in the Southern)

Since the wind speed defined in E3-1 is a function of slowly-varying meteorological parameters, the averaging time is assumed to be of the order of 10-20 minutes. The horizontal pressure gradient is computed using the modified exponential formula (E2-2b). This defines the gradient balance windfield as:

$$Vgb(r,\alpha) = \frac{1}{2}(VT \cdot \sin\alpha - fr) + \left\{\frac{1}{4}(VT\sin\alpha - fr)^2 + B\frac{\Delta p}{\rho}\left(\frac{RMAX}{r}\right)^B \varepsilon^{-\left(\frac{RMAX}{r}\right)^B}\right\}^{\frac{1}{2}} \qquad E3-3$$

Δp = central pressure difference
B = pressure-profile exponent
$RMAX$ = radius of maximum winds

Figure 3.1 shows an example of the resulting windfield for a tropical cyclone with parameters typical of a fairly intense storm using the above gradient balance equations. The most significant contribution to the wind pressure in the vicinity of the maximum winds arises from Δp, the central pressure difference. The circulation is symmetric about an east-west cut through the centre for a northward moving storm. The maximum wind speed occurs at $\alpha = 90°$ and near $r = RMAX$. In this case the pressure gradient dominates the second term under the square-root sign in E3-3 and the maximum wind speed can be closely approximated by:

$$Vgb, max = \frac{1}{2}(VT - fRMAX) + 0.61\sqrt{\left(B \cdot \frac{\Delta p}{\rho}\right)} \qquad E3-4$$

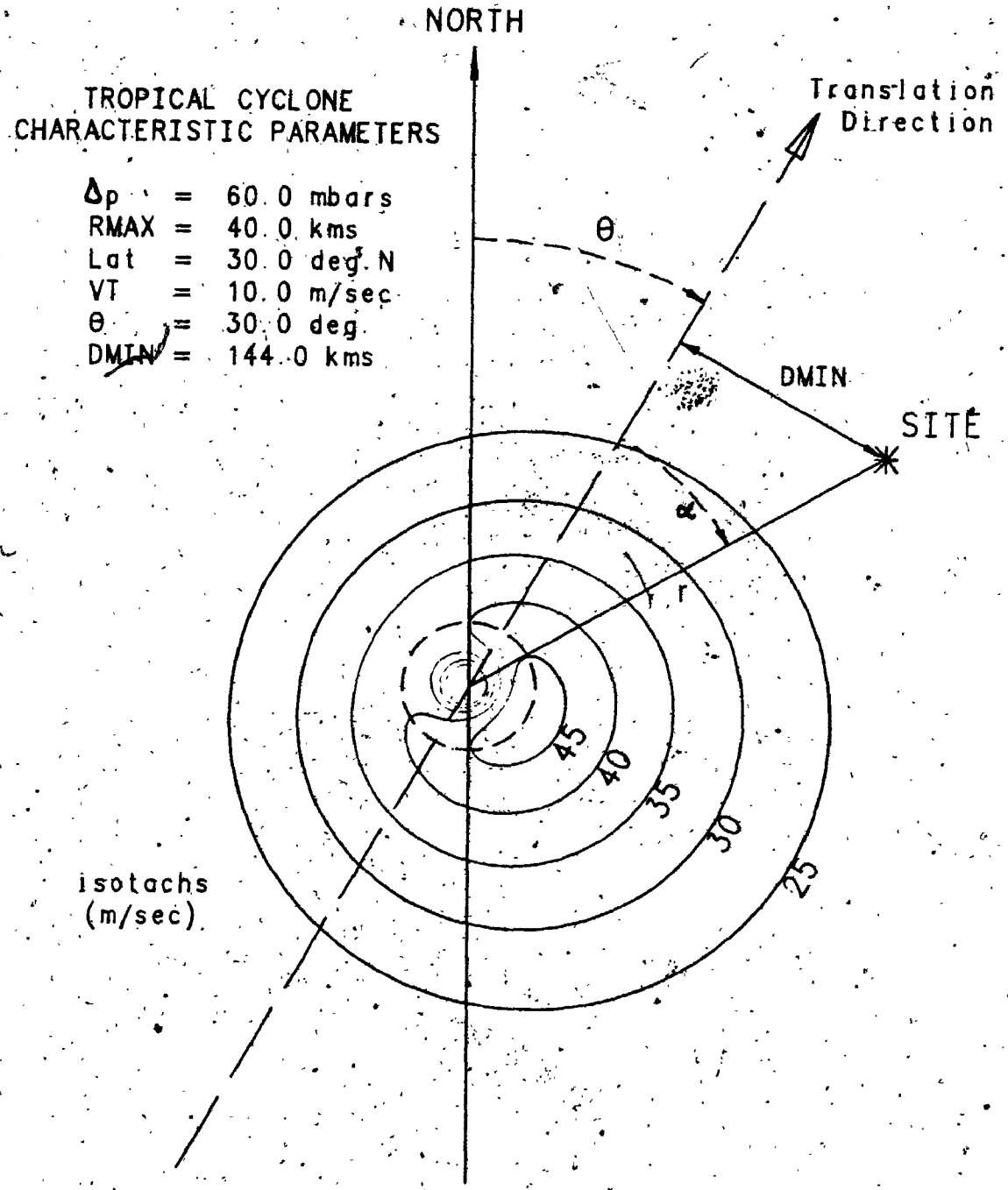

FIGURE 3.1 Example Gradient Balance Windfield

3.3 Over-Water 500 Metre Height Windfield

An inflow layer is distinguished in the present windfield model in order to reproduce the asymmetrical circulation observed in tropical cyclones resulting from the combined influence of surface friction and storm translation. The inflow layer is assumed to consist of two sub-layers (i) an upper section extending from the 700 mb level down to the 500 metre height in which the vertical wind shear is assumed to be negligible and (ii) the tropical cyclone boundary layer, assumed to extend from the 500 metre height down to the surface. The zero shear upper layer is assumed to act as a slab and is designated in the simulation windfield model as the 500 metre height windfield, V_{500}.

The V_{500} windfield is determined by making use of Shapiro's (1983) hurricane boundary layer model, herein referred to as the SHBL model. In Chapter 2 it was shown that the SHBL model is able to reproduce asymmetries in the inflow layer windfield of moving storms in agreement with actual storm observations. Use of the SBHL model is attractive because it is a dynamic model whose input parameters are precisely the same as those needed to define the gradient balance windfield. A difficulty exists with implementation of the SHBL model in that the momentum equations are solved for a slab boundary layer of constant depth. Thus it is not possible to define at exactly what height model-predicted wind speeds and directions apply. Consideration of the boundary layer profile suggests that SHBL model wind speeds apply well up in the inflow layer. What is required then is a reference point in the windfield where the wind speed magnitude is known and which can be related to some point in the SHBL model windfield.

The reference point chosen is the eyewall. Here, observations show that wind speeds between the 500 metre height and 700 mb level are almost constant. Hence, the azimuthally-averaged tangential component of wind speed at the 500 metre height should be very close to being in gradient balance. The SHBL model winds can then simply be adjusted so that the azimuthally-averaged tangential component at the radius of maximum winds is made to equal the gradient balance value. Wind speeds at all other radii are

then scaled accordingly. Thus the simulation model V_{500} wind speed magnitude is given by:

$$V_{500}(r,a) = V_{SHBL}(r,a) \cdot \frac{V_{gb}(RMAX)}{V_{SHBL}(RMAX)} \qquad E3-5$$

V_{500} = 500 metre height wind speed at (r, a)
$V_{SHBL}(r, a)$ = SHBL model wind speed at (r,a)
$V_{SHBL}(RMAX)$ = SHBL model azimuthally-averaged tangential wind speed component at $r=RMAX$
$Vgb(RMAX)$ = gradient balance azimuthally-averaged wind speed at $r=RMAX$

Wind direction at the 500 metre height is calculated assuming that SHBL model wind directions are representative of surface inflow angles and making use of the composite inflow angle data presented in section 2.3. The inflow angle in all quadrants is greatest at the surface (10 metre level) and decreases in a roughly linear fashion with height. Comparisons of aircraft data with simultaneous ocean buoy data support the quantitative decrease in inflow angle between the surface and 500 metre height shown in Figure 2.10. Assuming that the reduction in inflow angle will be of the same order at all azimuths, wind directions for the model 500 metre height windfield are specified as:

$$\theta_{500}(r,a) = \theta_{SHBL}(r,a)/3.0 \qquad E3-6$$

$\theta_{500}(r,a)$ = 500 metre height wind direction at (r,a)
$\theta_{SHBL}(r,a)$ = SHBL model wind direction at (r,a)

Figure 3.2 shows the 500 metre level windfield corresponding to the storm shown in Figure 3.1. The windfield maximum has moved towards the front of the storm. Wind speeds are slightly increased in the eyewall region and decreased further away from the eyewall. In Figure 3.3 the 30.0, 35.0 and 45.0 m/sec contours from both windfields have been replotted, showing the counter-clockwise rotation of the wind maximum. It can be seen that the area of winds greater than 45.0 m/sec at the 500 metre height is greater than the

Tropical Cyclone
Characteristic Parameters ... same as for Figure 3.1

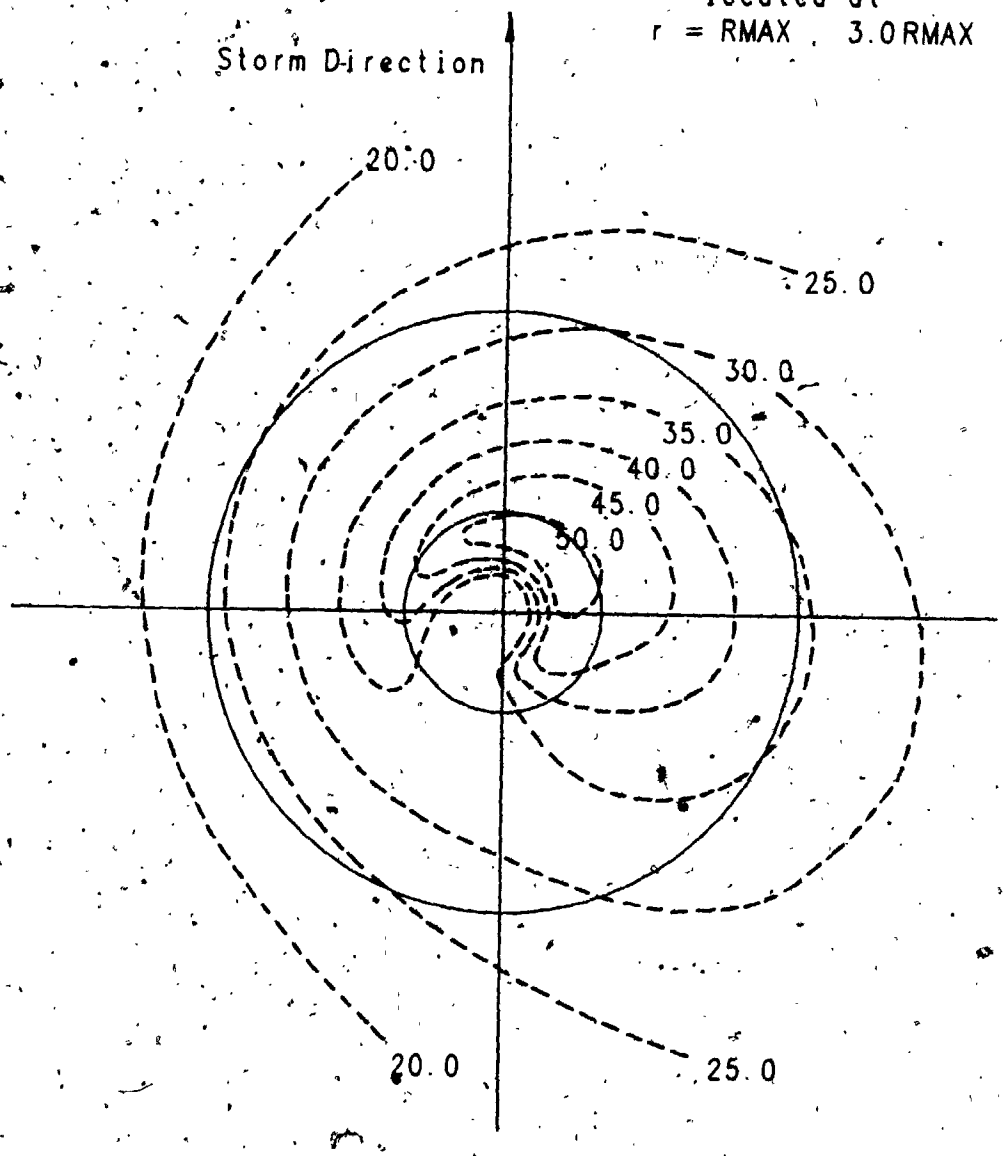

FIGURE 3.2 Example V_{500} Windfield Corresponding to Gradient Balance Windfield shown in Figure 3.1

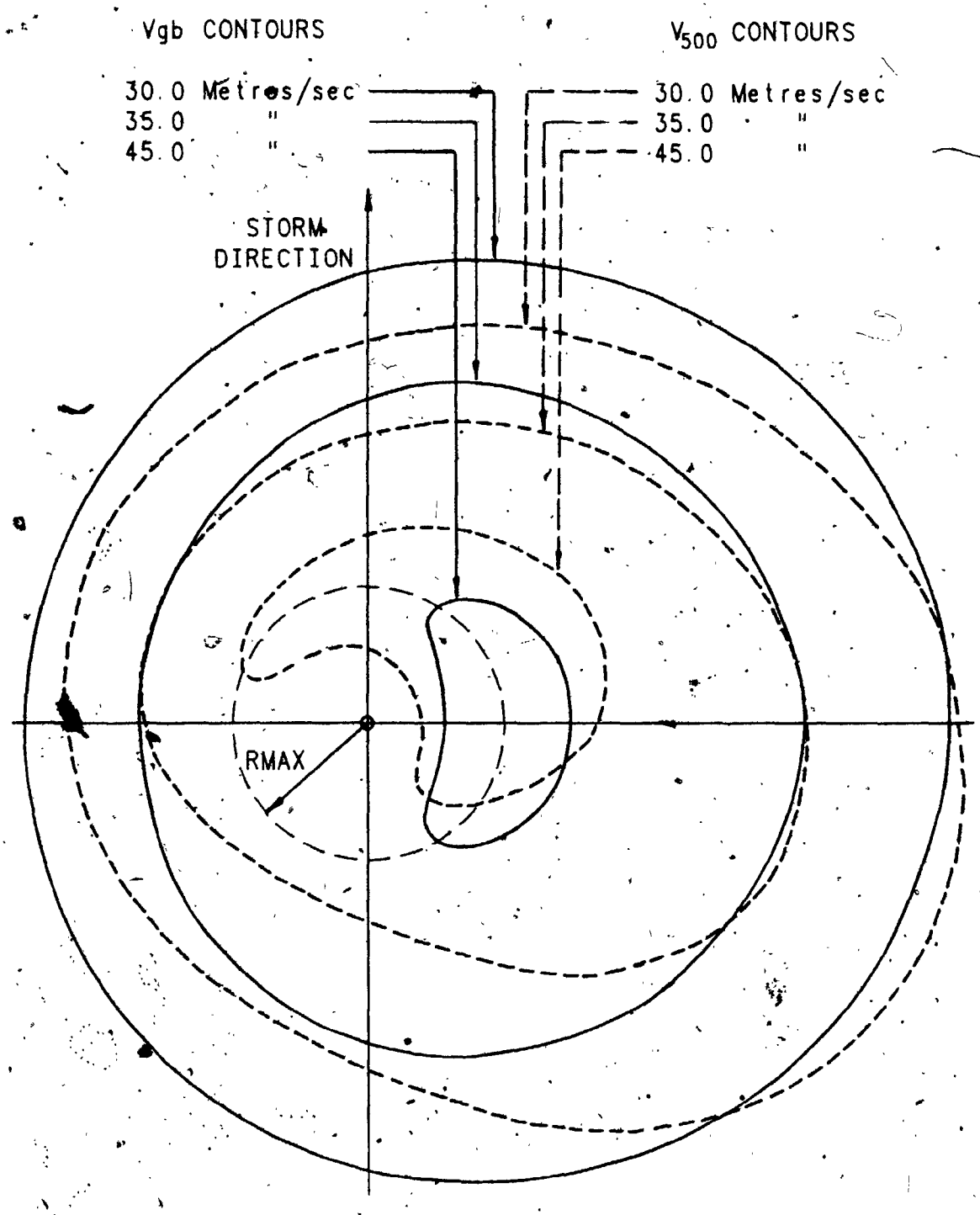

FIGURE 3.3 Comparison of 30.0, 35.0 and 45.0 m/sec Contours for the Vgb and V_{500} Windfields

equivalent area at the 700 mb level, whereas the opposite occurs for the 30.0 m/sec contour.

A number of points can be made about the use of the SHBL model to define the simulation model 500 metre height windfield. Firstly, since wind speed magnitudes near the radius of maximum winds are essentially the same as those at the gradient balance height, extreme wind speed estimates obtained from the simulation procedure yield almost the same predicted speeds at both the 500 metre height and the gradient balance height. The significance of the 500 metre height windfield within the simulation is the influence upon the circulation, particularly wind directions, of the storm translation speed and the consequent effects on building response estimates which in many cases can be extremely sensitive to wind direction. Secondly, any loss in accuracy resulting from the conversion of the SBHL model to the simulation 500 metre height windfield is considered to be more than compensated for by the ability to reproduce realistic features of the tropical cyclone inflow layer hitherto unrecognized in other simulation procedures.

3.4 Adaption of Shapiro's Numerical Model for Simulation Usage

A greater difficulty in adapting the SHBL model to the current simulation windfield model arose because of computer time limitations. The SHBL model requires approximately 280 CPU seconds of execution time on a Cyber Model 835 to achieve a convergent solution for a single windfield evolution. This is of the same order as the time required in typical Monte-Carlo simulations to run through a complete extreme wind speed prediction, involving the generation of approximately two thousand storms. Thus it was not possible to make use of the SHBL model directly in the simulation procedure. The output from the SHBL model is a series of coefficients at discrete radial intervals (typically $\delta r = 0.125RMAX$) which can be used to compute the wind speed and direction at any azimuth for the radial intervals specified. At any particular fixed geographical location the input parameters required in the SHBL model consist of storm parameters ($\Delta p, RMAX, VT$) and model constants (ρ, f, Cd, K) (section 2.4). It can be simply shown using dimensional analysis that SHBL

model wind speeds should then be a function of the following dimensionless parameters:

$$\frac{V_{SHBL}(r,a)}{fRMAX} = fn\left[\frac{\Delta p}{\rho(fRMAX)^2} ; \frac{VT}{fRMAX} ; \frac{K}{fRMAX^2} ; C_d\right] \qquad E3-7$$

Two model storms run with the same dimensionless parameters should yield identical dimensionless windfields. As indicated in Shapiro (1983) and as was determined after running several SHBL windfield simulations, the resulting winds are relatively insensitive to the choice of drag coeffcient, Cd, and eddy coefficient, K. Hence, the SBHL model windfield is effectively determined by two parameters, $\pi_1 = \Delta p/\rho(fRMAX)^2$ and $\pi_2 = VT/(fRMAX)$. Figure 3.4 illustrates the effect that a change in the π parameters has on the circulation. The six windfield examples shown have the following storm parameters:

All storms: ρ = 1.15 kg/m^3 , latitude = 30.0°N

Set 1:	Δp	= 60 mb	π_1	=	617
	$RMAX$	= 40 km			
	VT	= 0.0, 5.0, 10.0 m/sec	π_2	=	0.0, 1.72, 3.44
Set 2:	Δp	= 20.0, 60.0, 100.0 mb	π_1	=	206, 617, 1028
	$RMAX$	= 40 km			
	VT	= 5.0 m/sec	π_2	=	1.72

The relative changes in the windfields are illustrated in Figure 3.5, showing the ratio of the azimuthally-averaged SHBL tangential component to the gradient balance wind speed as a function of radius. Increasing either of the π parameters causes the winds to be more sub-gradient outside the radius of maximum winds and more super-gradient just inside the radius of maximum winds. When the radial component is taken into account it can be seen that after normalizing the SHBL windfield so that the average tangential component at the radius of maximum winds is equal in magnitude to the gradient balance value, the overall changes in magnitude from the

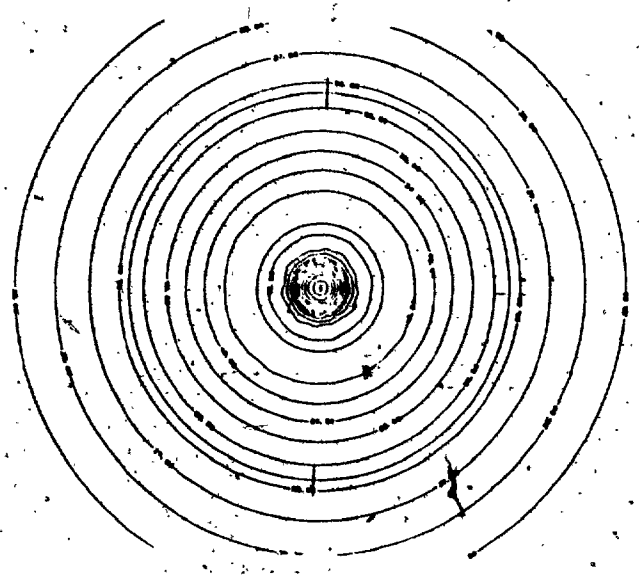

(a) VT = 0.0 metres/sec

(b)

VT = 5.0 m/sec

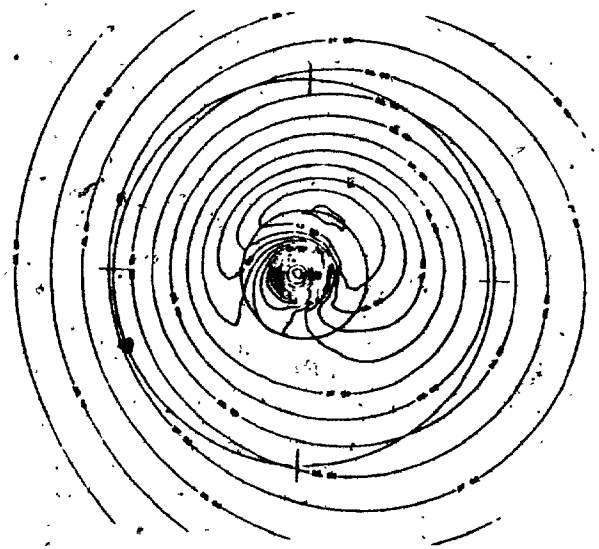

(c)

VT = 10.0 m/sec

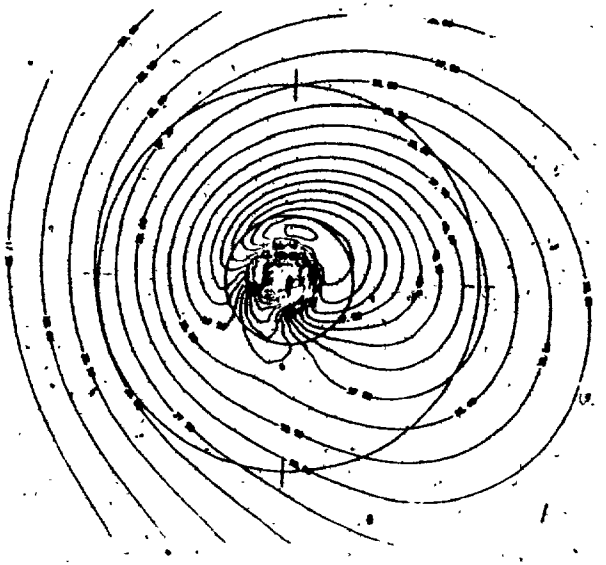

All cases { Δp = 60.0 mb, RMAX = 40.0 km

FIGURE 3.4 Example SHBL Windfields Showing Effect of Varying n Parameters. This Page, Increased Translation Velocity

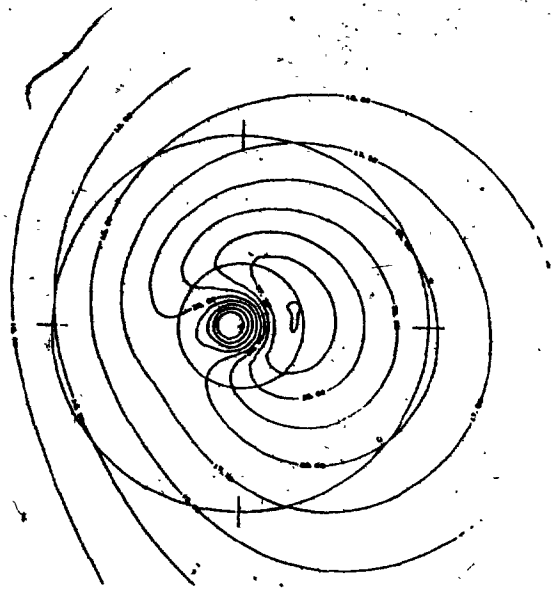

(a) Δp = 20.0 mb

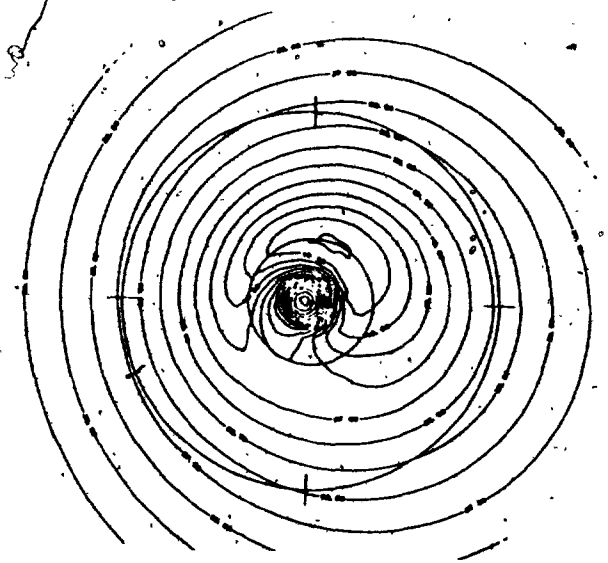

(b)

Δp = 60.0 mb

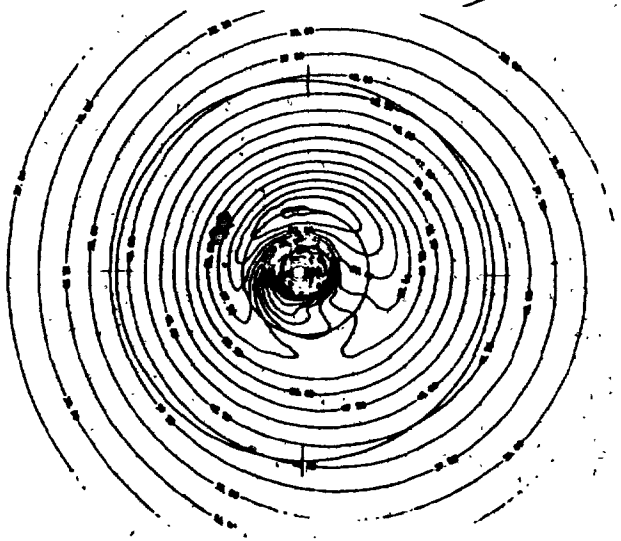

(c)

Δp = 100.0 mb

All cases { VT = 5.0 m/sec, RMAX = 40.0 km

FIGURE 3.4 (cont'd) Example SHBL Windfields Showing Effect of Varying Parameters. This page, Increased Central Pressure Difference

gradient balance values throughout the storm circulation are generally less than 20%. This is as expected. In the previous chapter it was shown that a large number of storm observations indicate that the winds at the surface rarely fall below 70% of the 700 mb winds, and that there is very little shear between the 700 mb level and 500 metre height winds. The major change then in the model 500 metre height windfield is the location of the maximum winds and the inflow angle distribution.

A further check on the realism of the normalized SHBL windfield was obtained by computing exponent constants for radial profiles of wind speed at different azimuths assuming a relationship of the form given by E2-1b. For the six windfields shown in Figure 3.4 the profiles gave exponents ranging from 0.45 to 0.60. This is in good agreement with the observed average value of 0.5 in previous studies (Gray, 1981). Increasing either of the π parameters gave sharper wind profiles. This is also in agreement with the composite data of Shea and Gray (1973) showing fast moving storms having sharper wind profiles than slow moving storms and the same tendency for more intense storms compared to weaker storms.

Figure 3.5 shows that the SHBL model windfield varies systematically with changes in the π parameters. This allows the possibility of interpolating between reasonably spaced π parameters to obtain intermediate solutions. This was the approach taken to adapt the SHBL model to the simulation procedure. A series of SHBL windfields were computed for a range of π parameters that covered the estimated range of possible $(\Delta p, RMAX, VT, \rho, f)$ values for North Atlantic storms. The output windfields were normalized as per E3-5 and E3-6 and the azimuthal coefficients stored in a data base under the particular π_1 and π_2 value. As a storm was generated in the simulation, the value of $V_{500}(r,a)$ was determined by a two-dimensional interpolation between the nearest π parameters. The orderly variation of windfield changes between the π parameters resulted in errors arising from the interpolation process of the order of 5% and less.

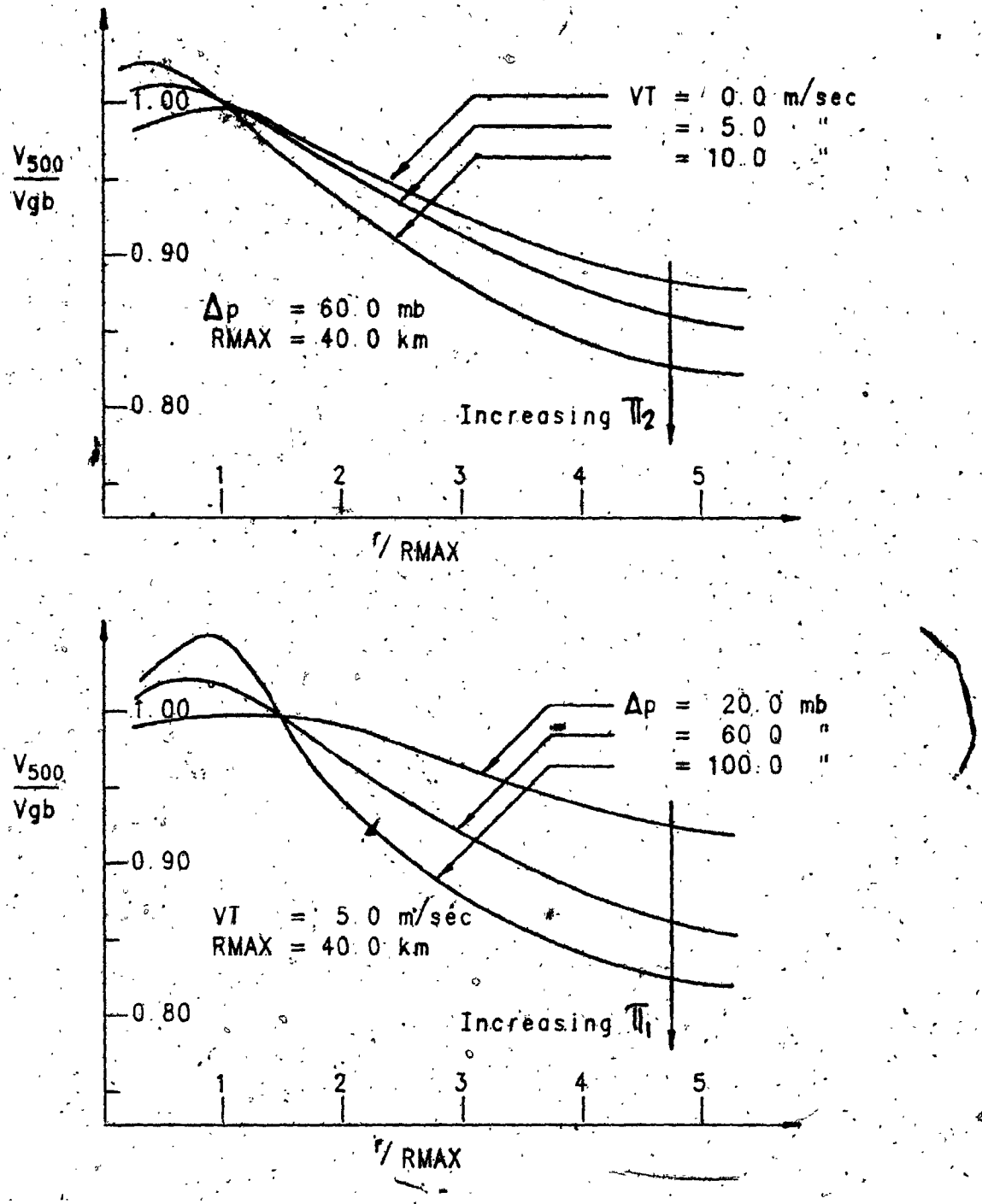

FIGURE 3.5 Ratio of V_{500} to Vgb Wind Speeds for Radial Profiles taken at $\alpha = 45°$

3.5 Over-Water Surface (10 metre) Height Windfield

The surface (10 metre) height windfield model in the simulation is defined using an empirical model to compute wind magnitudes and the SBHL model windfield to determine wind directions, specified as:

$$V_{10}(r,a) = \phi_\omega \cdot V_{500}(r,a) \qquad E3-8a$$

$$\theta_{10}(r,a) = \theta_{SHBL}(r,a) \qquad E3-8b$$

ϕ_ω = over-water surface to 500 metre mean wind speed reduction factor, a function of $(r/RMAX)$

The variation of ϕ_ω is shown in Figure 3.6. At any given radial distance the reduction factor is assumed to be constant for all azimuths. The ratio of surface to 500 metre height mean wind speed defined in E3-8a was determined keeping in mind the observational data discussed in section 2.5, which suggest near constant ratios of 0.75 throughout most of the surface windfield, with the possibility of slightly higher ratios near the eyewall and lower ratios in the right-rear quadrant away from the eyewall. The ratios chosen for the simulation windfield model are thus very slightly conservative. The wind directions given by the SHBL model are in agreement with observed surface inflow angles. Maximum inflow is concentrated in the right-front quadrant of the storm. Figure 3.7 shows the surface windfield corresponding to the example tropical cyclone depicted in Figures 3.1 and 3.2.

3.6 Over-Water Boundary Layer Profile

The tropical cyclone boundary layer is defined in the simulation windfield model as extending from the surface to the 500 metre height. The simulation boundary layer profile is defined in a relative fashion because of the varying surface to 500 metre height wind speed ratios in the windfield model. The profile is based on a logarithmic relationship defined by:

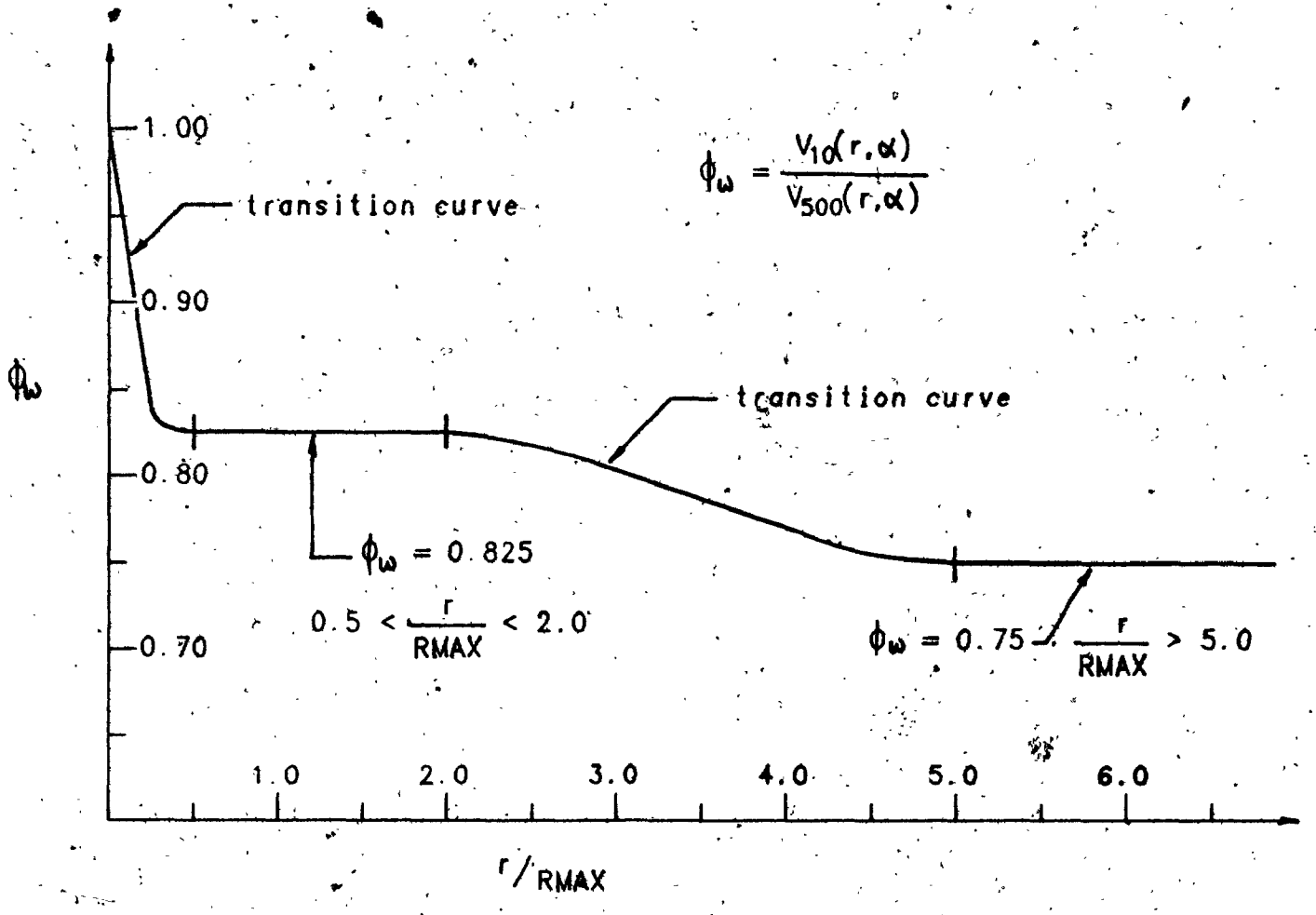

FIGURE 3.6 Ratio of Over-Water 10 Metre to 500 Metre Mean Wind Speed

Tropical Cyclone
Characteristic Parameters — same as for Figure 3.1

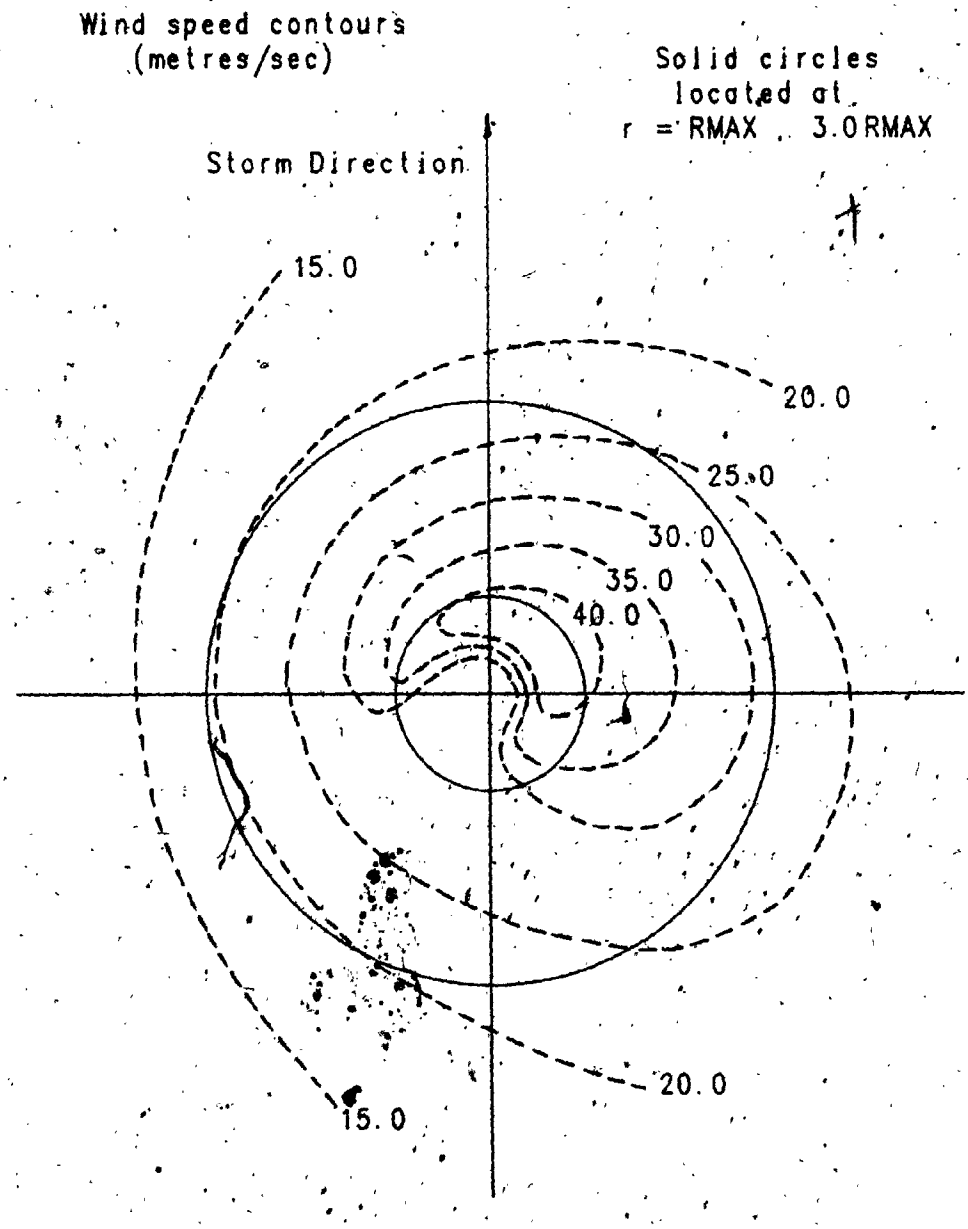

FIGURE 3.7 Example V_{10} Windfield Corresponding to V_{500} Windfield shown in Figure 3.2

for all (r,a) $\quad V(z) = V_{10} + P(z)\,\Delta V$ $\quad$ E3-9

where $P(z) = ln[az^2 + bz + c]$

z = height (metres)

$\Delta V = V_{500}(r,a) - V_{10}(r,a)$

a,b,c = constants defined such that $P(10) = 0.0$, $P(ZI\omega) = 0.5$, $P(500) = 1.0$

$ZI\omega$ = over-water boundary layer intermediate height

The function $P(z)$ defines a logarithmic variation of wind speed in the boundary layer between any two values of surface and 500 metre height wind speed. This is illustrated in Figure 3.8. The logarithmic shape of the profile is in agreement with the data presented in section 2.5. The three constants a,b,c are fixed once the value of the intermediate height, $ZI\omega$, is chosen. $ZI\omega$ defines the height where the wind speed is exactly mid-way between the value at the surface and at the 500 metre height, i.e. if $V_{10} = 0.8V_{500}$, then $V(ZI\omega) = 0.9V_{500}$. This is a convenient way in which to vary the basic logarithmic shape for different exposure conditions. Figure 3.8 also shows the resulting boundary layer profiles for $ZI\omega = 100, 150, 200$ *metres*, $V_{500} = 50.0$ *m/sec* and $V_{10} = 0.8V_{500}$. For over-water profiles the data suggest that the intermediate height lies at about the 150 metre level. This is the $ZI\omega$ value used for the boundary layer profile in the simulation over-water windfield model. Within the boundary layer the wind direction is linearly interpolated between the surface and 500 metre height values. Using the definition of the 500 metre height windfield, a linear boundary layer variation in wind direction is assumed:

$$\text{for all } (r,a) \qquad \theta(z) = \left[\frac{745 - z}{735}\right]\theta_{10} \qquad E3-10$$

z = height (metres)

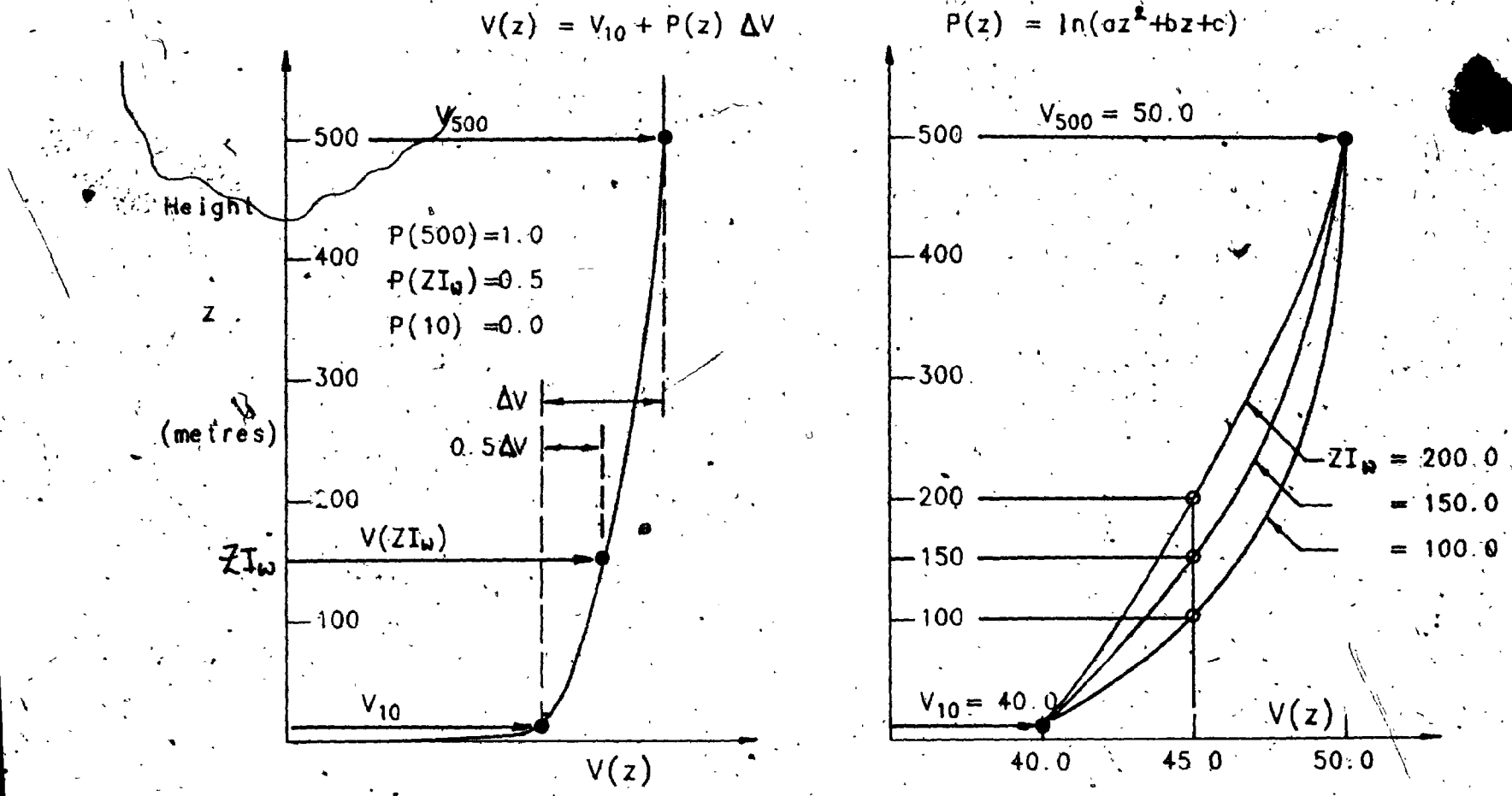

FIGURE 3.8 Simulation Model Over-Water Boundary Layer Profile

3.7 Separation of Landfall Effects on Different Levels Within the Tropical Cyclone Circulation

The behaviour of landfalling storms and resulting changes to the windfield are considerably complex especially at the lower levels within the circulation. Interest however is normally restricted to sites located near the coast where the risk is highest. The simulation windfield model separates the effects of landfall on the evolution of the tropical cyclone windfield into three distinct components.

(i) As the eye passes over land the central pressure difference of the storm is decreased. This affects wind speeds at all levels, since Δp is an input parameter to both the gradient balance and the 500 metre height windfields and since surface winds are derived in the simulation from the 500 metre winds. Other storm parameters are assumed to retain their over-water values, i.e. the radius of maximum winds, translation velocity, storm direction etc. remain unchanged.

(ii) Surface winds are further decreased to account for very much larger surface friction sustained over land. In the simulation windfield model this is accomplished in a two-stage approach by computing what an equivalent over-water surface wind speed would be and multiplying by a factor to convert to an over-land surface speed. A similar procedure is used to correct for the local inflow angle, by converting an equivalent open-water value to a representative over-land one.

(iii) The simulation windfield model recognizes the possibility of enhanced inflow activity in the immediate landfall area to the front and right of a storm approaching land. This is taken into account by varying the value of the over-land boundary layer intermediate height, ZI_l, as a function of distance inland from the coastline and position relative to the storm circulation.

The method of computing winds within the boundary layer using the three-stage approach outlined above is considered adequate for sites located near the coast. Some time after landfall is made, say 100 to 200 km inland, the

tropical cyclone boundary layer will take on extra-tropical characteristics. At this point the estimation of surface speeds may be better calculated directly from the upper-level speeds assuming strong wind neutral boundary layer conditions. The following three sections detail the manner in which each of the three components is defined in the proposed windfield model.

3.8 New Filling Rate Model

In section 2.6 it was shown that filling characteristics of North Atlantic storms vary with geographical location. In Miller (1963) and Schwerdt, Ho and Watkins (1979) the filling rate was modelled as a function of time elapsed after landfall. This is the approach adopted in most simulations. An initial examination of the drop in central pressure difference for U.S. landfalling storms however indicated a substantial degree of scatter in the filling rate when plotted this way. Schwerdt, Ho and Watkins (1979) note that in their sample of 16 landfalling tropical cyclones, the more intense storms tended to fill the fastest except over the Florida peninsula where the opposite was observed to occur. Tuleya, Bender and Kurihara's (1984) numerical landfall model indicated a faster filling rate for more intense storms. Other studies (Malkin, 1959; Goldman and Ushijima, 1974) have suggested that other parameters might influence the filling rate, such as storm size ($RMAX$), speed (VT) etc.

From the National Hurricane Center's historical records, track and central pressure data were obtained for 26 landfalling tropical cyclones. Their paths prior to and after landfall are shown in Figure 3.9. They were subdivided geographically into four groups which had approximately equal sample numbers:

Group	I	-	Western Gulf (U.S.-Mexico border to Houston)	8 storms
	II	-	Mid Gulf (New Orleans to Appalachicola)	5 storms
	III	-	Florida Peninusla	7 storms
	IV	-	Atlantic (Charleston to U.S.-Canada border)	6 storms

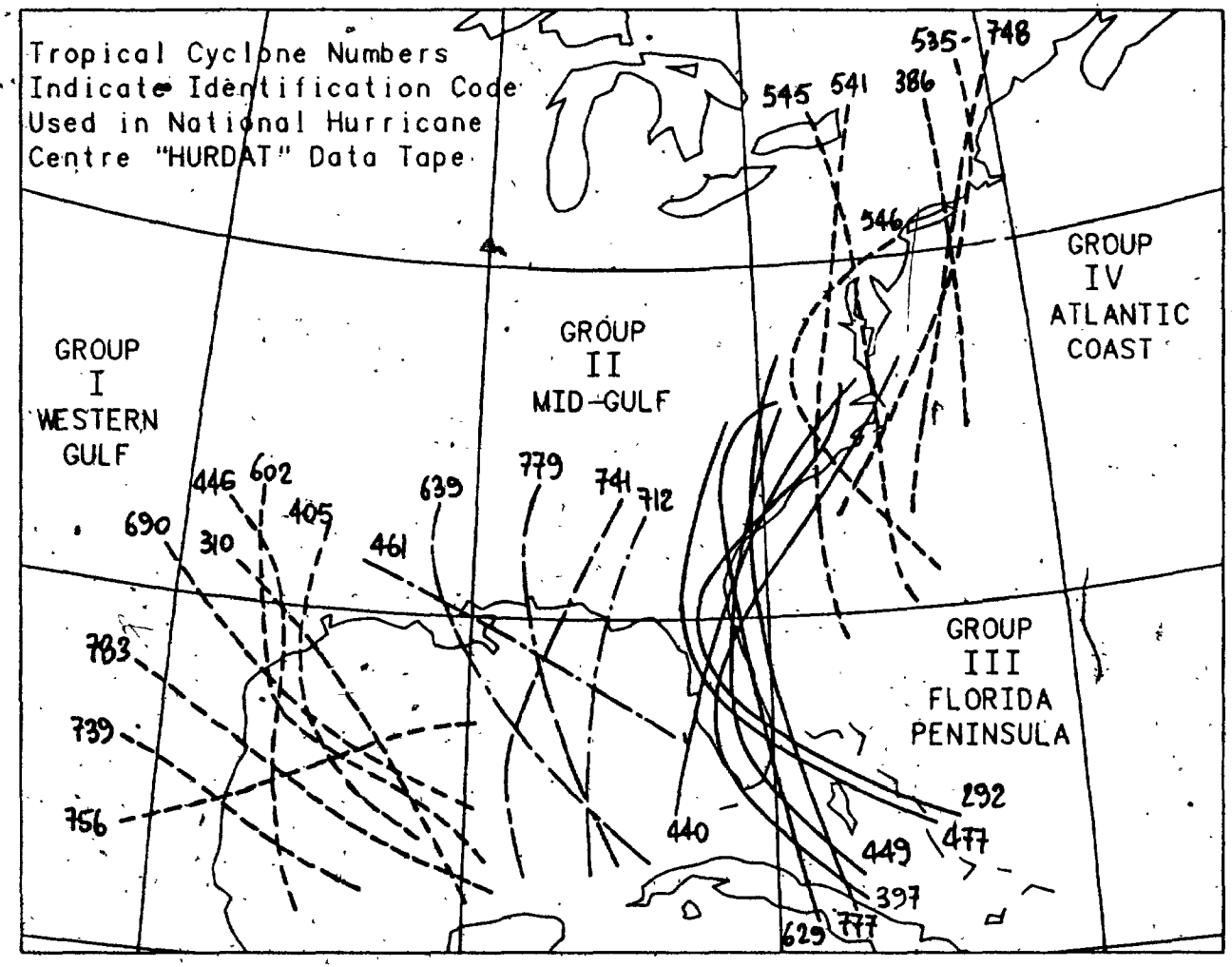

FIGURE 3.9 U.S. Landfalling Tropical Cyclones Used to Determine Simulation Filling Model

In order to take into account the initial intensity at the time of landfall, values of $\Delta p/\Delta p_o$ were computed for each storm, Δp_o being the value of the central pressure difference at landfall. This ratio was then plotted against four variables chosen as being parameters which might affect the filling rate of each storm. These were (a) "t", time elapsed after landfall (b) "d" $= VT.t$, distance travelled inland after landfall (c) "$t/RMAX$" and (d) "$VT.t/RMAX$". The variation of the central pressure difference ratio, $\Delta p/\Delta p_o$, with the four parameters is shown in Figures 3.10 and 3.13. Groups I and IV show considerable scatter for the "t" set. All groups are well-behaved for the "d" set with the lone exception of a single tropical cyclone in Group I. Considerable scatter is shown by the "$t/RMAX$" set in Groups III and IV and by the "$VT.T/RMAX$" set in Groups I and IV.

From these comparisons it emerged that the $\Delta p/\Delta p_o$ ratio was best expressed as a function of "d", the distance travelled inland after landfall. The shape of the decay curves shown in Figure 3.11 led to the following relations being adopted for the tropical cyclone filling rate in the simulation windfield model :

Before Landfall

Regions I, II, III $$\frac{\Delta p}{\Delta p_o} = 1.0 \qquad E3-11a$$

Region IV $$= 1.0 + \frac{DW}{1500.0} \qquad E3-11b$$

After Landfall:

Regions I, II, III $$\frac{\Delta p}{\Delta p_o} = \frac{1.0}{1.0 + \left(\frac{d}{FD}\right)^2} \qquad E3-12a$$

Region IV $$= exp\left|-\frac{d}{FD}\right| \qquad E3-12b$$

DW = distance to the landfall point (km)
d = distance travelled inland after landfall (km)
FD = filling parameter for each regional Group, equal to 150.0, 350.0, 450.0, 1000.0 for Regions I, II, III, IV resp..

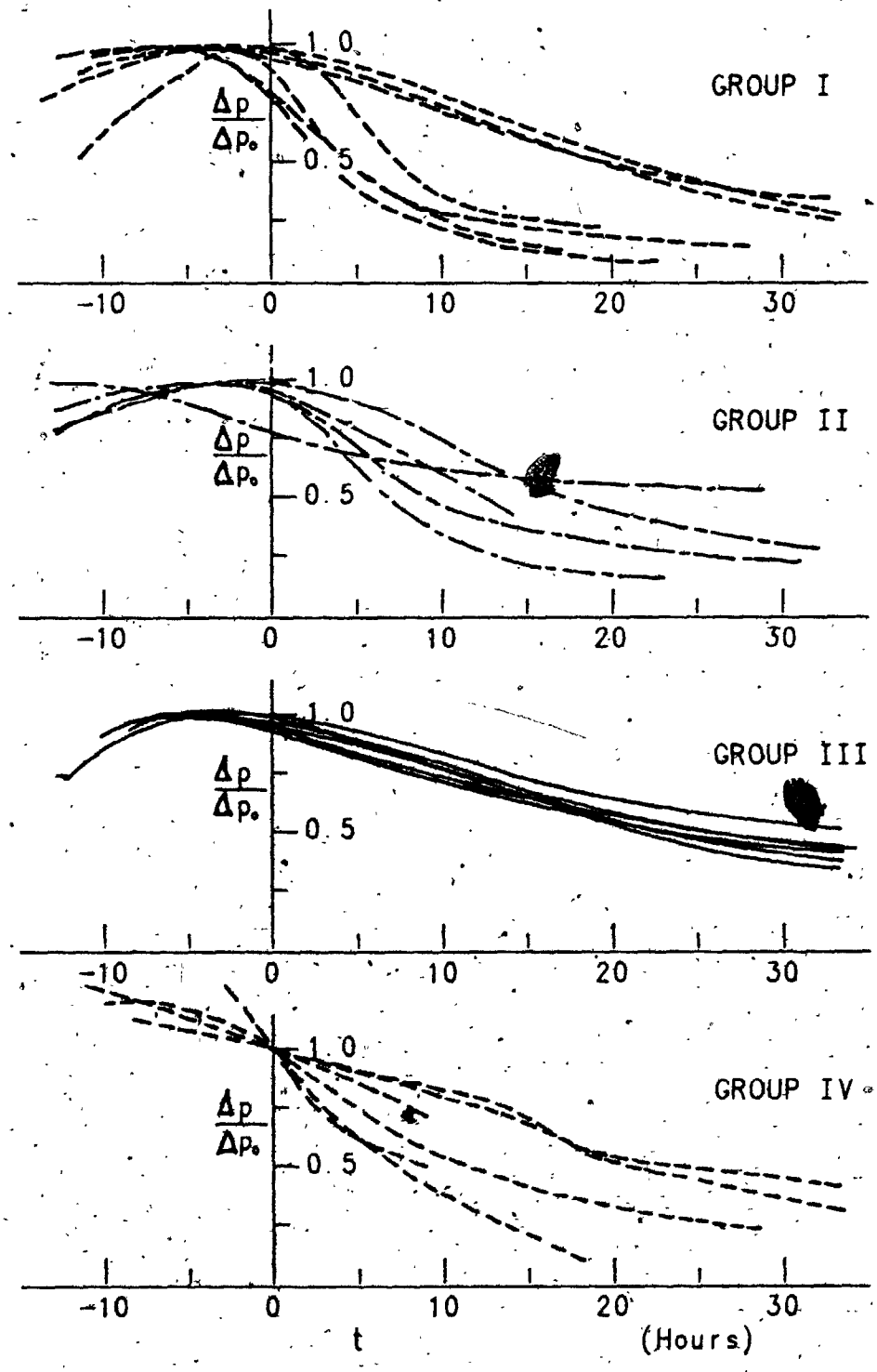

FIGURE 3.10 $\Delta p/\Delta p_o$ Versus "t"

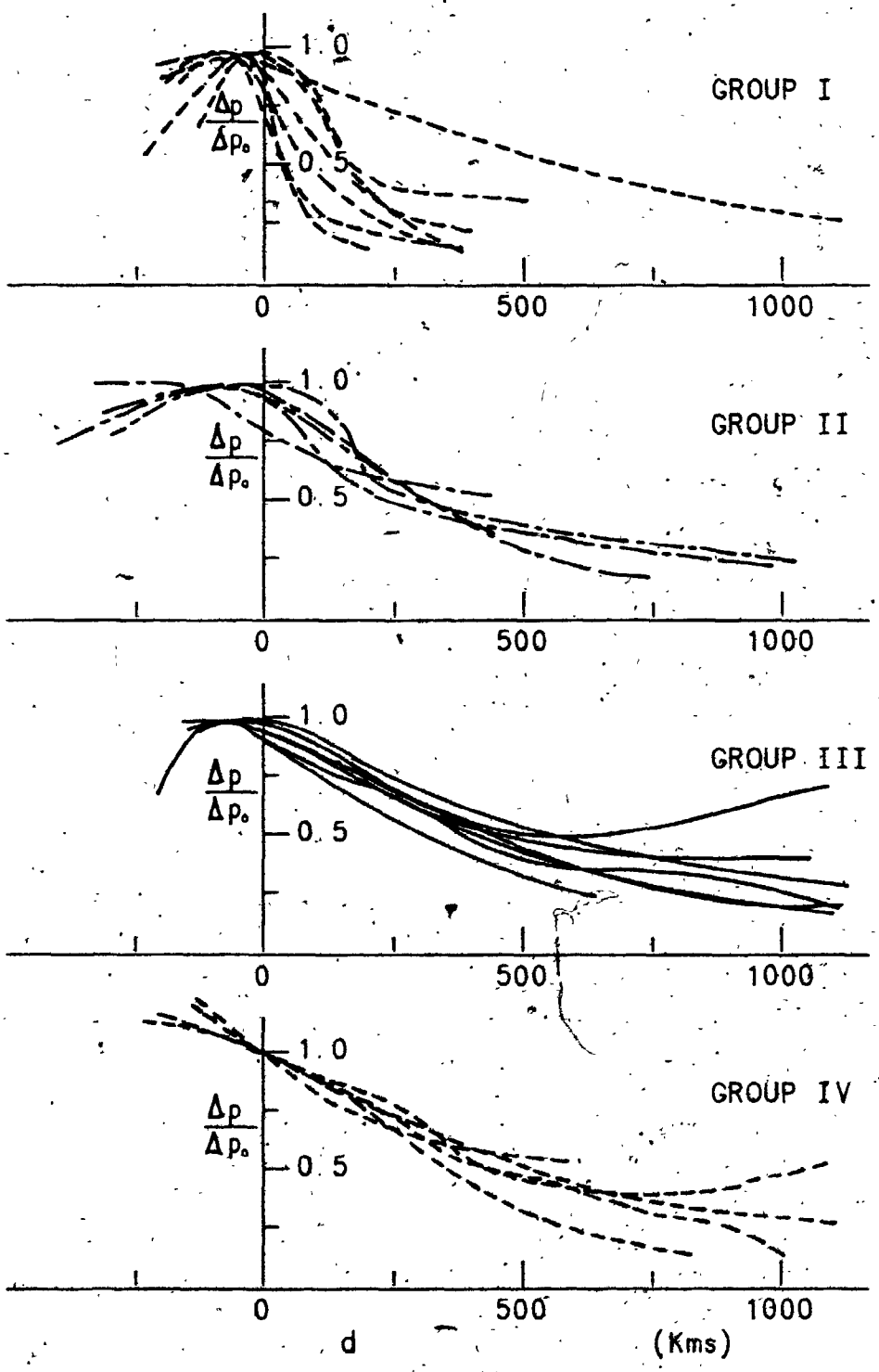

FIGURE 3.11 $\Delta p/\Delta p_o$ Versus "d"

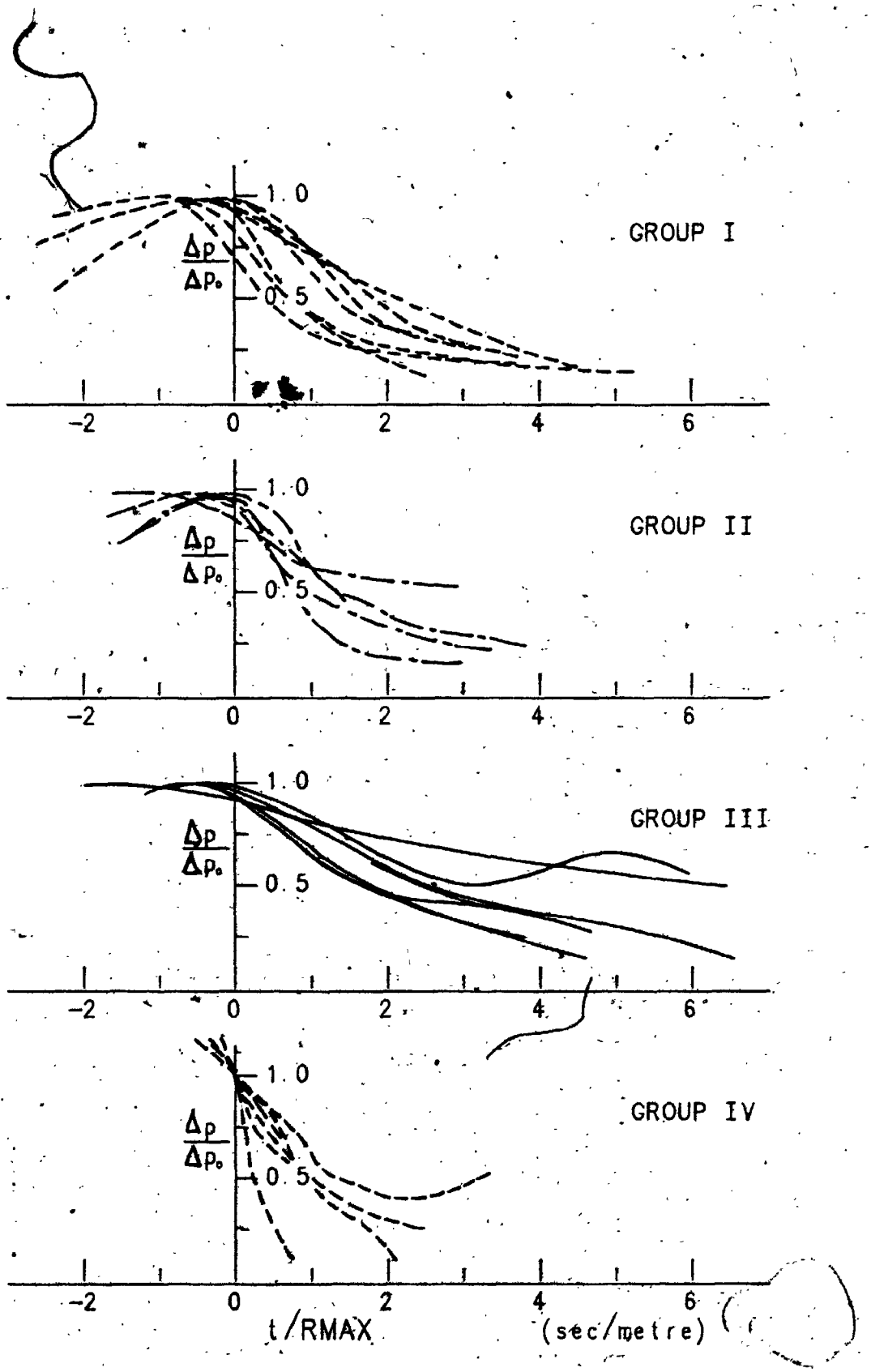

FIGURE 3.12 $\Delta p/\Delta p_o$ Versus "t/RMAX"

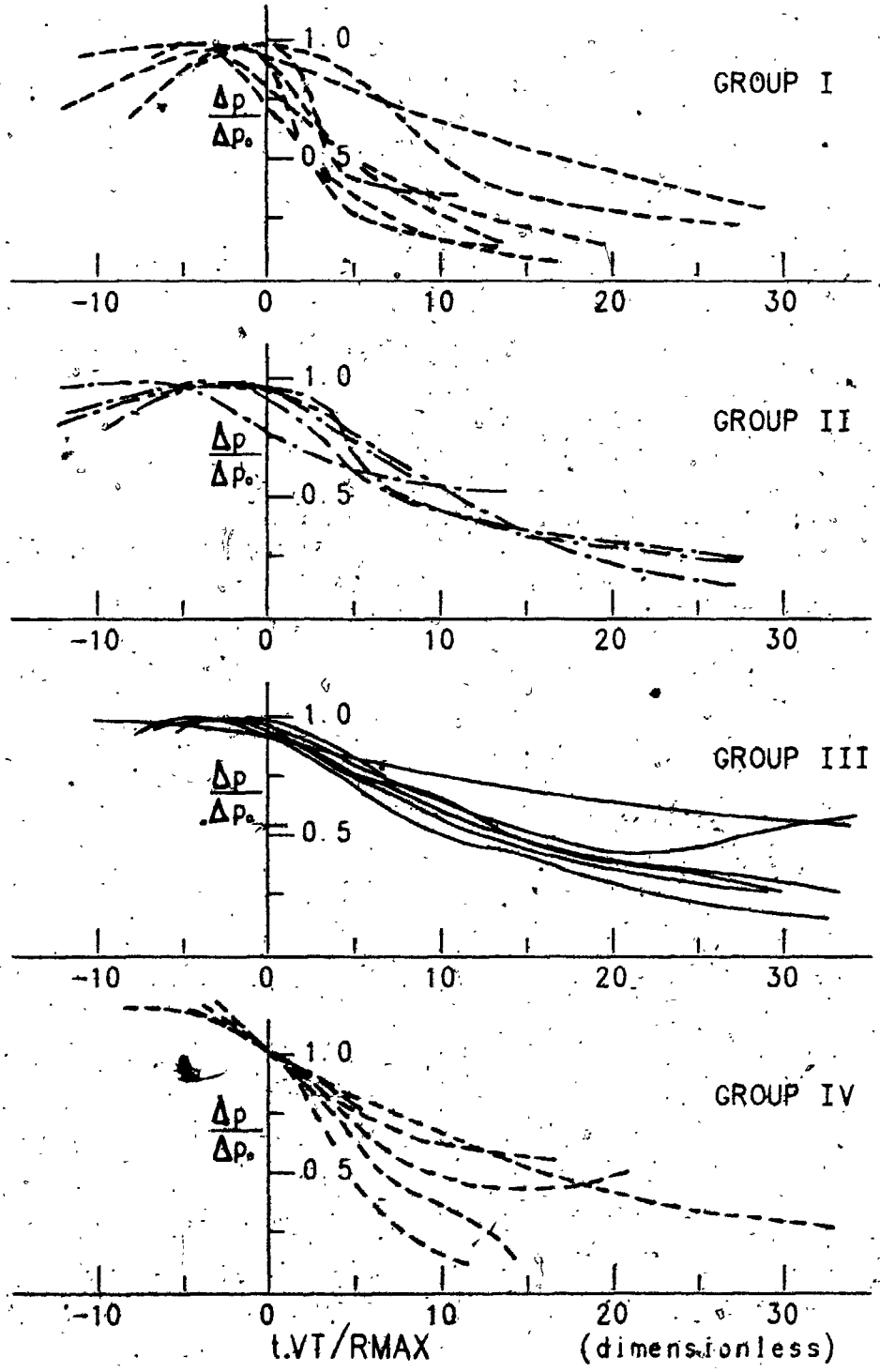

FIGURE 3.13 $\Delta p/\Delta p_o$ **Versus "t.VT/RMAX"**

The mathematical forms chosen have a physical significance. Storms making landfall in Regions I, II and III are typically in a mature, steady-state or sometimes in the process of deepening. Their central pressure is typically observed to be the same or even less than that registered at the time of landfall and a delay is usually observed at the time of landfall before the central pressure begins to rise (see Figure 3.11). For this reason, tropical cyclones modelled in Regions I, II and III are assumed in the simulation windfield model to have a constant central pressure difference while they are over open-water. A bell-shaped polynomial curve is then used after landfall is made. This has the effect of allowing a smooth transition for the onset of central pressure rise at landfall. In contrast, storms on the Atlantic seabord are typically in the process of weakening even before they have made landfall, as they move northwards over increasingly colder waters in the higher latitudes. Following the trend indicated in Figure 3.11 the filling process for storms in Region IV is assumed in the windfield model to be taking place over water as well as over land, and a linear over-water filling rate is followed at landfall by an exponential over-land curve.

The *FD* constant values were subjectively determined to give representative decay curves for each regional group that were slightly on the conservative side of the average of the individual storm curves. The four regional decay curves are shown in Figure 3.14. A transition equation was computed to allow for a smooth change in the filling rate along the coastline between the four groups.

This filling model represents a significant development over ones used in previous simulations. Apart from the choice of a different dependent variable, "*d*" rather than "*t*", the coastline is separated into four basic regional groupings with distinct filling rates and the weakening of storms in higher latitudes over open-water is taken into account.

3.9 Over-Land Surface Speed Reduction Factors

While it is possible to account for the effect of uniform changes in terrain roughness, changes in topography or built-up areas in the centres of large

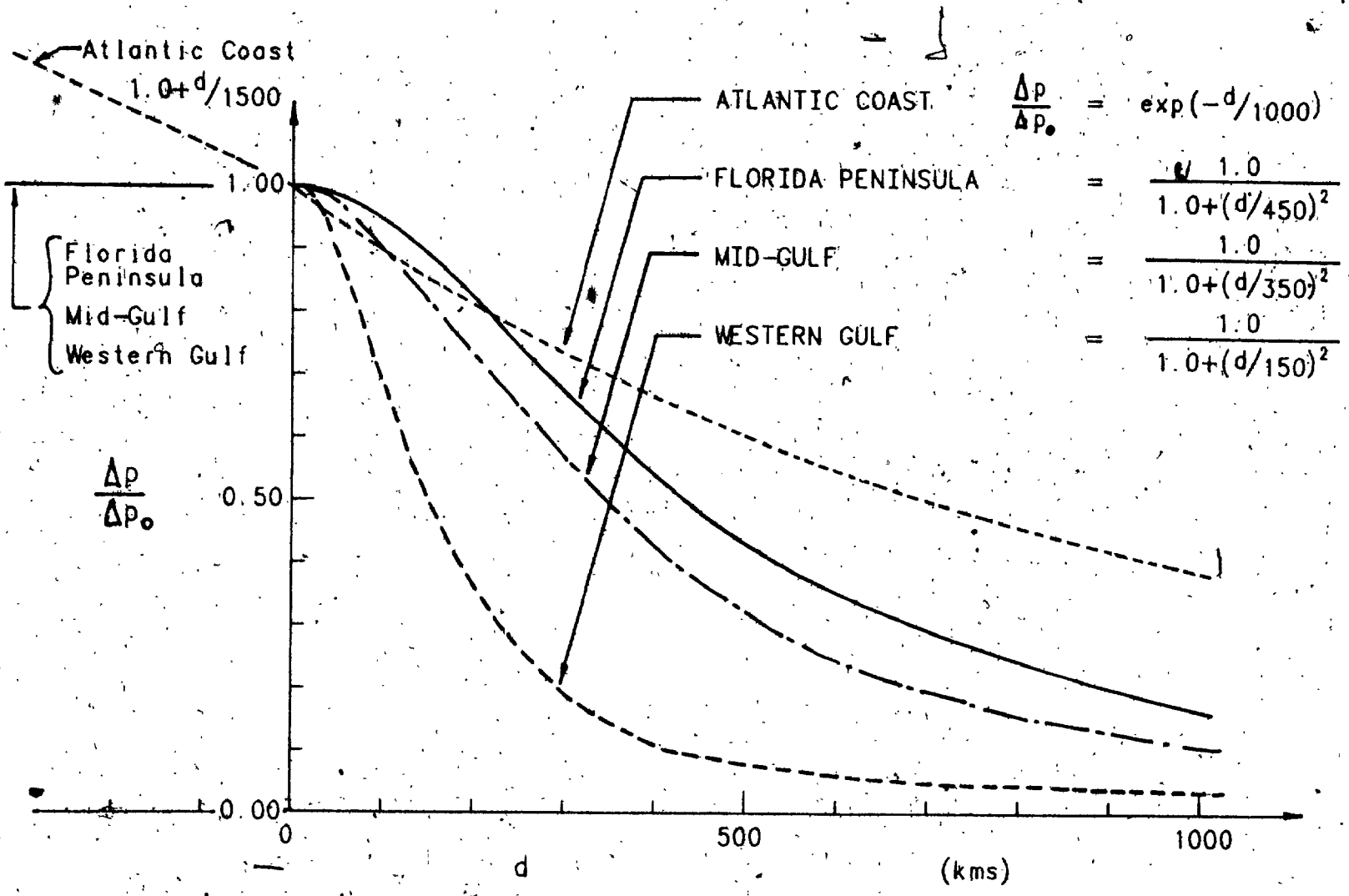

FIGURE 3.14 Smoothed Filling Rate Curves for U.S. Landfalling Storms

cities can induce complicated speed-up and retardation effects. These are beyond the scope of the simulation procedure but may be taken into account by combining the results of the simulation with detailed topographic test results performed in a wind tunnel through some common reference wind speed, typically at a height above the influence of surface friction.

A number of studies (e.g. Schwerdt, Ho and Watkins, 1979) have differentiated between the reduction factors applicable to surface over-land speeds for off-water and off-land trajectories. In contrast, the two recent case studies of Powell (1982) and Powell, Marks and Black (1984) indicate fairly uniform reduction factors for the ratio of over-land to over-water surface (10 metre height) wind speeds, approximately equal to 0.8. These ratios were observed during the landfall of Hurricanes Frederic (1979) and Alicia (1983), and apply to flat, open terrain. The reduction in surface speeds was observed to take place for sites located right on the coastline. Built-up urban areas or dense forest areas would presumably sustain higher reductions in mean surface speeds, as long as the topography remained fairly flat. In the simulation windfield model over-land surface speeds are computed by multiplying the equivalent over-water speed (i.e. at the same value of (r,α)) by a reduction factor defined by :

$$\begin{aligned} \phi_l &= 1.0 - 0.015\,DC && 0 \le DC \le 10.0 \\ &= 0.875 - 0.0025\,DC && 10.0 < DC \le 50.0 \\ &= 0.75 && DC > 50.0 \end{aligned} \qquad \text{E3-13}$$

[redacted] = over-land to over-water surface mean wind speed ratio
= distance inland from the coast (km)

The variation of ϕ_l lies somewhat on the conservative side of the observational data for coastal locations exhibiting generally flat, open terrain. In situations where the topography becomes severe, or in the core areas of large cities, it is recommended that simulation winds are corrected at surface locations with the aid of topographic correction factors computed from wind tunnel or, if available, full-scale speed-up wind measurements. Wind direction over land is computed by adding an inflow angle component to the equivalent over-water value based on the data gathered during the landfall of

Hurricanes Frederic (1979) and Alicia (1983). The increase in surface inflow angle is assumed to be slightly greater near the coastline and is defined as:

$$\begin{aligned} \Delta\gamma_l &= (2.0\,DC)^o && 0 \le DC \le 10.0 \\ &= (22.5 - DC/4.0)^o && 10.0 < DC \le 50.0 \\ &= 10^o && DC > 50.0 \end{aligned} \qquad \text{E3-14}$$

$\Delta\gamma_l$ = increase in inflow angle for over-land location
DC = as per E3-13

3.10 Over-Land Boundary Layer Profile

The 500 metre height windfield in the simulation is only allowed to change in magnitude through the decrease in central pressure difference. Observational data however indicate that the location of the maximum wind speed within the boundary layer increases to well above the 500 metre level. This means that the ratio of 500 metre height over-land to over-water winds should decrease slightly, although not nearly as much as the corresponding surface winds. Hence, leaving the 500 metre height windfield unchanged except for the effect of the reduced central pressure difference is a slightly conservative assumption. Increased friction over land should deepen the boundary layer profile. This would imply that a value for the over-land boundary layer intermediate height, ZI_l, defining the $P(z)$ boundary layer profile function should be greater than that chosen for the over-water windfield.

Opposing these effects are the data discussed in Chapter 2, which indicate the possibility of enhanced inflow and consequently higher winds close to the ground in the immediate landfall area to the front and right of the landfall location. Increased winds near the surface can also result from the enhanced downward transfer of momentum within rainbands, particularly the primary bands close to the eyewall. These features are handled in the simulation windfield model by defining an over-land intermediate height, ZI_l, such that:

$$ZI_l = 100.0 \qquad -90^o < \alpha < 90^o \qquad E3\text{-}15$$
$$0 \le DC \le 50.0.$$
$$-2.5\,RMAX \le RC \le 5.0\,RMAX$$

$$= 250.0 \qquad 90^o < \alpha < 270^o$$
$$DC > 50.0$$
$$RC < -2.5\,RMAX \quad RC > 5.0\,RMAX$$

RC = distance along coastline to the right *(+ve)* and left *(-ve)* of the landfall point *(km)*

The boundary conditions placed upon the ZI_l values allow for a variation in boundary layer profile as the storm is approaching land. Greatest inflow and hence the lower value of ZI_l occurs in the front of the storm *($-90^o \le \alpha \le 90^o$)*, as far as 50 km inland *($DC \le 50$ km)* and over a slightly greater area to the right of the storm than to the left *($-2.5RMAX \le RC \le 5.0RMAX$)*. Further than 50 km inland the higher value of ZI_l is adopted. In between, a linear transition is applied. The effect of this variation in ZI_l value is to produce somewhat conservative speeds within the tropical cyclone boundary layer for locations situated close to the coastline as a storm is approaching, conservative in the sense of being somewhat greater than their open-water equivalents.

3.11 Parameters Required by the Proposed Simulation Windfield Model

The over-water windfield model begins with the specification of the gradient balance circulation. The SHBL model windfield is then generated using the same pressure gradient and storm parameters. SHBL model wind speeds and directions are converted to define the 500 metre level circulation. The surface windfield is determined by factoring the 500 metre height wind speeds through the ϕ_w function and using the SHBL model wind directions directly. Within the boundary layer, the vertical wind speed profile is computed using the logarithmic transition curve, $P(z)$, after specifying the intermediate height value, $ZI\bar{w}$. At landfall the windfield is adjusted by reducing the central pressure difference using the filling rate relationships,

factoring the 10 metre height speeds by ϕ_l and fixing the over-land value of ZI_l according to the site location. The parameters required by the windfield model may be split into model constants and storm parameters. These are listed in Table 3.1.

The latter group of storm parameters are referred to as tropical cyclone characteristic parameters. During the execution of a simulation at a particular site, the model constants do not vary from storm to storm. It is the characteristic parameters which are generated in a probabilistic manner during the simulation that give rise to the ensemble of tropical cyclones used to reconstruct the tropical cyclone wind climate at the site of interest. To these windfield characteristic parameters must be added those which define the occurrence of storms at any particular location in both time and space. These will be discussed in Chapter 5.

TABLE 3.1

WINDFIELD MODEL PARAMETERS AND FUNCTIONAL RELATIONSHIPS

Model Constant Parameters :

ρ	=	air density	
f	=	Coriolis parameter	functions of
B	=	pressure profile exponent	latitude
FD	=	filling rate constant	
Cd	=	drag coefficient	
K	=	eddy diffusion	
Φ_w	=	over-water surface to 500 metre height mean wind speed ratio	
ZI_w	=	over-water boundary layer intermediate height	
Φ_l	=	surface over-land to over-water mean wind speed ratio	
$\Delta\gamma_l$	=	added-surface over-land inflow angle component	
ZI_l	=	over-land boundary layer intermediate height	

Storm Parameters :

Δp	=	central pressure difference
$RMAX$	=	radius of maximum winds
VT	=	translation velocity

CHAPTER 4

EVALUATION OF PROPOSED TROPICAL CYCLONE WINDFIELD MODEL

4.1 General

In the current study an attempt was made to base the simulation windfield model on an extensive data base of reliable tropical cyclone observations. The model is now evaluated by comparing wind speeds and directions predicted by the model with actual wind traces recorded during tropical cyclone events. Comparisons include storms from the North Atlantic, Northwest Pacific and Australian regions. While many such anemometer records are available, only few are located in areas where reasonable correction factors can be estimated to convert observed speeds to a common reference height and standard averaging time.

The mean wind speed and direction histories chosen for comparison were determined from the raw anemometer data by smoothing the records to extract the "sustained" wind (a form of running average) characterizing the steady-state behaviour of the storm and representative of mean winds with averaging times of 10-20 minutes. The model-predicted wind speeds and directions were computed assuming constant values of the storm parameters, $(\Delta\tilde{p}, RMAX, VT, \theta, DMIN)$, usually assigned their landfall values. While this placed a constraint on the ability of the windfield model to correctly reproduce the observed wind speeds and directions, the wind traces thus calculated were the same as would be created during a simulation given the respective landfall data values.

4.2 North Atlantic Hurricanes

Particular emphasis is laid in this section on two recently occurring hurricanes, Frederic (1979) and Alicia (1983). Uniquely for the North Atlantic, wind records obtained during these storms were subjected to

intensive study and corrected to standard averaging times and heights. In addition, these two storms were part of the Hurricane Landfall Program run by the Hurricane Research Division of A.O.M.L. (Miami), so that a multitude of data including aircraft observations, ocean buoy data, radar data and land station records were assimilated and analyzed. It was thus possible not only to compare wind speeds and directions predicted by the simulation windfield model to individual anemometer station observations, but to compare the circulation as a whole using observed "composite" windfields and model circulation windfields at the centre of the composite period.

(i) Hurricane 'ALICIA'

Alicia developed from a weak low-pressure area into a tropical storm at 1800 Greenwich Mean time (GMT) on August 15, 1983 in the central Gulf of Mexico, about 350 km south of New Orleans. Alicia became a hurricane at 00 GMT on August 17 while moving slowly northwestward with a translation speed varying between 2.0 to 5.0 m/sec. Landfall was made at 0730 GMT at the southwest tip of Galveston Island, at which time Alicia was moving north-northwestward at about 4.0 m/sec. The central pressure dropped to its minimum value of 962 mb just after landfall at 0840 GMT. The storm then passed very close to Alvin before moving over the western sectors of Houston from 1230 to 1400 GMT. At the point of closest approach, Alicia's wind centre lay approximately 12 km to the west of the downtown Houston area. Figure 4.1 shows the storm track and location of several of the land stations from which were recovered wind records.

A number of individual wind trace comparisons are made first. These were chosen from the 17 sites analyzed by Marshall (1984), who determined correction factors for the local exposure conditions and type of instrumentation at each of the sites. Those shown here are considered to be relatively unaffected by the surrounding urban or land topography and represent original records at heights of 10 metres and greater above the ground. Four comparisons are shown in Figures 4.2a-d, for the records obtained from (a) U.S. Coast Guard Cutter Buttonwood, (b) Baytown Exxon Tower, (c) Dow Chemical Plant "A" and (d) Houston Intercontinental Airport respectively. These four sites were not only located in relatively unobstructed

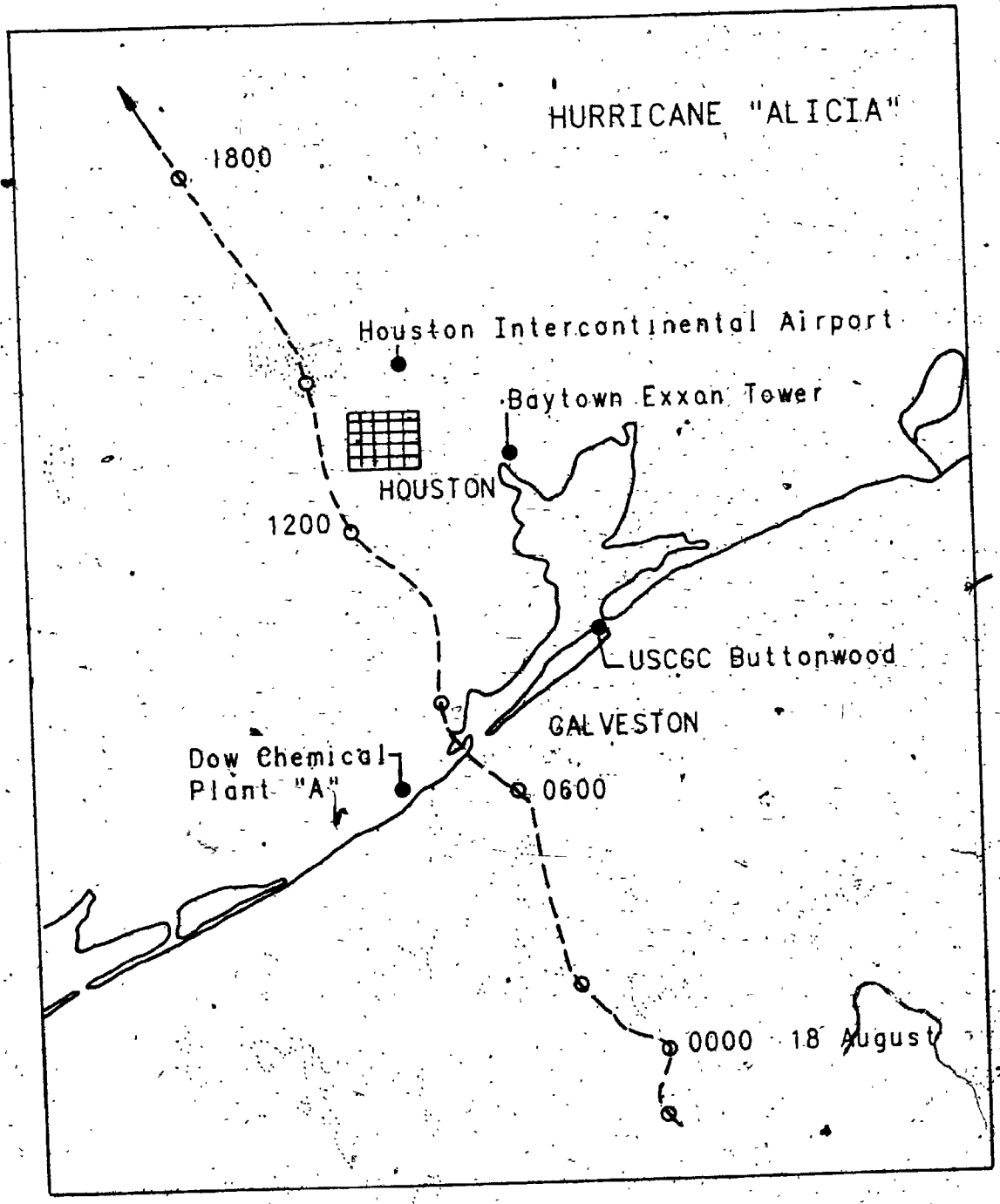

FIGURE 4.1 Hurricane Alicia Location Map

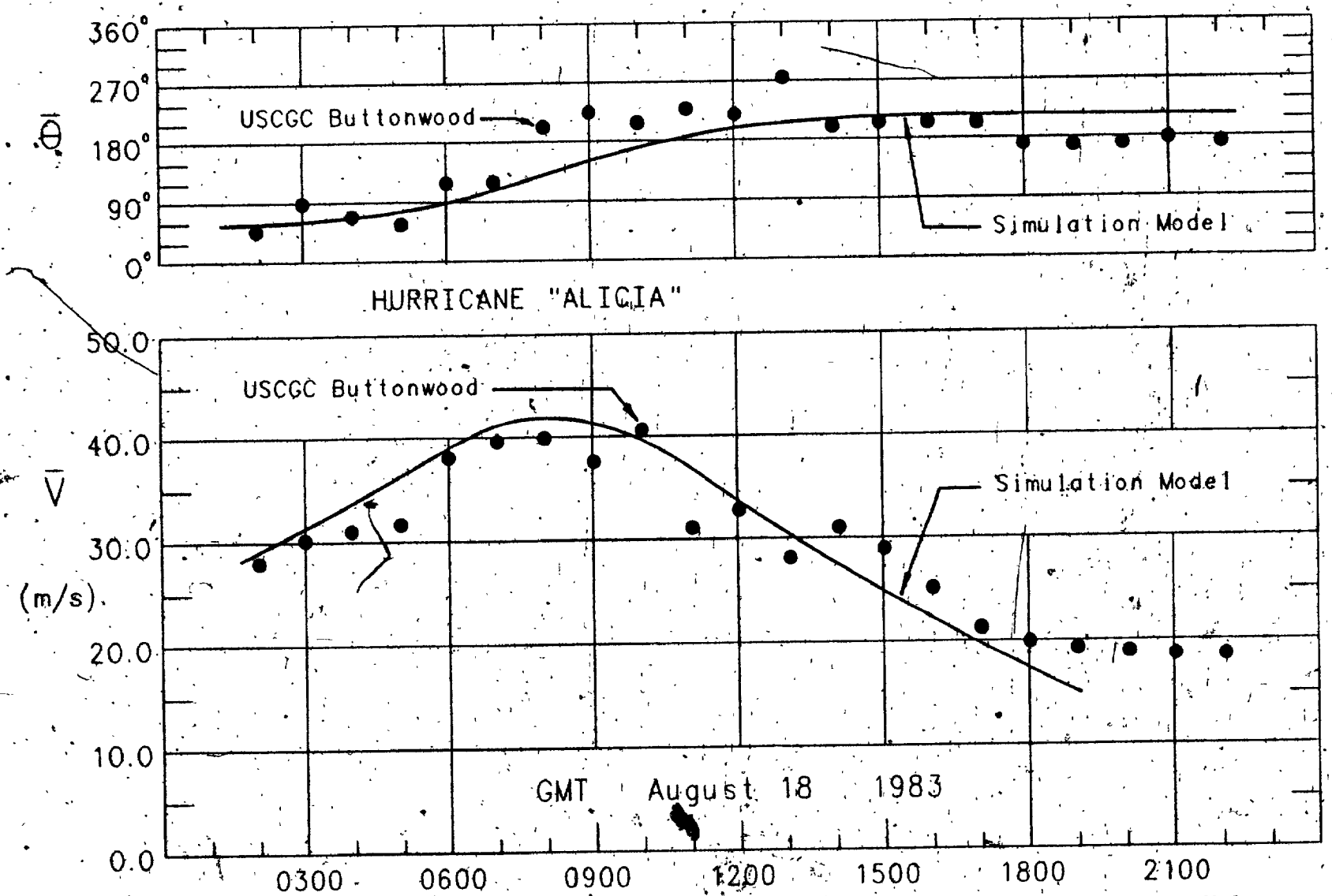

FIGURE 4.2 **Comparison of Observed and Model-Predicted Wind Speeds During Hurricane Alicia**
(a) U.S.C.G.C. Buttonwood Record

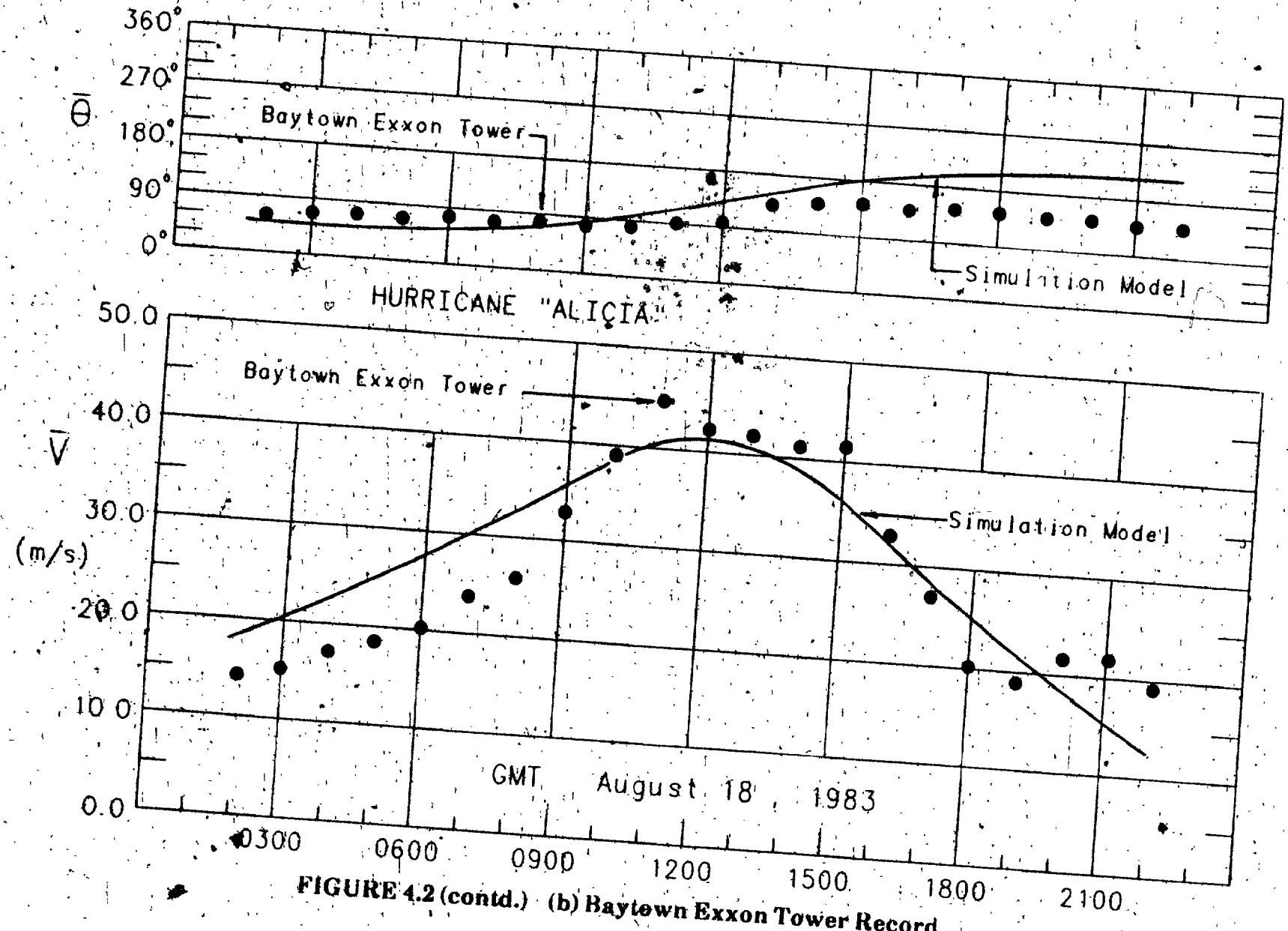

FIGURE 4.2 (contd.) (b) Baytown Exxon Tower Record

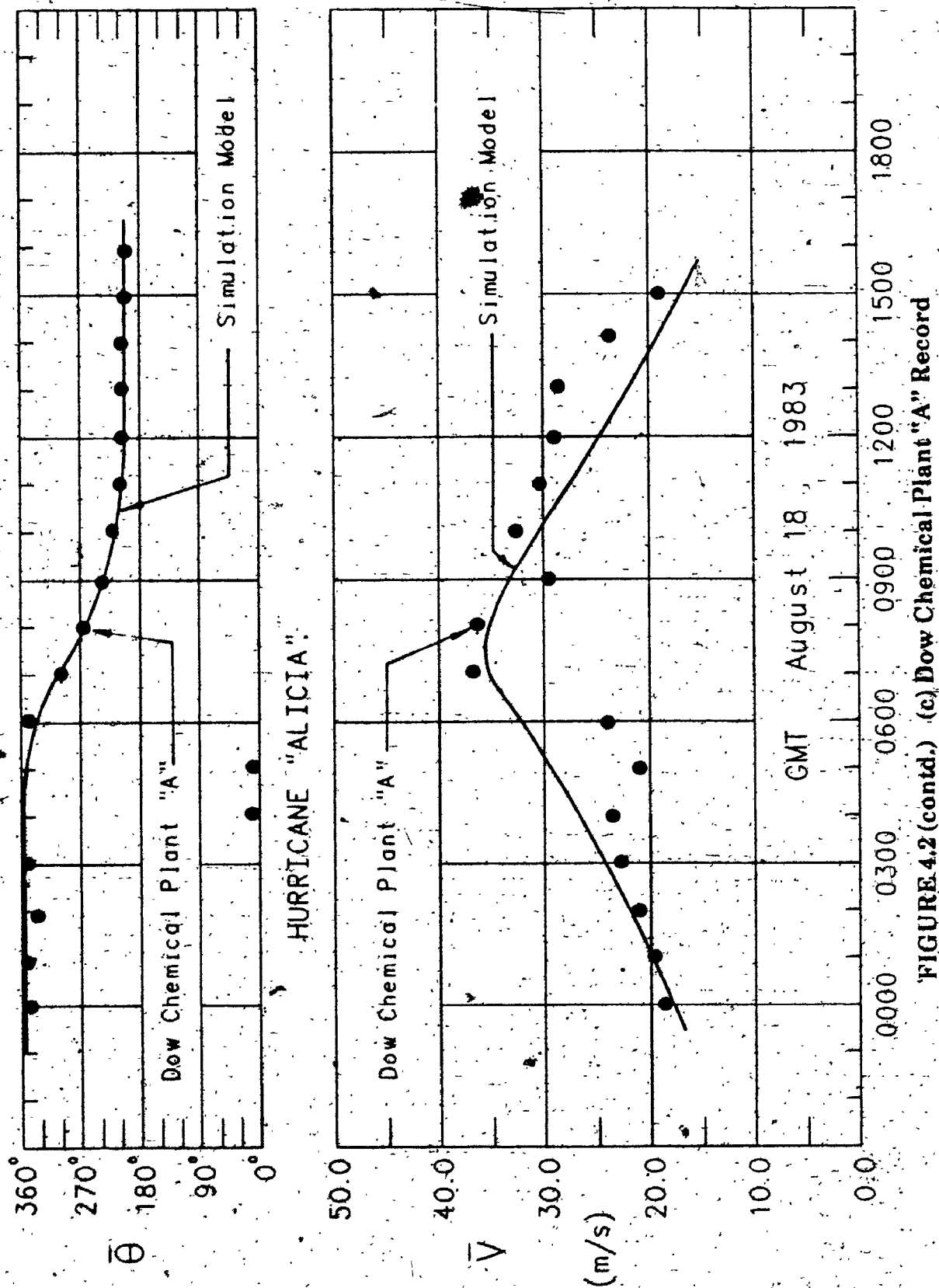

FIGURE 4.2 (contd.) (c) Dow Chemical Plant "A" Record

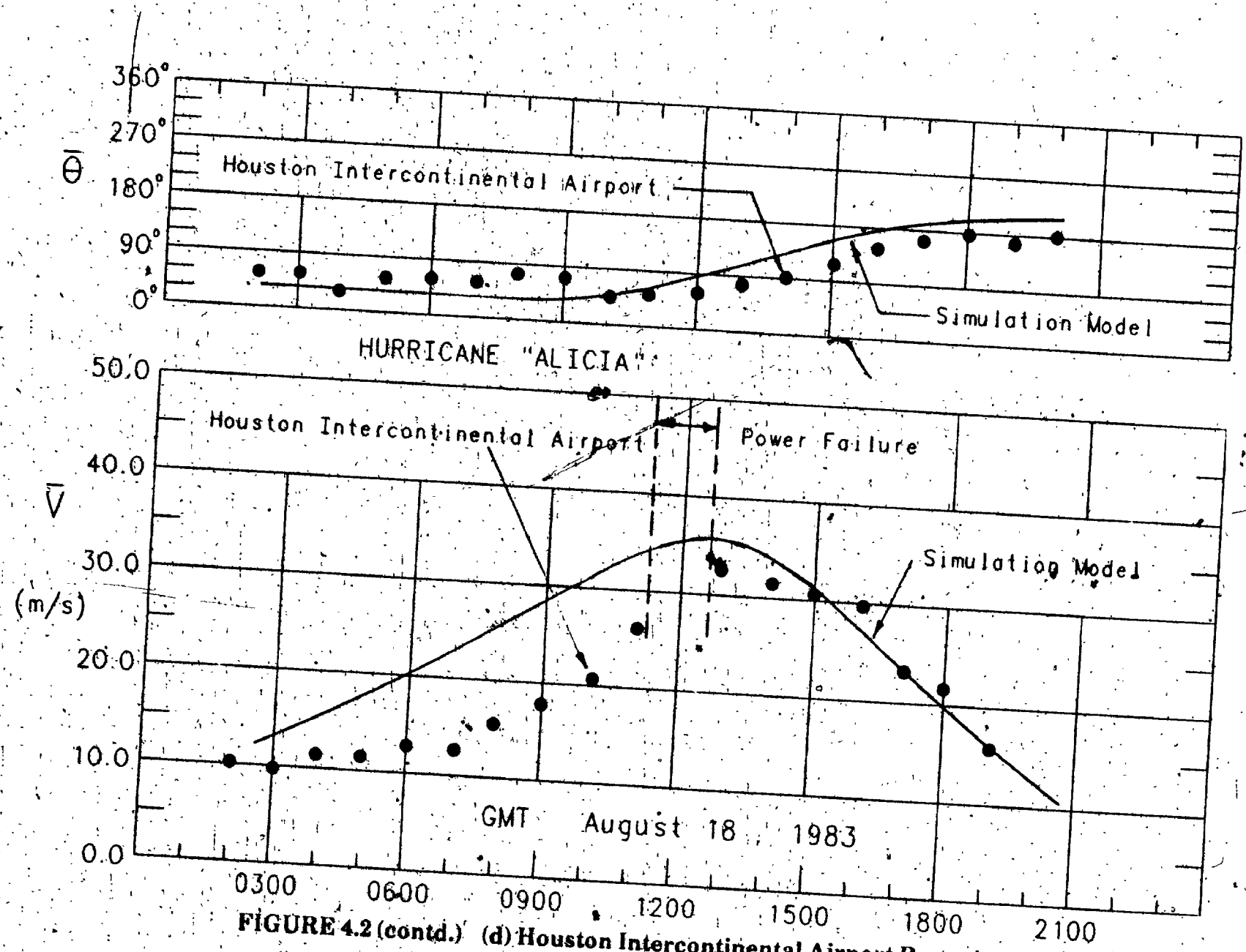

FIGURE 4.2 (contd.) (d) Houston Intercontinental Airport Record

exposures, but cover a large area affected by Alicia both at the coastline to the right and left of the landfall position and some distance inland.

In each case a comparison is made between the over-land 10 metre height wind speed and direction predicted by the simulation windfield model and that computed from the converted anemometer data. Some errors are expected to arise from the limitation imposed upon the simulation windfield model of having to specify constant values for Δp, *RMAX*, *VT*, θ and *DMIN* throughout the passage of the storm, during which time several of the actual parameters fluctuated significantly. Maximum wind speeds are well-predicted for the U.S.C.G.C. Buttonwood record although the observed wind directions vary, both greater and less than the predicted ones, by in some cases over 60°. The Baytown Exxon Tower wind speeds are slightly under-estimated by the simulation model at the time of the maximum winds and over-estimated prior to that point. This record exhibits a sharper wind profile than indicated by the model and may be related to the strong rainband activity occurring in the Baytown area at the time. Wind speeds are also slightly under-estimated at the maximum point for the Dow Chemical Plant "A" record although the wind directions are faithfully reproduced. The higher than predicted winds at this site may be due to the secondary wind maximum that was located in the left quadrant of the storm as it approached land (see Figure 4.3). Wind speeds are over-estimated for the Houston Intercontinental Airport site prior to the point of closest approach and well predicted subsequently.

Such specific comparisons must be assessed bearing in mind the local mesoscale variations in the windfield, particularly the presence of rainband activity. Hurricane Alicia's circulation was significantly affected after landfall by the strong convective activity in the storm. Intense rainbands outside the radius of maximum winds kept forming in the southeast quadrant and propogating in a counter-clockwise and outwards sense relative to the storm centre. These rainbands contributed to the formation of secondary wind maxima, producing high winds at the eastern end of Galveston Island and in the Baytown area even though these locations were well away from the radius of maximum winds.

With the great amount of data gathered during the storm's passage, it was possible to check other features of the simulation windfield model. Figure 4.3 shows the over-water 1600 metre level composite windfield for Alicia seven hours before landfall was made. The height of this composite windfield lies roughly midway between the gradient balance height (700 mb) and the 500-metre height. Secondary wind maxima to the right and left of the storm circulation in addition to the primary maximum in the front quadrant can be seen. However it may be noted that most of the high winds lie to the front and slightly to the right of the storm centre and that the streamlines are almost circular, indicating that the tangential component of the horizontal wind vector was close to gradient balance. An azimuthally-averaged tangential wind profile was computed from the above composite windfield, shown in Figure 4.4. After the storm translation velocity had been subtracted from wind vectors in all quadrants, the wind speeds were converted to 10-minute means taking into account the aircraft speed (110 m/sec) and the aircraft data averaging time (30 seconds). Also shown in Figure 4.4 is the profile that would have been obtained assuming gradient balance with a storm central pressure of 966 mb and radius of maximum winds equal to 28 km, the observed values at the time. The agreement between the actual profile and the theoretically derived gradient balance profile is good, particularly at the radius of maximum winds.

Hurricane Alicia was not one of the storms analyzed in section 3.8 determining filling rates for North Atlantic tropical cyclones. Thus it could be used to independently check the validity of the decay model used in the simulation. Figure 4.5 shows the decrease in central pressure difference after landfall was made and that predicted by the windfield model for Region I category filling. The initial bell-shaped form of the simulation filling model is supported by the observed data and the central pressure difference drop is well predicted if just slightly conservative during the first few hours after landfall.

(ii) ALLIED BANK PLAZA Case Study

A unique opportunity arose with the passage of Hurricane Alicia past downtown Houston, created by the fortuitous recording of the accelerations on the top floor of the Allied Bank Plaza building during Alicia's approach. The

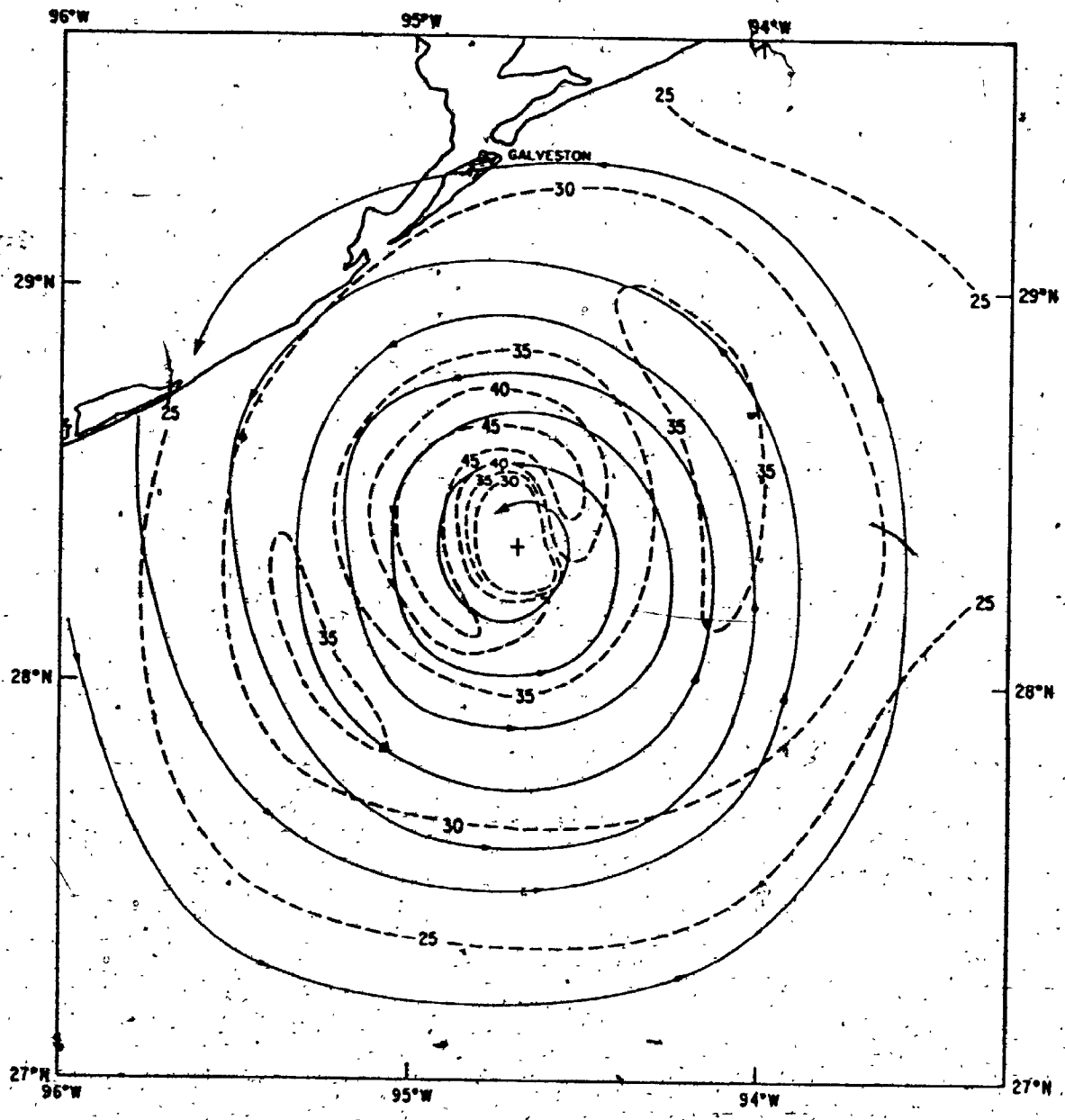

FIGURE 4.3 1600 Metre Height Streamline and Isotach Composite Analysis for Hurricane Alicia, Centred on 0300 GMT August 18 1983 (Powell, Marks and Black, 1984)

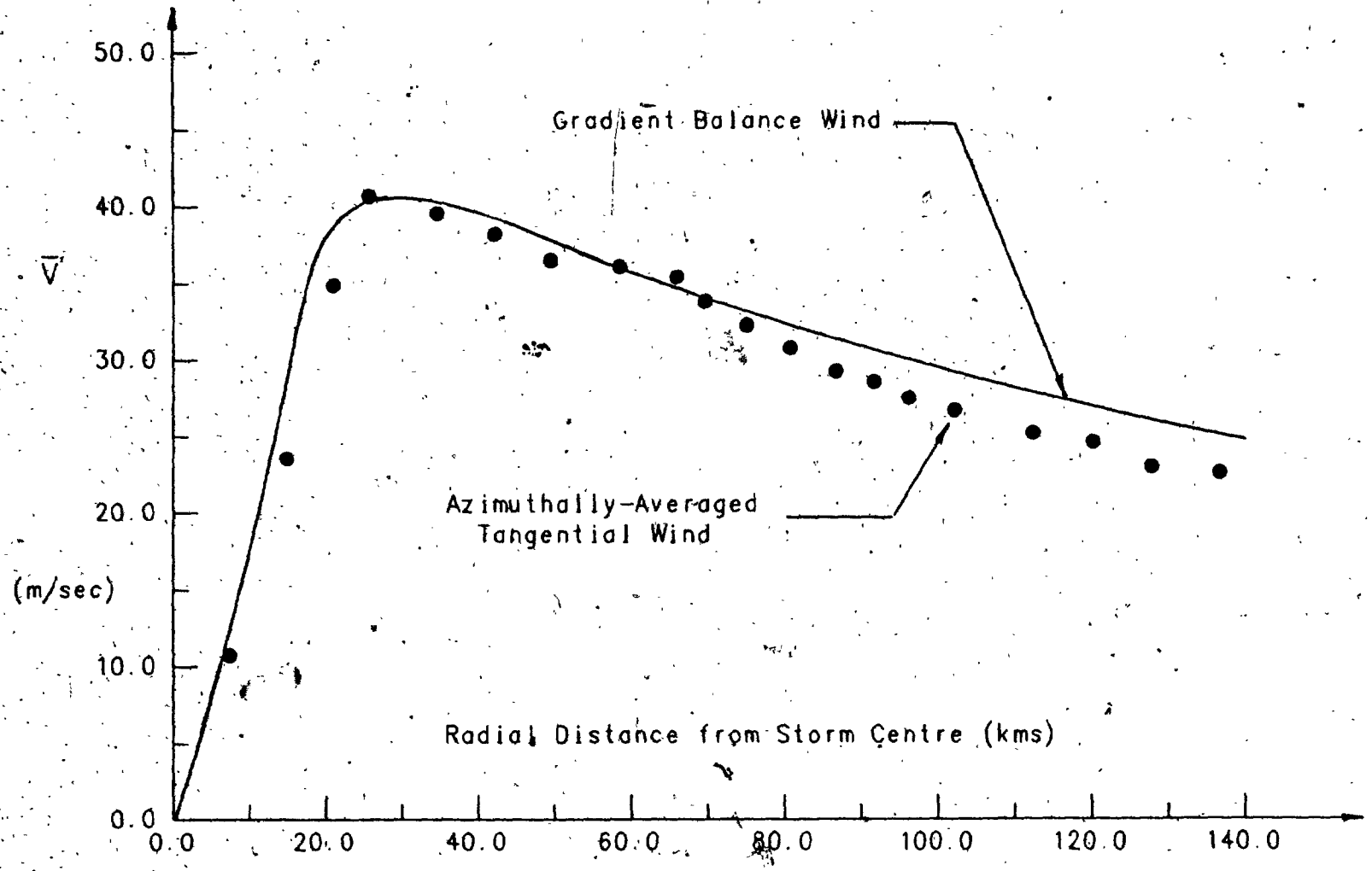

FIGURE 4.4 **Comparison of Alicia Over-Water Azimuthally-Averaged Tangential Wind Profile With Gradient Balance Wind Profile**

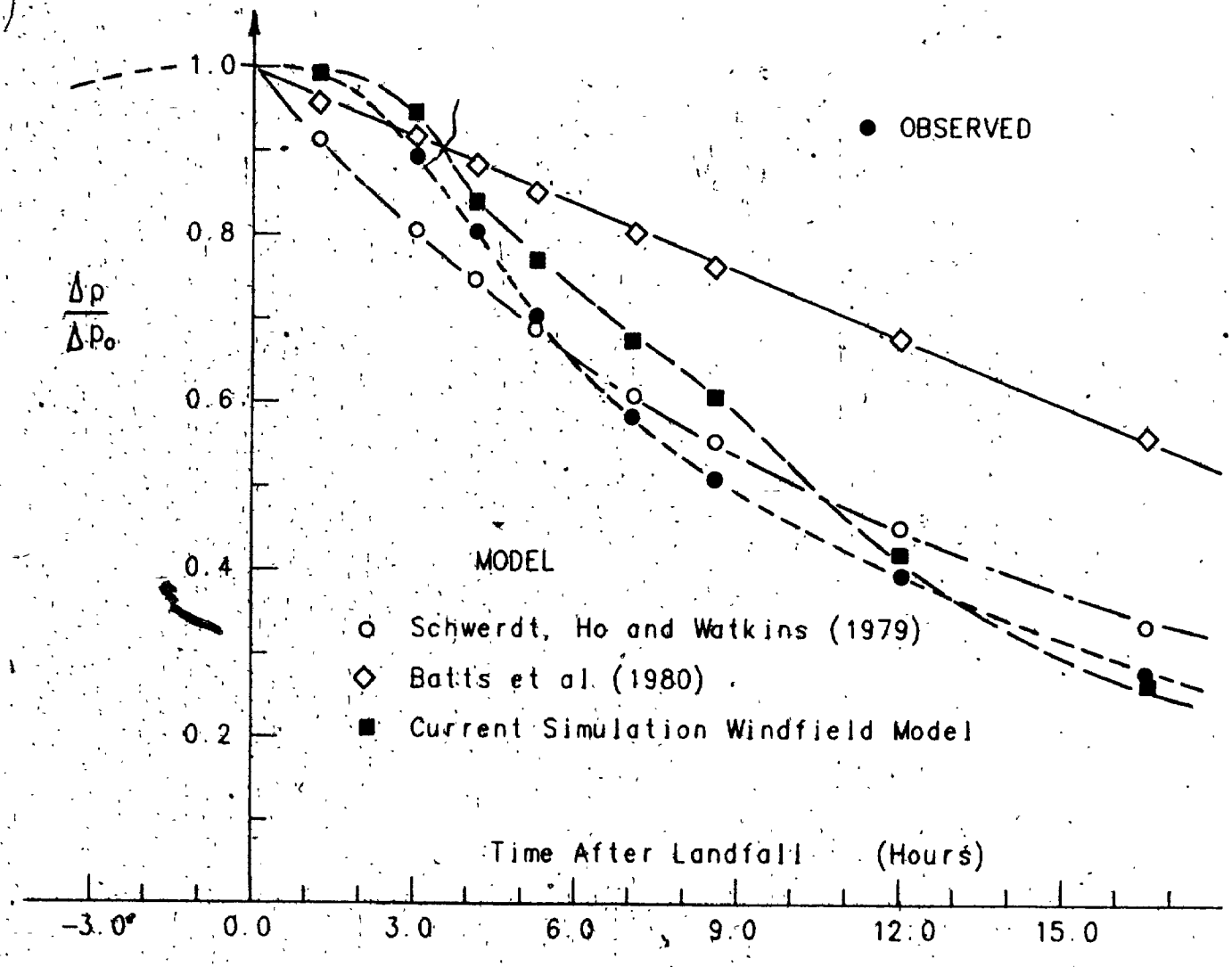

FIGURE 4.5 Comparison of Actual Filling Rate Behaviour for Hurricane Alicia With Several Theoretical Models

Allied Bank Plaza, a 71-storey structural steel office tower, became the tallest building in the downtown Houston area when it was completed in late 1982. A wind tunnel study was carried out at the Boundary Layer Wind Tunnel Laboratory of the University of Western Ontario, to provide information on the wind-induced response of the tower in a variety of wind conditions, including severe events such as hurricanes. As part of this study, accelerometers were mounted on the top floor of the tower to monitor the dynamic behaviour of the building. Despite the extreme hazard evident at the time, personnel from the consulting firm responsible for the architectural and structural design of the building, Skidmore, Owings and Merrill, were able to reach the top of the building and operate the accelerometers manually. An acceleration record was obtained lasting approximately 90 minutes just before the peak of Alicia's influence on the Houston downtown area. The coincidence provided by the availability of the wind tunnel test information for the building and the recording of the accelerations sustained during the storm led to the idea of reconstructing the windfield "seen" by the building during Alicia's passage to obtain estimates of the accelerations and to compare these with the actual measured ones.

The wind speeds and directions experienced at the Allied Bank Plaza site were reconstructed from the large data base of meteorological information gathered through the Hurricane Landfall Program previously mentioned. Much of this information is reported in Powell, Marks and Black (1984). The Allied Bank wind trace was developed by moving forward composite windfields of the type shown in Figure 4.3 taking into account the relative position of the Bank site. Several nearby anemometer stations were used to supplement these data to determine the local wind speeds and directions. Details of the reconstruction can be found in Powell, Georgiou, Isyumov and Halvorsen (1985). The estimation of the Bank site wind history clearly contains a large degree of subjective analysis. However, by simultaneously computing what an equivalent upper-level, open-water trace and surface, inland trace would have appeared as, reasonable upper and lower bounds could be established for the variation of wind speeds and directions at the site. The final reconstructed wind history is shown in Figure 4.6. The estimated accuracy of the wind trace is ± 5.0 m/sec for the speeds and $\pm 10^{\circ}$ - 20° for the wind directions.

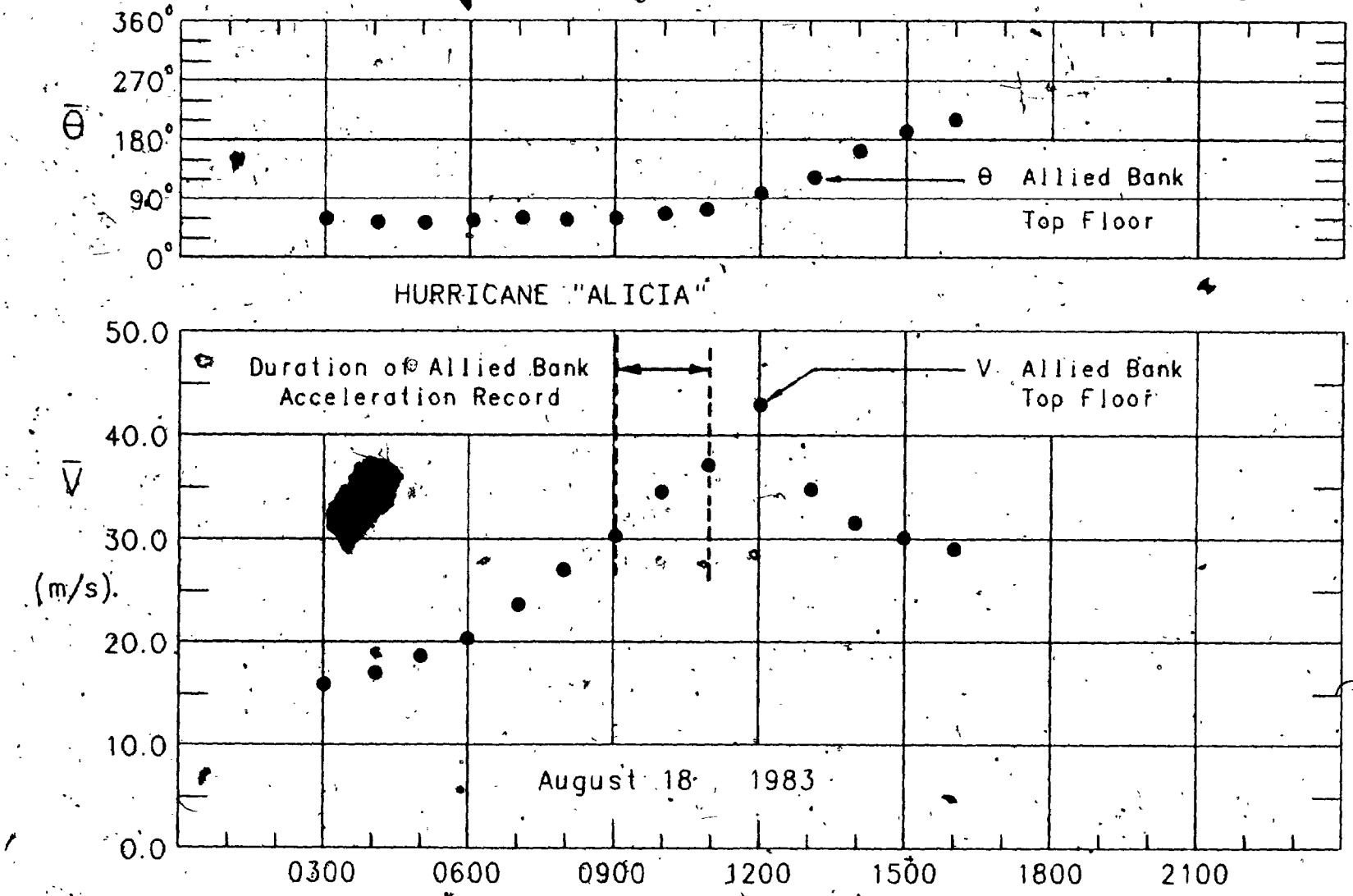

FIGURE 4.6 **Reconstructed History of Wind Speeds and Directions Experienced at the Allied Bank, Downtown Houston, During Hurricane Alicia**

The wind tunnel model studies carried out for the Allied Bank Plaza tower are described in detail in Isyumov and Churth (1980a,b). They included aeroelastic model tests, an example of which is shown in Figure 4.7 showing resultant sway accelerations of the building at a full-scale height of 275 metres. Corrections were made to account for differences in the fundamental vibration modes and structural damping values between the wind tunnel test and those observed from the acceleration traces, to adjust the wind tunnel test data accelerations to the accelerometer height and to adjust the wind tunnel gradient wind speed reference value to reflect the different boundary layer profile during the passage of the storm. The resultant acceleration data was then subjected to the reconstructed wind history at the site and the resultant peak sway accelerations calculated. To allow for uncertainties in the wind conditions at the site, accelerations were computed for a range of possible speeds and directions (± 2.5 m/sec and $\pm 5°$ respectively). The upper and lower bounds of the estimated accelerations are shown in Figure 4.8.

Also plotted in Figure 4.8 are the accelerations that would have been predicted by the simulation windfield model given the storm Δp, *RMAX*, *VT*, θ and *DMIN* values at the landfall point, coupled with the wind tunnel test data. In an actual computer simulation, these accelerations would be the ones generated by the model for a storm with Alicia's landfall characteristics. The comparison of the accelerations utilizing the reconstructed wind history with the actual observed accelerations is excellent, most of the points falling near the middle of the bounded range. The accelerations predicted using the simulation windfield model-generated estimates do not fare quite as well, in particular during the latter stages of the storm's passage. This is predominantly due to the inability of the simulation model to account for the unique rainband activity that accompanied Alicia and which undoubtedly affected the winds experienced in the downtown Houston area. Considering the errors introduced by this limitation, the estimated accelerations show encouraging agreement. The good agreement however between the observed accelerations and those predicted using the reconstructed wind history provides a unique and valuable validation of wind tunnel model studies, illustrating the reliability of wind tunnel modelling within the design process for tall buildings.

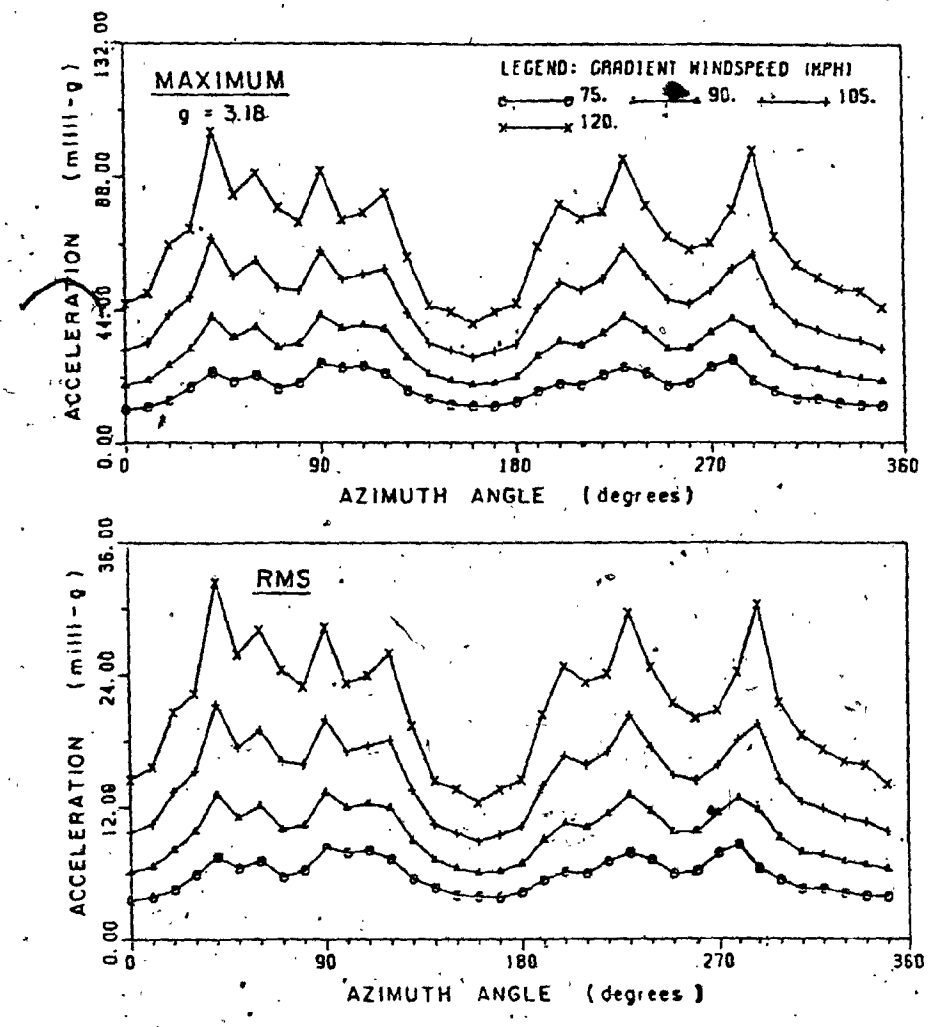

FIGURE 4.7 **Wind Tunnel Aeroelastic Model Test Results; Resultant Sway Accelerations at the 900-Foot Level of the Allied Bank, Houston. (Structural Damping equal to 1.5%) (Isyumov and Church, 1980)**

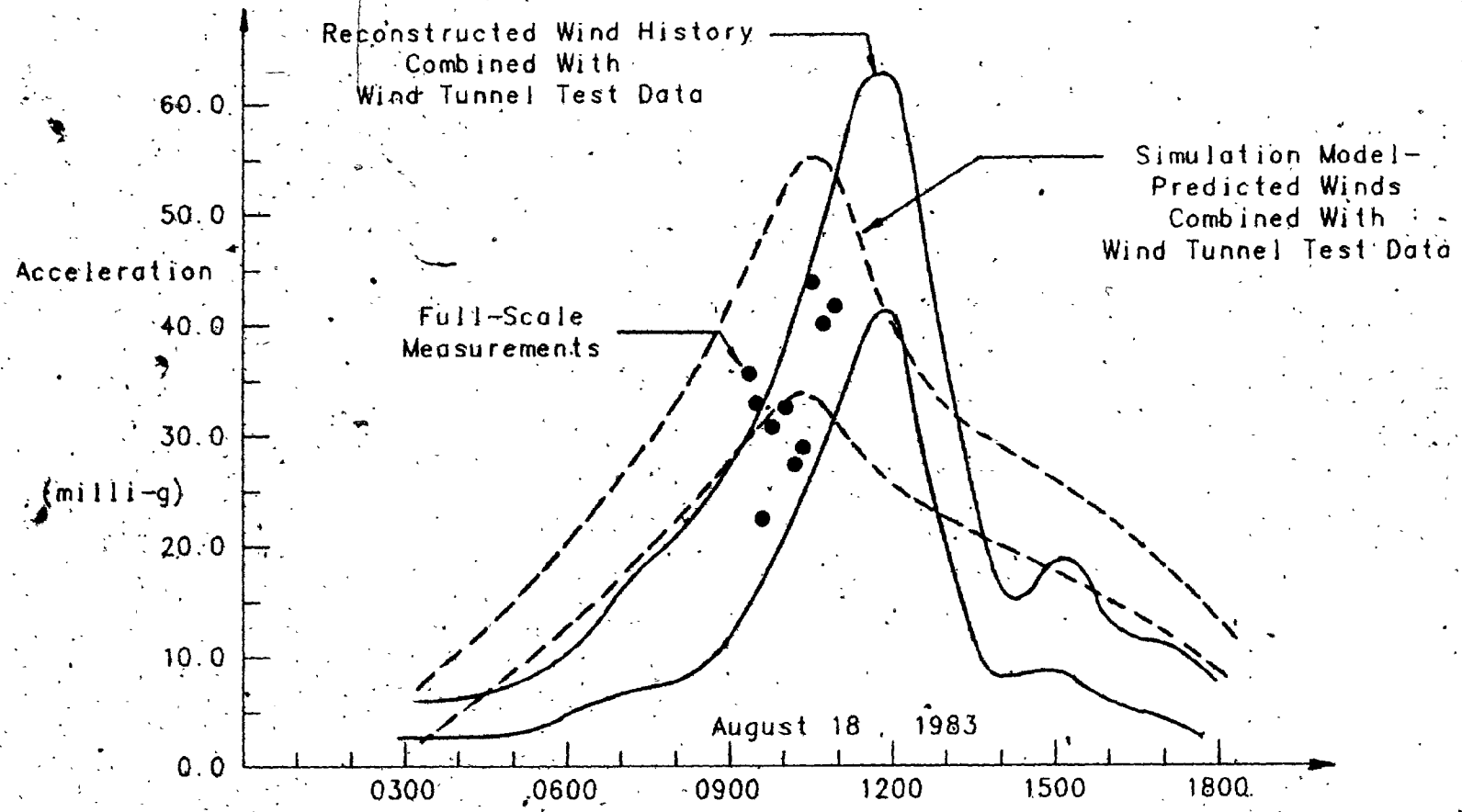

FIGURE 4.8 **Comparison of Observed and Predicted Peak Accelerations at the 71st Floor of the Allied Bank During Hurricane Alicia**

(iii) Hurricane "FREDERIC"

Hurricane Frederic moved through the Caribbean during the beginning of S[redacted]er 1979. As it passed the islands of Puerto Rico, Hispaniola and [redacted]rederic remained relatively weak. On leaving the northwest coast of Cuba on September 10, the storm intensified rapidly as it moved over warm Gulf waters. By the time Frederic made landfall just to the east of the Mississippi-Alabama border the central pressure had fallen from 980 mb off the coast of Cuba to 946 mb at landfall. Frederic's track approaching the coastline is shown in Figure 4.9. The landfall storm translation velocity was 6.4 m/sec.

Hurricane Frederic was the first U.S. landfalling tropical cyclone to be part of the HRD Hurricane Landfall Program. Some of the information gathered as a result of this Program was discussed in Chapter 2. In particular, it was shown that Frederic's 500 metre over-water windfield strongly resembled the basic qualitative features of the Shapiro numerical model circulation used in the current simulation windfield model.

Since much of the data gathered during Frederic's occurrence formed the basis of various sections of the simulation windfield model, independent assessment of the model is restricted in this section to comparisons of observed and model-predicted wind speeds and directions for land stations in the Pascagoula, Mississippi to Mobile, Alabama area. A description of some of these sites may be found in Reinhold (1981). Figure 4.9 also shows the location of the Dauphin Island Bridge (DIB) and Ingalls Shipbuilding (ISB) anemometers and Pensacola Regional Airport (PRA), the stations chosen for comparison. The wind speed comparisons are shown in Figures 4.10a-c for the DIB, ISB and PRA records respectively. In both the DIB and ISB comparisons the second wind maximum is over-estimated by the simulation windfield model. The maximum winds for all three sites are generally well predicted, two cases showing under-estimates of 5-10%. Wind directions after landfall are generally less well modelled than those at and before landfall.

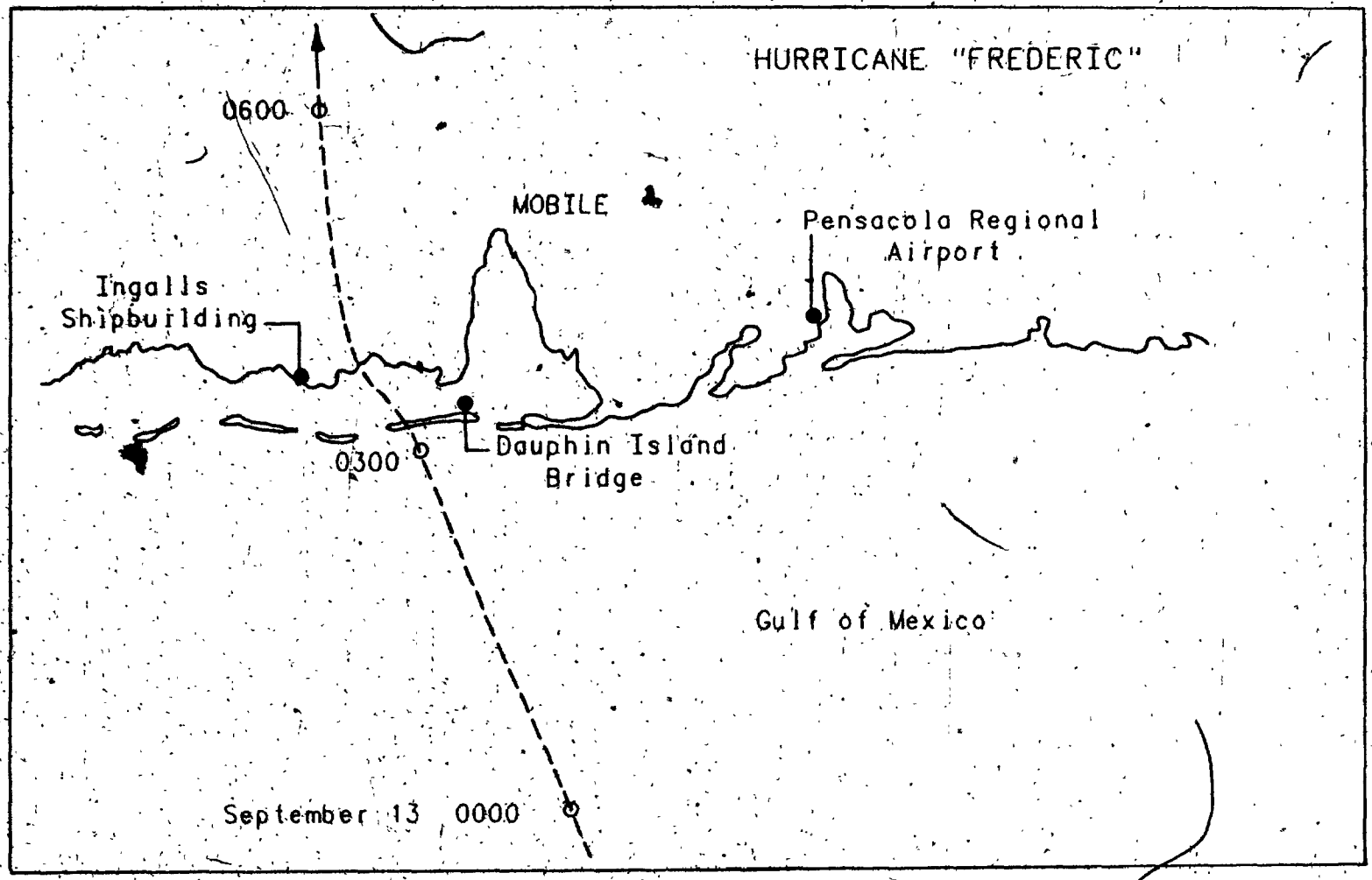

FIGURE 4.9 Hurricane Frederic Location Map

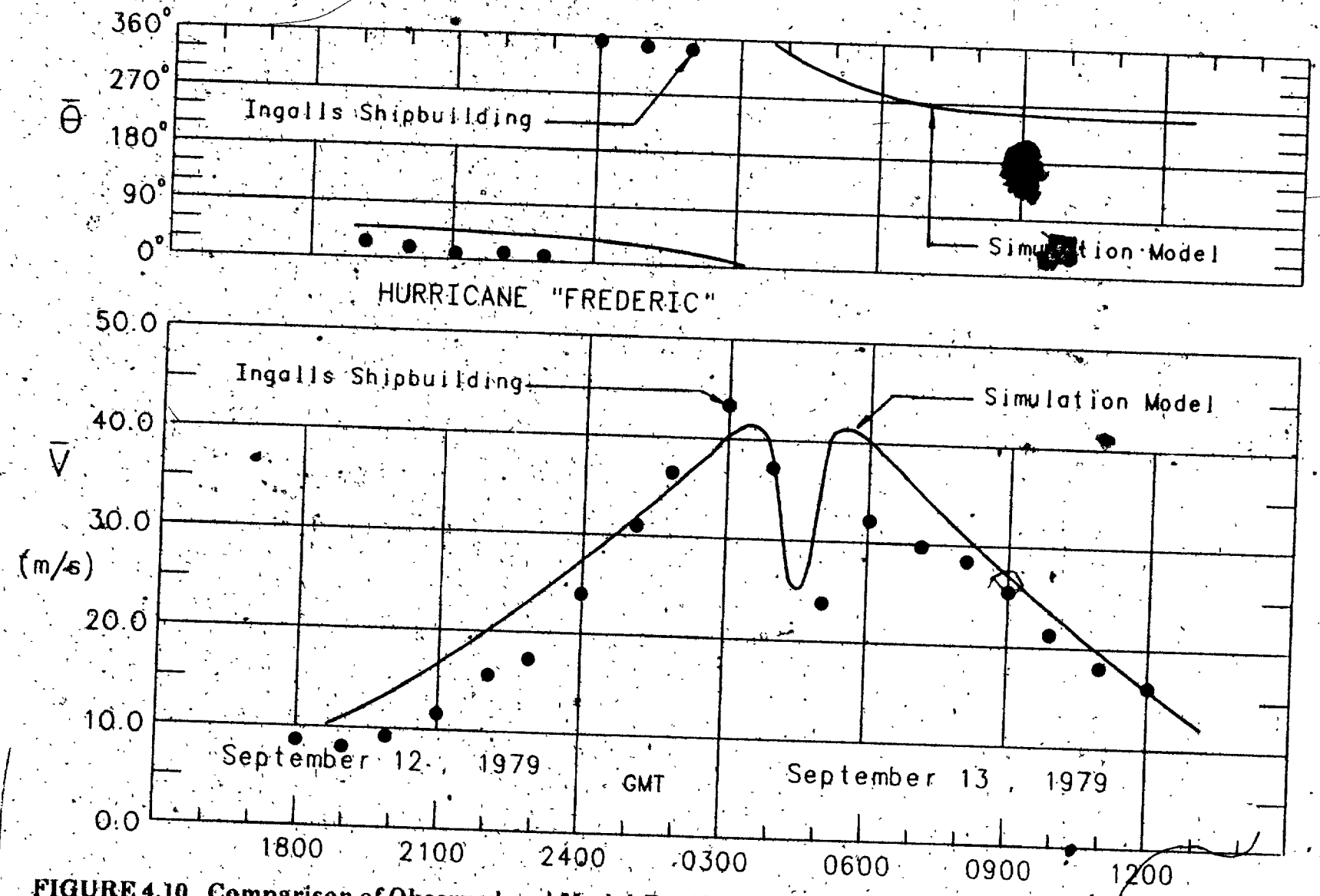

FIGURE 4.10 Comparison of Observed and Model-Predicted Wind Speeds During Hurricane Frederic
(a) Ingalls Shipbuilding Record

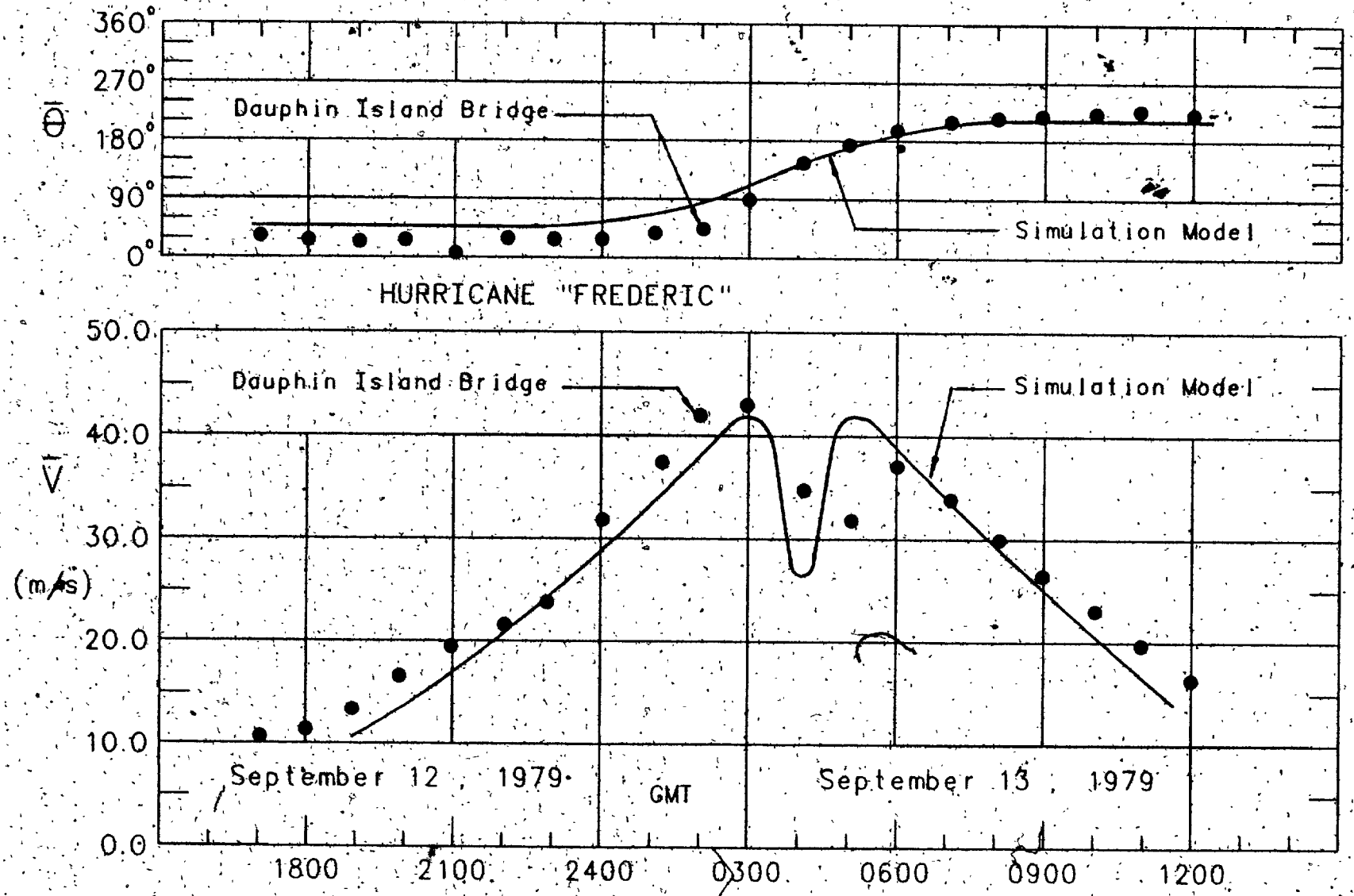

FIGURE 4.10 (contd.) (b) Dauphin Island Bridge Record

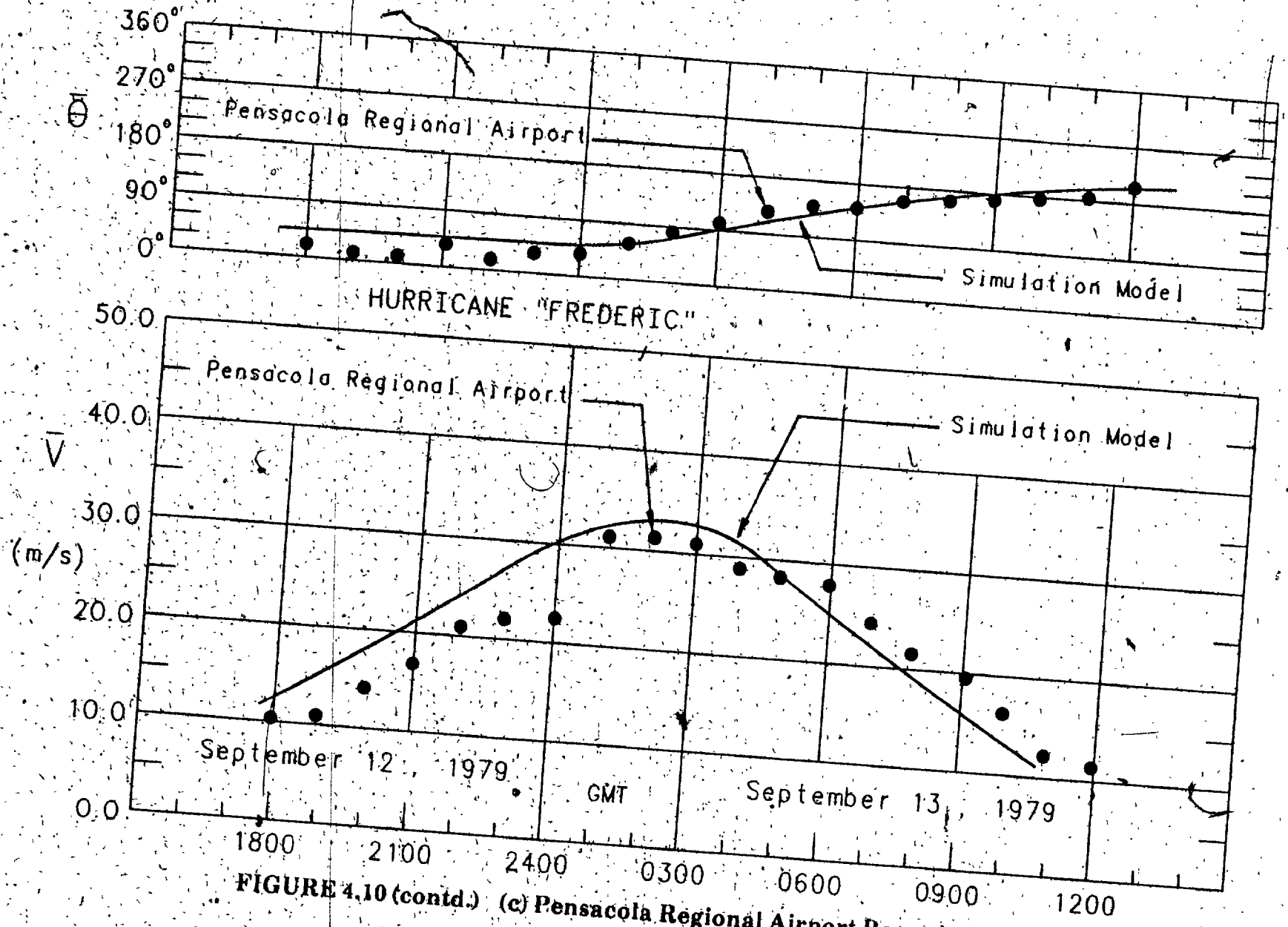

FIGURE 4.10 (contd.) (c) Pensacola Regional Airport Record

4.3 Northwest Pacific Typhoons

During the course of this study, a wind engineering project was conducted at the UWO Boundary Layer Wind Tunnel Laboratory, sponsored by Ove Arup and Partners, Hong Kong Limited, aiding in the design of the new headquarters of the HongKong and Shanghai Bank. Recognizing the dominant influence of tropical cyclones in the region, a study was made of the Hong Kong area wind climate, in particular the expected wind speeds for typhoon conditions. In support of the wind climate study of the region, wind records were made available by the Royal Observatory, Hong Kong (ROHK), from a number of anemometer stations in the area, including the Observatory itself, Kai Tak International Airport, Cheung Chau, Waglan Island and the King's Park observation station. The exposure conditions of these stations are described in Chen (1975) and their location shown in Figure 4.11. Two deserve special mention; ROHK, for its remarkable length (1884-present) and Waglan Island, for its relatively good, open-water exposure from most directions. Changes to the surrounding urban landscape however have significantly affected the ROHK records making it difficult to apply corrections to convert the ROHK anemometer data to standard reference heights (Chin and Leong, 1978). The Waglan Island data do not suffer from this drawback. Rather the wind records only have to be adjusted to take into account the aerodynamic influence of the island's shape on wind speeds. Accordingly, a topographic-model wind tunnel study of Waglan Island at a scale of 1:500 was undertaken, reported in Surry et al (1981). Results of the study included a series of directional factors relating anemometer winds to equivalent upper-level (500 metre) and surface (10 metre) winds for the four anemometer locations during the life of the island's meteorological station (1953-present). Figure 4.12 shows the ratio of the anemometer height wind speed to the equivalent open-water 10 metre height wind speed measured upstream of the island. It can be seen that the interference effects caused by nearby buildings which affected the Waglan Island records at the second anemometer location (January, 1964 to July, 1966), causing it to be relocated, are well captured in the wind tunnel model tests. A number of such sets of correction factors were determined for different exposure conditions, i.e. different approaching boundary layer profiles. Using these correction factors it was possible to determine wind speeds and directions for the Waglan site at

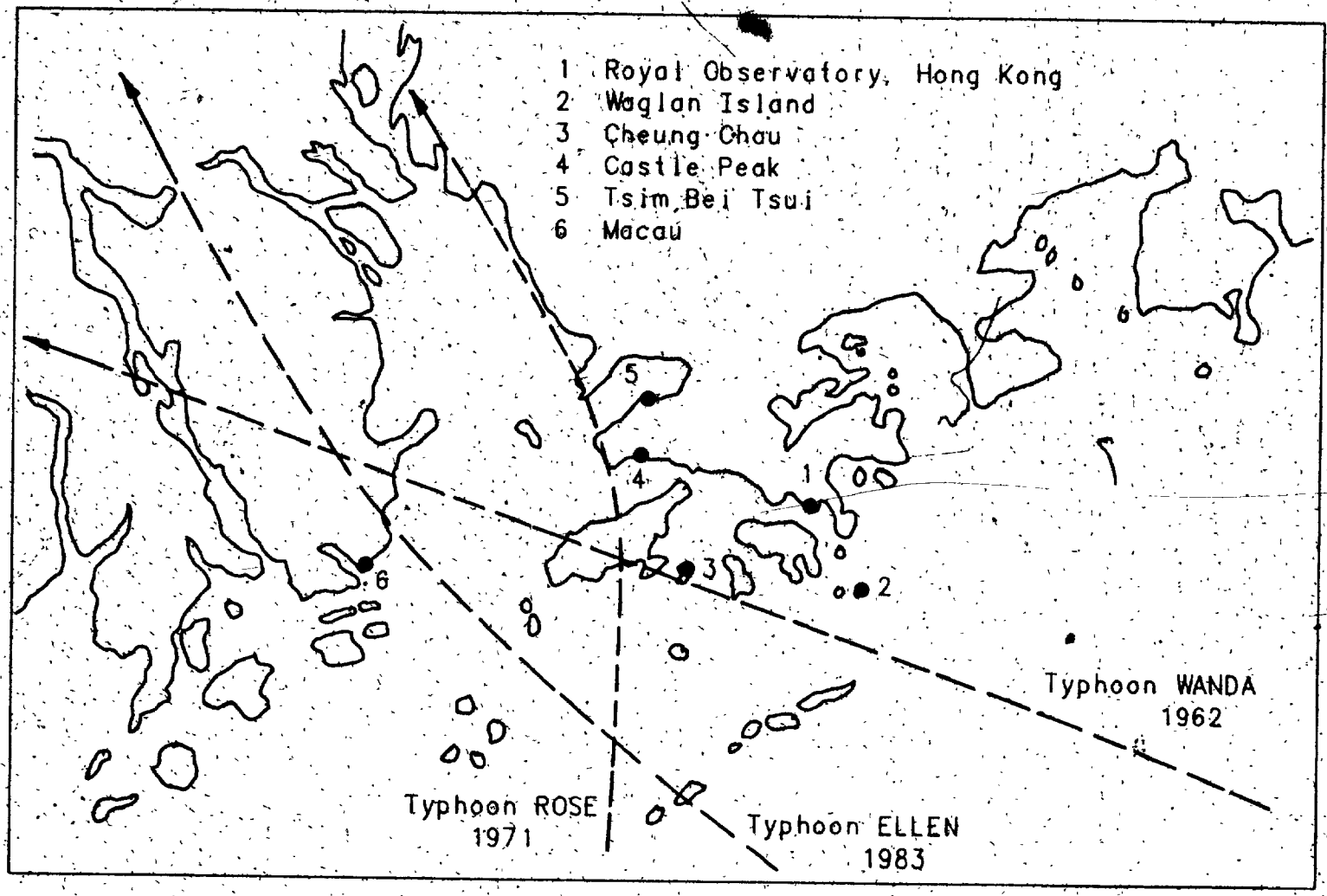

FIGURE 4.11 Location Map for Hong Kong Area Anemometer Stations and Tracks for Typhoons Ellen (1983), Rose (1971) and Wanda (1962)

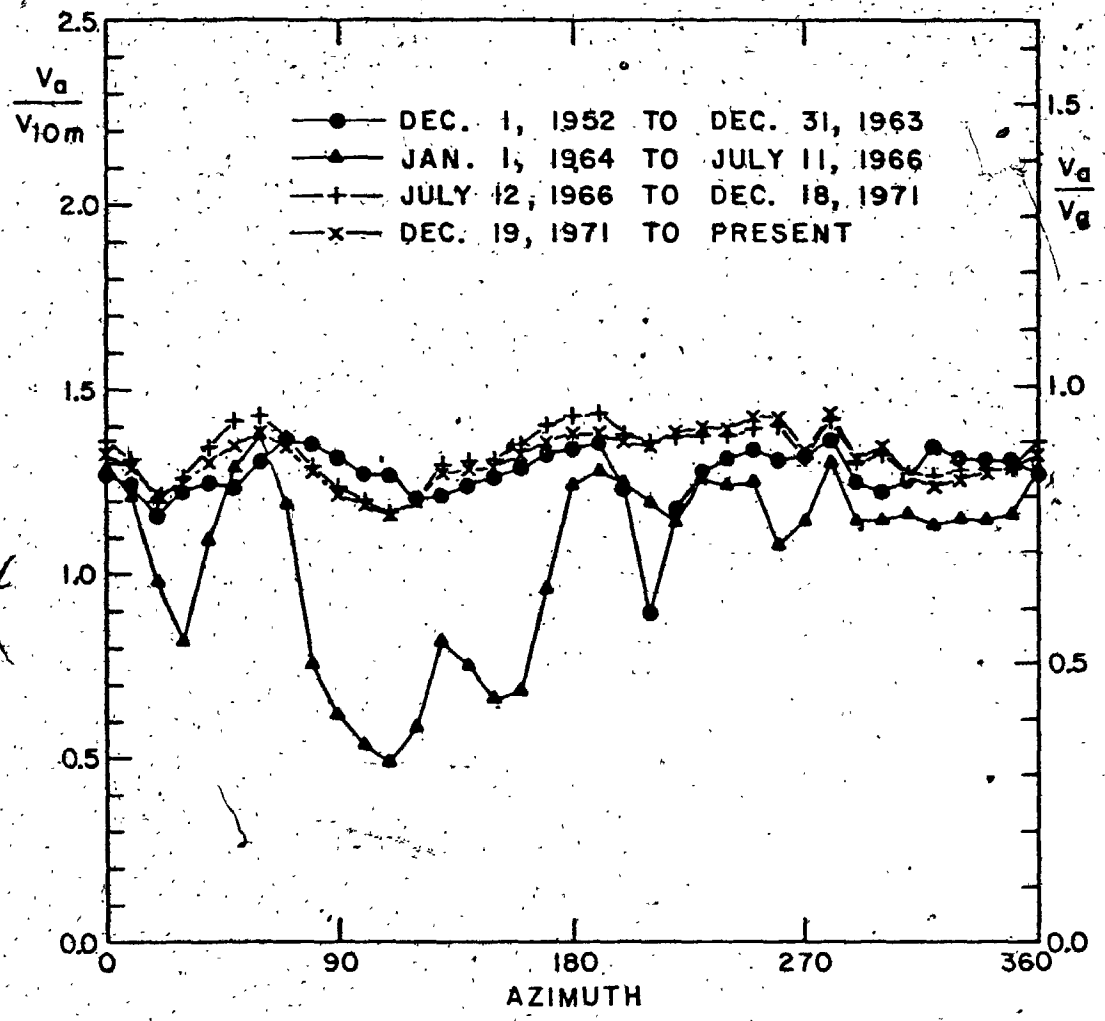

FIGURE 4.12 Ratio of Waglan Island Anemometer Wind Speed to Upstream 10 Metre Height Open-Water Wind Speed

the 500 metre and surface heights from the raw anemometer data. The wind tunnel corrections cannot include for obvious reasons the turning effect on wind directions caused by surface friction on upper-levels winds. Therefore, comparison of wind directions between the corrected Waglan data and simulation windfield model predictions is restricted to surface angles only.

ROHK also provided general meteorological data relevant to storms passing through the Honk Kong area. These included the 1968-1982 ROHK "Annual Tropical Cyclone Summaries". From these were derived the input data for the simulation windfield model. The storms chosen for comparison between simulation model-predicted winds and the actual recorded winds all passed by Waglan Island with tracks that resulted in wind directions from the long fetches of clear, open sea surrounding the island.

(i) Typhoon "ELLEN"

Typhoon Ellen originated as a tropical depression near the Marshall Islands on August 29 1983 and reached typhoon strength (equivalent to hurricane intensity) on September 4. As Ellen passed the northern tip of Luzon the central pressure of the storm rose from a minimum of 928 mb to 966 mb. Ellen re-intensified slightly in the South China Sea. The central pressure fell to 960 mb and remained at that level till landfall was made on September 9. Figure 4.11 shows Ellen's path in the vicinity of Hong Kong. The eye crossed the mainland coast just to the north of Macau at about 0845 local time. The storm then adopted a more northerly path into Guangdong Province where it weakened rapidly later that night. Meteorological data recorded during Ellen's passage past Hong Kong indicated that the circulation was in a steady-state during that time. The radius of maximum winds in this time period was 45 to 50 km and the storm translation velocity 3.7 m/sec.

Typhoon Ellen ranks as one of the most intense typhoons ever to strike Hong Kong. Hurricane-force winds lasted for record periods at the Waglan Island and Cheung Chau anemometer stations. Several stations in the area recorded their maximum-ever values of mean and/or peak gust wind speed. Figure 4.13 shows wind records from three stations in the area, identified in Figure 4.11. All three stations were briefly inside of the radius of maximum

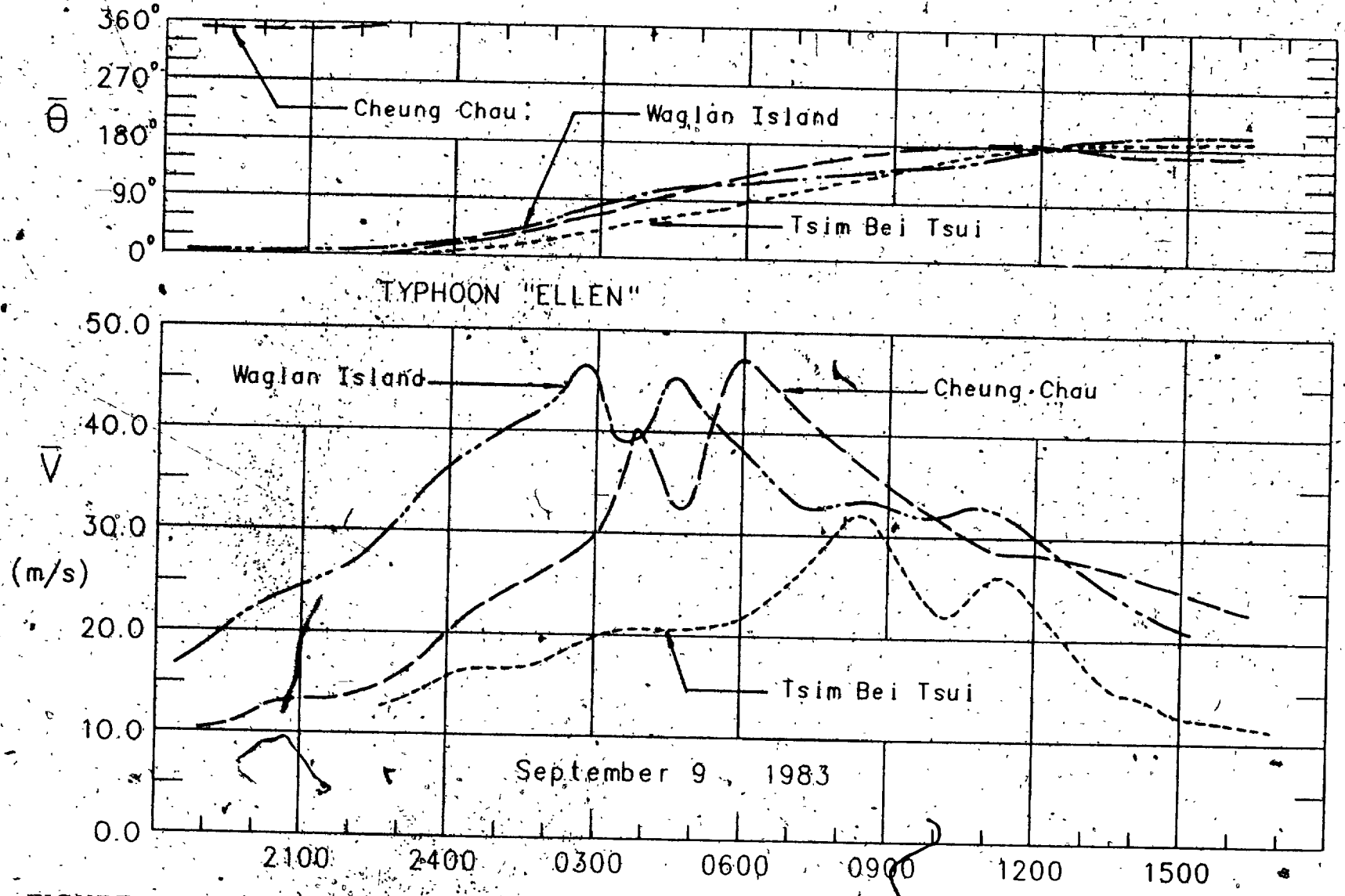

FIGURE 4.13 Comparison of Wind Records Obtained During Typhoon Ellen at Waglan Island, Cheung Chau and Tsim Bei Tsui

winds and located to the right of the storm path as Ellen moved in a northwesterly path through Hong Kong. The Waglan Island speeds show two maxima of almost equal magnitude, consistent with the assumed steady-state nature of the circulation at the time. The Tsim Bei Tsui record clearly shows the weakening of the circulation once landfall was made, evidenced by the 20% reduction in the second peak of the trace. The Cheung Chau wind speed history shows an increase in the second wind maximum as the storm passed the site. An examination of the wind directions associated with the two mean maxima (0400 and 0600 local time) shows that in the former case the winds had passed over Hong Kong Island and Lamma Island before reaching Cheung Chau, while for the second maximum the winds were off-water. These variations show the problems encountered in correcting surface winds where substantial changes in topography and terrain are present, thereby emphasizing the unique value of the Waglan Island data.

The simulation windfield model-predicted wind speeds and directions for Typhoon Ellen at the 500 metre and surface heights were compared to the Waglan Island data, converted to the same heights, using the results of the topographic model test correction factors. The results are shown in Figure 4.14. Wind speeds are over-estimated while the storm was approaching, but can be seen to match well during and after the hours when Ellen's maximum winds were experienced on the island.

(ii) Typhoon "ROSE"

Typhoon Rose developed as a tropical depression about 175 km west of Guam on August 10 1971. Rose traversed the northern end of Luzon early on August 14 and entered the South China Sea later that day. During the next day, the storm translation speed slowed down to about 3.6 m/sec and Rose underwent a period of intensification during which the central pressure fell to 959 mb by midnight of August 15. The 36 km diameter eye became well-defined and the storm veered northwards towards Hong Kong. The edge of Rose's eye passed close to the west of Cheung Chau at about 0115 local time on August 17 with a central pressure of around 961 mb. After crossing the western coast of Castle Peak, Rose moved away from Hong Kong north-northwestwards towards Canton. An unusual phenomenon accompanying the

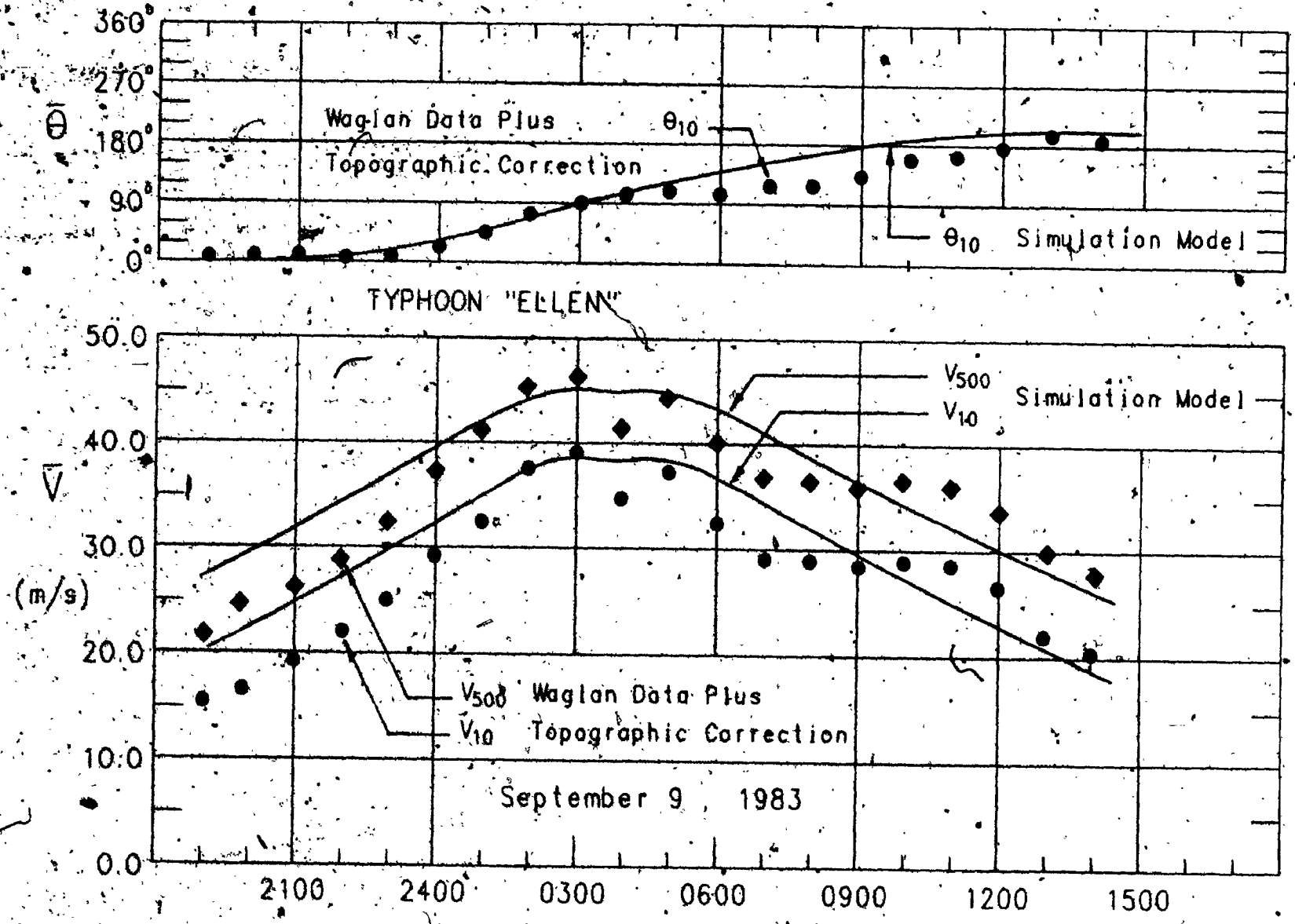

FIGURE 4.14. Comparison of Observed and Model-Predicted Wind Speeds Suring Typhoon Ellen, Waglan Island Corrected Record

passage of Rose was the development of sea fog at Waglan Island, Cheung Chau and Cape Collinson on the morning of August 18, most probably caused by the lowering of the sea surface temperature after the storm's passage. Rose's track past Hong Kong is shown in Figure 4.11.

As with Typhoon Ellen, the wind record obtained from Waglan Island exhibited wind directions from predominantly off-water trajectories, making the comparison of observed with simulated wind speeds possible with only the topographic test correction factors necessary to convert the island anemometer data. This comparison is shown in Figure 4.15. The wind speeds are slightly under-estimated by the windfield model at the 500 metre and surface heights. The observed wind directions show a greater amount of veering than predicted by the model, especially after the point of closest approach. This may be due partly to the more northwesterly movement of the storm after leaving the Hong Kong vicinity. The simulation wind speeds were computed assuming a constant direction of storm translation northwards, which was the value of approach angle at the closest point of the storm to Waglan Island.

(iii) Typhoon "WANDA"

Typhoon Wanda formed on August 29 1962 as a tropical depression about 2000 km to the southeast of Hong Kong. Moving west-northwest towards the Luzon Strait at 7.8 m/sec, it gradually intensified, exhibiting an unusually large circulation with a diameter of 1500 km. Winds reached gale force on Waglan Island at 0200 local time on September 1 when the storm was centred about 170 km away and moving towards Hong Kong with a translation speed of 5.6m/sec. Wanda passed through the colony during the period 0900 to 1200 local time. The path is shown in Figure 4.11. With the typhoon passing so close to the south there was a rapid veering of winds to the southeast over the whole area and many recording stations registered a temporary lull in wind strength during this time. The storm then moved inland over Guangdong Province and weakened rapidly during the morning.

The storm minimum central pressure of 953 mb recorded by the Royal Observatory was (and remains) the lowest ever. Damage from the storm was

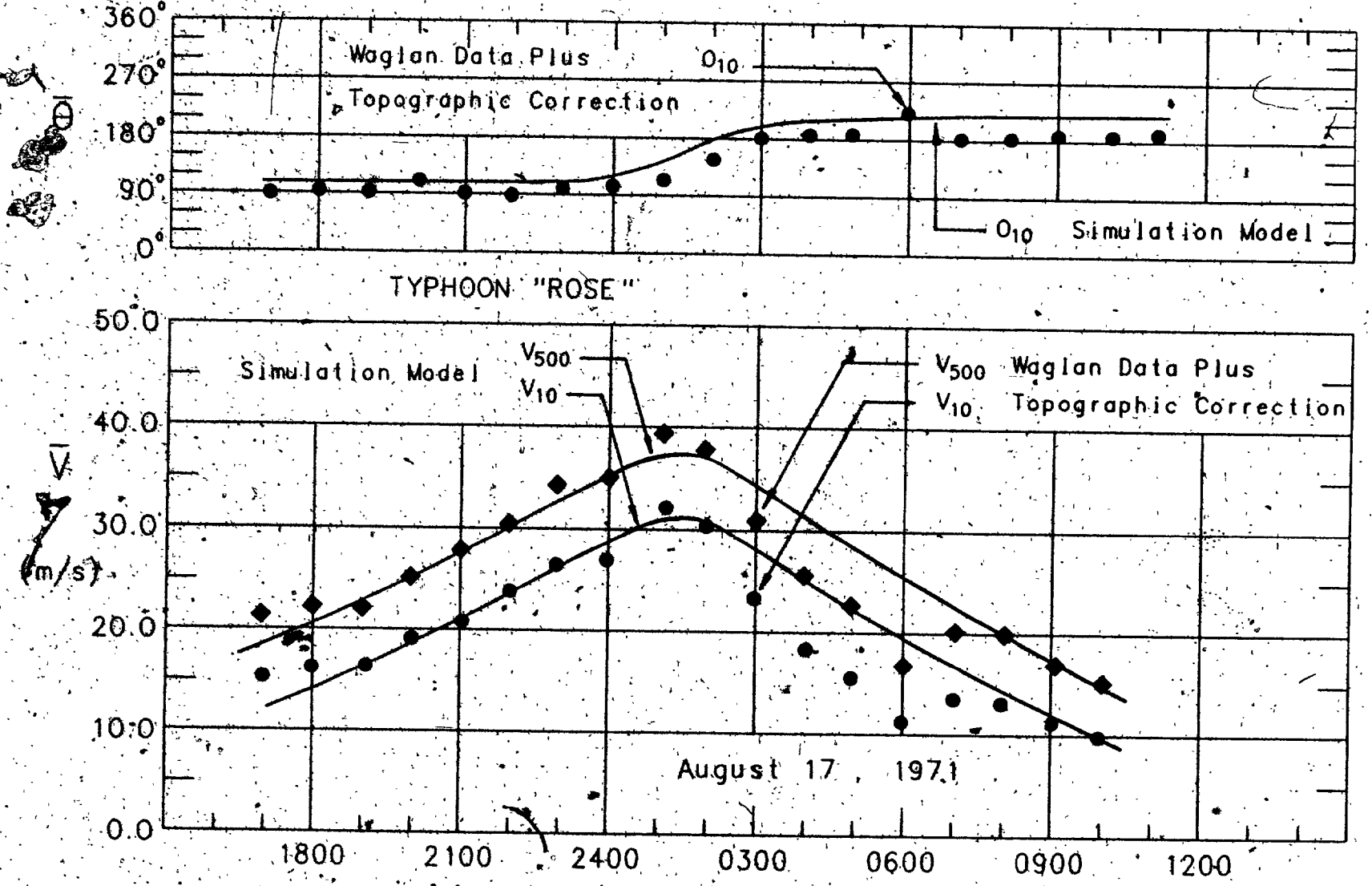

FIGURE 4.15 Comparison of Observed and Model-Predicted Wind Speeds During Typhoon Rose, Waglan Island Corrected Record

severe, with 130 fatalities, 53 missing and over 72,000 registered homeless. Figure 4.16 shows the comparison of observed and model-predicted wind speeds at Waglan Island. In this case the model wind speeds are slightly over-conservative at the time the maximum winds were occurring. The wind directions are well predicted by the simulation windfield model.

4.4 Australian Cyclones

Two tropical cyclones are examined in this section, Cyclones Tracy and Althea. In each case, these storms passed close to major cities (Darwin and Townsville respectively) where anemometer stations, operated by the Australian Bureau of Meteorology and located at the respective city airports, recorded wind speeds and directions during the passage of the storms. In both cases the anemometer stations were situated close to the coast and surrounded by generally flat, open terrain. Since both anemometer heights were at the 10 metre level, no adjustment was made to the anemometer records except to average the actual raw data to compute the mean recorded speeds and directions.

(i) Cyclone "TRACY"

Cyclone Tracy developed from a tropical low which formed 700 km northeast of Darwin early on December 20 1974. This low moved slowly southwest and had intensified into a tropical cyclone by the next evening. After continuing to move very slowly southwestwards for two days, Tracy changed direction on the morning of December 24 to the east-southeast and headed directly for Darwin. It remained on this path and passed almost directly over Darwin the next morning making landfall at 0330 local time. Figure 4.17 shows Tracy's path approaching and after making landfall at Darwin.

At the time of landfall the central pressure was about 940 mb and the translation speed never greater than 2.5 m/sec. Radar pictures indicate that Tracy possessed a very small eye, varying in diameter between 10 to 15 km. Meteorological reports also indicate that the eye diameter was contracting as

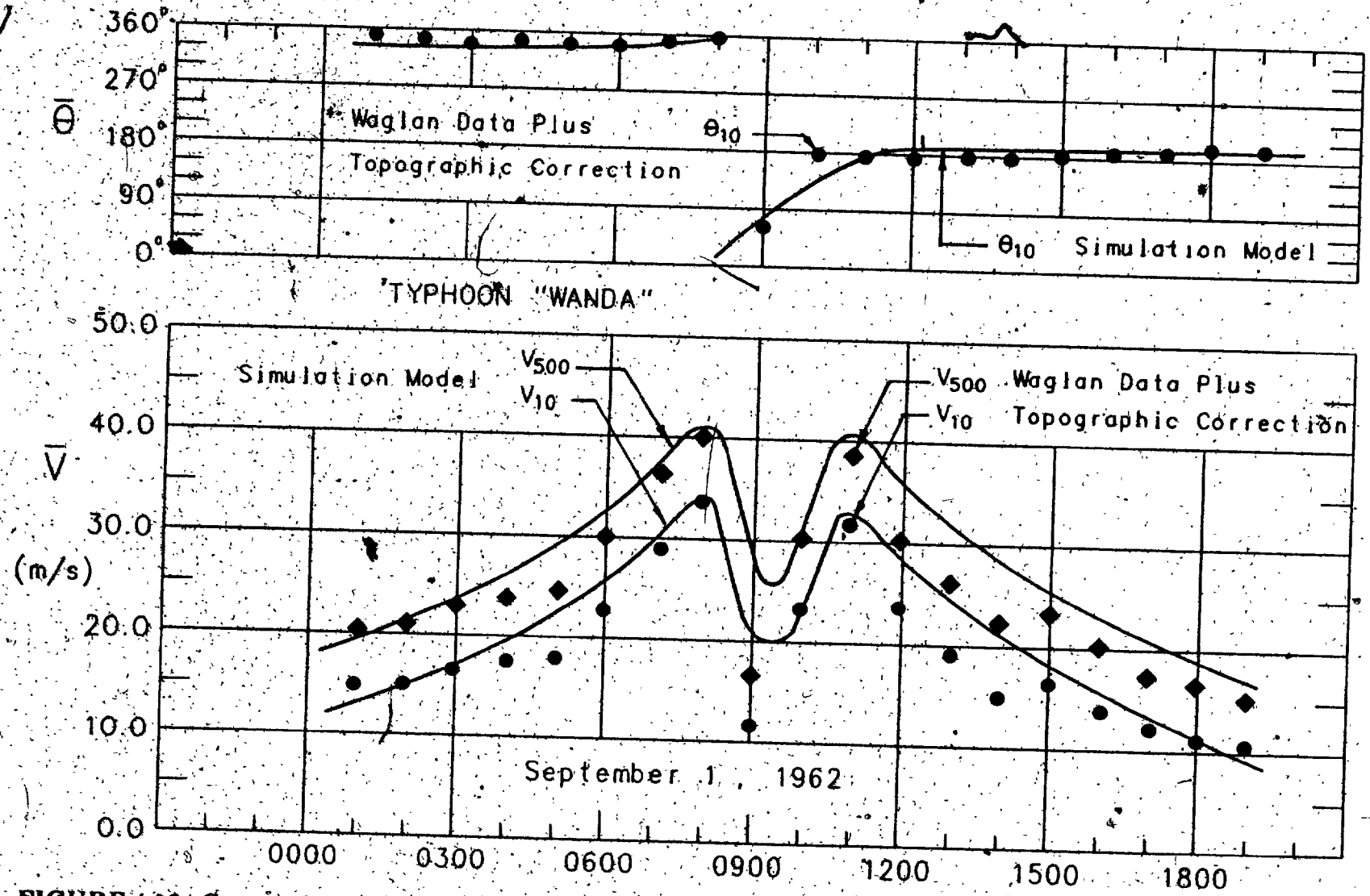

FIGURE 4.16 Comparison of Observed and Model-Predicted Wind Speeds During Typhoon Wanda, Waglan Island Corrected Record

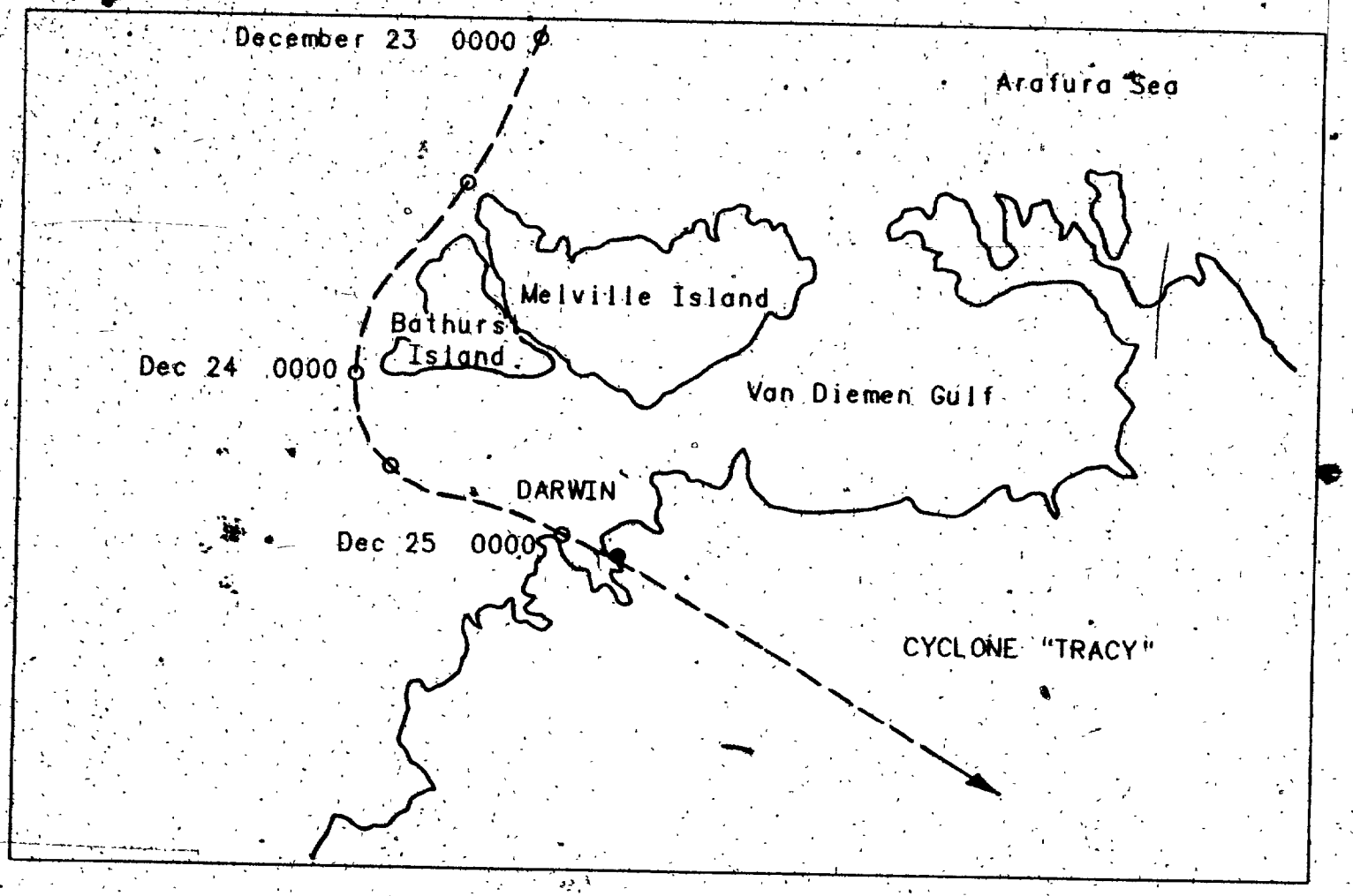

FIGURE 4.17 Cyclone Tracy Location Map

Tracy approached Darwin. This may have been accompanied by intensification of the circulation and hence the wind speeds and directions sustained in the Darwin area may not be representative of a steady-state storm.

Wind speeds and directions were recorded at the Darwin Airport anemometer station. At 0235 local time the anemometer was recording mean winds over 30.0 m/sec with gusts up to 50.0 m/sec. Unfortunately, the anemometer was struck by debris and ceased to function at 0305 local time. Just prior to failure the record showed gusts over 60.0 m/sec, although verbal reports suggest strongly that the winds went higher, as the eye passed by an hour or so later. Figure 4.18 shows the comparison between the airport wind record and the simulation windfield model wind speeds and directions. Airport wind speeds and directions are available only up to the failure time.

(ii) Cyclone "ALTHEA"

Cyclone Althea crossed the North Queensland coast just north of Townsville at 1900 GMT on December 23 1971. The central pressure of the storm had held very steady at 970 mb as it approached the coastline. The eye was not well-formed and had a diameter that varied between 60 to 65 km. Townsville thus did not experience the full force of Althea's winds, the landfall position being some 48 km to the north. During Althea's approach to the coastline the translation velocity of the storm remained steady at 5.1 m/sec. Figure 4.19 shows Althea's track.

Wind speeds and directions were recorded at Townsville's Garbutt Airport anemometer statioin. The station is located close to the coast and is surrounded by predominantly flat terrain, except for a number of nearby hills. These include Castle Hill (286 metres), 5 km to the east-southeast, and Mt. Stuart (580 metres), 10 km to the south-southeast. These hills therefore have some effect on the wind flow at the airport for winds in the southeast quadrant, which coincides with the direction of the winds experienced at Townsville during Althea's approach and at landfall.

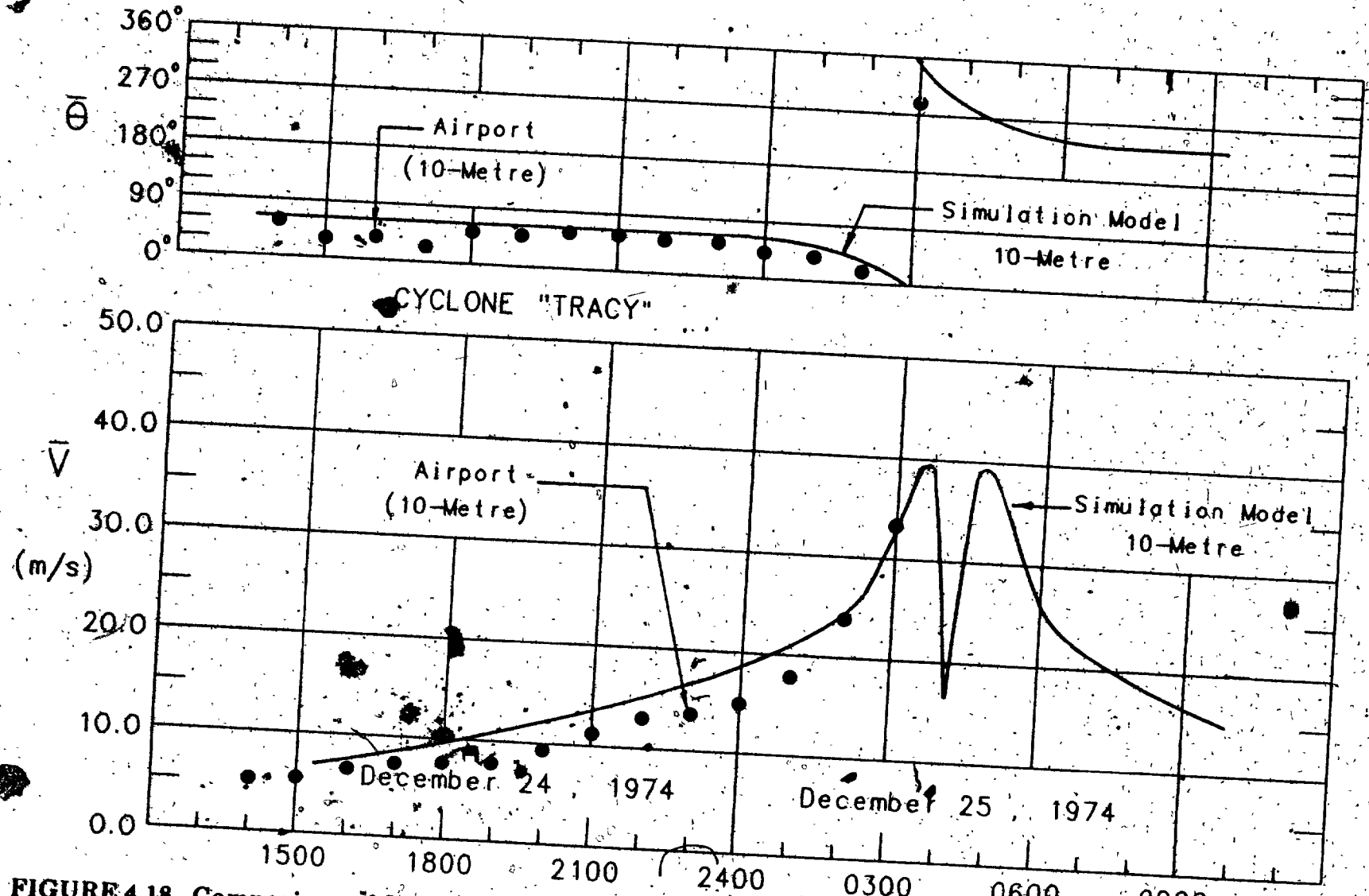

FIGURE 4.18 Comparison of Observed and Model-Predicted Wind Speeds During Cyclone Tracy, Darwin Airport Record

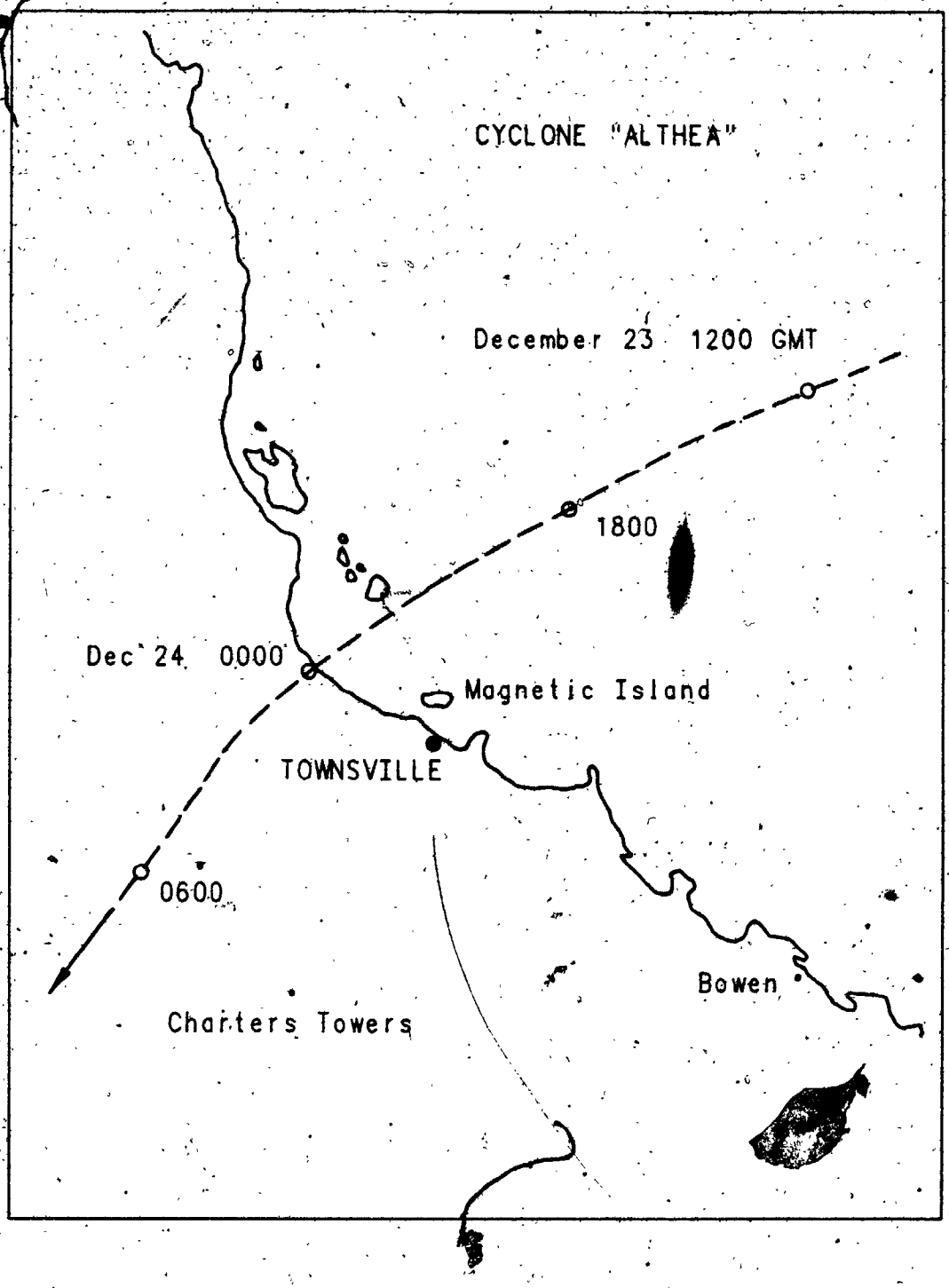

FIGURE 4.19 Cyclone Althea Location Map

Figure 4.20 shows the wind history recorded by the Garbutt station and the simulated wind speeds and directions predicted by the windfield model at the 10 metre height. The simulated wind speeds were computed assuming the site to be located in open terrain. The maximum wind speeds are reproduced well but the corresponding wind directions show significant deviations. These however are for directions where the nearby hills may have interfered with the wind flow at the time of landfall.

4.5 Discussion

The comparisons given in this chapter are important for two reasons :

(a) They are the only independent means by which the simulation windfield model can be shown to be capable of reasonably reproducing the mean windfield in tropical cyclones given the necessary characteristic parameters. It is not possible to say that the comparisons given in the preceding sections prove this beyond doubt. Each particular tropical cyclone studied had its own unique features added to the question of the suitability of the measuring sites chosen for the comparisons. In general however the simulation windfield model seemed to adequately reproduce the mean wind speeds and directions observed at surface locations near the coast.

One limitation of the comparisons is that they all dealt with fairly intense tropical cyclones. All had minimum central pressures less than 970 mb at the time of landfall. Thus the apparent success of the comparisons should be qualified to refer only to tropical cyclones of hurricane-force intensity. It should be noted however that the purpose of the simulation procedure itself is to determine design wind speeds for engineering structures. Interest is therefore centred on the high wind speed range. For this reason, attention was focused in this chapter on those storms which would have the greatest impact on the final predictions made by the simulation.

(b) The comparisons offer a relatively simple means by which to attach error estimates to model-predicted wind speeds and directions. An alternative approach would involve estimating errors for each sequence in the windfield

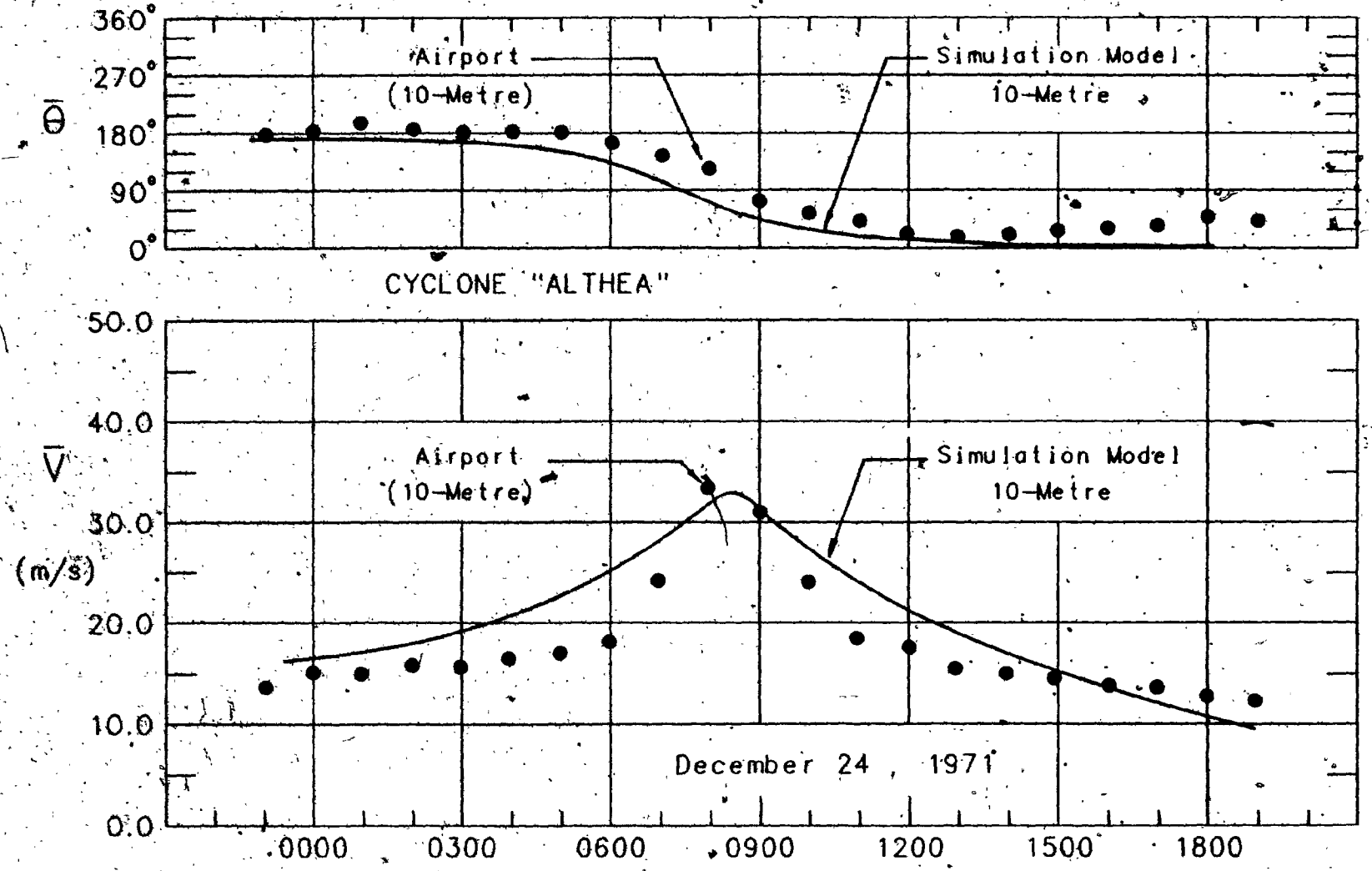

FIGURE 4.20 Comparison of Observed and Model-Predicted Wind Speeds During Cyclone Althea, Townsville Garbutt Airport Record

computations, the gradient balance assumption, the SHBL circulation computation, the 500 metre to 10 metre conversion, etc. Excluding Cyclone Tracy (the maximum winds were not observed) the comparisons showed no bias in the windfield model to consistently over-estimate or under-estimate observed wind speeds. Of the examples included in this chapter, all model speeds were within ±10% of the observed speeds at the time the maximum winds were being recorded. Over half the comparisons were within ±5%. Away from the region of maximum winds, the model wind speeds in some cases differed from observed ones by as much as 20%. In these cases it is difficult to assess whether the deviation is due to deficiencies in the windfield model or extraordinary features exhibited by the particular storm in question.

Wind directions showed generally greater variation than wind speeds. However, in some cases, e.g. Cyclone Althea, exposure conditions existed which undoubtedly affected the observed directions which could not be taken into account by the simulation windfield model. Therefore a likely estimate of the variability of the model wind directions is ±20-30°.

CHAPTER 5

DETERMINATION OF THE PROBABILITY DISTRIBUTION FUNCTIONS FOR THE TROPICAL CYCLONE SIMULATION CHARACTERISTIC PARAMETERS

This chapter presents the data analysis devoted to improving the statistical representation of the tropical cyclone characteristic parameters used in the simulation procedure. This covers six storm variables : the annual occurrence rate (λ), central pressure difference (Δp), radius of maximum winds (*RMAX*), translation velocity (*VT*), approach angle (θ) and minimum approach distance (*DMIN*). Statistical models used in previous studies were examined as well as alternative distributions which seemed likely to fit the data. In several cases new probability distribution functions were proposed, with significant impact on the final extreme wind estimates given by the procedure.

5.1 . Data Sources

Although the primary function of the National Hurricane Center (NHC), Miami, Florida, is in the area of forecasting, it has developed, under the leadership of Dr. C.J. Neumann, an additional capability as a data collection agency. The single most important source for this study is the NHC computer file of dates, tracks, central pressure values and wind speed estimates (if available) for all tropical cyclones occurring in the North Atlantic region over the 98-year period, 1886 to 1983. This file is herein referred to as the HURDAT (HURricane DATa) tape.

The HURDAT tape contains four pieces of information for each tropical cyclone recorded : time and date, latitude and longitude position, maximum sustained wind speed and central pressure (if available). Observing systems used to compile the storm data found in the HURDAT tape are described in Jarvinen, Neumann and Davis (1984). The major change in the overall

effectiveness of the data gathering systems came in 1944 with the start of organized aircraft reconnaissance. Prior to this date some storms occurring over the ocean may have gone undetected, particularly if they were short-lived storms moving over areas unused as shipping lanes. This shortcoming did not affect the recording of tropical cyclone occurrences along the coastline. After 1944, continuous monitoring of tropical cyclones by aircraft reconnaissance allowed the continuous recording of a storm's track, maximum winds and central pressure. A significant increase in pressure data at this date reflects this. The continuous coastal radar network which began functioning in 1955 increased the amount of track information available mainly for landfalling storms. A second major breakthrough occurred with the introduction of weather satellites with visible and infra-red sensor capability, offering continuous monitoring of tropical cyclone systems at any point of the globe. In 1977, for the first time, meteorological information was relayed from reconnaissance aircraft to the National Hurricane Center via almost instantaneous communication through a geostationary satellite.

An example of the data compiled in the HURDAT tape is given in Figure 5.1, showing the tracks of all tropical cyclones originating in the month of July for the period 1886-1977. Tropical cyclone tracks found in the HURDAT tape are often referred to as "best tracks". They are constructed during a post-storm analysis taking into account all the available information, satellite pictures, reconnaissance aircraft data, land-based radar fixes, ship reports and ocean data buoy records. Tropical cyclones often exhibit small oscillatory motions in their tracks. Generally these trochoidal track loops are smoothed out in the "best" track defined for a storm, so that the storm path reflects the larger scale storm motion rather than the precise location of the path taken by the eye. Track positions for tropical cyclones recorded in the HURDAT tape are noted at six-hourly intervals at 0000, 0600, 1200 and 1800 Greenwich Mean Time (GMT). The latitude and longitude positions are given to the nearest 0.1 degree.

The current version of the HURDAT tape has been revised several times. It includes wind speed estimates at each storm position. These are sustained (1-minute average) surface speeds, given in knots (1 knot = 0.5144 m/sec) and rounded off to the nearest 5-knot value, i.e. 45, 50, 55 etc. The veracity of

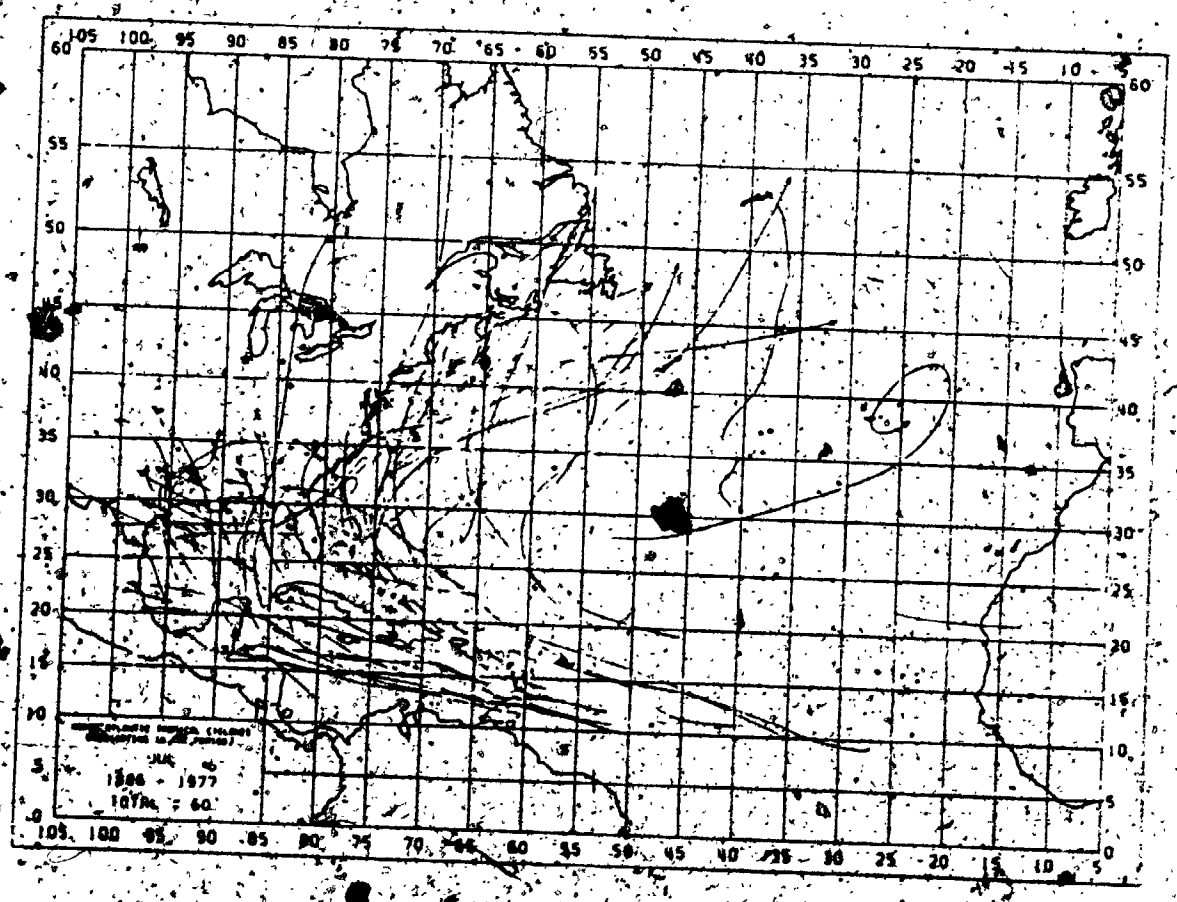

FIGURE 5.1 North Atlantic Tropical Cyclones Originating in July, 1886-1977.

these wind speed estimates must be considered to be limited. Over the ocean speeds are determined from ship reports and state-of-the-sea assessments. Even when wind speed estimates are made from aircraft reconnaissance these are based once again on subjective estimates of the sea-state or tables relating flight-level winds to surface winds. For tropical cyclones over land, wind speed estimates have more recently been made from anemometer stations operated by the National Weather Service. Initially no attempt was made to account for the wide variation in heights, locations and exposure at these stations. Finally wind speed values entered in the HURDAT tape are sometimes computed from Kraft's (1961) minimum pressure-maximum wind equation (section 2.2).

Figure 5.2 contains final surface wind and pressure profiles for Hurricane Anita (1977), as well as the original information used to determine the profiles. The wide scatter in the wind speed data compared to the pressure data is evident. In contrast to wind speed estimates, pressure values noted in the HURDAT tape are observed values, not determined via any other source of data. Central pressure is recorded for a storm only if reported within 2 hours of the four HURDAT standard track times. It is clear from the raw pressure data shown in Figure 5.2 that central pressure is a much more conservative property of a tropical cyclone than the windfield. This is also true of the other storm parameters examined in this chapter. The tropical cyclone windfield defined using these parameters is thus a steady-state windfield varying with time scales of the order of an hour.

A second important source of data used in this chapter is NOAA Technical Report NWS23 (Schwerdt, Ho and Watkins, 1979) herein referred to as NWS23, setting out meteorological criteria to compute wind speeds for the so-called Standard Project Hurricane and Probable Maximum Hurricane. NWS23 is an extension and revision of a number of earlier efforts to summarize the climatology of North Atlantic tropical cyclones (Graham and Nunn, 1959; Ho, Schwerdt and Goodyear, 1975). This report includes the most extensive compilation of tropical cyclone radius of maximum wind and periphery pressure data available, which are not covered in the HURDAT tape.

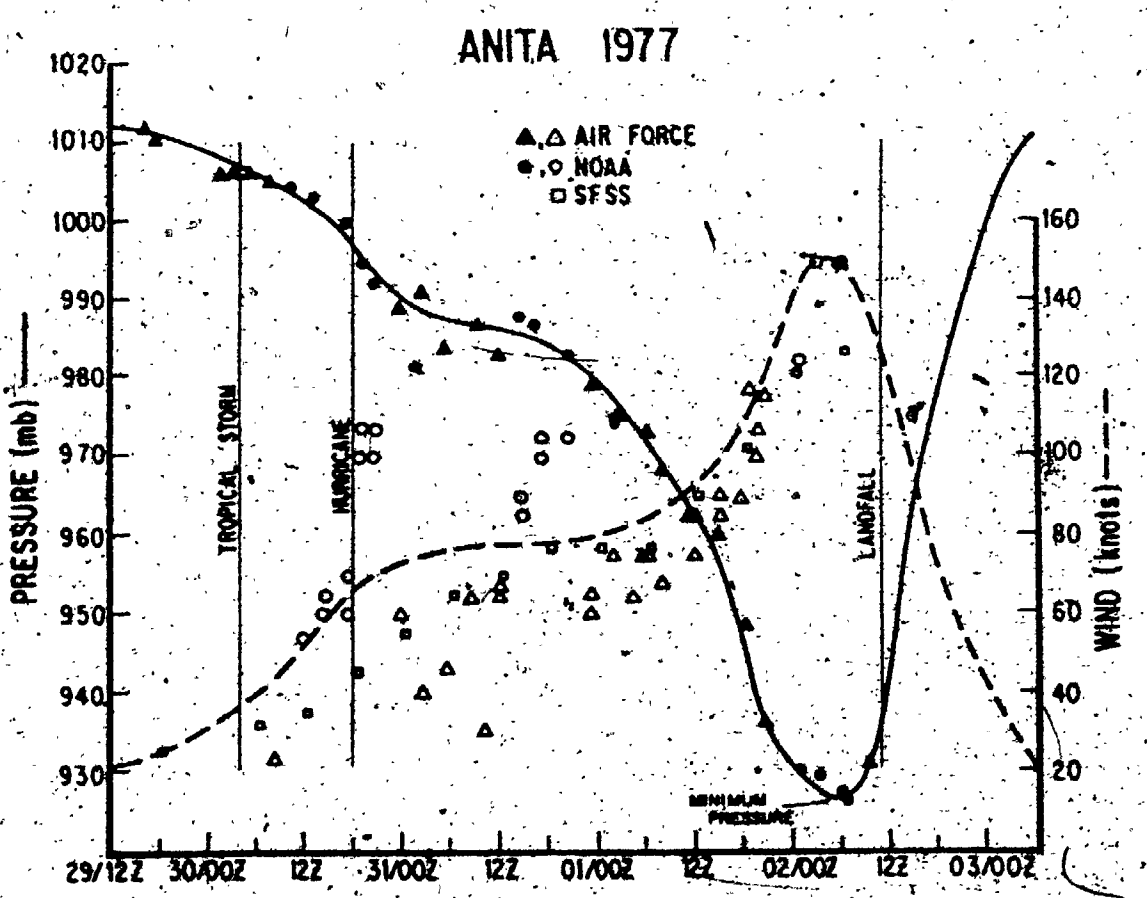

FIGURE 5.2 **Final Wind and Pressure Profiles and Actual Data for Hurricane Anita (1977)**

5.2 Methodology of the Tropical Cyclone Landfall Approach in Specifying the Simulation Characteristic Parameters

Within the simulation procedure tropical cyclones generated are assumed to be in steady-state while over water and modified only if landfall is made, according to the manner prescribed in Chapter 3. Various methods have been used for choosing the tropical cyclones from which to define the climatological storm data required by the simulation at any particular site. Some previous studies have used linear coastal segments and only considered data from landfalling storms. This excludes much relevant information especially for sites along the Atlantic Coast. In the current procedure a circle around the site of interest is utilized. All tropical cyclones whose paths (as determined from the HURDAT tape) have entered the circle are then used to assimilate sample sets of Δp, VT, etc., from which the probability distribution functions are defined.

Two factors influence the choice of data circle size : (i) the total number of tropical cyclones entering the circle which dictates the sample size for determining the parameter distribution functions and (ii) the sensitivity of the parameters to geographical location. Statistically speaking, the more tropical cyclones within each data circle the better, and hence the larger the required circle diameter. However, as will be seen, all the model parameters were found to display moderate to high sensitivity to changes in position along the coastline, especially the central pressure difference, Δp. This argues for the use of smaller data circles to preserve the geographical variation of the parameters. Initial examination of the data suggested that data circles with a diameter of 500 km represented the best compromise between the above two constraints.

In order to examine the characteristic parameters systematically, data circles were located along the United States Gulf and Atlantic Coasts at one radius distance apart (250 km) to ensure reasonable overlapping. Figure 5.3 shows the location of the 24 resulting data circles used to define the characteristic parameters and the "milepost" scale that has been utilized in previous U.S. hurricane risk studies.

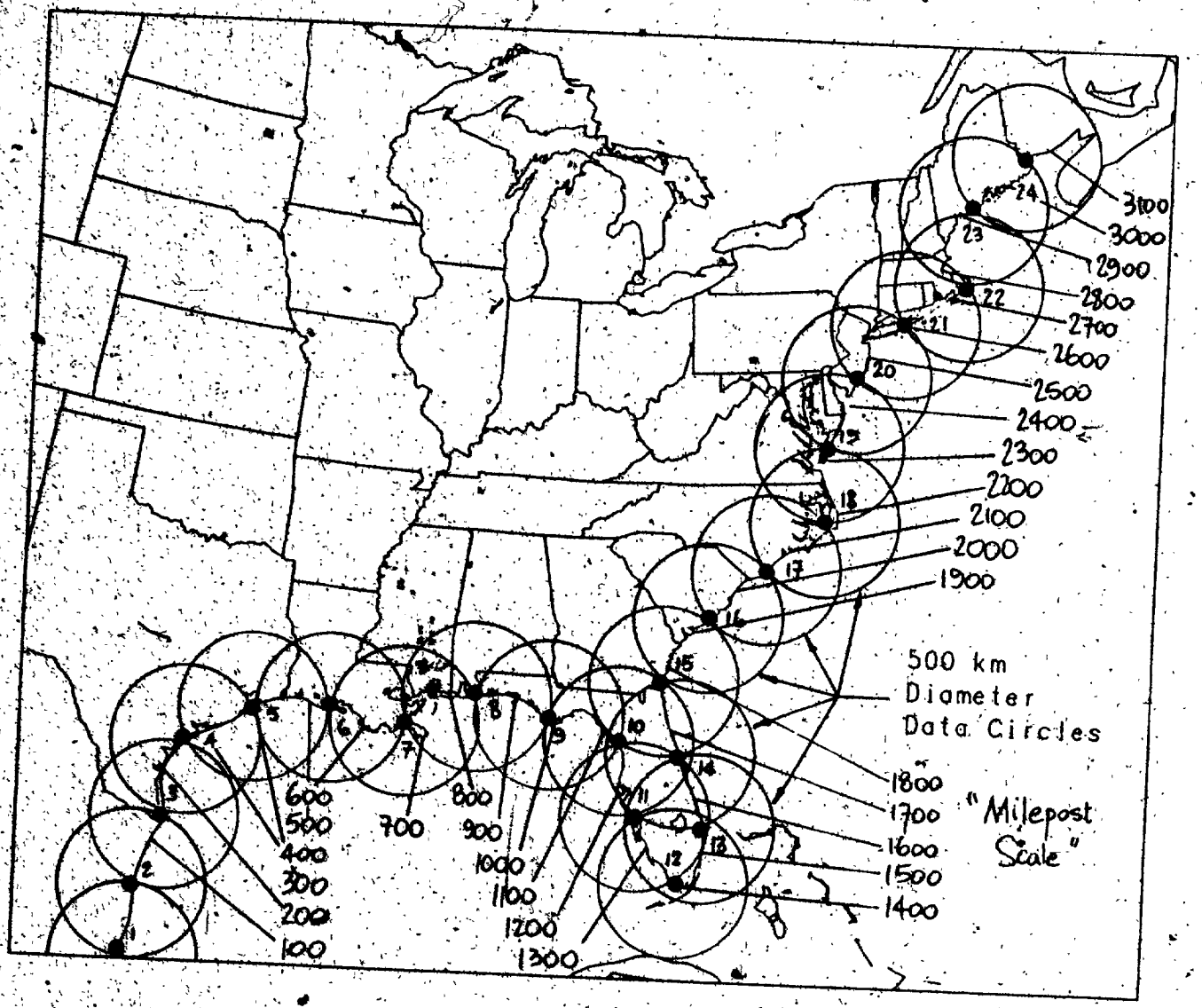

FIGURE 5.3 Location Map for U.S. Coastal Data Stations and "Milepost" Scale

Figure 5.4 shows the way in which the storm model parameters are defined. The central pressure value chosen from a storm entering the data circle is the one closest to the station of interest. Values of translation velocity and approach angle are determined as the average values exhibited within the data circle. The value of minimum approach distance is determined from the path of the storm represented as a series of straight line segments joining the 6-hourly HURDAT track points.

5.3 Annual Occurrence Rate - "λ"

It is well known that tropical cyclones occur mostly in the hot months of late summer and early fall, when warm ocean waters favour their genesis and intensification. In the North Atlantic, the main season commences at the end of July reaching a maximum around mid-September. Activity virtually ceases by the end of November. A typical tropical cyclone simulation however may generate a wind history spanning many thousands of years. Therefore the monthly and seasonal variations of tropical cyclone occurrence are not of immediate interest. What is required in the simulation is the annual variation of tropical cyclone occurrence, specifically a discrete probability distribution yielding the expected number of tropical cyclones occurring every year over the span of the simulation.

There are a number of possible candidates. However there are compelling reasons for seeking a distribution whose mathematical form is related to the climatology underlying the process. The occurrence of tropical cyclones is a rare event. Even on a regional basis the annual frequency is small. This feature suggests the use of the Poisson distribution to define the annual occurrence rate. An additional requirement affecting the suitability of the Poisson distribution is that there be no correlation between the occurrence of succeeding storms. There is evidence however that there are years during which the formation of tropical cyclones is indeed favoured. The incidence of active tropical cyclone periods in time has been noted in all formation areas of the world (Gray, 1979). In the North Atlantic, hurricane activity seemed to concentrate around Florida in the 1940's, on the Atlantic seaboard in the 1950's and along the Gulf Coast during the next two decades. A number of recent

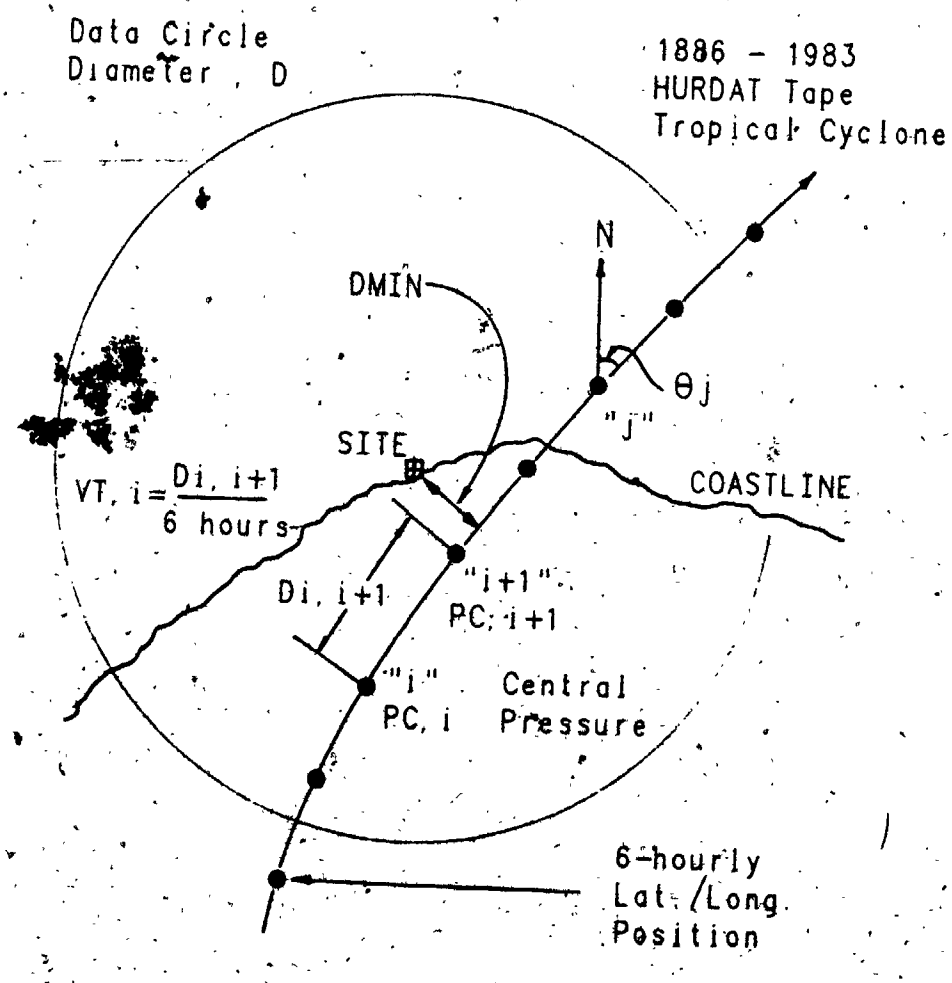

$$\lambda_D = \frac{\text{no. of tropical cyclones in data circle}}{\text{no. of years (=98)}}$$

$PC = PC, i$ (closest to the SITE)

$VT = \overline{VT, i}$ (mean VT within circle)

$\theta = \overline{\theta i}$ (" θ " " ")

FIGURE 5.4 **Definition Diagram for Tropical Cyclone Characteristic Parameters**

studies have suggested links between these observed inter-annual variations and regional and global climatological patterns. Shapiro (1982a,b) analyzed North Atlantic hurricanes in the period 1899-1978 and found that both the annual occurrence and regional shifts in hurricane activity were related to the Quasi-Biennial Oscillation (QBO) of sea-level pressure and 700 mb height winds in the region. Gray (1984a,b) demonstrated that tropical cyclone activity in the North Atlantic was related to four factors : (i) the occurrence of El Nino events, (ii) the QBO zonal wind direction, (iii) the QBO zonal wind change and (iv) the April-May Caribbean Basin sea-level pressure anomaly. For example, the average annual occurrence rate of tropical storms and hurricanes in the period 1900-1983 is 5.3 and 9.0 for El Nino and non-El Nino years respectively.

The question then arises whether the dependence of tropical cyclone occurrence upon the climatological parameters identified in Gray's study (or any other study) favours a distribution defining the occurrence rate not compatible with the assumption of a randomly occurring rare event, i.e. is there reason to suppose that some period other than an annual one is the basis of tropical cyclone occurrence and that some correlation between events exists. Of the four parameters cited in Gray's study, the two related to the QBO do in fact have very regular periodicity, of the order of 26 months. The other two, the occurrence of an El Nino event and the Caribbean Basin sea-level pressure anomaly, have no evident periodicity. Both Shapiro and Gray found that the contribution of the QBO correlations to tropical cyclone frequency explained only a very small portion of its total variance. Thus, even though it has been demonstrated that the occurrence of tropical cyclones in the North Atlantic is subject to climatological constraints, these include factors which appear to be completely random in character. Therefore it would seem that at the present time there exists no alternative other than the historical records from which to estimate the variation of tropical cyclone occurrence.

The first attempt to model the annual tropical cyclone occurrence rate was made by Thom (1970), who investigated the incidence of both tropical storms and hurricanes striking the New England coast. In comparing the occurrence of hurricanes in the southern North Atlantic Ocean with those reaching the

U.S. Atlantic coast, a gradual increase in the mean frequency was observed for the ocean data but not for the land data. Over the ocean it is quite possible that smaller, weaker storms went undetected in the years preceding the introduction of aircraft reconnaissance. Over land however the data gathering systems, at least in so far as the simple recording of a tropical cyclone occurrence, seem to have been quite uniform for the period of interest, 1886-present. Thom fitted distributions of the Poisson and negative binomial type to the annual frequency series of tropical cyclones for the whole southern North Atlantic region and for those incident upon the U.S. Atlantic seabord. The negative binomial distribution is representative of a process in which rare events occur in time but with some correlation existing between successive events. The negative binomial distribution was found to model the whole ocean series the best, while the Poisson was found to give the best fit to the coastline incident series. Chi-square tests performed for the fit of the Poisson distribution to the coastline series showed remarkable agreement. Thom suggested that while the data did indicate some correlation between occurrence of events on a whole-ocean regional basis, the occurrence at any particular coastal location appeared to be more random in nature through the simple reduction in chance of incidence.

A further reason for the success of the Poisson distribution at particular coastal locations lies in the observation that any correlation that does exist between successive storm occurrences is strongest at the genesis stage, typically many thousands of miles way from any potential U.S. landfall site. The path that a tropical cyclone takes after its genesis, determining if and where landfall will be made, is dependent upon climatological factors and regional steering currents quite independent of those affecting its genesis, and in no sense predictable. Thus the complete set of physical processes dictating the character of the coastal incidence of tropical cyclones in the United States tends to produce an annual frequency pattern of random occurrences rather than correlated ones, supporting the use of the Poisson distribution to represent the annual occurrence rate.

The appropriateness of the Poisson distribution has been confirmed by Hope and Neumann (1968) and Neumann (1971) for the annual occurrence of tropical cyclones at other U.S. coastal locations and Xue and Neumann (1985)

for Northwest Pacific locations. These studies showed that the annual storm frequency of occurrence could be closely modelled fitting Poisson distributions to the data, where the Poisson parameter was estimated from the sample mean. The Poisson distribution gives the probability of having k occurrences in any one year as:

$$p(k) = \frac{\lambda^k e^{-\lambda}}{k!} \qquad k = 0, 1, 2, 3, \ldots \qquad E5-1$$

λ = Poisson parameter

The mean and standard deviation (rms) of this distribution are both equal to the Poisson parameter, λ. At any particular locality the value of λ can be specified as:

λ_D = the average number of tropical cyclones per annum occurring within a circle, diameter D, centred around that locality

Figure 5.5 shows the variation of λ_D for 500 km diameter data circles around the U.S. Gulf and Atlantic coastline determined from the HURDAT tape. The increased frequency evident at Cape Hatteras is due to its geographically-exposed location on the Atlantic seabord. For any particular data circle size it is possible to back-multiply by the record length (98 years) to calculate the number of historical tropical cyclones passing within each respective data circle. This number is important because it indicates the sample size from which the distributions of the other parameters, e.g. track angle, translation speed etc., must be derived at any particular site. For 500 km diameter data circles this number ranges from 50 to 140 occurrences with well over half the coastal sites experiencing more than 90 incidences.

The events which make up the population from which the characteristic parameters are determined are the occurrences of tropical cyclones which have reached sufficient intensity so as to be observed and hence compiled in the historical records. Thus the probability distribution functions developed in the following sections for Δp, VT etc., should be considered to be conditional ones in the sense that they are determined from a population of

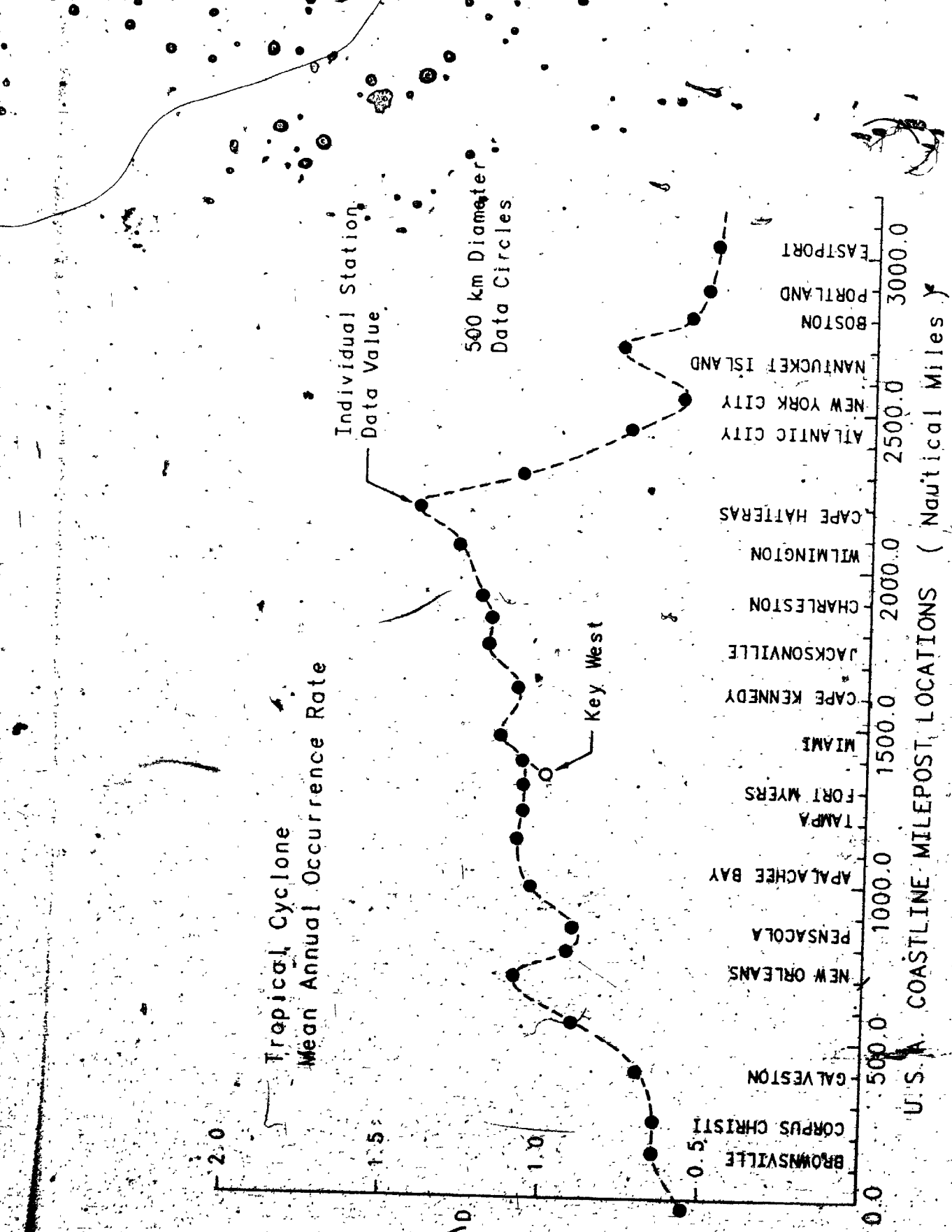

FIGURE 5.5 U.S. Coastline Mean Annual Occurrence Rate, λ_D

events limited by some intensity level. This should be borne in mind in comparing the statistical parameters now examined with those in other studies, where the relevant populations may have been truncated to include only those tropical cyclones reaching tropical storm intensity or hurricane intensity.

5.4 Central Pressure Difference - "Δp"

The central pressure difference, Δp, is the universally accepted index of a tropical cyclone's intensity. It is defined as the difference between the periphery pressure, Pn, at the outer limits of the storm circulation, and the minimum central pressure, Pc, at the storm centre. The gradient balance equation (E3-3) defining the 700 mb windfield indicates that, all else being equal, the square of the wind speed varies directly with Δp. Δp is fundamental to the whole tropical cyclone circulation. The storm surge height induced by a landfalling storm is approximately proportional to Δp, all other parameters being held constant. Much importance was thus attached to determining the character of Δp around the coastline. Statistical results concerning Δp derived in this section were subject to some uncertainty. Continuous reliable observations of Pn and Pc have been taken only since about 1944. The use of 500 km diameter data circles for individual site analysis resulted in samples which in certain cases had to be considered as limited ones. Hence for the analysis of Δp, a parallel set of statistics was generated based on 1000 km diameter data circles. The final form of the assumed Δp distribution was shaped by a certain amount of meteorological judgement in addition to the quantitative statistical tests performed.

The periphery pressure, Pn, is frequently defined as the average pressure around a hurricane where the isobars change from cyclonic to anticyclonic flow. The most comprehensive data set of Pn values can be found in NWS23, listing 74 Gulf Coast and 55 Atlantic Coast hurricanes. Values of Pn were determined at or near the time of a storm's minimum central pressure within 150 nautical miles (278 km) of the coast. This does not quite coincide with the way the central pressure is defined in the simulation procedure i.e. the closest recorded value of central pressure to any particular site. Also, the HURDAT

tape contained many more values of central pressure, for which there were no accompanying values of periphery pressure. Hence for the purpose of this analysis it was decided to define the central pressure difference using a constant value for Pn equal to 1013.0 mb. This is the average value that Pn takes in NWS23 and is also equal to the value of standard sea-level pressure. The coefficient of variation of Pn in the NWS23 compilation is 2.5 mb. Prior to NWS23 the most complete listing of Pn was contained in NHRP Staff (1957). These were mostly values of asymptotic pressure i.e. the value to which an exponential pressure profile (equation E2-2a) is asymptotic. By coincidence the average value of the Pn set determined by this method also turned out to be 1013.0 mb. Most interest is necessarily directed towards the behaviour of Δp at high values, where small deviations in the value of Pn have the least effect.

Figure 5.6 shows the variation of the mean and rms values of Δp along the coastline for both 500 and 1000 km diameter data circles. The 500 km data circle values show significantly greater variability along the coastline than the 1000 km data values. Clearly the transition from the smaller sized data circles to the larger ones induced a smoothing effect so that "local" characteristics (within several hundred kilometres of any one site) were lost. The major peaks in the mean Δp values occurring near Brownsville, Pensacola, the southern Florida peninsula and just north of New York City were virtually eliminated in the 1000 km diameter data sets. Therefore in the analysis of Δp the 500 km data circles are used to preserve the local characteristics of the central pressure difference while the 1000 km data circles are included to enhance the statistical reliability of the various tests.

Various attempts have been made to model the statistical variation of Δp along the U.S. coastline. In NWS23 two limiting values of Δp were obtained for the Standard Project Hurricane and the Probable Maximum Hurricane windfields based on smoothed averages of the lowest 7 recorded values of P_c in 500 nautical mile stretches of coastline spaced at 50 nautical mile centres. Gomes and Vickery (1976) and Tryggvason, Surry and Davenport (1976) defined Δp using the lognormal distribution. Batts, Cordes, Russell, Shaver and Simiu (1979) also used the lognormal distribution but imposed an upper limit for Δp of 135 mb. A preliminary examination of the data suggested that

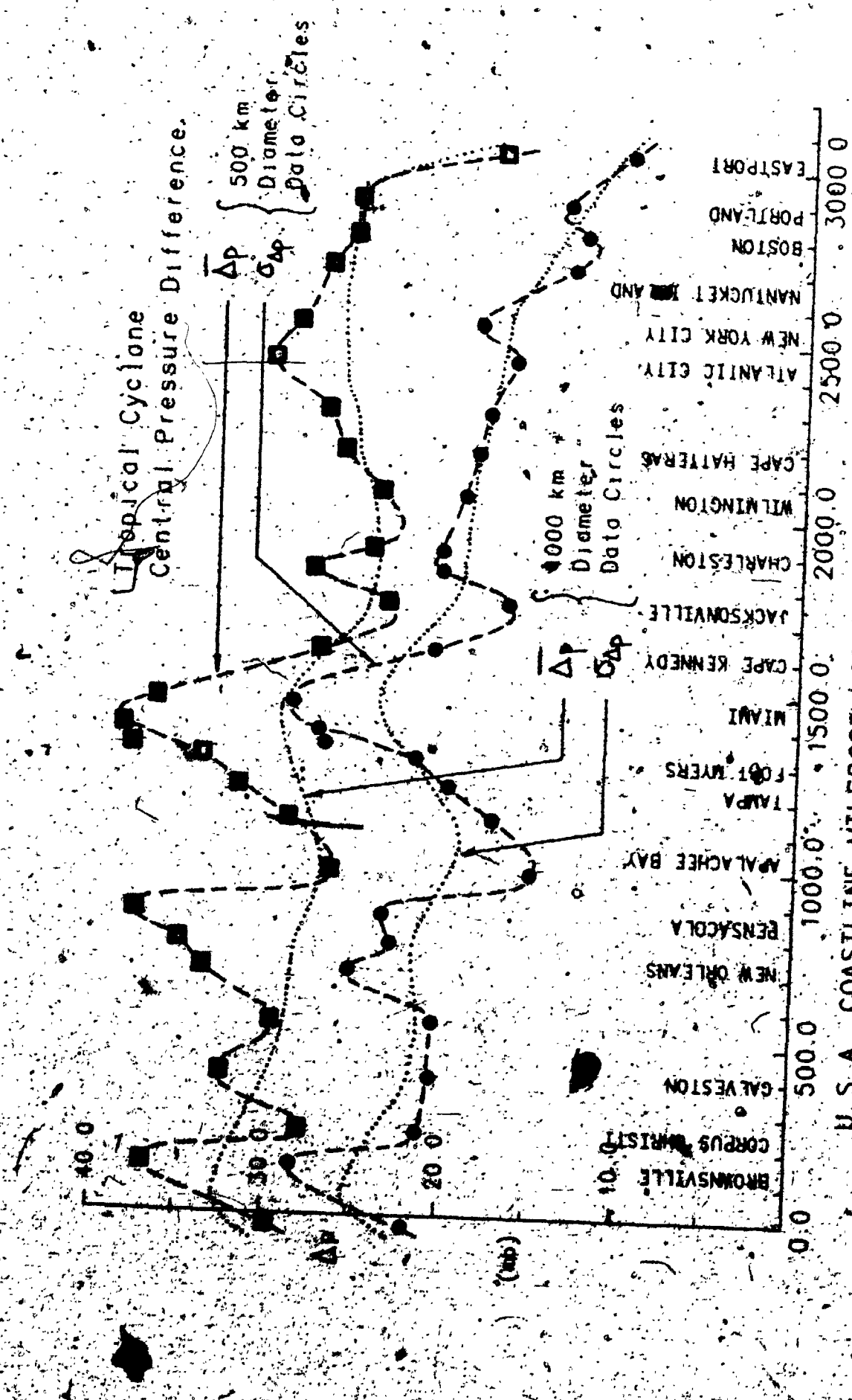

FIGURE 6.6 U.S. Coastline Central Pressure Difference Variation

the Weibull distribution might also suitably fit the data so comparitive tests were made on the Δp sets for stations along the U.S. coastline using three predictor distributions, (i) Weibull L.S.F. (least squares fit), (ii) Weibull M.L.F. (maximum likelihood fit) and (iii) lognormal M.L.F. The Weibull cumulative distribution function (CDF) and lognormal probability density function (PDF) are respectively :

$$\text{Weibull CDF } F(\Delta p) = 1.0 - exp\left[-\left(\frac{\Delta p}{C}\right)^{k}\right] \qquad E5-2$$

$$\text{Lognormal PDF } f(\Delta p) = \frac{1.0}{\Delta p \sqrt{2\pi}\, S_{ln\Delta p}} exp\left[-\frac{1}{2}\left\{\frac{ln\Delta p - m_{ln\Delta P}}{S_{ln\Delta p}}\right\}^{2}\right] \qquad E5-3$$

C, k = Weibull constants

$m_{ln\Delta p}, s_{ln\Delta p}$ = mean and rms values of distribution of $log(\Delta p)$

Statistical analysis of the three predictor equations comprised (a) Chi-square tests and (b) visual examination of the predictor CDF fitted curves for goodness-of-fit to the data samples.

(a) Chi-Square tests : these involve the calculation of a statistic related to the deviations of the sample data values from the predicted values. For a particular data set separated into N classes, the number of degrees of freedom, k, attached to the Chi-square (χ^2) statistic is equal to $(N-1)$ minus one each for every parameter estimated in the distribution. Attached to the statistic is a level of signifciance, α, defined such that the $prob(\chi^2(sample) > \chi^2(\alpha,k)) = \alpha$. High values of "$\alpha$" imply that the deviations found when using a particular predictor distribution function from the sample data are quite likely. The χ^2 statistic is additive, so it is possible to lump the individual data station χ^2 values together to give an idea as to the goodness-of-fit of a particular distribution over the whole coastline. A conservative estimate of the smallest number of observations possible in a χ^2 class is 5 to 10 (Cramer, 1956 ; Mald, 1952). Recent studies (Lindley, 1956; Fisz, 1963) have shown that tests based on as few as two observations per class give satisfactory results. Sample sizes for the 500 km and 1000 km data circles

ranging from 10 to 80 led to the choice of 8 and 16 for the number of classes to be used for the χ^2 statistic. The computed values for the three predictor equations are summarized in Table 5.1. In all cases the Weibull MLF candidate distributions exhibited the lowest χ^2 values and highest "α" values making it the most favoured.

(b) Goddness-of-fit tests : when initially comparing the three predictor CDF functions to the sample data sets it was found that standard linear CDF plots could be ambiguous to the extent that both Weibull and lognormal fitted curves appeared equally suitable. The Weibull distribution can be rewritten in the form :

$$ln\left[-ln(1.0-F(<\Delta p))\right] = k\,ln\Delta p - k\,lnC \qquad E5-4$$

Data sample pairs of $(log\Delta p,\ log[-log(1.0-F(\Delta p))])$ thus yield linear relationships for data following Weibull distributions. On the same axes lognormal distribution functions appear as monotonically increasing convex-upwards curves. Four examples are shown in Figure 5.7. The general trend exhibited by the data did not favour the lognormal distribution. In fact, a slightly concave-upward trend persisted in virtually all the data samples. Most importantly, in the critical area of the graphs (i.e. the high Δp end) the sample points showed no sign of a curving trend in compliance with the lognormal distribution. The CDF goodness-of-fit tests thus also favoured the Weibull MLF distribution.

As a final criterion upon which to base the choice for the Δp distribution, the Weibull MLF and lognormal MLF predictor curves were combined with the local occurrence rate to calculate the estimated Δp value associated with a 100-year return period storm along the coastline. The results are shown in Figure 5.8. From a meteorological point of view it is impossible to justify the excessive values indicated by the lognormal predicted curve for a majority of the coastal sites (e.g. the expected 100-year return period hurricane for Miami would have a minimum central pressure around 750 mb). The values predicted by the Weibull MLF curve seem reasonable although somewhat conservative in the Florida peninsula area.

ranging from 10 to 80 led to the choice of 8 and 16 for the number of classes to be used for the χ^2 statistic. The computed values for the three predictor equations are summarized in Table 5.1. In all cases the Weibull MLF candidate distributions exhibited the lowest χ^2 values and highest "α" values making it the most favoured.

(b) Goddness-of-fit tests : when initially comparing the three predictor CDF functions to the sample data sets it was found that standard linear CDF plots could be ambiguous to the extent that both Weibull and lognormal fitted curves appeared equally suitable. The Weibull distribution can be rewritten in the form :

$$ln\left[-ln(1.0-F(<\Delta p))\right] = k\,ln\Delta p - k\,lnC \qquad E5-4$$

Data sample pairs of $(log\Delta p,\ log[-log(1.0-F(\Delta p))])$ thus yield linear relationships for data following Weibull distributions. On the same axes lognormal distribution functions appear as monotonically increasing convex-upwards curves. Four examples are shown in Figure 5.7. The general trend exhibited by the data did not favour the lognormal distribution. In fact, a slightly concave-upward trend persisted in virtually all the data samples. Most importantly, in the critical area of the graphs (i.e. the high Δp end) the sample points showed no sign of a curving trend in compliance with the lognormal distribution. The CDF goodness-of-fit tests thus also favoured the Weibull MLF distribution.

As a final criterion upon which to base the choice for the Δp distribution, the Weibull MLF and lognormal MLF predictor curves were combined with the local occurrence rate to calculate the estimated Δp value associated with a 100-year return period storm along the coastline. The results are shown in Figure 5.8. From a meteorological point of view it is impossible to justify the excessive values indicated by the lognormal predicted curve for a majority of the coastal sites (e.g. the expected 100-year return period hurricane for Miami would have a minimum central pressure around 750 mb). The values predicted by the Weibull MLF curve seem reasonable although somewhat conservative in the Florida peninsula area.

TABLE 5.1

χ^2 STATISTIC TESTS : ΔP DATA

		Distribution		
		WEIBULL LSF	WEIBULL MLF	LOGNORMAL MLF
(1) 500 km Diameter Data Circles				
8-Class	χ^2	272.9	167.8	200.3
	α(%)	26.2	42.1	36.9
16-Class	χ^2	471.4	418.4	429.4
	α(%)	39.5	43.2	42.6
(2) 1000 km Diameter Data Circles				
8-Class	χ^2	299.1	167.4	249.3
	α(%)	22.8	42.1	29.5
16-Class	χ^2	502.3	474.5	537.0
	α(%)	38.0	39.7	35.9

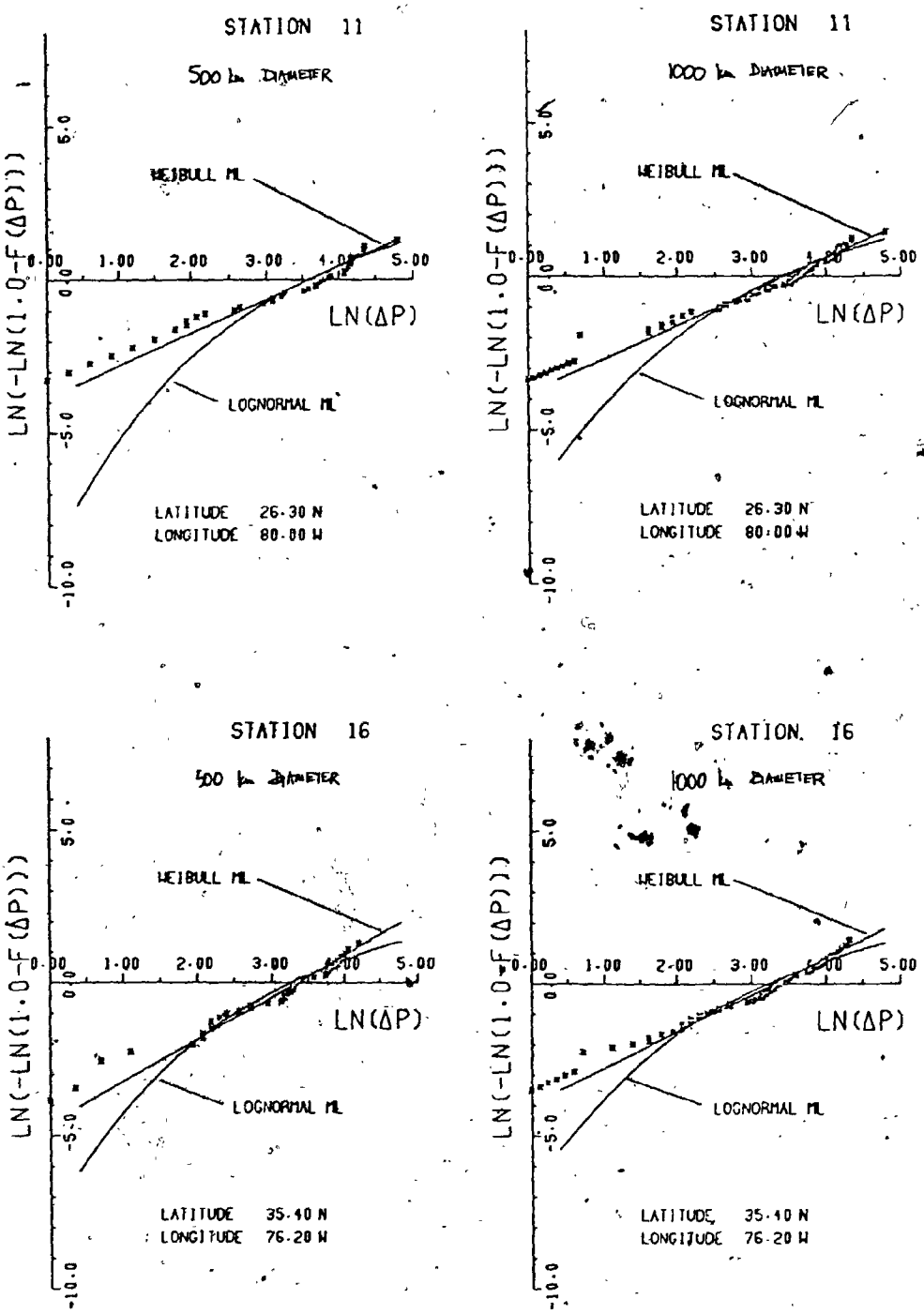

FIGURE 5.7 Δp Data Goodness-of-Fit Tests

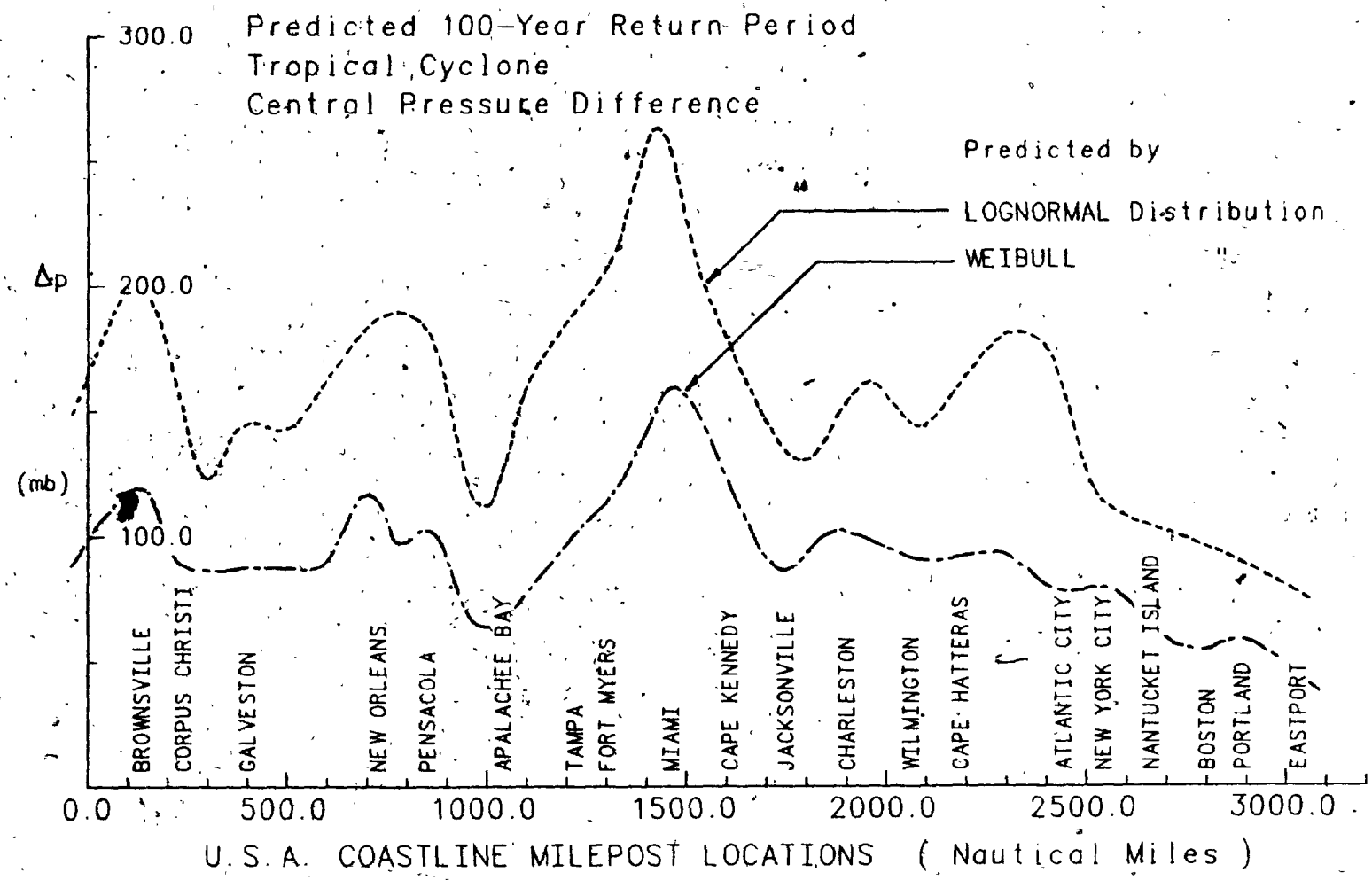

FIGURE 5.8 U.S. Coastline 100-Year Return Period Δp Variation

The unrealistically high values of Δp generated in a simulation running several thousands of years utilizing the lognormal distribution is a defect which has in fact been recognized by researchers who use this distribution. The problem has been remedied in these cases by introducing an artificial cut-off point (e.g. $\Delta p = 135$ mb in Batts et al, 1980). Storms generated in the simulation which have a Δp value greater than the cut-off value are then either completely rejected or the Δp value reduced to the cut-off point. Such artificial mechanisms only serve to warp the resulting extreme values at the upper end and do nothing to rectify the errors in modelling the body of the Δp distribution. The effects of such artificial cut-offs are discussed further in section 6.5. These considerations combined with the Chi-square and goodness-of-fit tests led to the choice of the Weibull distribution as the one best suited to represent Δp.

5.5 Radius of Maximum Winds - "RMAX"

The radius of maximum winds, *RMAX*, is the primary measure of the lateral extent of a tropical cyclone and is an important factor in the generation of storm surge. A tropical cyclone that is both large and intense has enormous destructive power. Intense tropical cyclones tend to have small values of *RMAX* and storms in northerly latitudes have larger *RMAX* values than those in southerly latitudes. For example, two of the most intense North Atlantic tropical cyclones ever recorded, the Labour Day hurricane of 1935 ($Pc = 892mb$) and Hurricane Camille in 1969 ($Pc = 908mb$), both had well-formed vortices with small values of *RMAX*, 11 and 15 km respectively. The 12 Northwest Pacific typhoons which had minimum central pressures below 900 mb in the period 1960-1973 had a mean value of *RMAX* equal to 15 km, with the largest value in the group equal to 32 km. This compares to the overall *RMAX* average of 25 km for all Northwest Pacific tropical cyclones in the same period, with more than 20 storms having *RMAX* values greater than 50 km.

Several studies have examined the correlation between *RMAX* and other tropical cyclone characteristic parameters. Myers (1954) applied a kinetic

energy evaluation to coastal hurricanes and found a suggestion of an inverse relation between size (*RMAX*) and intensity (Δp) for the more intense storms. Kuo (1959) showed that from theoretical considerations the eye diameter should decrease if the central pressure was reduced. These notions were reinforced in Colon's study (1963) which showed that in a majority of observed cases the widening of the storm eye accompanied weakening of a storm and vice versa.

Depperman (1959) examined data from 195 tropical cyclones which crossed the Philippines and concluded that deeper storms tended to have smaller eyes. Shea and Gray's (1973) composite data analysis (section 2.3) confirmed this trend for the North Atlantic. Figures 5.9 and 5.10, taken from their report, show the variation of *RMAX* with maximum wind speed and latitude respectively. These graphs indicate large variability in *RMAX* values at particular wind speeds and latitudes but nevertheless exhibit a definite pattern correlating *RMAX* inversely with maximum wind speed, and hence intensity, and inferring increasing *RMAX* values with increasing latitude. An analysis of *RMAX* versus *Pc*, the minimum central pressure, found in Ho, Schwerdt and Goodyear (1975) supported the same conclusion. However, when the latitudinal trend present in both *RMAX* and *Pc* was removed, it was found that the relationship between these two variables weakened considerably. Graham and Hudson (1959) had previously suggested that there was no latitudinal trend in *RMAX* once the *RMAX-Pc* inter-relation was removed. A final study worthy of note is that of Bell (1974), examining tropical cyclone eye observations in the Northwest Pacific for the period 1958-1973. Table 5.2 shows the distribution of *RMAX* values separated into groups by their minimum central pressure. It can be seen that the mean *RMAX* values decrease with increasing intensity. One particularly interesting feature is that for values of *Pc* greater than 980 mb the mean *RMAX* value begins decreasing again. This feature agrees with an often observed characteristic of tropical cyclones in their formative stage to begin by increasing their size until they are properly organized and then once tropical storm intensity has been achieved for the eye to begin contracting.

Tryggvason, Surry and Davenport (1976) and Russell (1976) both assumed *RMAX* to be distributed as a lognormal random variable with constant

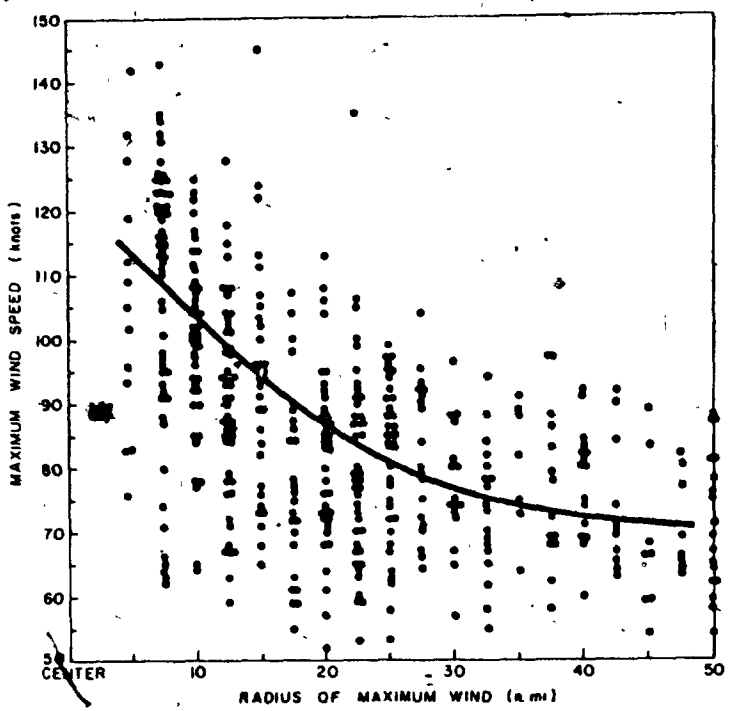

FIGURE 5.9 Variation of RMAX with Maximum Wind Speed for Lower Tropospheric Data (Shea and Gray, 1973)

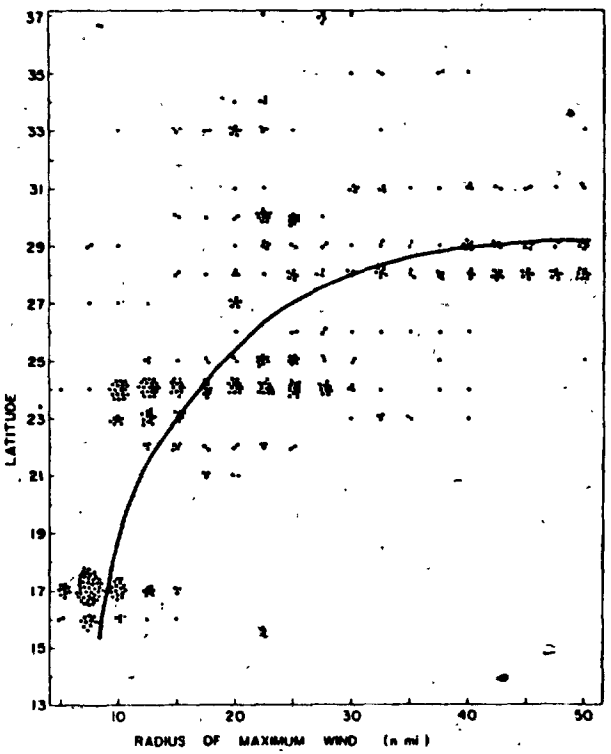

FIGURE 5.10 Variation of RMAX with Latitude for Lower Tropospheric Data (Shea and Gray, 1973)

TABLE 5.2

FREQUENCY DISTRIBUTION OF NORTHWEST PACIFIC TROPICAL CYCLONE EYE DIAMETER VERSUS EYE PRESSURE
1958-1968

Total Number of Storms = 2013

Eye Diameter (n. miles)	Eye Pressure (mb) -919	920-939	940-959	960-979	980-	TOTAL
0-20	72.0	52.4	46.6	41.0	49.4	47.8
21-40	24.7	44.1	40.9	41.7	36.8	38.9
41-60	2.1	3.5	8.0	12.6	7.7	8.6
61-80	1.0	-	2.9	2.9	3.7	2.9
81--	-	1.7	1.9	2.4	1.8	
TOTAL	4.6	8.4	17.4	29.5	40.1	100.0
MEAN DIAMETER (km)	36.0	44.5	52.7	55.2	51.9	
RMS DIAMETER (km)	21.6	19.8	33.5	33.7	37.7	

variance and its median linearly dependent upon Δp in the former case and its mean linearly dependent upon $log(\Delta p)$ in the latter case. Gomes and Vickery (1976) found the best correlation to exist between the mean of $log(RMAX)$ and $log(\Delta p)$. Batts et al (1980) also assumed $RMAX$ to be lognormally distributed. The governing distribution was censored however so that $8km < RMAX < 100km$, to avoid unrealistically "tight" or "broad" storms. Tryggvason et al (1976) also placed limits upon the median of $RMAX$, so that $14\,km < median(RMAX) < 93\,km$.

NWS23 formed the basis of the analysis of $RMAX$ data in this study, comprising 49 Atlantic Coast hurricanes (1900-1978), 67 Gulf Coast hurricanes (1900-1978) and 179 Northwest Pacific typhoons (1960-1974). The first two sets relevant to the United States list values of $RMAX$ at or near the time of lowest minimum central pressure within 150 nautical miles of the coast, for tropical cyclones with Pc less than 982 mb. The cut-off used for the typhoon data was 985 mb. $RMAX$ values were determined from land station wind speed records, eye radii from aircraft radar, eye radii from aerial reconnaissance wind reports, estimates from pressure profile data and narrative or tabular data documented in the Monthly Weather Review Journal (pre-1950). A screening process was used in compiling the data which rejected questionably high values of $RMAX$ for a number of tropical cyclones. Figure 5.11 shows the complete set of U.S. tropical cyclone $RMAX$ values used to develop the governing probabilistic relationships around the coastline. While considerable scatter is evident, the correlation between $RMAX$ and Δp is borne out by the monotonically decreasing upper limit of $RMAX$ values with increasing Δp. There also appears to be a higher percentage of tropical cyclones with large $RMAX$ values at any given value in the Atlantic Coast sample set than for the Gulf Coast set. The correlations between $RMAX$, minimum central pressure and latitude and longitude determined in NWS23 are given in Table 5.3.

Establishing the joint probability relationship between two parameters with a given degree of reliability requires a larger sample of data than that needed in determining a single parameter probability density function. Clearly much more data than presently available would be necessary to establish conclusively the joint probability relationship between $RMAX$ and

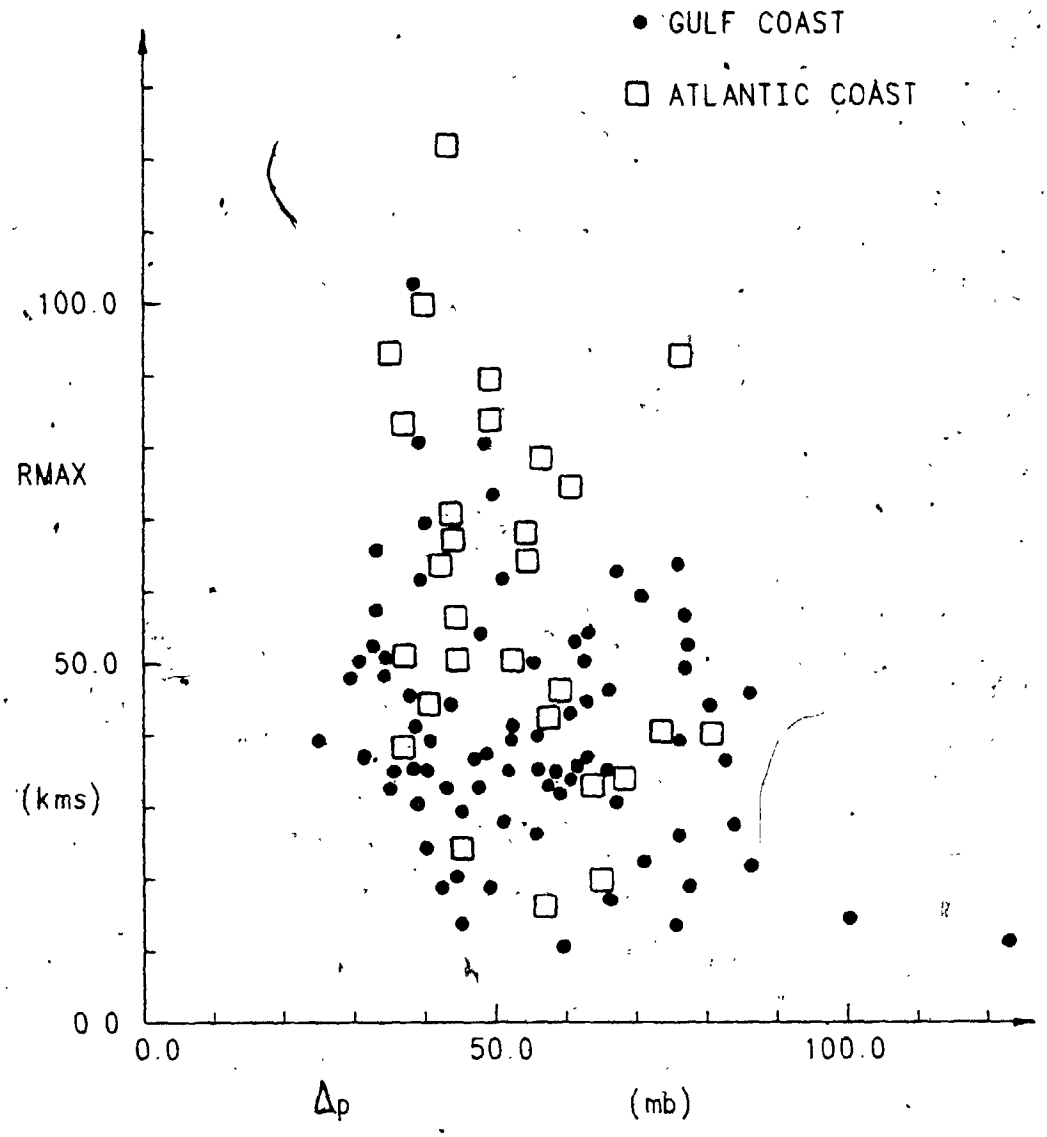

FIGURE 5.11 **RMAX Versus Δp for 116 Gulf and Atlantic Coast Tropical Cyclones (Central Pressure < 985 mb)**

TABLE 5.3

CORRELATIONS BETWEEN RMAX, Pc, LATITUDE AND LONGITUDE FOR NORTH ATLANTIC AND NORTHWEST PACIFIC TROPICAL CYCLONES

CORRELATION COEFFICIENT ρ_{xy}

	x			
	RMAX	Pc	Latitude	Longitude
y				
(1) GULF COAST				
RMAX	-	0.33	*	-0.06
Pc	0.33	-	*	-0.02
Latitude	*	*	-	*
Longitude	-0.06	-0.02	*	-
(2) ATLANTIC COAST				
RMAX	-	0.39	0.52	*
Pc	0.39	-	0.27	*
Latitude	0.52	0.27	-	*
Longitude	*	*	*	-
(3) NORTHWEST PACIFIC				
RMAX	-	0.20	0.26	*
Pc	0.20	-	0.18	*
Latitude	0.26	0.18	-	*
Longitude	*	*	*	-

*Not Applicable

Δp. Hence some meteorological judgement tempered the statistical analysis that follows.

The data were examined in three groups - Gulf Coast, Atlantic Coast and Gulf and Atlantic Coasts combined, referred to as groups G, A and C respectively. Relationships between various parameters were investigated in terms of their variation with $log(\Delta p)$, in particular the mean and rms value of $RMAX$, $\{m(RMAX), s(RMAX)\}$, and the median and rms value of $log(RMAX)$, $\{med(RMAX), s(log(RMAX)\}$. Initially, data pairs of (Δp, $RMAX$) were separated into an equal number of groups on the basis of increasing Δp. Correlations between the various parameters cited above proved to be quite high, so the lognormality assumption of the distribution of $RMAX$ was tested in the following manner. The following relationships were assumed:

$$med(RMAX) = \frac{C_1}{\Delta p^x} \qquad (E5-5)$$

$$s(log(RMAX)) = \frac{C_1}{\Delta p^y} \qquad (E5-6)$$

C_1, x, C_2, y = positive constants

The values of C_1, x, C_2 and y were determined by maximum likelihood analysis assuming $RMAX$ to be lognormally distributed. In order to examine the suitability of relationships suggested by previous authors, the analysis was performed three times with (i) all four parameters maximized, (ii) C_1, x, C_2 maximized and $y = 0.5$, and (iii) C_1, C_2 maximized and $x = 0.5$, $y = 0.0$. The results of the analysis are given in Table 5.4. Distinct differences appeared in the parameters determined for groups G and A for all three analysis runs. Parameters C_1 and x showed only small differences between analyses (i) and (ii). The value of C_2 hardly changed at all for analyses (ii) and (iii). These results suggested a further examination of the data to test (a) whether the Gulf and Atlantic Coast data belonged to statistically separate populations and (b) whether the simpler, and hence more attractive

TABLE 5.4

MAXIMUM LIKELIHOOD RELATIONSHIPS BETWEEN MED(RMAX), S(LOG(RMAX)) AND ΔP

Analysis		Tropical Cyclone Group		
		Gulf "G"	Atlantic "A"	Combined "C"
(i)	Med(RMAX)	$\frac{234.4}{\Delta p^{0.466}}$	$\frac{1693.6}{\Delta p^{0.896}}$	$\frac{435.2}{\Delta p^{0.603}}$
	S(log(RMAX))	$0.149\ \Delta p^{0.271}$	$0.141\ \Delta p^{0.284}$	$0.274\ \Delta p^{0.130}$
(ii)	Med(RMAX)	$\frac{254.7}{\Delta p^{0.487}}$	$\frac{1796.8}{\Delta p^{0.911}}$	$\frac{459.9}{\Delta p^{0.617}}$
	S(log(RMAX))	0.443	0.430	0.459
(iii)	Med(RMAX)	$\frac{268.1}{\Delta p^{0.5}}$	$\frac{360.0}{\Delta p^{0.5}}$	$\frac{289.4}{\Delta p^{0.5}}$
	S(log(RMAX))	0.443	0.439	0.460

Maximized Relations : $\text{Med(RMAX)} = \frac{C1}{\Delta p^{x}}$

$\text{S(log(RMAX))} = \frac{C2}{\Delta p^{y}}$

Analysis (i) no restrictions on C1, x, C2, y
(ii) set $y = 0$
(iii) set $x = 0.5, y = 0$

relationships for analysis assumption (iii) with $x=0.5$ and $y=0.0$ were adequate. This was done through the use of the standard "t"-test.

Each of the three tropical cyclone groups were tested in the following manner. Data pairs (Δp,$RMAX$) of group I say were assumed to obey the functional relationships that had been determined for group J. Unit normal variates for each data pair could then be computed and this new sample set subjected to the t-test under the hypothesis of a Gaussian population $N(0,1)$. The results are shown in Table 5.5 expressed in terms of the cumulative distribution percentage of each sample's "t" parameter. A very high percentage indicates that the sample is very likely to have come from the assumed population, and vice versa. As expected, each group did well when it was assumed to be part of a population whose parameters (C_1, x, C_2, y) were determined by its own data pairs. However both the Gulf Coast and Atlantic Coast groups fared badly, especially the Atlantic Coast group, when they were assumed to belong to the Combined distributions. The hypothesis that the Atlantic Coast group could be represented by the functional relationships derived for the Combined group (Gulf plus Atlantic Coasts) is strongly rejected. As a second outcome of the t-test analysis, it can be seen that the three parameter assumption groups (i), (ii) and (iii) fared equally well amongst each data group. In fact, group (iii) with $x=0.5$ and $y=0.0$ appears to be slightly more acceptable.

For the sake of completeness, the same statistical analysis was repeated with the (Δp,$RMAX$) data groups to see if relationships assuming $RMAX$ to be Gaussian or Weibull distributed gave better fits to the data. The results gave very poor fitting relationships compared to the lognormal analysis. Thus it was decided to define $RMAX$ as being lognormally distributed and conditionally dependent upon Δp. On the basis of the t-tests it was decided to adopt the simpler form of the relationships examined, $x=0.5$ and $y=0.0$, with a view to checking the sensitivity at a later stage within the simulation procedure itself. It may be noted that the simpler form of the resulting equations facilitated certain analytical formulations subsequently performed in conjunction with the running of the simulation procedure. The governing relationships thus chosen to describe the $RMAX$ parameter are:

TABLE 5.5

GULF AND ATLANTIC COAST RMAX "t"-TESTS

		Group J (Sample) Tropical Cyclone Group		
		Gulf "G"	Atlantic "A"	Combined "C"
Group I (Assumed Population)				
Gulf			(%)	
Analysis	(i)	99.0	-	-
	(ii)	99.7	-	-
	(iii)	99.9	-	-
Atlantic				
Analysis	(i)	-	99.8	-
	(ii)	-	99.9	-
	(iii)	-	99.9	-
Combined				
Analysis	(i)	7.2	0.8	99.0
	(ii)	8.0	0.9	98.5
	(iii)	6.8	0.8	99.9

Analysis Groups (i), (ii) and (iii)
Same as per Table 5.4

Gulf Coast

$$med(RMAX) = \frac{268.1}{\sqrt{\Delta p}} \qquad E5.7a$$

$$s(log(RMAX)) = 0\ 443 \qquad E5-7b$$

Atlantic Coast

$$med(RMAX) = \frac{260\ 0}{\sqrt{\Delta p}} \qquad E5-8a$$

$$s(log(RMAX)) = 0\ 439 \qquad E5-8b$$

Figures 5.12 and 5.13 show the chosen relationships between $RMAX$ and Δp for both coastal regions along with the actual data values.

5.6 Translation Velocity - "VT"

In contrast to the two preceding parameters the tropical cyclone translation velocity, VT, was found to behave in a most regular manner. The translation velocity dictates how long a particular location will be under a storm's influence. It is responsible for the added component of wind velocity on the right-hand side of the storm circulation above the inflow layer and the right-front quadrant wind maximum within the boundary layer. It is also an important parameter in the potential storm surge a landfalling tropical cyclone can generate.

In Figure 5.14 can be seen the coastal variation of the mean and standard deviation of the translation velocity, VT. VT increases monotonically with latitude. The tropical cyclone translation velocity has previously been described using the lognormal distribution. By way of comparison, coastal data sets of VT were also fitted using least squares fit and maximum likelihood Weibull distributions in exactly the same manner as had been done for the central pressure differentce, Δp. The comparison of the three predictor distributions was based, as for Δp, on (a) Chi-square tests and (b) visual examination of the data sets for goodness-of-fit to the assumed cumulative distribution functions.

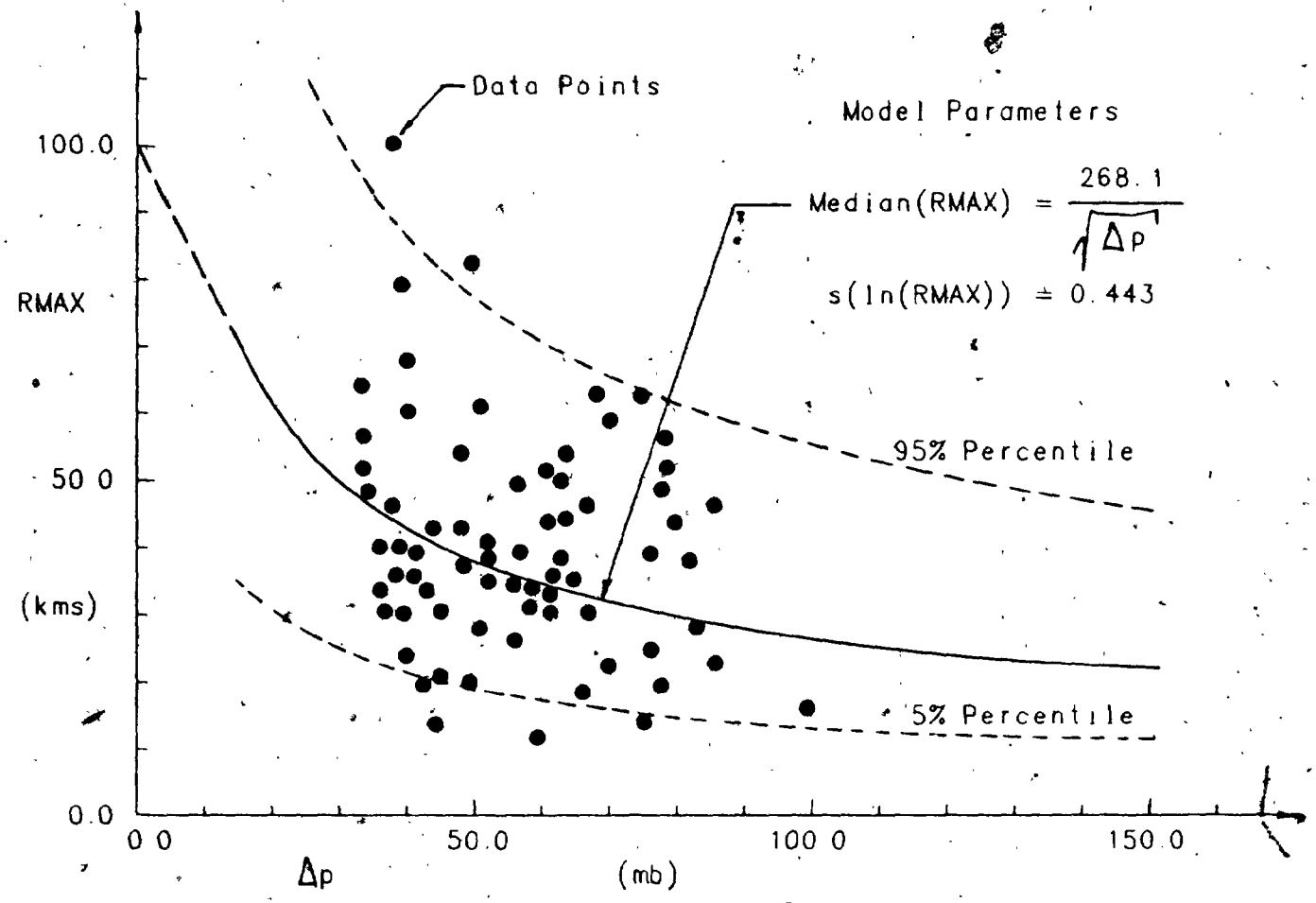

FIGURE 5.12 Comparison of Observed with Predictor Values of RMAX Versus Δp - Gulf Coast Storms

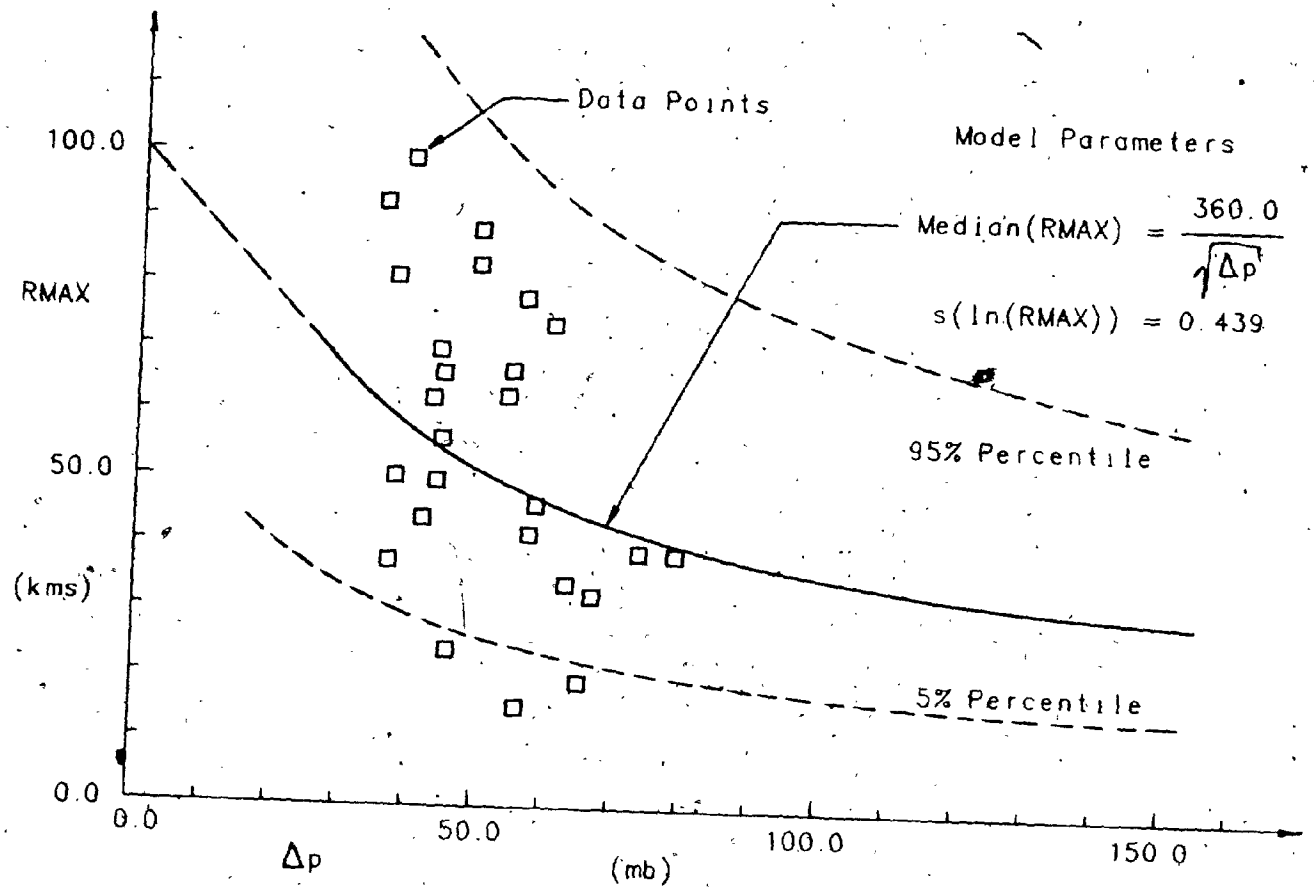

FIGURE 5.13 Comparison of Observed with Predictor Values of RMAX Versus Δp - Atlantic Coast Storms

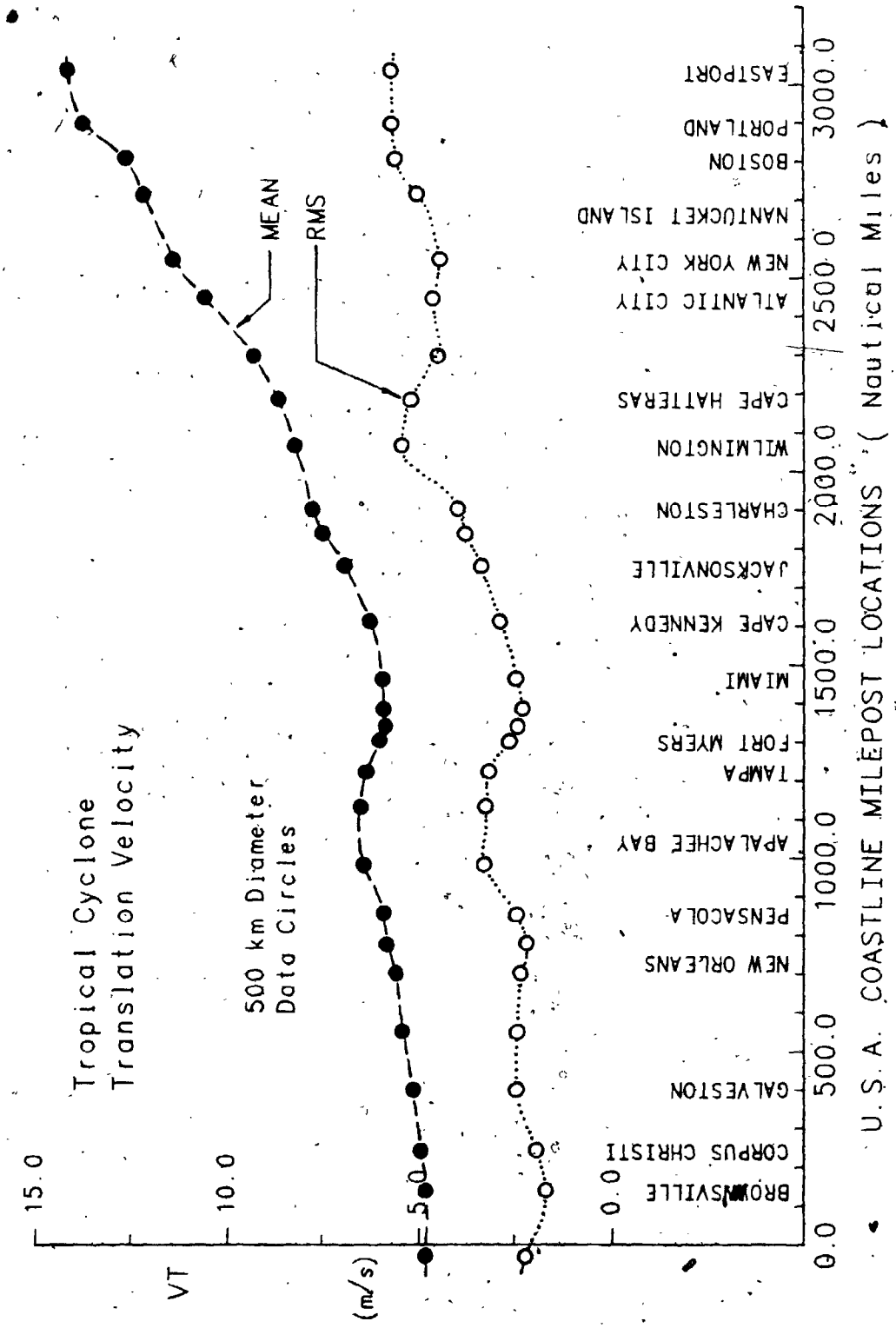

FIGURE 5.14 U.S. Coastline Translation Velocity Variation

(a) Chi-square tests : these were applied to each predictor equation using three class sizes, 8, 12 and 20. The results are summarized in Table 5.6 showing values of χ^2 (all stations) and the significance level of this value for each distribution tested. The lognormal distribution becomes superior as the number of classes increases. This trend arises because for the 8-class tests, the first and last classes are not as sensitive to the deviations in the distribution at their extremes as for the 20-class tests. The Weibull distributions become less satisfactory as the number of classes increases, whereas the lognormal distribution appears to retain a satisfactory level of acceptance in all cases.

(b) Goodness-of-fit tests : graphs of the CDF of the translation velocity were plotted in the same manner as for the central pressure difference. As mentioned before, the vertical double-logarithmic scale chosen linearizes data belonging to Weibull-type distributions, but results in monotonically increasing convex-upwards curves for lognormal distributions. Graphs for three coastal locations are shown in Figure 5.15. These were typical of the entire coastline. The data follow the lognormal predictor equations much better than the Weibull curves. It can also be seen that for the central portion of data points, both distributions fit the data well, explaining the approximately equal Chi-square values for the 8-class tests. It was the extreme points which really showed up the bias in the data towards the lognormal fitting curves.

Thus both the Chi-square tests and CDF goodness-of-fit tests strongly supported the adoption of the lognormal distribution to describe the tropical cyclone translation velocity. The predicted mean and rms values of the VT data sets, assuming that they are lognormally distributed, are:

$$m^P(VT) = exp\left[m(log(VT)) + \frac{1}{2}\, s^2(log(VT))\right] \qquad E5-9a$$

$$s^P(VT) = m^P(VT)\left[exp\left\{s^2(log(VT)) - 1.0\right\}\right]^{\frac{1}{2}} \qquad E5-9b$$

TABLE 5.6

X^2 STATISTIC TESTS : VT DATA

		DISTRIBUTION		
		LOGNORMAL MLF	WEIBULL LSF	WEIBULL MLF
500 km Diameter Data Circles				
8-Class	X^2	147.4	144.6	198.5
	α(%)	29.3	30.3	14.2
12-Class	X^2	217.4	233.7	281.4
	α(5)	43.1	37.1	22.8
16-Class	X^2	422.8	527.0	533.6
	α(%)	41.3	18.5	17.0

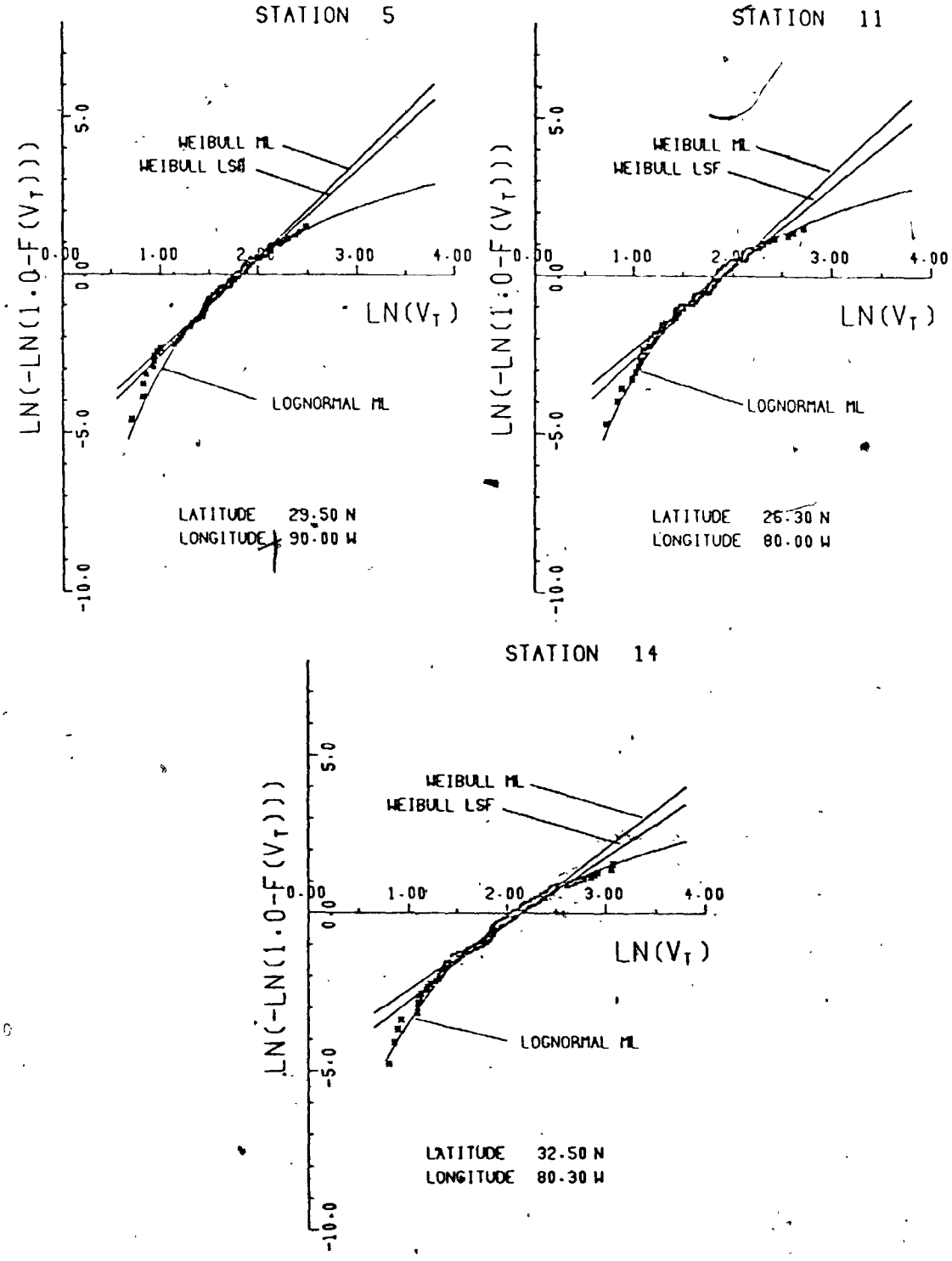

FIGURE 5.15 VT Data Goodness-of-Fit Tests

$m(log(VT)), s(log(VT))$ = observed mean, rms of $log(VT)$
$m^P(VT), s^P(VT)$ = predicted mean, rms of VT

Using equations E5-9a and b it was possible to compare the observed mean and rms values of VT to the ones predicted under the lognormality assumption. The comparison of the means was extremely close, with slightly greater variation between predicted and observed rms VT values. Figure 5.16 shows the variation of the observed mean and rms values of $log(VT)$ data used to define the distribution of the tropical cyclone translation velocity.

5.7 Approach Angle - "θ"

The tropical cyclone approach angle was determined as the average angle exhibited by a storm within each 500 km diameter data circle. This angle, θ, is the average storm heading taken clockwise positive from North (=0°). While a tropical cyclone may change its translation direction considerably within a circle of diameter 500 km, the average angle will usually be very close to the actual value at the centrepoint where the track is closest to the site of interest. Since most interest is concentrated on the time when the storm is reasonably close to the particular site no attempt is made to account for track curvature within the simulation procedure. The approach angle has a significant effect on the simulation results when these are combined with wind tunnel test data for structures whose dynamic response is sensitive to wind direction. The variation of approach angle along the coastline has an added significance with respect to the risk associated with line-like structures such as transmission lines, dealt with in Chapter 7.

The occurrence of tropical cyclones moving with track headings in the range $90° < \theta < 270°$ is rare. Those storms with values in the range $180° < \theta < 270°$ occur under the influence of deep northeasterly flows and have only been observed in several instances on the west coast of the Gulf of Mexico and two cases in the region of the Florida Peninsula. NWS23 in fact totally excludes the possibility of hurricanes moving with headings in the range $90° < \theta < 250°$. Figure 5.17 shows the variation of the mean and rms value of θ around the U.S. coastline. At the western end of the Gulf of Mexico the storms

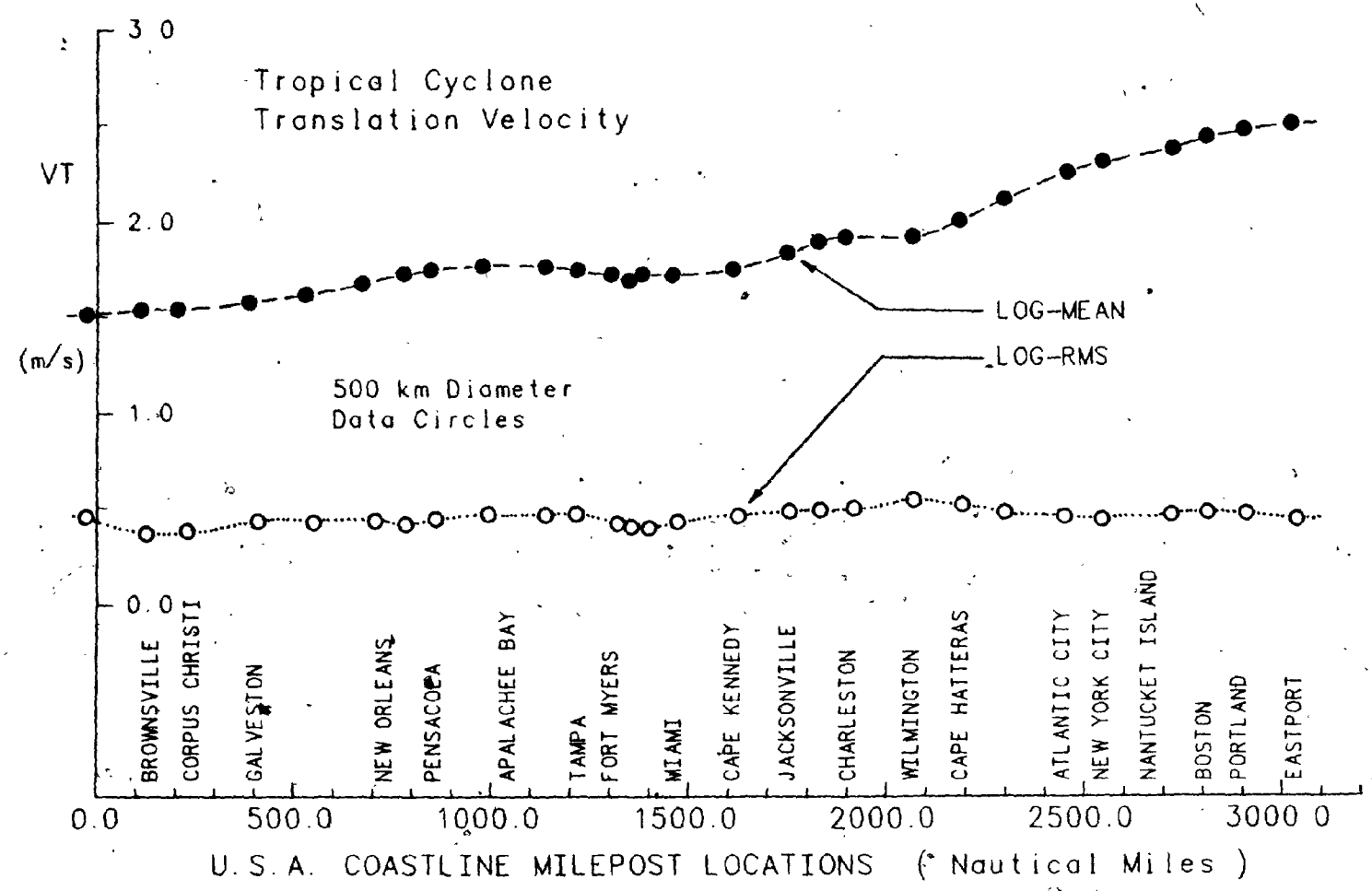

FIGURE 5.16 U.S. Coastline VT Predictor Distribution Parameters

are typically moving west-northwest and northwestward. From New Orleans till the Florida west coast the mean value of θ is almost exactly zero (due North). North of the 30° latitude tropical cyclones turn northeastward. The rms value of θ lies in the range, $40° \leq s(\theta) < 50°$, over most of the coastline, except for the Atlantic north of 30° latitude, where it falls to about half this value.

The analysis of the tropical cyclone approach angle, θ, made in most previous studies was not viewed as being critical to the outcome of the results of a simulation, except in cases involving the estimation of storm surge. In most simulations the distribution of θ was assumed to be uniform within some empirically determined range spanning the observed mean value. Tryggvason (1980) used the von Mises distribution. This distribution plays a central role in statistical inference on the circle where its importance is somewhat similar to that of the normal distribution on the line. Its PDF is defined by:

$$f(\theta) = \frac{1}{2\pi I_o(k)} \exp\left[\frac{\cos(\theta - \theta_o)}{\frac{1}{k}}\right] \qquad E5-10$$

$I_o(k)$ = modified Bessel Function, 1st kind, zero order
θ_o = mean approach angle
k = concentration parameter

As $1/k$ becomes very large the von Mises distribution reduces to the uniform distribution. For small $1/k$, θ is distributed as a normal distribution with mean equal to θ_o and rms equal to $1/k$. The smaller that $1/k$ becomes, the more concentrated the distribution of θ becomes about its mean θ_o. This flexibility makes it a natural one to choose as the distribution governing the approach angle. An initial examination of CDF plots of θ data sets confirmed the suitability of both the von Mises and normal distributions. For further comparison, Weibull CDF curves were fitted to the data sets. Figure 5.18 shows two comaprisons, typical of what was observed for all the coastal sites. The von Mises and normal distributions were for all intents and purposes identical. The Weibull fitted distributions showed significant deviation for a

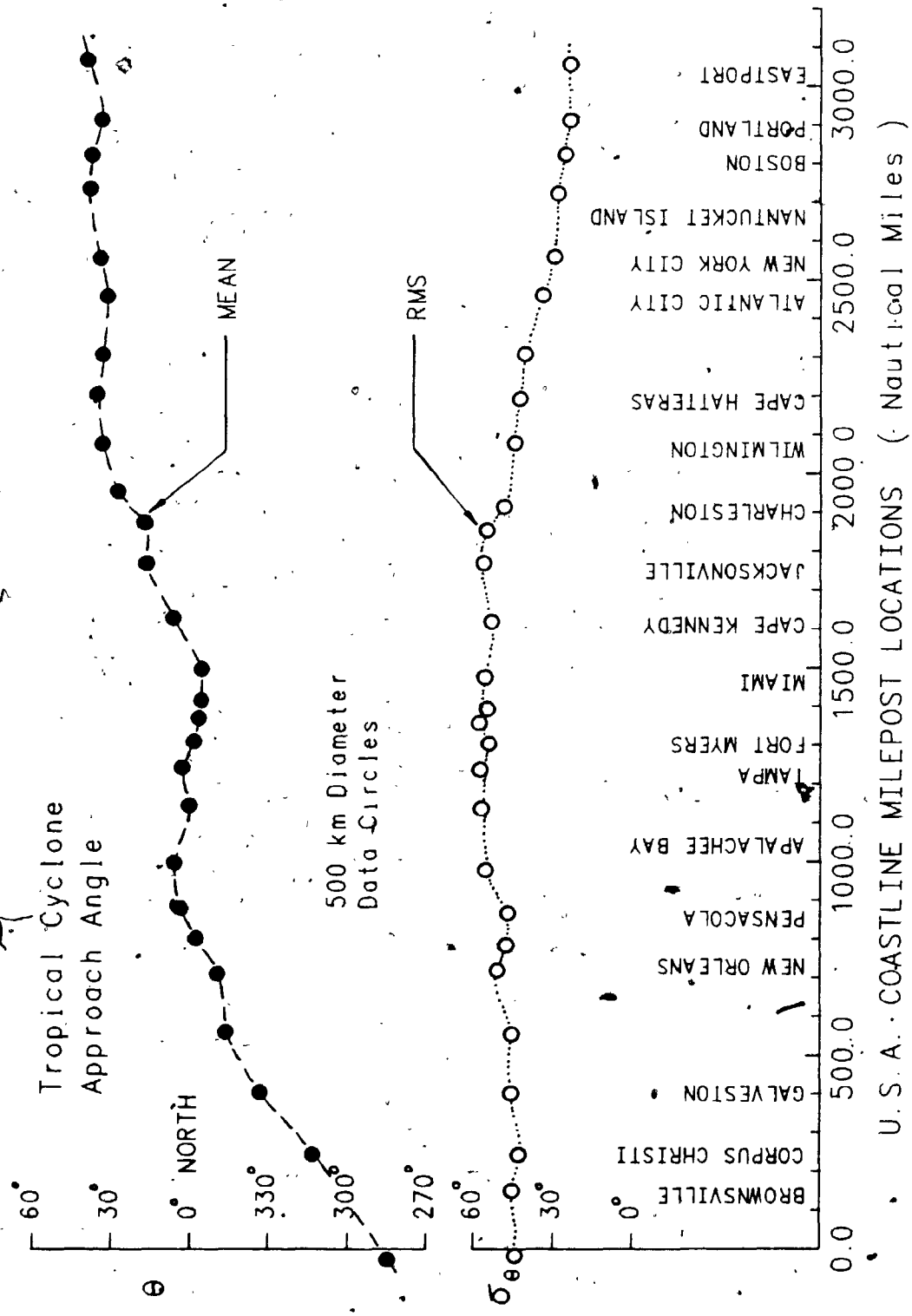

FIGURE 5.17 U.S. Coastline Approach Angle Variation

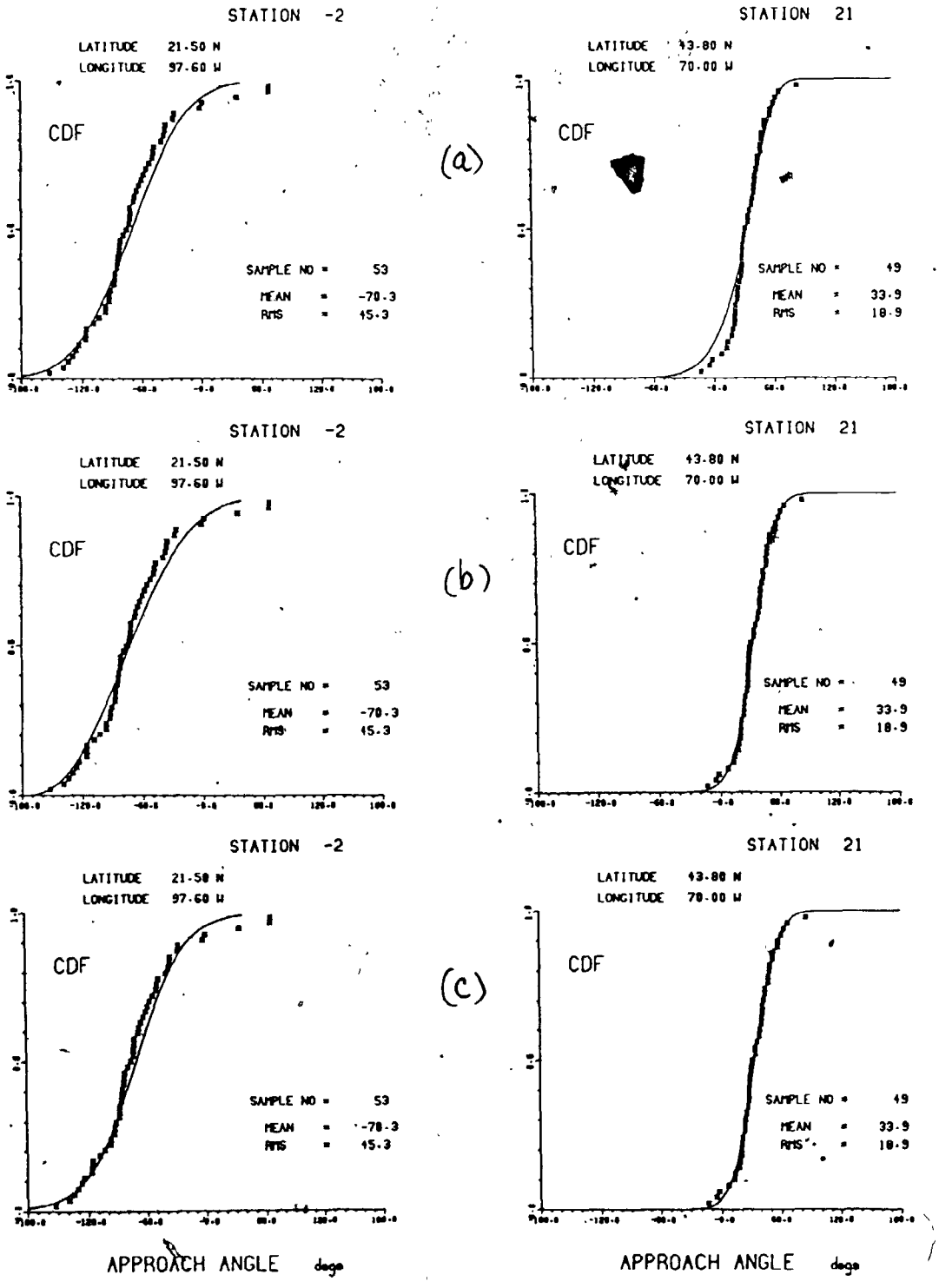

FIGURE 5.18 **θ Data CDF Comparisons : (a) Weibull, (b) Normal and (c) von Mises Distributions**

number of data sets particularly the Atlantic coastal sites. Chi-square tests reflected the visual assessment of the CDF fitted curves.

For these reasons it was decided to adopt the von Mises distribution as the one best suited to describing θ. Figure 5.19 shows values of θ_o and $1/k$ around the U.S. coastline used to generate the distributions of approach angle at any particular site. It may be recalled that lower values of $1/k$ indicate greater concentration of θ values about the mean θ_o.

5.8 Minimum Approach Distance - "DMIN"

The minimum approach distance, *DMIN*, was obtained from the track data as the distance from the closest point on the track to the particular site in question assuming straight line segments between each 6- hourly recording of the tropical cyclone's latitude and longitude. If the site was to the right-hand side of the storm as it passed by at its closest point, *DMIN* was taken to be positive. Figure 5.20 shows the variation of the mean and standard deviation of *DMIN* taken around the U.S. coastline. It can be seen that more tropical cyclones pass to the right of coastal locations from Miami northwards i.e. there are more storms on the ocean side of Atlantic coastal sites than on the landward side.

A first approximation to the distribution governing *DMIN* might be the uniform distribution i.e. an equal chance of a storm having any value of *DMIN* within the allowable limits ($\pm$250 km for a 500 km diameter data circle). This would require that *DMIN* should have zero mean and a standard deviation equal to its range divided by $\sqrt{12}$ (equal to 144.3 km for 500 km diameter data circles). The coastal variation shown in Figure 5.20 does not conform closely to these conditions. The deviations of the *DMIN* mean values from zero however are more prominent than the deviations of the rms values from their predicted value of 144.3 km. This suggests that the PDF of *DMIN* may be adequately described using either a linear or quadratic model. *DMIN* PDF's were generated accordingly for coastal data sets. Four examples are shown in Figure 5.21. The deviations of the data from the fitted curves are generally small and the differences between the linear and quadratic curves

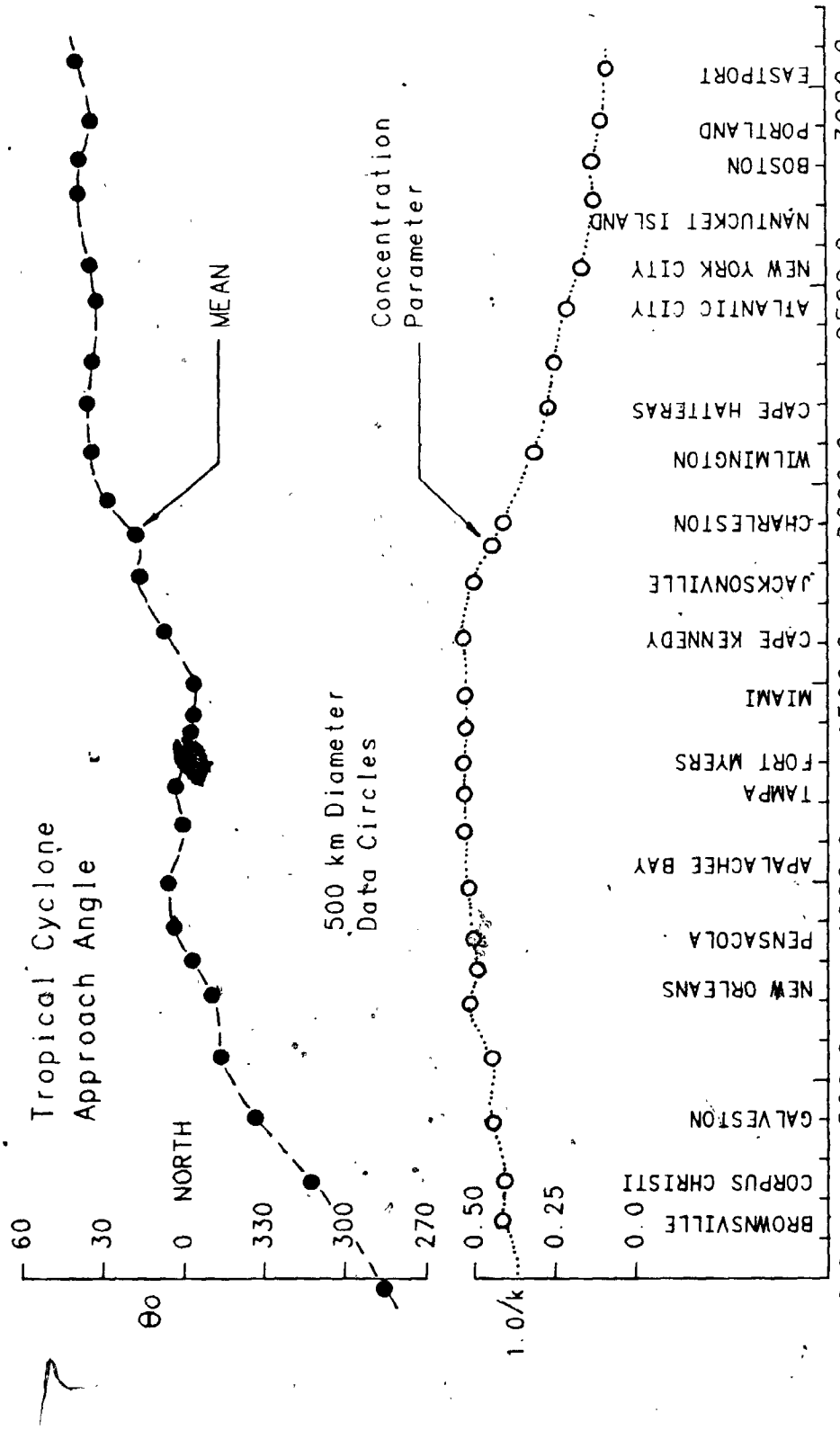

FIGURE 5.19 U.S. Coastline Predictor Distribution Parameters

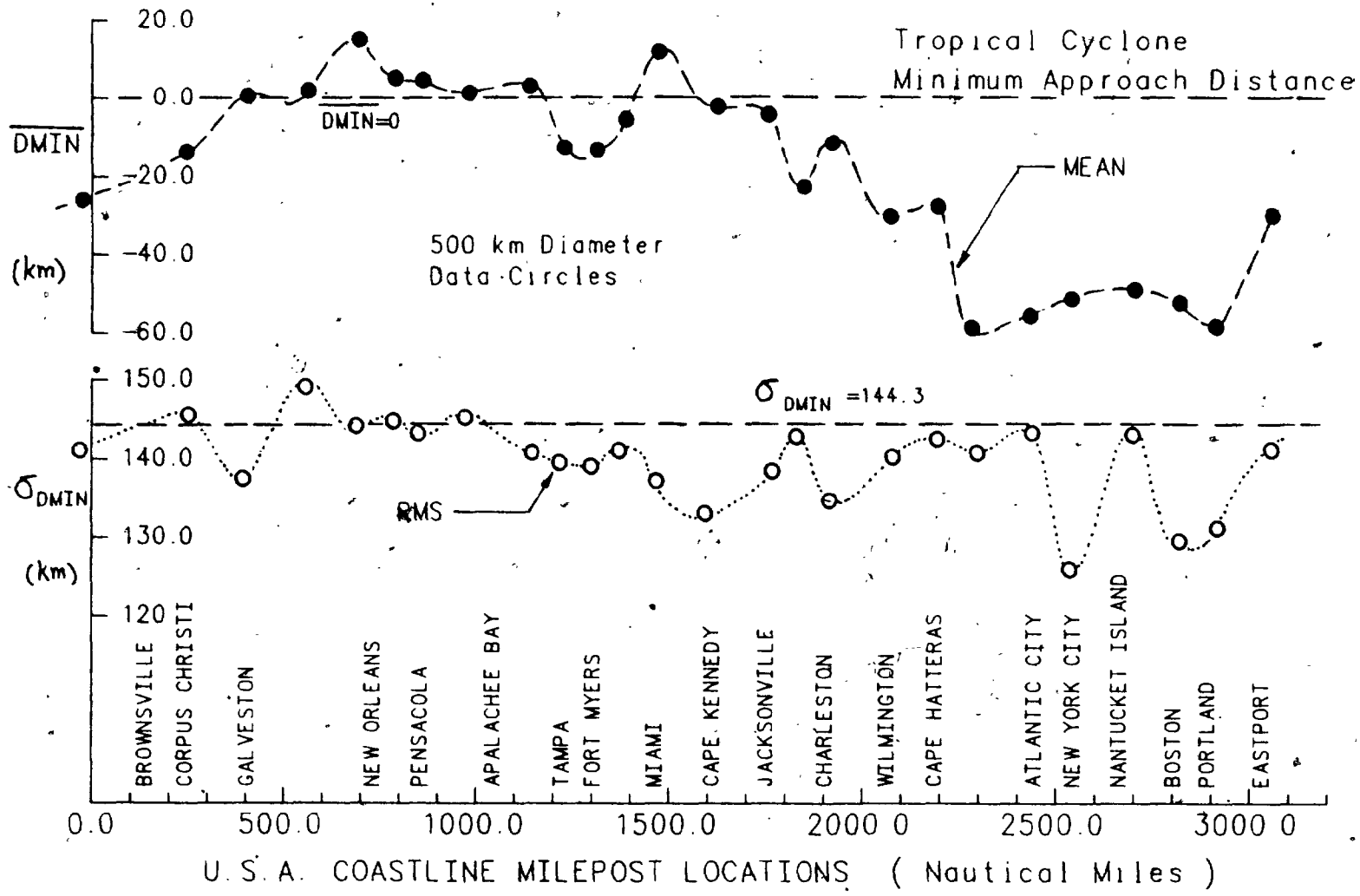

FIGURE 5.20 U.S. Coastline Minimum Approach Distance Variation

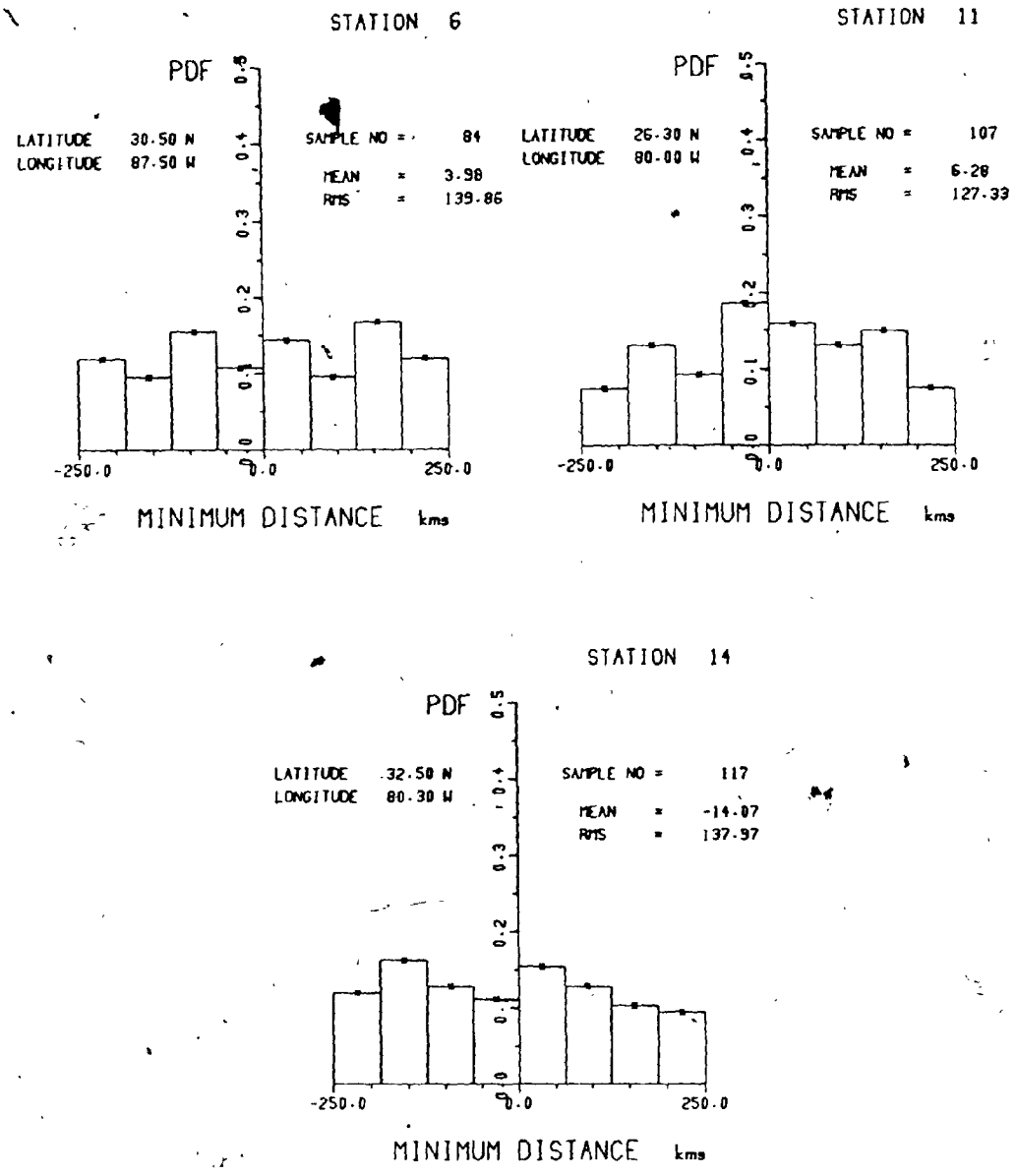

FIGURE 5.21 DMIN Data PDF Examples

small. The CDF represents the integration of the PDF, so the linear and quadratic PDF fitted curves have quadratic and cubic CDF equivalents:

$$F_q(DMIN) = q_o + q_1 DMIN + q_2 DMIN^2 \qquad E5-11$$

$$F_c(DMIN) = C_o + C_1 DMIN + C_2 DMIN^2 + C_3 DMIN^3 \qquad E5-12$$

q_i, c_i = constants

The polynomials were constrained to satisfy the boundary conditions, $F(-250.0)=0.0$ and $F(250.0)=1.0$, i.e. the probability that a storm occurred outside the data circle was zero. The coastal data sets were fitted with polynomials Fq and Fc. These were found universally to be monotonically increasing functions. Figure 5.22 shows the comparison of fitted curves to the data. Both the quadratic and cubic CDF curves were found satisfactory in almost all cases. In an attempt to compare the two fitted curves on a quantitative basis, a parameter DD was evaluated at each coastal site, defined as:

$$DD = \frac{1}{N} \sum_{i=1}^{N} \frac{(DMIN_{,o}^{i} - DMIN_{,p}^{i})^2}{DMIN_{,o}^{i}} \qquad E5-13$$

$DMIN_o^i$ = observed $DMIN$ values, with CDF value $i/(N+1)$
$DMIN_{,p}^i$ = predicted $DMIN$ value from $F(i/(N+1))$
N = number of data sample points

The average value of DD for the quandratic and cubic CDF curves was 4.2 and 3.5 km respectively. In only 3 out of the 24 coastal sites examined was the individual DD value smaller for the quadratic than the cubic CDF curve. While the comparisons favoured the choice of the cubic CDF curve over the quadratic, the generally satisfactory agreement of both seemed to suggest that further investigation of higher order polynomials was an unnecessary refinement whose effect on the overall simulation results would be minimal at best. Thus the cubic polynomial CDF was chosen as the distribution most suited to defining the minimum approach distance, $DMIN$.

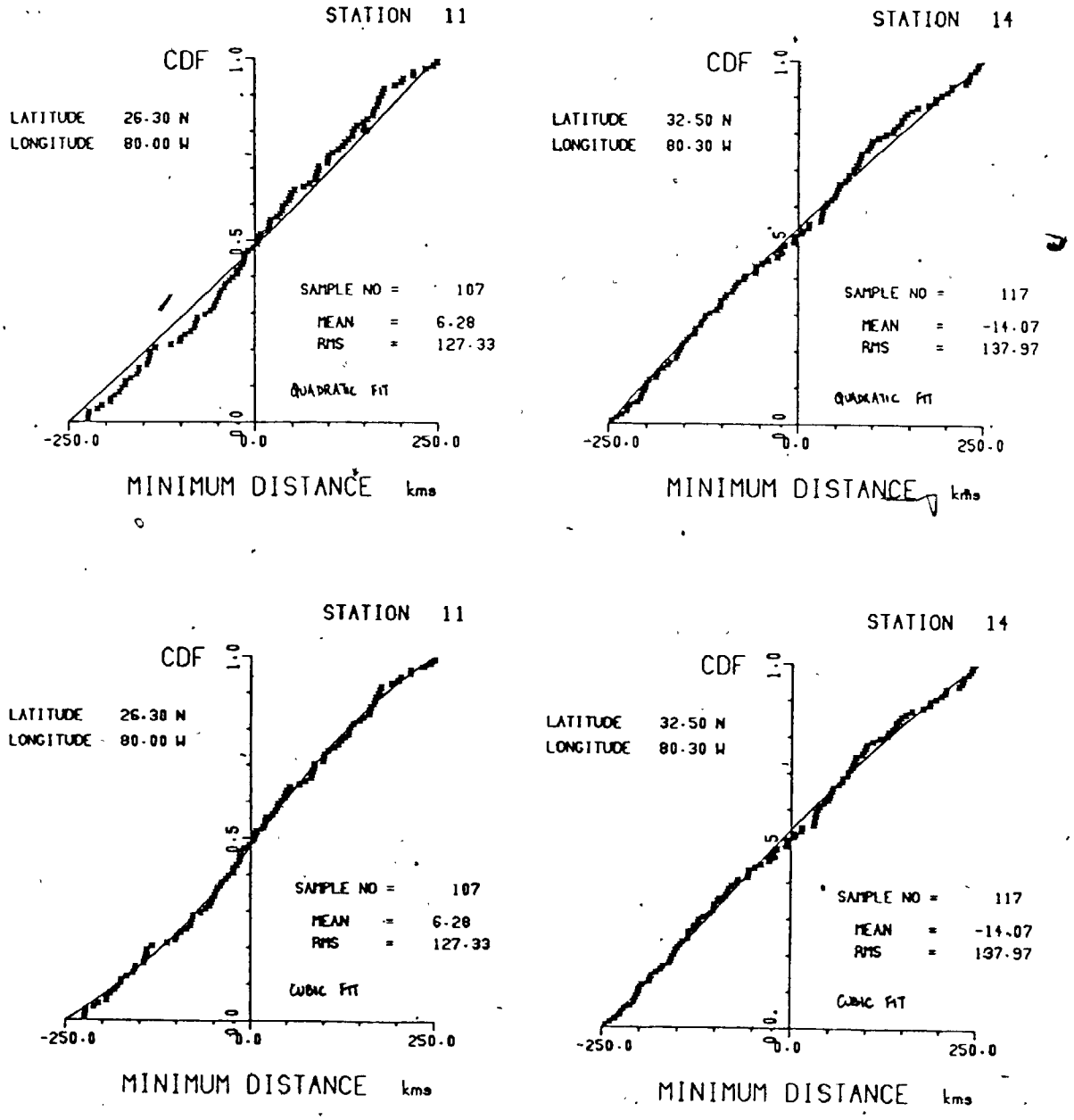

FIGURE 5.22 DMIN Data CDF Comparisons (a) Quadratic and (b) Cubic

CHAPTER 6

APPLICATION OF THE SIMULATION PROCEDURE TO HURRICANE-PRONE REGIONS OF THE UNITED STATES

6.1 Simulation Methodology and Choice of Global Parameters

The computational procedure used in the simulation is illustrated in Figure 6.1. It is assumed that the distribution functions describing the tropical cyclone characteristic parameters (λ, Δp, *RMAX*, *VT*, θ, *DMIN*), have already been calculated. During the execution of the simulation program a separate record is kept of all wind speeds and their respective directions as well as the peak speeds registered in each storm. The former are used to calculate the parent distribution of wind speed and direction, the latter, the extreme-value distribution. The simulation procedure requires the setting of a number of "global" parameters. These include (a) the size of the area used in the simulation, (b) the computational method used to estimate the parent and extreme-value distributions and (c) the number of storms generated in the simulation to ensure statistically reliable wind speed estimates.

Two factors influence the choice of simulation circle diameter. The first is the geographical sensitivity of the climatological parameters governing the input to the simulation. In the previous chapter it was shown that, for the North Atlantic, the choice of 500 km diameter simulation circles preserves the local character of the meteorological parameters while ensuring that enough data points can be obtained from the HURDAT tape to reliably determine the statistical functions for these parameters. The second factor is the potential "area of influence" that a storm has, i.e. how far away from any particular site of interest does the passing of a tropical cyclone influence the wind speeds, especially the extremes, at the site. There are two consequences of using a finite-size circle for the simulation. Firstly, the wind data used to compute the parent distribution are incomplete at the lower end because the simulation wind speeds and directions recorded at the site do not begin and end at their zero points but at the values computed at one radial distance from the site. Secondly, the set of extremes obtained at the end of the simulation will be

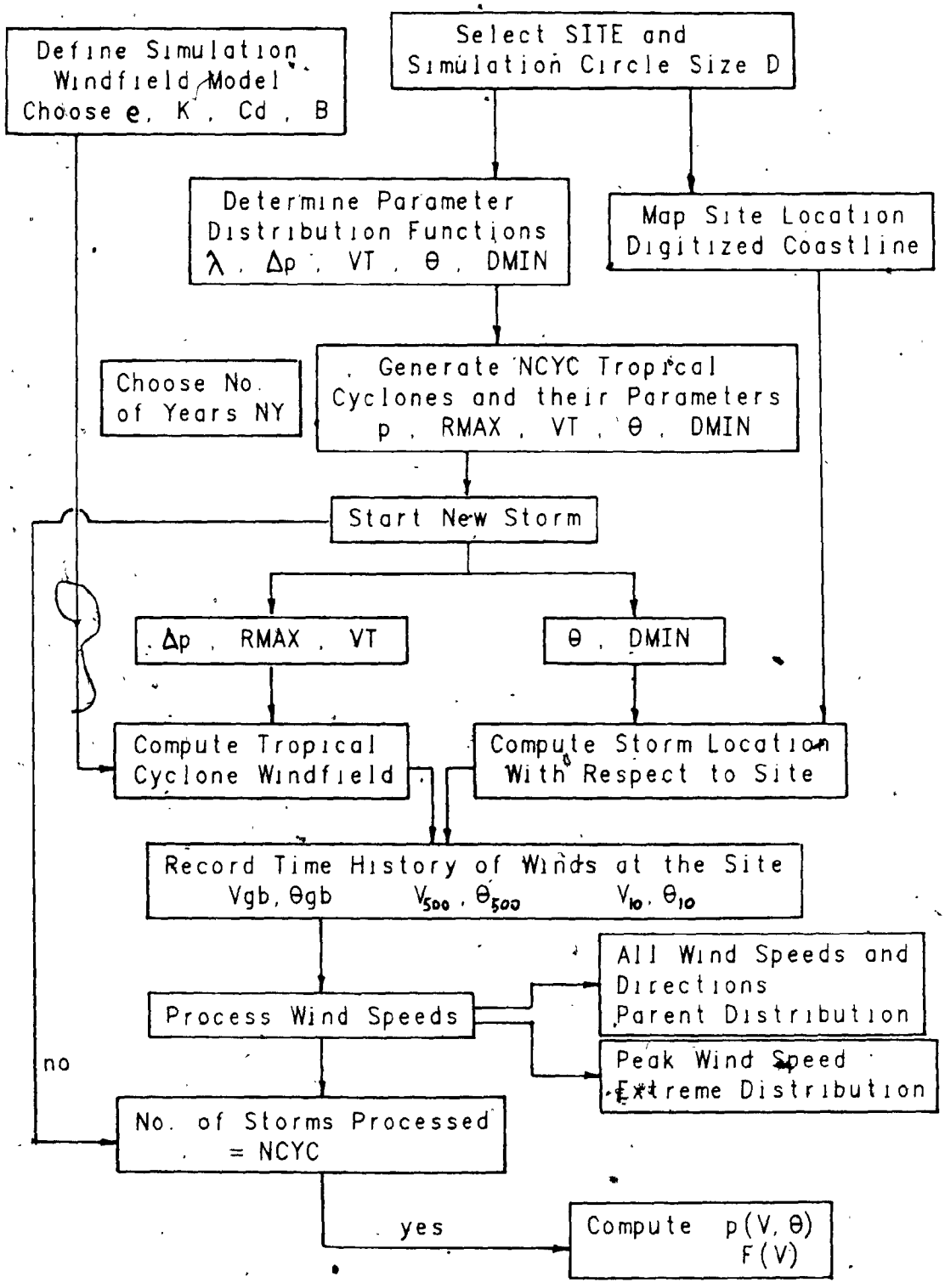

FIGURE 6.1 Simulation Procedure Flow Diagram

"missing" the values from storms that would have passed by the site outside the circle. For example, an extremely intense and large storm ($\Delta p = 100mb$, $RMAX = 80\ km$) that passed a site 255 km away at the closest approach point would still have registered a peak wind at the surface close to 20.0 m/sec at the site. This value is effectively missed if the area simulated around the site is limited to 250 km in radius. This truncation affects the extreme-value distribution mostly at the lower end and may be avoided by basing the computations on the upper end of the distribution. In section 7.2 it will be shown using an alternative and independent approach for computing the extremes that, for the North Atlantic, the effective area of influence of tropical cyclones is consistent with the use of 500 km diameter simulation circles.

Different methods are used in the current procedure to calculate the parent and extreme-value distributions. The parent distribution is derived by separating the data into 22.5° sectors, and fitting each sectorial sub-group individually by conditional probability distribution functions. The joint probability density function of wind speed and direction, i.e. the parent distribution, is then calculated by multiplying by the marginal probability that the wind will be in each given sector, equal to the relative frequency of occurrence of all wind speeds in that sector. From a number of trial runs it was found that the sectorial data were well-modelled using the Weibull distribution. Thus the probability of exceeding a wind speed, V, when the wind direction is in sector "i" is given by:

$$prob\left\{ > V | sector\ "i" \right\} = \frac{N(\theta_i)}{NT}\ exp\left[-\left\{ \frac{V}{C(\theta_i)} \right\}^{k(\theta_i)} \right] \qquad E6-1$$

$C(\theta_i), k(\theta_i)$ = Weibull parameters, for sector "i" winds

$N(\theta_i)$ = total number of hours when tropical cyclone winds occur with wind direction in sector "i"

NT = total number of hours when tropical cyclone winds occur

The 16 sectorial $N(\theta_i)$, $C(\theta_i)$ and $k(\theta_i)$ values can be Fourier-fitted to derive a continuous variation with azimuth. This is usually done using the first four expansion terms, e.g.:

$$C(\theta) = C_o + \sum_{i=1}^{4} \left\{ C_i^c \cos i\theta + C_i^s \sin i\theta \right\} \qquad E6-2$$

$C_o, C_1^c, C_1^s, C_2^c, C_2^s, \ldots$ = Fourier coefficients

During initial trials, it was noticed that the extremes seemed to follow the Weibull distribution at the upper end but exhibited a persistent upward "swing" at the lower velocity range. This upward trend is coincidentally evident in the extremes obtained in the Batts et al (1980) simulation (their Figure 7). It is suspected that this phenomenon is caused by the loss of wind speed maxima resulting from the finite-size circle used in the simulation. Computation of the extremes is accomplished in the current procedure using a modified approach that avoids this effect. If a process is Poisson distributed with an average rate, "n", the probability of no events occurring in time "T" is given by $Prob(0) = exp(-nT)$. Trial runs indicated that the exceedance rate of the extremes, $N(>Vo)$, for some velocity, Vo, followed the Weibull distribution, i.e.:

$$N(>Vo) = \lambda \varepsilon^{-\left(\frac{Vo}{C}\right)^k} \qquad E6-3$$

λ = annual occurrence rate
C, k = Weibull parameters

Since the exceedances of high velocities are rare and independent, they can be considered to be Poisson distributed. Hence the probability that no storm wil have a velocity greater than Vo will be given by $Prob(0) = exp(-N(>Vo)T)$. This is identical to the situation where all velocities are less than Vo, and hence equivalent to the extreme-value distribution value of Vo. If unit time is taken as annual the extremes are then defined by:

$$F(<V) = exp\left[-\lambda \varepsilon^{-\left(\frac{V}{c}\right)^k} \right] \qquad E6-4$$

In the simulation, the extremes are computed using the maximum likelihood technique, maximizing all three constants λ, C and k. A lower cut-off point is designated so as to bypass the problem area in the low wind speed range. By maximizing the value of λ, and not simply assuming it to be the local value of occurrence rate used to generate the storms in the simulation, the calculation of the extremes is not affected by the loss of wind data resulting from the limited simulation circle size.

The number of storms which need to be generated to ensure statistical reliability depends upon whether the parent distribution is to be calculated in addition to the extremes. The stability of the simulation extreme-value estimates was investigated by running simulations for three locations - Galveston, Miami and New York City - using an increasing number of storms generated in each simulation. Figure 6.2 shows the convergence of 10-year, 100-year and 1000-year return period V_{500} extreme wind speed estimates with storm number for the three sites. The variability of the extreme estimates increases with return period. The Miami estimates take longer (more storms) to converge to a constant level. This may be due to the higher mean and standard deviation values of central pressure difference for this location. From these trial runs it appeared that a suitable number of tropical cyclones necessary in a simulation generating extreme wind speed estimates was 2500, so as to ensure reasonable reliability up to return periods of 1000 years.

When the parent distribution is to be determined, the number of storms necessary to simulate increases, since 16 separate sectorial distributions have to be fitted. However, the calculation of each sectorial distribution only requires the determination of the two Weibull parameters (c,k) and not a rate parameter, λ, as in the extremes. Trial runs indicated that a minimum adequate number of storms for the estimation of the parent distribution was 10,000. This typically resulted in the compilation of 10,000 or more hourly readings of wind speed in each of the 16 azimuthal sectors, providing enough data at the upper end to give an accuracy to the estimated parent distribution comparable to that of the extremes.

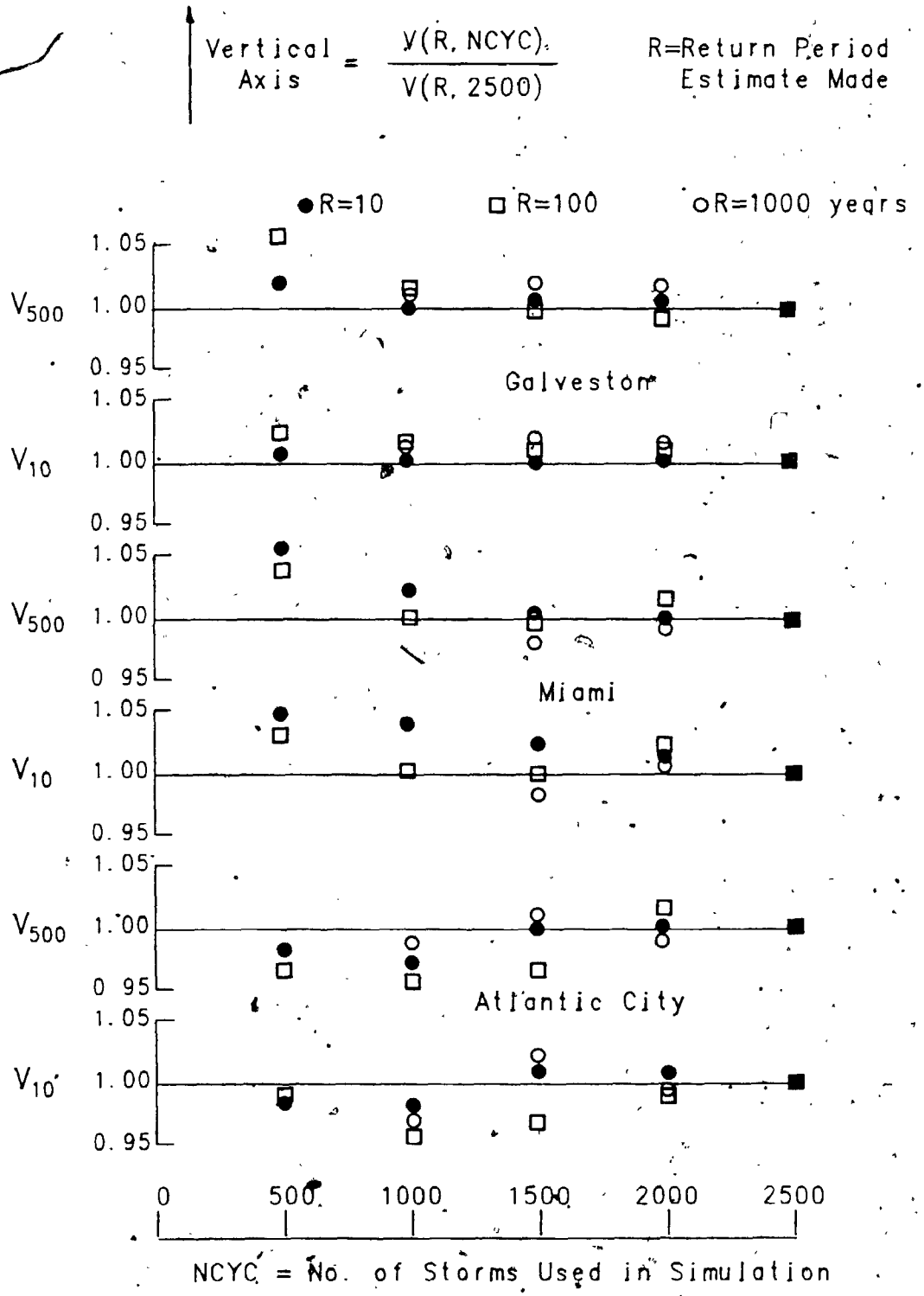

FIGURE 6.2 Simulation Tropical Cyclone Number Convergence Tests

6.2 Return Period and Risk

In the following sections extreme-value wind speed estimates are related to the notion of "return period" and "risk". In the case of tropical cyclone simulation estimates, these notions should be distinguished from their normal statistical meaning. In conventional terms, the risk of exceeding some value of say a velocity, is interpreted as the probability or chance that it will be exceeded in one year. This can then be related to the extreme-value distribution, $F(V)$. The velocity, Vo, which is exceeded $r\%$ of the time in any one year is given by $F(Vo) = 1.0 - r$.

If a velocity, Vo, is exceeded, on average, once every R years, the velocity is said to have a return period of R years. It then follows that $r = 1/R$. Thus, the 100-year return period wind speed can be thought of in two distinct ways, (i) as the wind speed which, on average, is exceeded once every 100 years, or (ii) as the wind speed which has a 1% chance of being exceeded in any one year.

Turning now to simulation extreme-value estimates, it can be noted that they are based on the analysis of meteorological data going back some 100 years. Therefore, when a wind speed is quoted as being the 100-year return period speed, it is reasonable to interpret the statement in both ways described above, i.e. that it will likely be exceeded once in the next 100 years or that there is a 1% chance of it being exceeded in any one year. However, a wind speed estimate with a 2000-year return period cannot legitimately be interpreted as being the value which will be exceeded roughly once in the next 2000 years, since this implies that the state of the climate is known over the next 2000 years. Clearly, no basis for such a claim exists. Rather, a simulation wind speed estimate quoted as having a return period of 2000 years should be interpreted strictly as the speed which has a 0.05% chance of being exceeded in any one year, based upon the current historical meteorological data base. In the following sections, although simulation extreme-value estimates are quoted in terms of their respective return periods, they should be viewed generally in terms of their risk percentages, especially for the higher return periods.

6.3 Example Simulation Run - Miami

The simulation procedure is illustrated using the computations and results for a single simulation run for Miami. The first step involves calculating the characteristic parameter distribution functions. A simulation circle is defined around the site of interest. The statistical relationships governing the parameters are then determined from the HURDAT tape using all tropical cyclones of record that have entered this circle. The usual North Atlantic simulation circle diameter of 500 km is used. Data obtained from the HURDAT tape showed that the average number of storm occurrences per year for this circle is 1.14.

A summary of the distribution functions used for the Miami simulation is given in Table 6.1 along with the numerical values specifying each particular distribution. The average value of approach angle, -11.4°, indicates that most tropical cyclones approach Miami moving slightly to the west of northward. The mean minimum approach distance of 8.4 km indicates an almost equal likelihood for storms passing to the west and east of Miami with a slight bias for storms to the west. The average translation velocity of tropical cyclones in the area is 5.8 m/sec. The parameter values for the central pressure difference suggest, not surprisingly, an area of intense hurricane activity; the estimated 100-year return period central pressure is the lowest for the whole coastline. Figure 6.3 shows the immediate geographical area covered in the Miami simulation indicating the model coastline used in the filling computations. The site of interest (at the circle centre) was located right on the coastline. The surface speeds calculated are open-water 10 metre height speeds.

Two simulations were run for Miami, for 2410 and 9630 years. This resulted in the generation of 2503 and 10023 tropical cyclones respectively. The extreme wind speed estimates for Miami were based on the shorter run. The longer run was used to compute the parent distribution function. The parent and extreme-value distributions computed from the simulated wind histories are shown in Figure 6.4 and 6.5 respectively. The contours of the parent distribution of wind speed and direction are nearly circular with somewhat higher exceedance probabilities from the south-southeast direction for the 500 metre windfield. The increase in inflow angle at the surface

TABLE 6.1

MIAMI SIMULATION STATISTICAL DATA SUMMARY

Parameter	Distribution	Simulation Value		
Annual Occurrence Rate (Tropical cyclones/year)	Poisson	mean	=	1.143
Central Pressure Difference (millibars)	Weibull	C	=	35.004
		k	=	1.038
Translation Velocity (metre/sec)	Lognormal	log-mean	=	1.673
		log-rms	=	0.436
Minimum Approach Distance (kilometres)	Polynomial	mean	=	8.423
		rms	=	140.42
Approach Angle (degrees)	Von Mises	mean	=	-11.42
		k	=	1.680

TABLE 6.2

MIAMI SIMULATION
MEAN HOURLY EXTREME WIND SPEED ESTIMATES
(metre/sec)

Return Period (years)	Gradient Balance Height	500 metre Height	Surface Height
10	39.5	39.8	32.0
25	47.1	47.6	38.8
50	52.5	53.1	43.6
75	55.2	56.0	46.2
100	57.1	58.0	47.8
200	61.6	62.5	51.9
500	67.3	68.4	57.1
1000	71.2	73.1	60.8

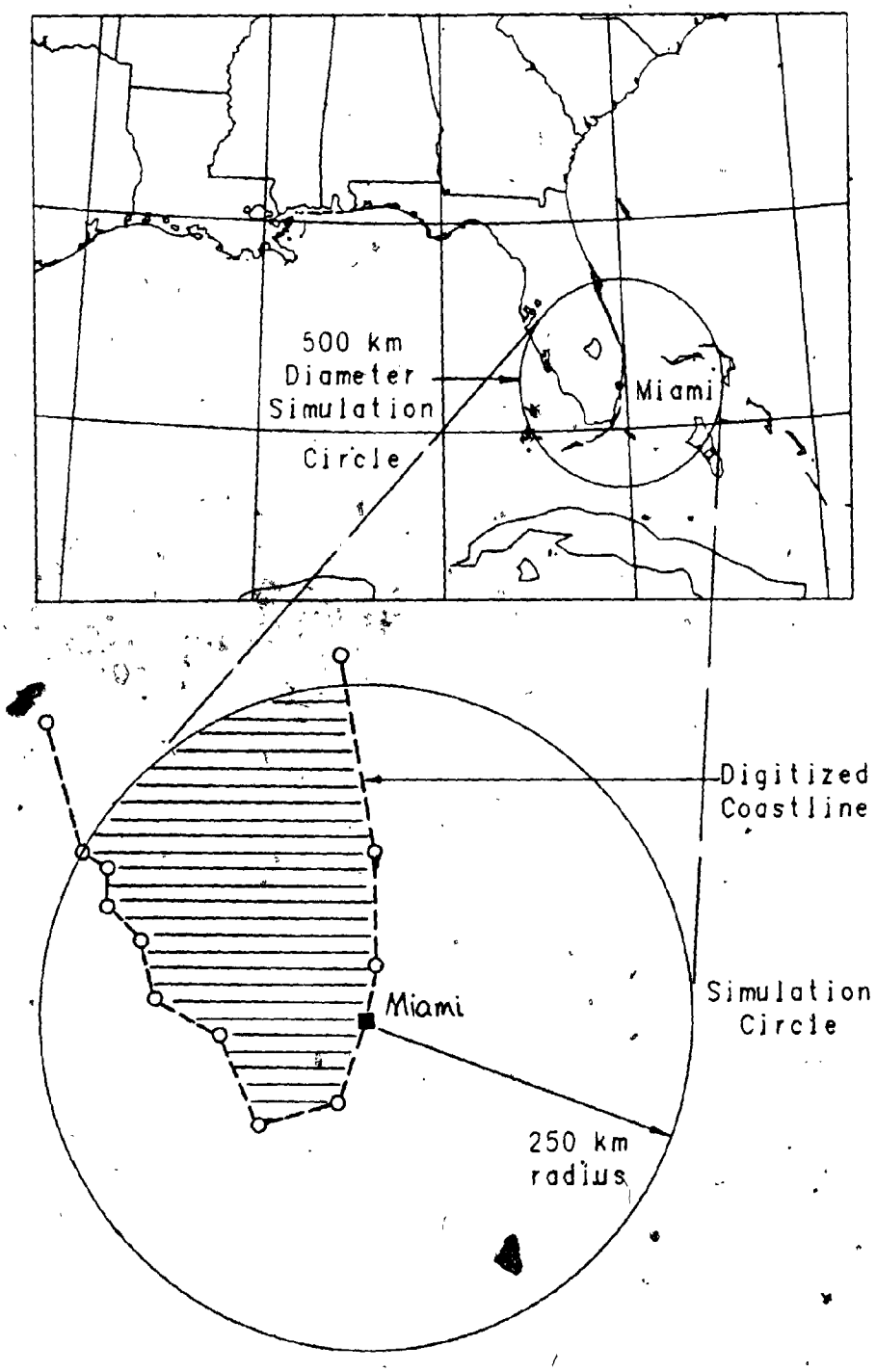

FIGURE 6.3 Geographical Area Covered in Miami Simulation

Contours show wind speeds which, for different directions, have equal probability of being exceeded. The probability of of wind speeds lying outside the hatched contour is 1%. Other contours represent probability levels of 0.1%, 0.01%, 0.001% and 0.0001% respectively

Radial distances indicate wind speeds in metres/sec

0 20 40

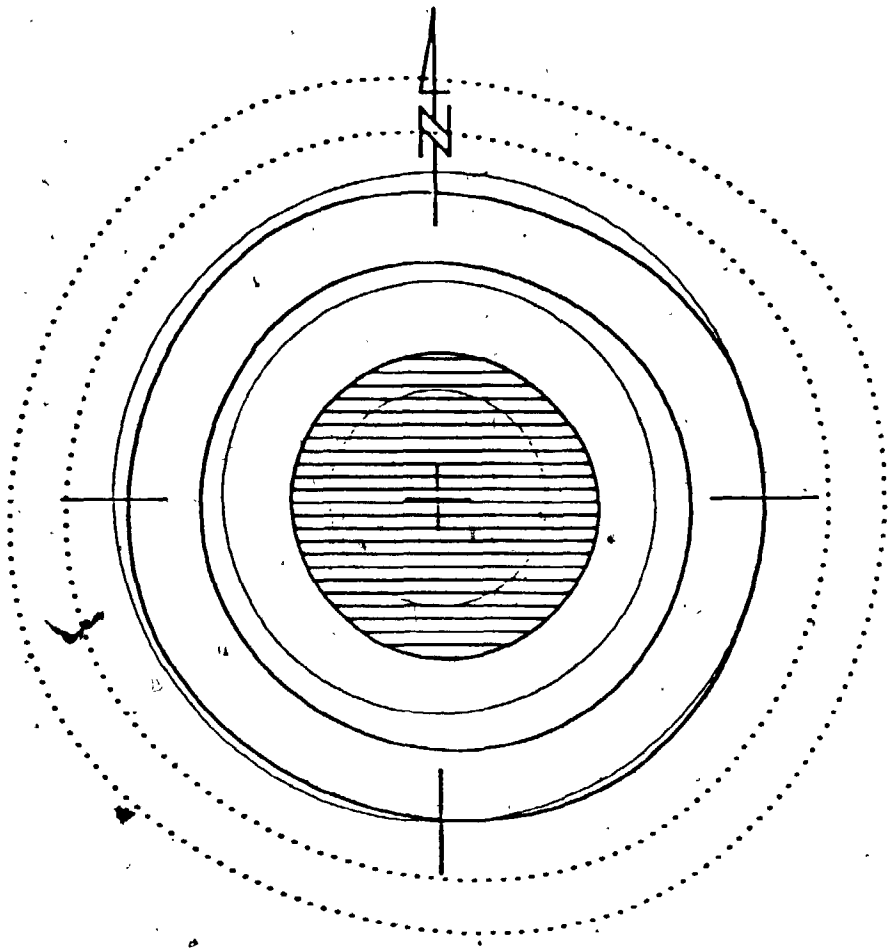

FIGURE 6.4 **Miami Simulation Parent Wind Speed Distribution $p(V,\theta)$, (a) 500 Metre Height**

Contours show wind speeds which, for different directions, have equal probability of being exceeded. The probability of of wind speeds lying outside the hatched contour is 1%. Other contours represent probability levels of 0.1%, 0.01%, 0.001% and 0.0001% respectively

Radial distances indicate wind speeds in metres/sec

0 20 40

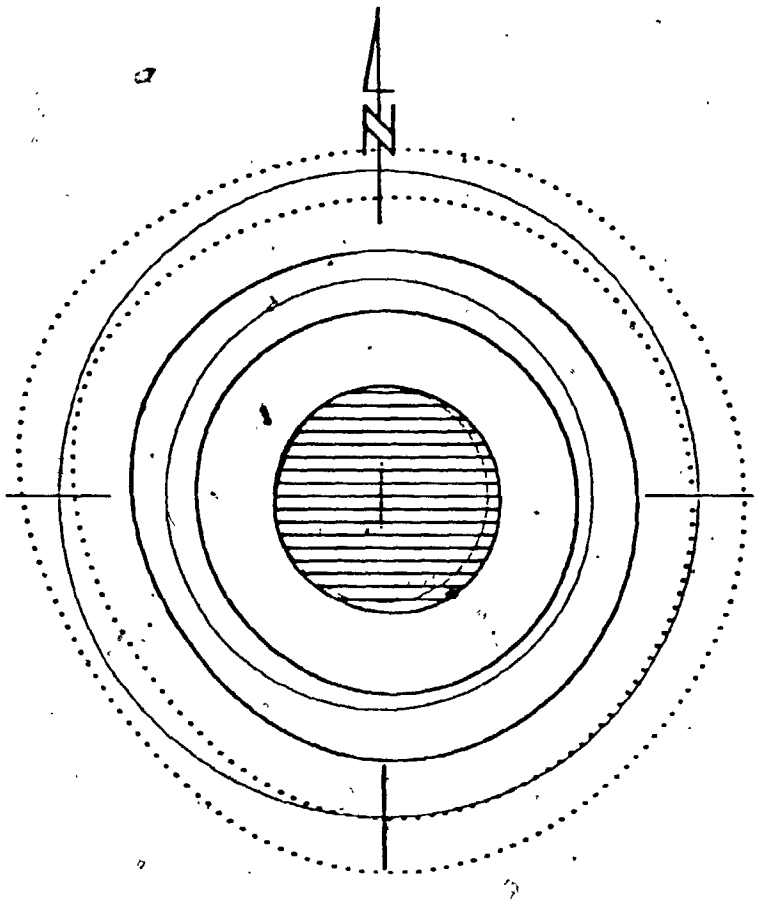

FIGURE 6.4 (contd.) (b) 10 Metre Height

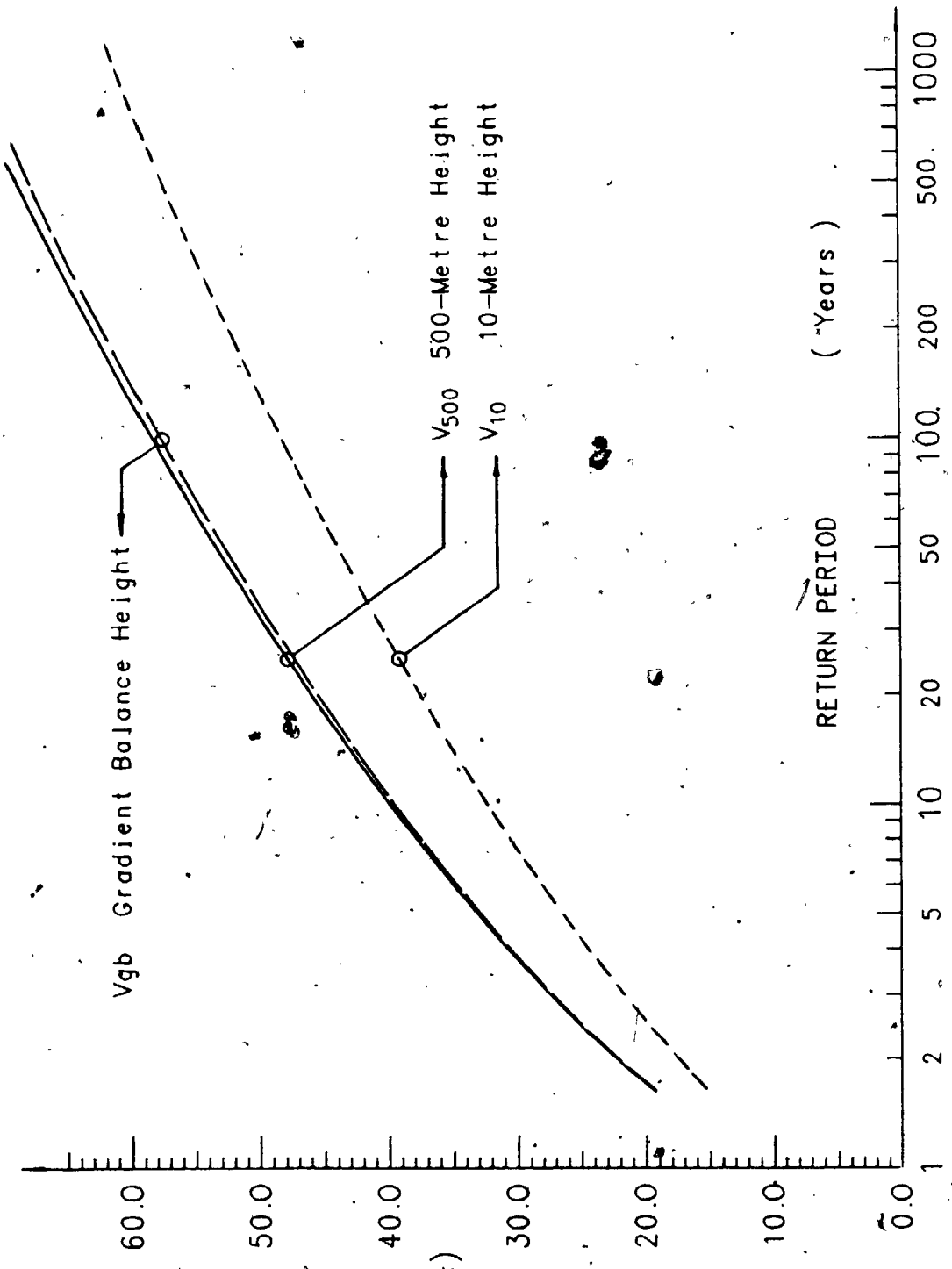

FIGURE 6.5 Miami Simulation Extreme-Value Mean Hourly Wind Speed Estimates

results in the bias moving to the east-southeast direction. The extreme-value analysis is summarized in Table 6.2 and indicates 100-year return period mean hourly wind speeds of 57.1, 58.0 and 47.8 m/sec for the gradient balance, 500 metre and 10 metre heights respectively. The mean gradient balance and 500 metre height extreme estimates are virtually identical. Because the simulation site was located on the coastline, locations several kilometres inland could expect a reduction in the surface speeds quoted. Both upper-level extreme estimates however would be unchanged.

6.4 Comparison of Hong Kong Simulation Extreme Wind Speed Estimates with Waglan Island Data

The simulation windfield model was evaluated in Chapter 4 by comparing actual wind records with model-predicted wind speeds and directions. The overall reliability of simulation extreme wind speed estimates could similarly be assessed by comparing simulation results with extremes obtained from actual tropical cyclone occurrences. In the North Atlantic this is not possible. No recording station has accumulated a sufficient data base of maximum wind speed measurements to allow such a comparison. This is possible however using tropical cyclone data obtained in the Hong Kong region.

Records of wind speed and direction obtained during tropical cyclone occurrences in the Hong Kong region were discussed in section 4.2. Due to the relatively high frequency of storm occurrence in the area records from two stations in the area have been used in past studies to estimate extreme wind speeds (Chen, 1975; Melbourne, 1984). These are (i) the Royal Observatory, Hong Kong (ROHK) with its remarkable length of record (1884-present) and the Waglan Island anemometer station with the long fetch of winds over water is most directions. While the ROHK record is almost 100 years in length, dramatic changes in surrounding building development have affected the uniformity of the data. For this reason, the Waglan Island record was chosen to estimate extreme wind speeds in the Hong Kong region.

The analysis of Waglan Island tropical cyclone wind speeds to obtain a distribution of extremes involved the same correction process which was used

to compare individual storm records in section 4.2. The raw anemometer winds were corrected for aerodynamic effects using the results of the wind tunnel topographic tests performed for the island (Surry, Lythe, Horvath and Davenport, 1981), and converted to the two reference heights used in this study, thereby obtaining two further data sets at the 500 metre and surface heights respectively.

The data made available by ROHK included maximum 10-minute mean winds for 175 tropical cyclones recorded in the period 1953-1982 and maximum mean hourly winds and peak gusts for 72 tropical cyclones recorded in the period 1973-1982. From this information eight data sets were derived, detailed in Table 6.3. The maximum 10-minute means were separated into two groups, one for the overall period 1953-1982 and a second for the period 1973-1982, so that a comparison could be made between hourly and 10-minute means and peak gusts for the same set of storms. For each data set, a parallel one was obtained by choosing the annual maximum recorded each year. The 1973-1982 sets comprised only 10 annual maxima and were clearly prone to high uncertainty. These final eight data sets were analyzed using standard maximum likelihood techniques, fitting Type I extreme-value distributions using the least squares method, an adjusted-weights method (Gumbel, 1958) and the Leiblien method (Leiblien, 1974).

The results are summarized in Table 6.4, showing the 100-year return period predicted wind speeds for each set. The estimates derived from the annual maxima sets are consistently higher than those obtained analyzing all storms and are not considered appropriate given the small sample number. The estimates for the 10-minute mean data sets are consistent between the 1953-1982 and 1973-1982 periods. From the raw data the average ratio of maximum 10-minute to hourly means was 1.06, and 1.47 for the ratio of peak gusts to maximum mean hourly winds. These ratios are preserved in the extreme estimates. A large discrepancy exists between estimates for the 1973-1982 period data sets depending upon the particular fitting technique chosen. This would appear to be related to the size of the sample as the 1953-1982 period estimates are not similarly affected. These considerations led to the decision to use the Leiblien calculated estimates for the "28/E/10" data set (28-year, 175-storm, maximum 10-minute mean winds) to define the extreme-

TABLE 6.3

WAGLAN ISLAND TROPICAL CYCLONE DATA SETS

Set Name	Record Length (years)	Sample Number	Storms Chosen	Speed Type
28/E/10	28	175	all storms	10-minute mean
28/A/10	"	28	annual maxima	"
10/E/10	10	72	all storms	10-minute mean
10/A/10	"	10	annual maxima	"
10/E/60	10	72	all storms	mean hourly
10.A/60	"	10	annual maxima	"
10/E/G	10	72	all storms	peak gust
10/A/G	"	10	annual maxima	"

TABLE 6.4

100-YEAR EXTREME-VALUE ESTIMATES FOR WAGLAN ISLAND DATA (metre/sec)

Set	Least Squares	Type I Analysis Adjusted-Weights	Leiblien
28/E/10	51.4	52.6	49.5
10/E/10	50.8	52.1	46.2
10/E/60	49.7	50.8	40.8
20/E/G	66.9	68.4	60.7
28/A/10	54.5	56.0	54.1
10/A/10	55.7	58.7	51.2
10/A/60	53.2	54.9	47.9
10/A/G	75.4	77.7	71.5

value distribution for Waglan Island and to convert the maximum 10-minute means to maximum hourly means using the 1.06 ratio value measured from the raw data. The Waglan Island estimates are in good agreement with those made by Chen (1975) using annual maximum hourly means for the period 1953-1975, as can be seen in Figure 6.6.

These estimates are now compared to those derived using the simulation approach. The simulation procedure was modified for use in the Hong Kong region in a number of important ways. These are discussed in detail in Georgiou, Mikitiuk, Surry and Davenport (1984). The most important changes were:

(a) The circle diameter used for the simulation prediction was increased to 1000 km, from the smaller 500 km size used for the North Atlantic. Data obtained from ROHK tropical cyclone data tapes showed that the average annual number of storms for this size circle was 5.8. This is close to the average annual number of tropical cyclones that necessitated the display of Tropical Cyclone Signals in the Hong Kong region in the period 1946-1982, equal to 6.3, and supports the inclusion of all historical tropical cyclones in the analysis, not just those reaching typhoon intensity. The larger circle required for the Hong Kong simulation also reflects the observed increase in mean storm size between Northwest Pacific and North Atlantic tropical cyclones (a 40% increase in the average storm radius; Merrill, 1984).

(b) Several of the parameter distribution functions were altered. In the Hong Kong region, the lognormal distribution was found to give a better fit to the central pressure difference data than the Weibull. The conditional dependence of the radius of maximum winds upon the central pressure difference was adjusted to fit the data compiled by Bell (1974).

The simulation procedure was run for a time period of 1702 years, which resulted in the generation of 10004 tropical cyclones, allowing the determination of the parent as well as the extreme-value distribution. The results of the Hong Kong simulation are shown in Figures 6.7 and 6.8 and summarized in Table 6.5. Also shown are the extreme wind speed estimates derived from the actual Waglan Island data as described above. The

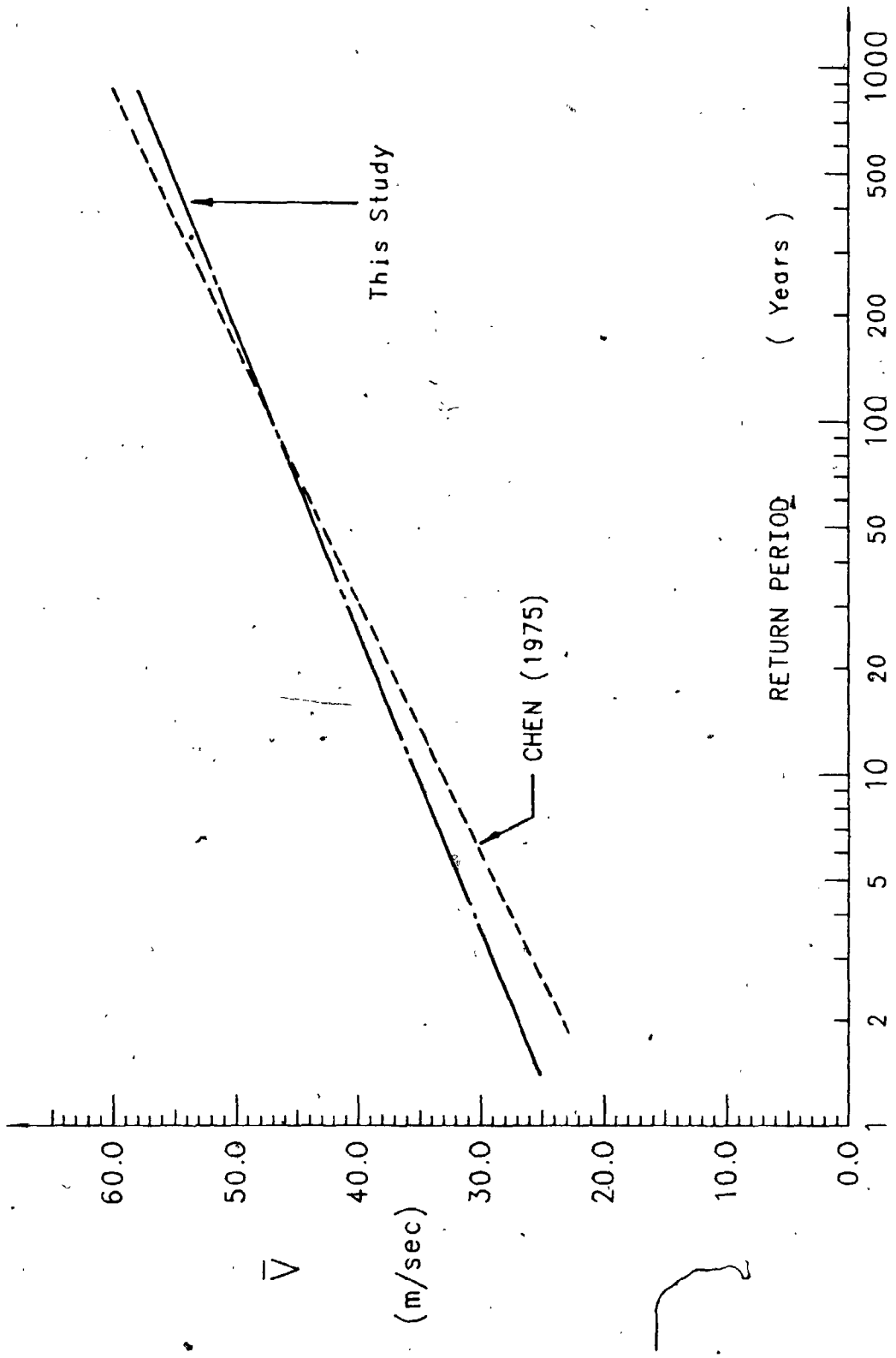

FIGURE 6.6 Waglan Island Predicted Extreme Mean Hourly Wind Speeds

Contours show wind speeds which, for different directions, have equal probability of being exceeded. The probability of of wind speeds lying outside the hatched contour is 1%. Other contours represent probability levels of 0.1%, 0.01%, 0.001% and 0.0001% respectively

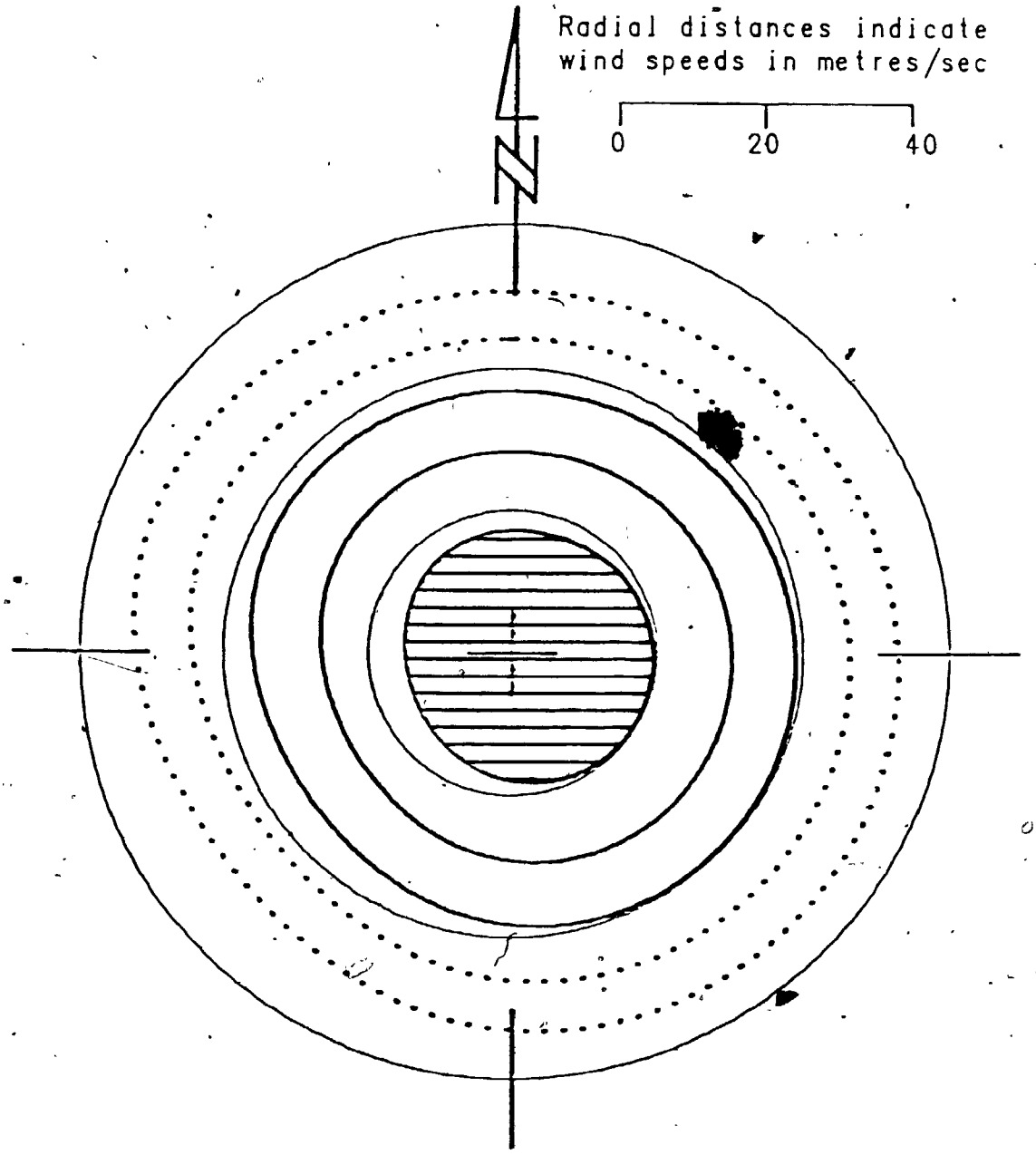

FIGURE 6.7 **Hong Kong Simulation Parent Wind Speed Distribution $p(V, \theta)$, 500 Metre Height**

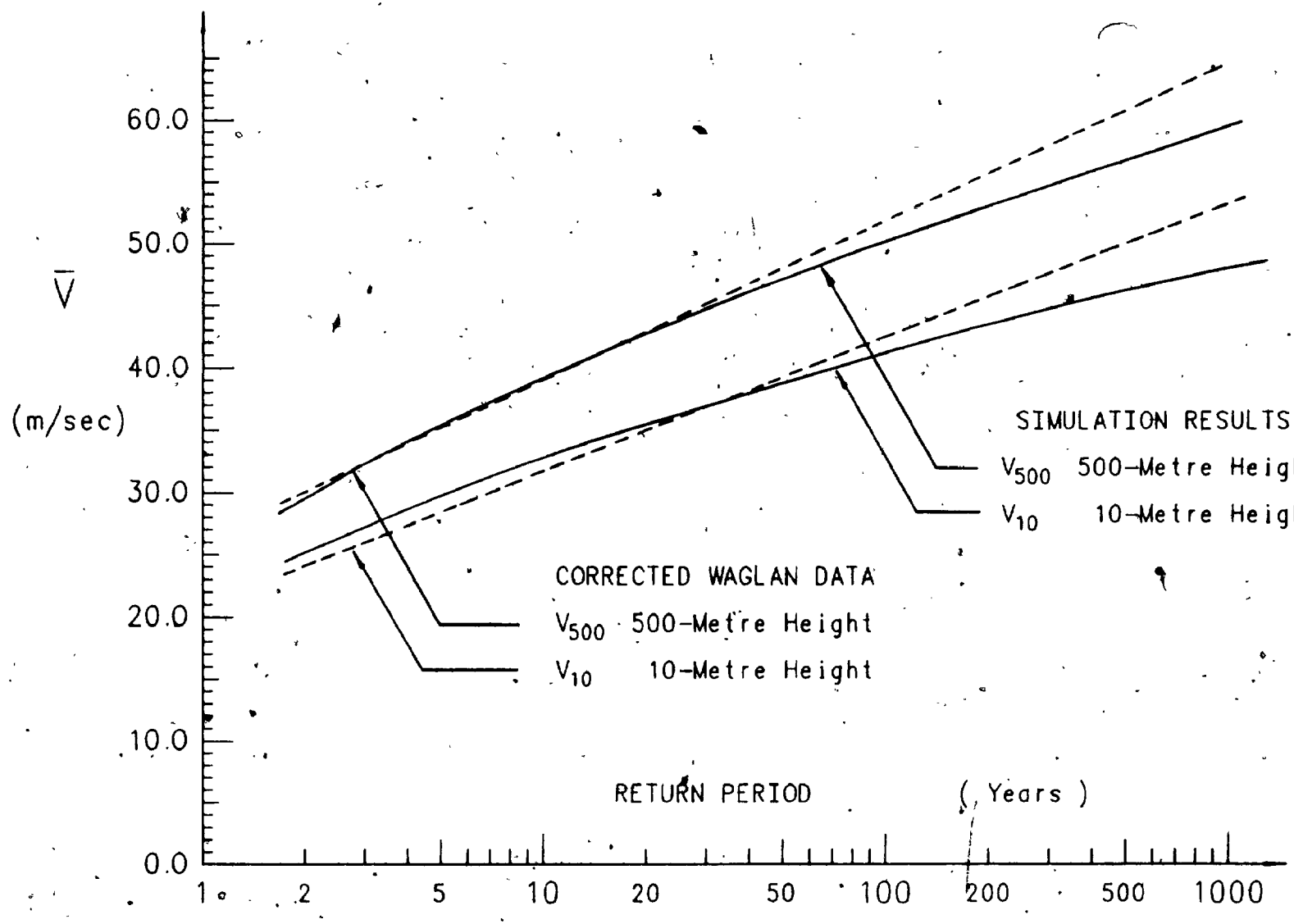

FIGURE 6.8 Hong Kong Extreme-Value Mean Hourly Wind Speed Estimates

agreement between the simulation predictions and the extremes derived from the Waglan data is encouraging, taking into account the uncertainties involved in converting the anemometer wind records to suitable reference heights and the statistical limitations imposed by the 28-year length of historical record available. The opportunity to make a direct comparison of actual recorded extremes with simulation predicted estimates is a unique one.

TABLE 6.5

COMPARISON OF SIMULATION WITH ACTUAL DATA DERIVED MEAN HOURLY EXTREME WIND SPEED ESTIMATES FOR WAGLAN ISLAND
(metre/sec)

Return Period (years)	500 metre level		Surface	
	Corrected Waglan Data	Simulation	Corrected Waglan Data	Simulation
10	39.0	38.8	31.8	32.5
50	47.7	46.8	39.0	38.6
100	51.6	50.0	42.0	40.9
200	55.4	53.0	45.1	43.2
1000	64.2	59.4	52.2	48.0

6.5 Tropical Cyclone Extreme Wind Speed Estimates for the United States Gulf and Atlantic Coasts

The simulation procedure was applied to the Gulf and Atlantic Coasts of the United States. Simulations were performed at 250 km intervals around the coastline, at the same locations chosen for the Chapter 5 parameter analysis and shown in Figure 5.3. Simulation circles with a diameter of 500 km were utilized. At each site, a constant number of tropical cyclones was generated, approximately equal to 2500. The actual simulation time length varied according to the site's local occurrence rate. Two parallel runs were performed initially, (i) for sites located right on the coastline and (ii) for sites located 100 km inland. Extra runs were made at various locations, both inland and offshore to make up a regional hurricane extreme wind speed map.

The coastal simulations were run assuming the sites to be located right on the coastline, i.e. the surface speeds are open-water equivalents. The inland site simulation runs were made assuming flat, open terrain exposure. Therefore inland surface speed estimates may vary considerably for eastern locations were the topography can become severe at moderate distances inland, as opposed to areas in the southwest and the Florida peninsula, where the terrain remains remarkably flat, often for a considerable distance inland from the coast. The results presented in Figure 6.9 to 6.14 do not include the gradient balance height extreme wind speed estimates, as they were found to be almost identical to the 500 metre height extremes.

Extreme wind speed estimates for the coastal sites are shown in Figures 6.9 and 6.10. Significant variation exists around the coastline. Five regions exhibiting local maxima are separated by "quiet" areas where the estimated extremes are considerably diminished. Local maxima occur at the U.S.-Mexican border, the Mississippi delta-Pensacola area, the lower Florida peninsula, the Charleston-Cape Hatteras area and Cape Cod. The overall maximum is found in the southern Florida region. The estimated 100-year return period extremes at the surface vary from 47.8 m/sec in the Miami area to less than 30.0 m/sec near the U.S.-Canada border. The differences between neighbouring sections of coastline can be large, e.g. the 100-year surface speed estimate drops from 42.5 to 36.5 m/sec in just 300 km from Pensacola to Apalachee Bay. The change along the eastern Florida coastline is even greater, dropping from 47.8 m/sec near Miami to 37.3 m/sec at Jacksonville, 500 km to the north. This 25% drop translates into a 50% difference in the value of the square of the wind speed, a direct measure of the expected wind-induced pressure loads.

Figures 6.11 and 6.12 show the simulation extreme wind speed estimates for the 100 km inland locations. The variation is similar to that of the coastal sites. Surface speeds for sites running down the centre of the Florida peninsula increase from 32.5 m/sec inland from Jacksonville to 38.0 m/sec inland from Palm Beach. The reduction in surface speeds within the Florida peninsula thus reflects mostly the reduction due to surface friction. For other coastal areas, a greater relative drop is experienced due to increased influence from filling, e.g. the drop in 100-year surface speeds along the western portion

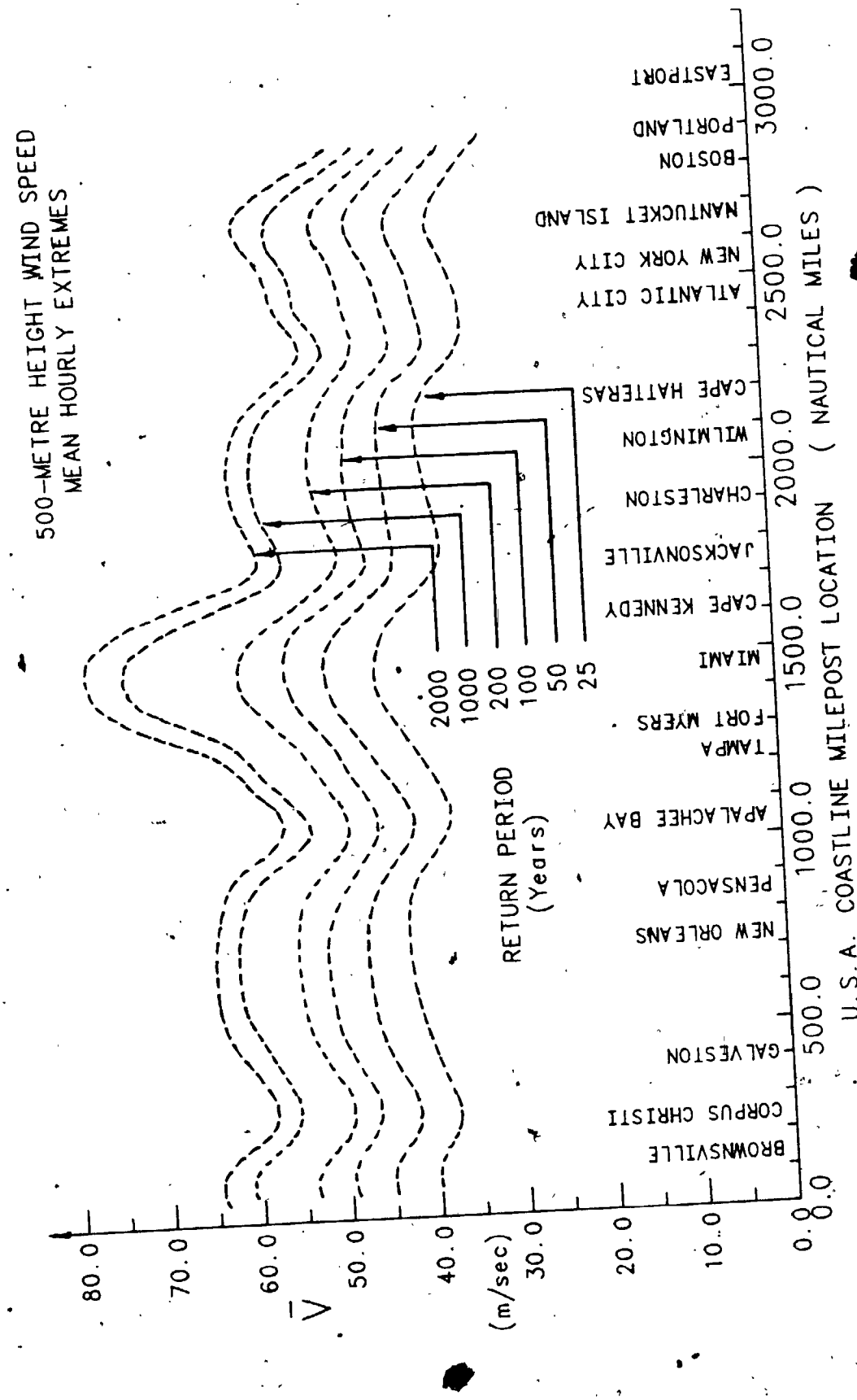

FIGURE 6.9 Simulation 500 Metre Height Extreme-Value Estimates for C[redacted] Locations

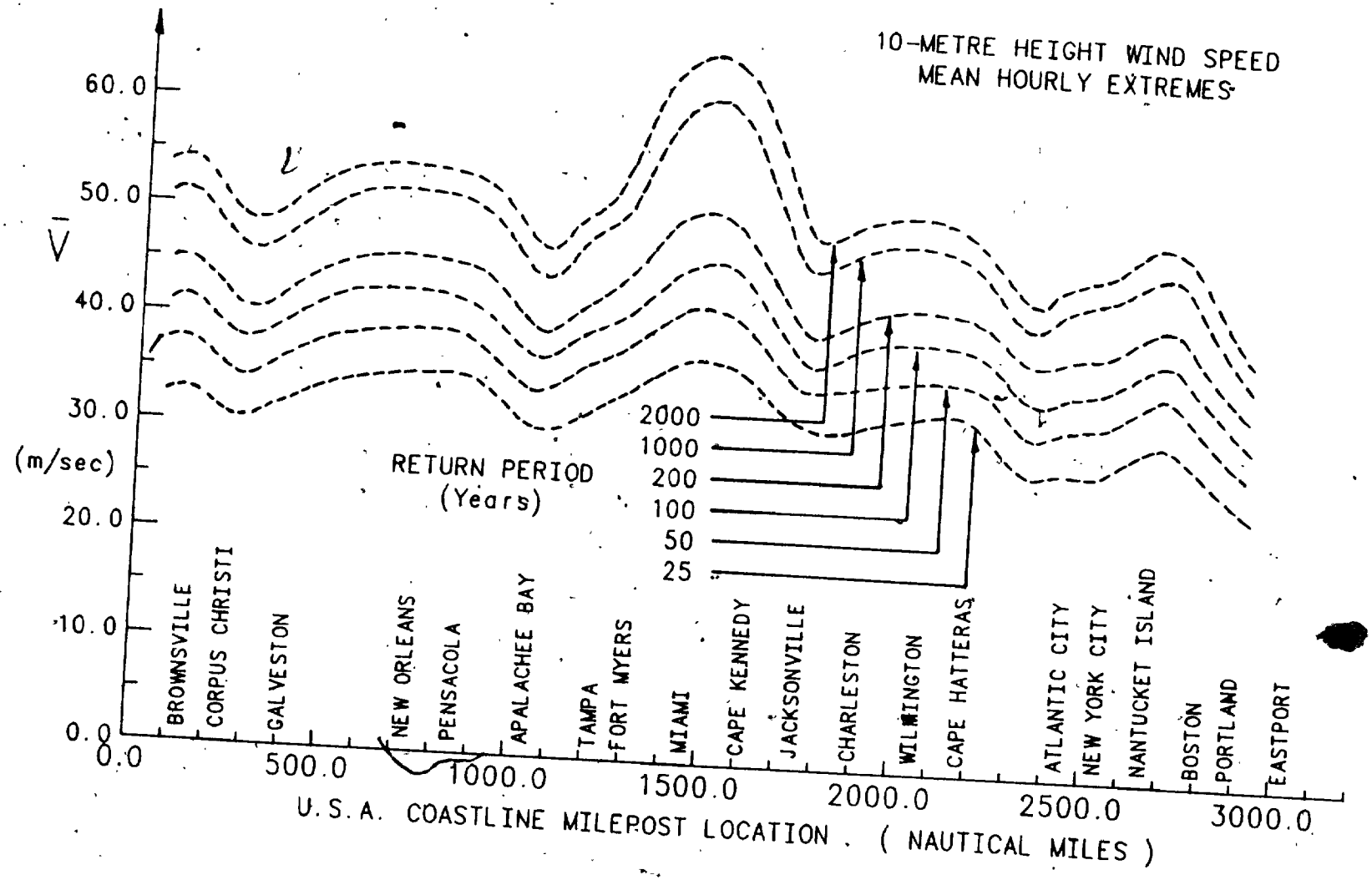

FIGURE 6.10 Simulation 10 Metre Height Extreme-Value Estimates for Coastal Locations

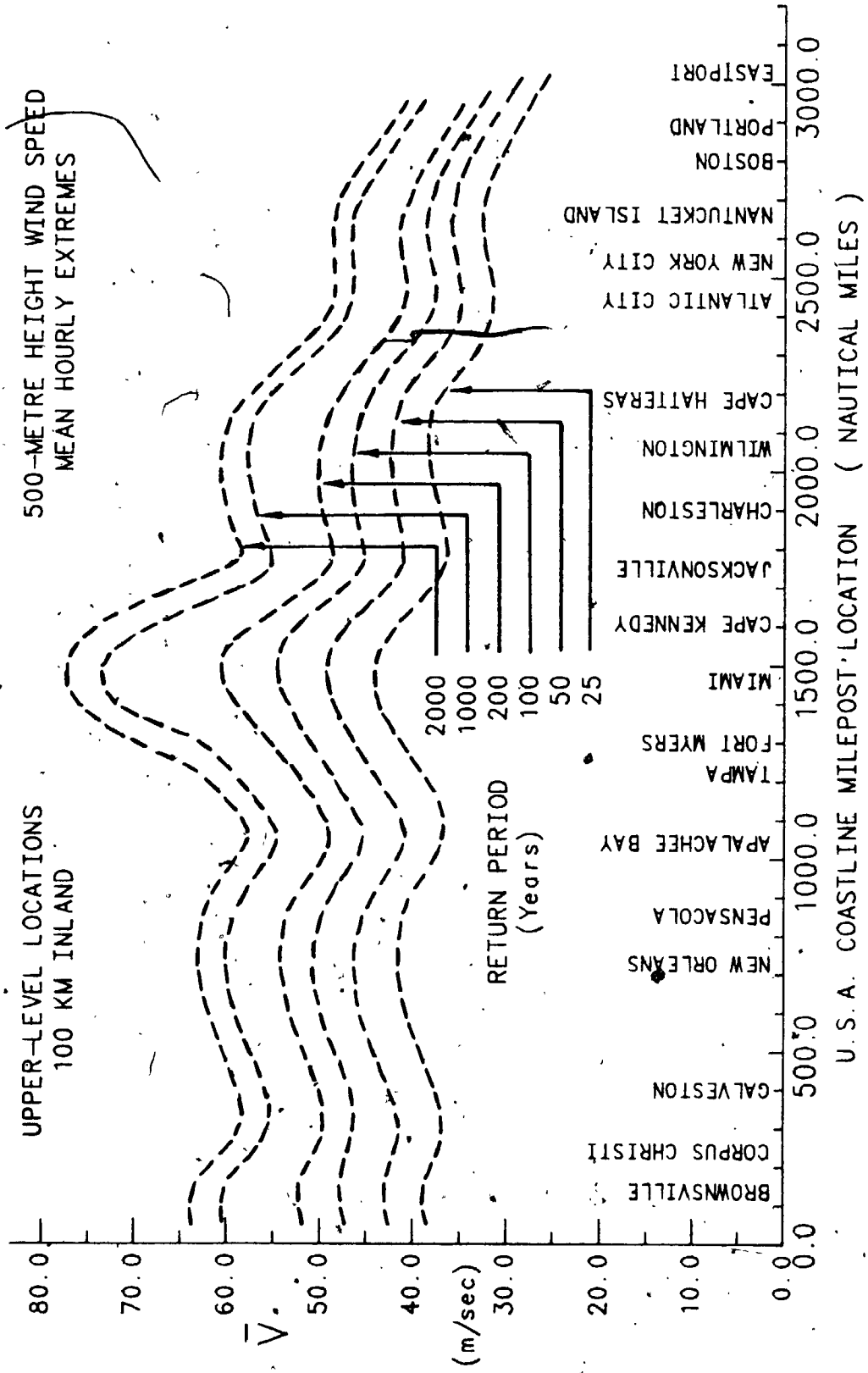

FIGURE 6.11 Simulation 500 Metre Height Extreme-Value Estimates for Locations 100 km Inland

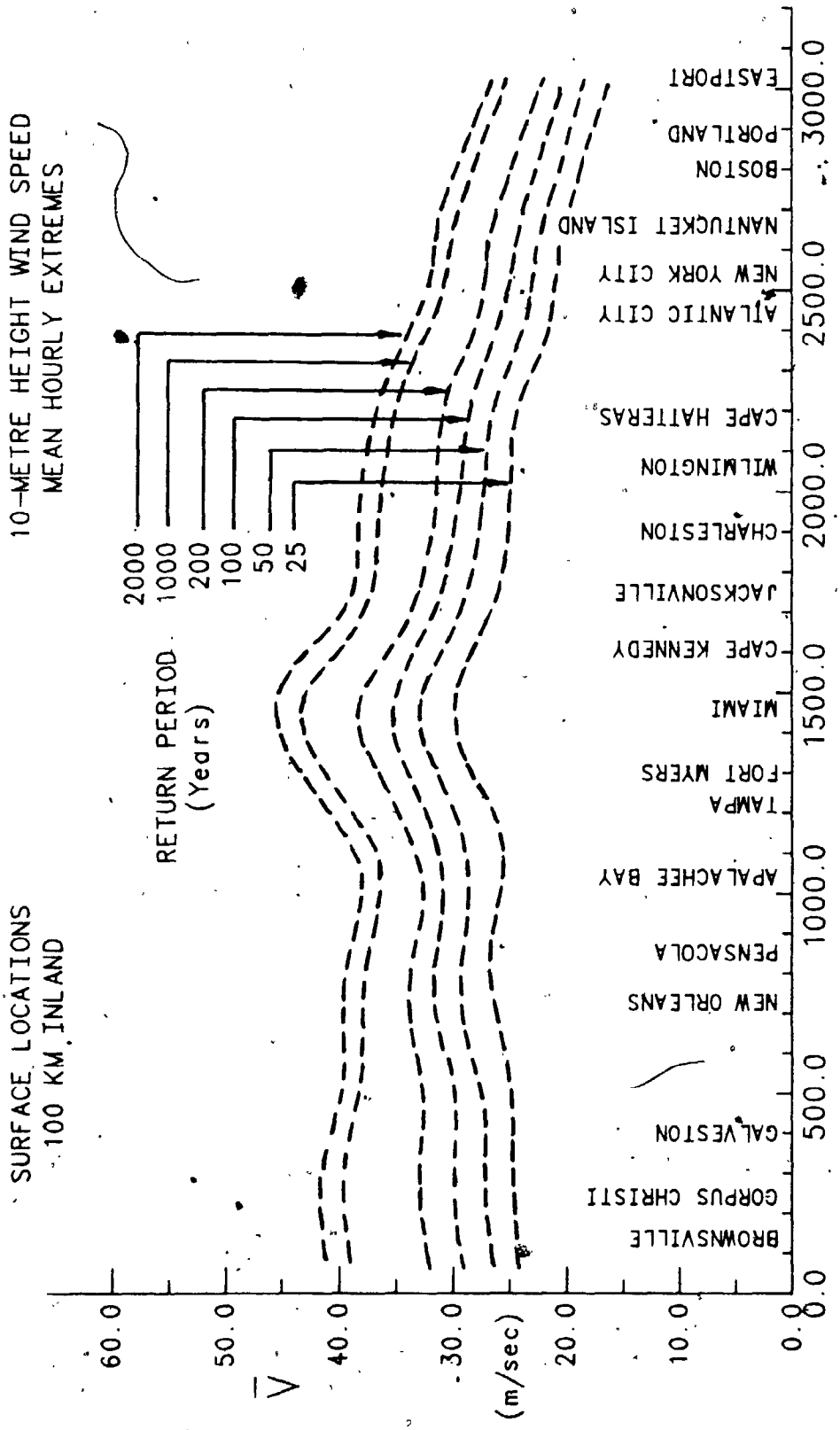

FIGURE 6.12 Simulation 10 Metre Height Extreme-Value Estimates for Locations 100 km Inland

of the Gulf Coast between coastal sites and 100 km inland is typically 70-75% compared to 80-85% for the Florida peninsula.

The results from all the simulation runs were used in the production of hurricane extreme wind speed risk maps, shown in Figure 6.13 and 6.14 for the 100-year return period estimates. The surface risk maps show marked discontinuities at the coastline compared to the 500 metre height map. The potential to identify areas where the risk is high is of considerable value to planners, engineers and other interested gorups (e.g. the insurance industry).

6.6 Comparison of Results with Previous Studies

The results of the present simulation may be compared to two recent studies examining hurricane risk in the United States. These are NOAA Technical Report NWS23 (Schwerdt, Ho and Watkins, 1979) and Batts, Cordes, Russell, Shaver and Simiu (1980), herein referred to as NWS23 and BCRSS respectively.

In NWS23, meteorological characteristics of North Atlantic tropical cyclones were used to develop estimated windfields for the so-called Standard Project Hurricane (SPH) and Probable Maximum Hurricane (PMH). The SPH is a steady-state hurricane having a severe combination of values of characteristic parameters (Δp, $RMAX$, VT, etc.). It is difficult to assign a return period to the SPH. Values of each hurricane parameter are chosen so that only few historical storms over a large region have had more extreme values. The process of choosing each parameter separately means that the actual probability of occurrence of the SPH is small, with a return period of perhaps several hundred years. The coastal variation of the 10 metre height open-water equivalent wind speed was calculated for a number of different SPH storms depending upon the choice of the highest or lowest possible value of storm translation velocity or radius of maximum winds. The results are shown in Figure 6.15. A range is given at any particular coastal site. The lower estimate was obtained assuming a high value for $RMAX$ and low value for VT, the upper curve for a low value of $RMAX$ and high value for VT.

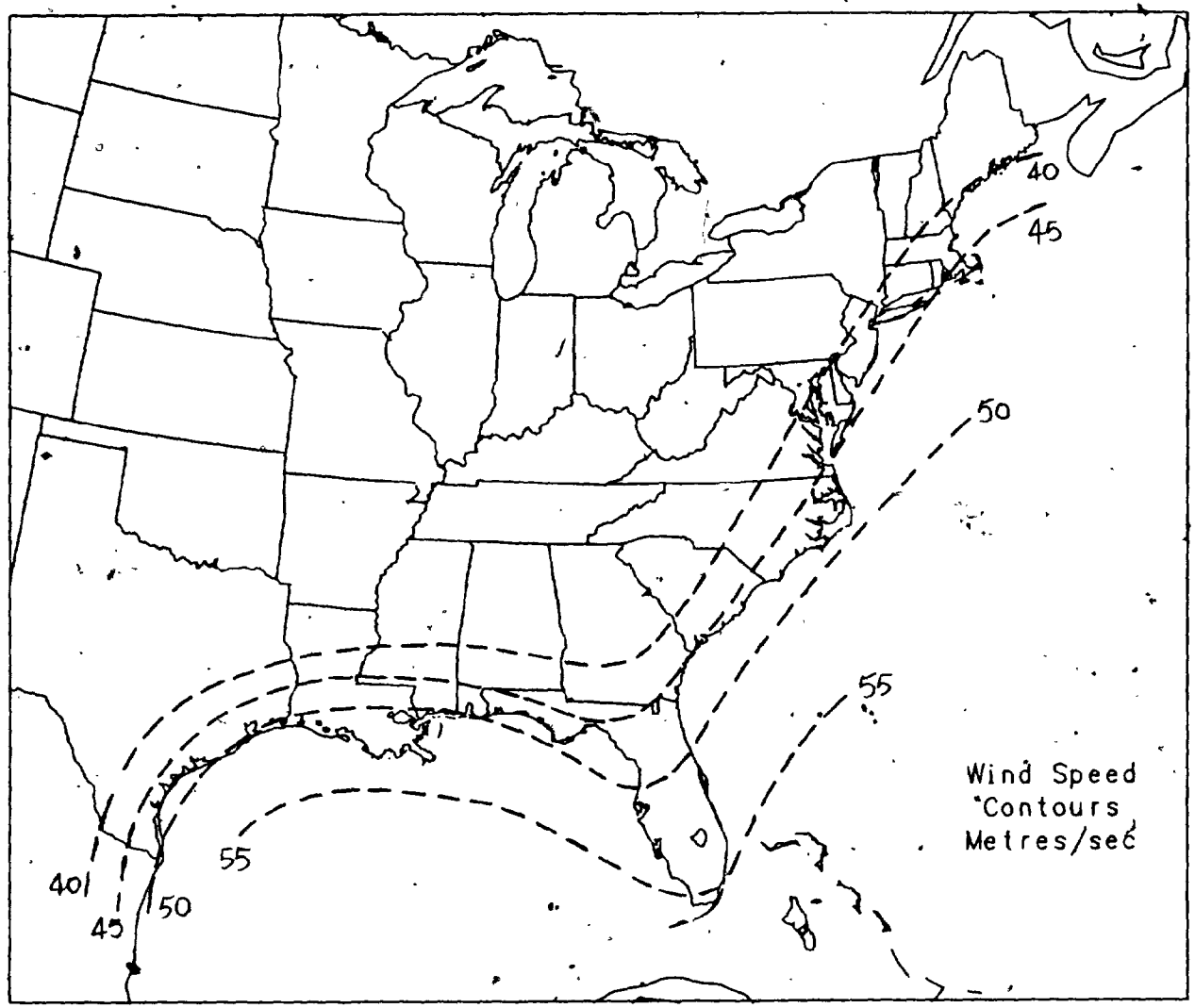

FIGURE 6.13 Simulation 100-Year Return Period Extreme-Value Estimates - 500 Metre Height Mean Hourly Wind Speeds

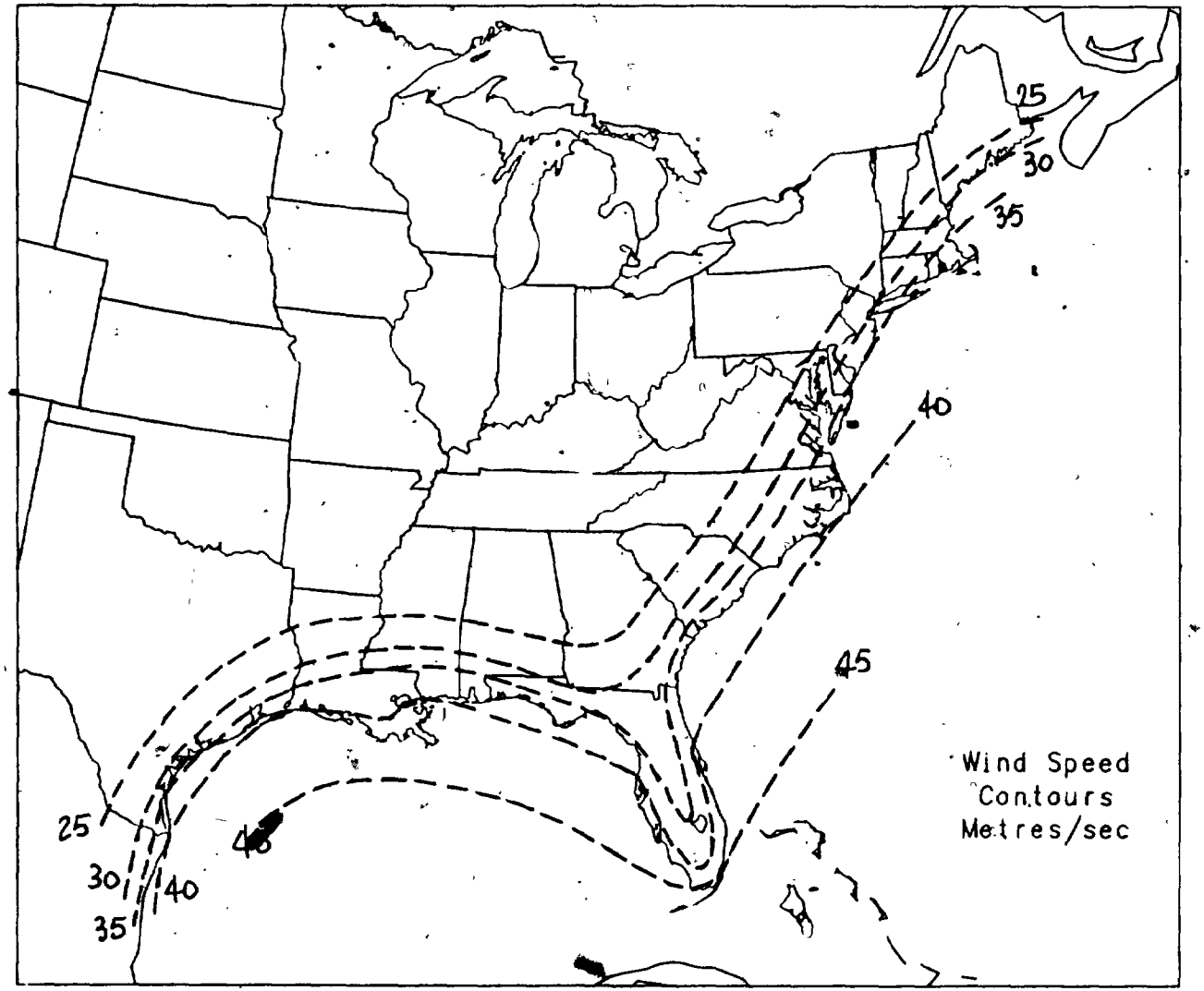

FIGURE 6.14 **Simulation 100-Year Return Period Extreme Value Estimates - 10 Metre Height Mean Hourly Wind Speeds**

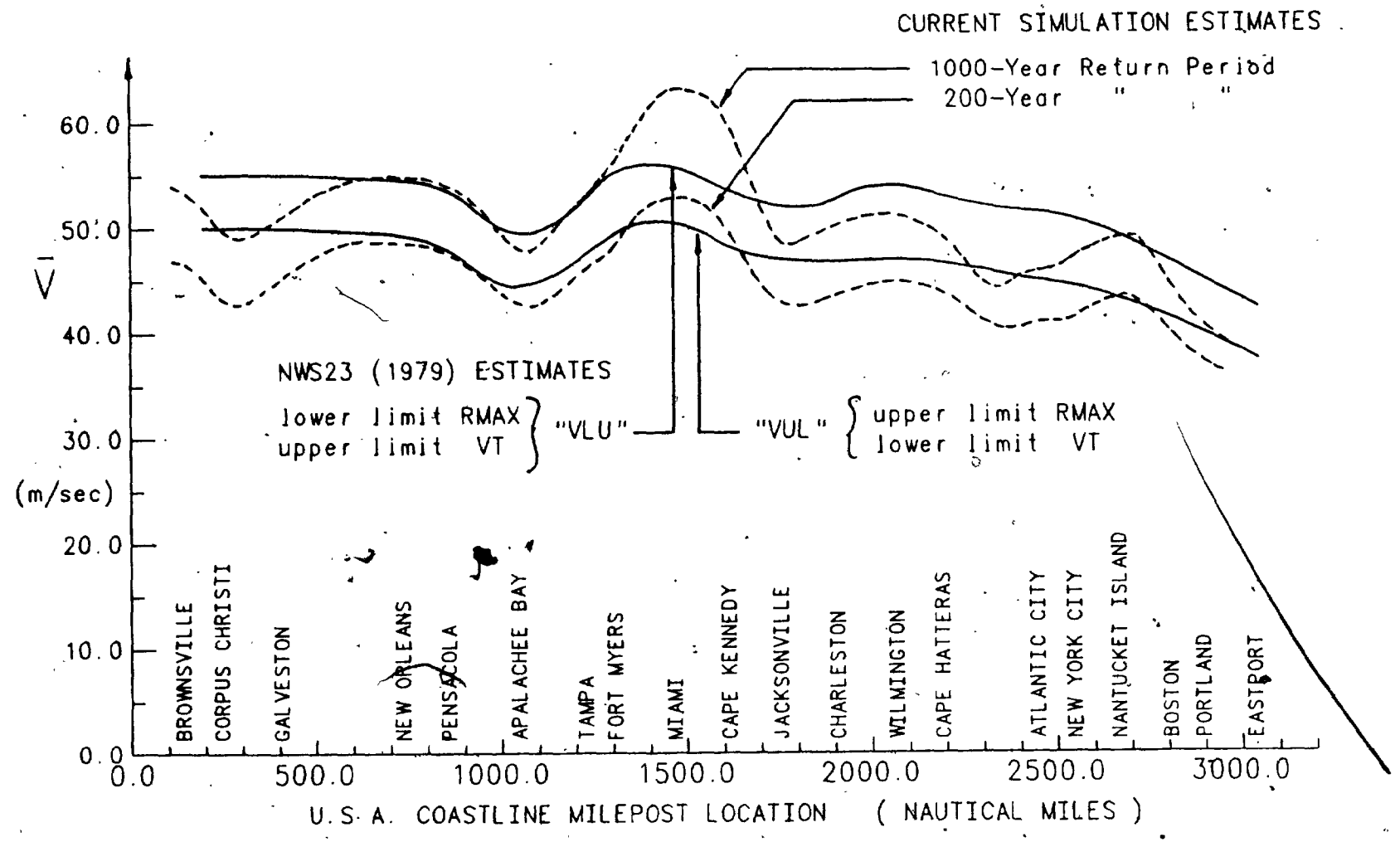

FIGURE 6.15 Comparison of Current Simulation Estimates with NWS23 Results

The variation in estimated maximum wind speeds is qualitatively similar to the results obtained using the present simulation. Wind speeds exhibit a gradual decrease from the Mexican border until around Pensacola, where a significant drop in predicted speeds occurs having a minimum in the Florida Panhandle area. The SPH winds quickly rise again to their overall maximum on the southeast coast of the Florida peninsula. Wind speeds decrease again until Wilmington where there begins a secondary maximum located just to the south of Cape Hatteras. Northwards, the winds gradually decrease. Without being able to attach an exact return period to the SPH storm extremes shown, it is not possible to compare the actual magnitudes shown in Figure 6.15 with the simulation extreme wind speed estimates, shown in Figure 6.10. The SPH curves however lie close to the simulation estimates in between the 200 and 1000 year return periods, in agreement with a subjective assessment in NWS23 of the likely return period for the SPH.

In BCRSS, a simulation procedure was used to obtain estimated fastest-mile extreme wind speeds at 10 metres above ground in open terrain near the coastline, and at 200 km inland. A constant factor of 0.85 was used to convert over-water to over-land surface wind speeds. Figure 6.16 shows the coastal extreme wind speeds computed in BCRSS after conversion of fastest-mile winds to mean hourly winds. The variation of extremes is qualitatively very similar to that obtained in the present simulation, although the magnitudes differ in a number of important respects. Local maxima are coincident with those shown in Figure 6.10. The 100-year and 2000-year return period present simulation results are included for comparison. The magnitudes of the 100-year curves are in close agreement. The 2000-year BCRSS curve is almost coincident in the Florida peninsula area but about 10-15% higher everywhere else. Inspection of the BCRSS curves shows that the ratio of expected extremes for a given site to the maximum value close to Miami increases with return period, e.g. the ratio of Cape Cod to Miami extremes increases from 80% to 90% between the 25-year and 2000-year return periods. A probable explanation for this trend which would account for the discrepancy between the 2000-year return period curves lies in the choice of distribution for a central pressure difference. In BCRSS, the lognormal distribution was chosen coupled with a truncation of Δp values at the 135 mb level. Thus the more intense hurricane regions would have a proportionately greater number

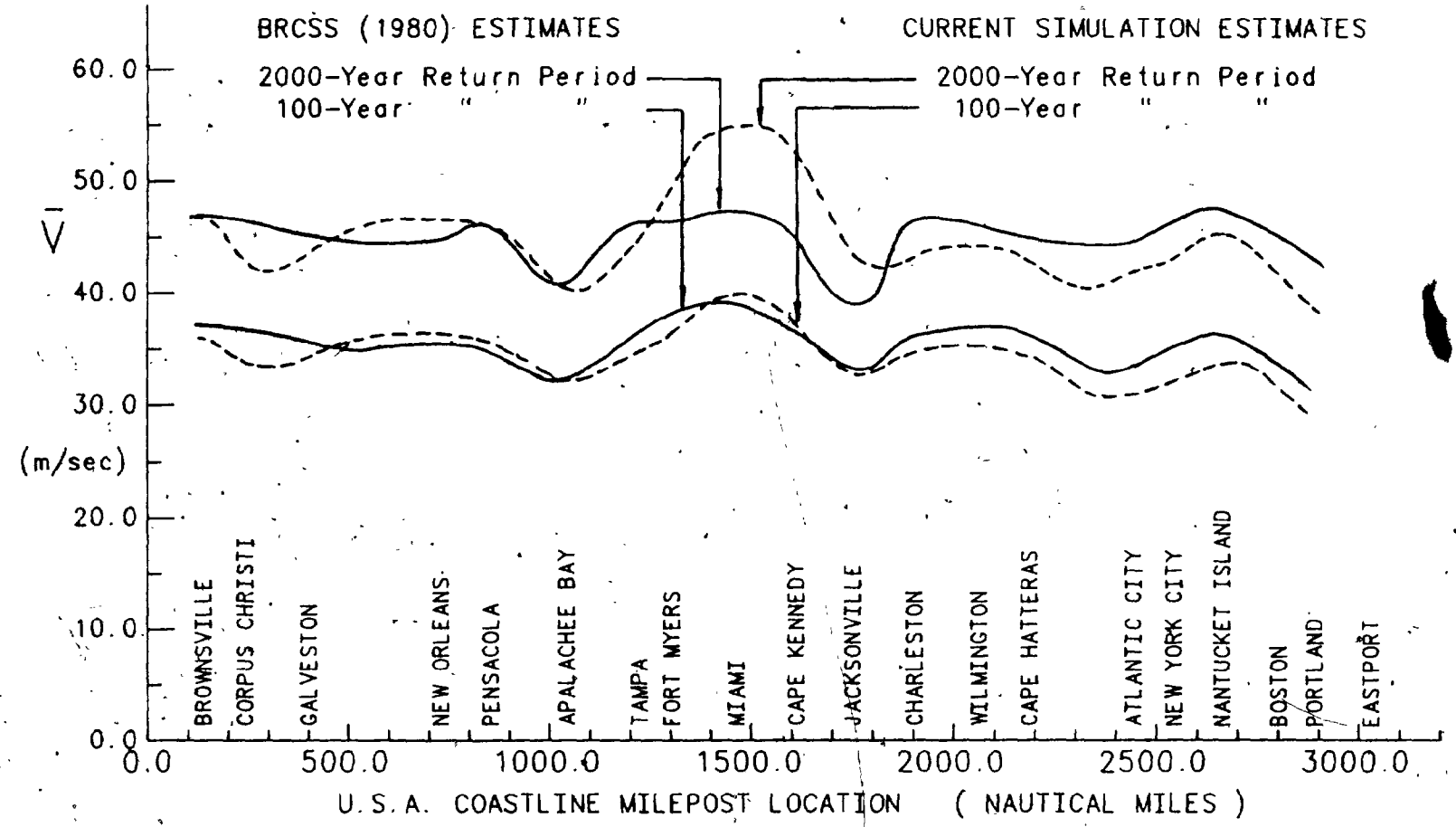

FIGURE 6.16. Comparison of Current Simulation Estimates With BCRSS Results

of storms within the simulation cut back to the truncation Δp value. This would lead to a relative overestimate in "quiet" areas (e.g. Florida's Panhandle) and relative underestimate in severe areas (e.g. Miami). There would thus be a tendency to level out the contours around the coastline for higher return periods, as is observed in the BCRSS results.

There is thus general qualitative agreement between extreme wind speed estimates obtained using the current simulation and the two studies discussed in this section, particularly for coastal locations. The characteristics of parent distributions for individual sites were not determined in NWS23 and BCRSS and hence comparisons of the parent distributions are not possible. The uncertainties associated with estimated extreme wind speeds obtained using the simulation approach were the subject of a recent study by Dorman (1983).

Dorman applied the simulation technique to a typical Australian cyclone-prone coastal site and varied input parameters within the simulation in order to assess the sensitivity of the approach on the final extreme estimates. The range of possible values for any particular variable was determined from the literature, with a supposedly substantial opinion supporting both the high and low values. Many of the studies from which representative data were obtained however are outdated and inappropriate. For example, the ratio of over-land to over-water mean (10-minute average) surface (10 metre) wind speed was allowed to vary from 0.79 to 1.0. This ratio is represented by the ϕ_l parameter in the current simulation procedure. The upper value, 1.0, was justified by the assumption that the surface roughness length over open-water in extreme wind conditions (e.g. hurricane conditions) corresponds to suburban terrain, i.e. a Z_o value of about 0.3 metres. This is in direct conflict with all observational data gathered in open-water conditions for North Atlantic tropical cyclone occurrences, as discussed in section 2.5, and as can be seen in Figure 2.20. A range of values from 0.7 to 0.9 was adopted for the ratio of open-water surface to gradient mean wind speed. The large amount of simultaneous aircraft and ocean data buoy measurements (see section 2.5) observed in tropical cyclones over open-water contradicts the upper value, 0.9, of the assumed range. The relationships chosen as well-substantiated candidates to define the gradient wind speed were taken from Myers (1957), Graham and Nunn (1959), Holliday (1969) and Atkinson and Holliday (1975),

even though in some cases they applied to different tropical cyclone oceanic regions. The limitations of these predominantly empirical formulae were discussed in section 2.1. Other model parameters which were allowed to vary included the simulation circle size, radial wind profile exponent, central pressure difference cut-off value and radius of maximum wind representation.

It is not surprising therefore that combinations of these parameters could be chosen to yield large differences in the final simulation extreme predictions. Dorman found that the 50-year return period over-water, surface mean wind speed and over-land, surface gust wind speed varied between 22.3 to 45.9 m/sec and 24.7 to 82.5 m/sec respectively. This wide range of simulation-derived estimates resulted however from inappropriate assumptions regarding tropical cyclone windfield characteristics coupled with an unnecessarily arbitrary choice of admissable global parameters (simulation circle size, wind profile exponent, radius of maximum wind limitations, etc.). Attention to recent advances in the understanding of tropical cyclones and reasonable care in defining simulation model global parameters would greatly reduce the uncertainties in the simulation-derived extremes in Dorman's study, uncertainties which are unduly pessimistic and certainly not supported by the results given in this chapter.

CHAPTER 7

EXTENSION OF THE SIMULATION PROCEDURE TO EXAMINE LINE-LIKE RISK AND STRUCTURAL RESPONSE COMPUTATIONS

The simulation procedure is extended to examine two problems of engineering design interest, the increased risk sustained by line-like structures such as transmission lines and the computation of structural response exceedances from the tropical cyclone wind climate. In addition to applying the simulation procedure directly to these problems analytical approaches are developed which aid in forming general solutions, reducing the computation time required and hence increasing the efficiency of the simulation method.

7.1 Line-Like Risk for United States Coastal Locations

The extreme wind speed estimates that were determined along the U.S. Gulf and Atlantic Coasts in the previous chapter are applicable to point structures, i.e. indicating the risk that an isolated building would experience. This risk can be expected to increase for line-like structures, most notably transmission lines. Apart from the actual length of the line, a number of other factors play a role in influencing the final risk. These include the position of the line relative to the coastline and the orientation of the line in relation to the mean storm approach angle.

In order to examine the line-like risk problem, three locations were chosen, shown in Figure 7.1, in the vicinity of Galveston, Miami and Charleston. At each of these locations two lines were defined, one running parallel to the coastline, the other running inland perpendicular to the coastline. Also shown is the mean tropical cyclone approach angle at each of the three sites. The three sites allow different relationships to be examined between the lines and the predominant direction of storm motion. The Galveston coastal line (GC) and inland line (GI) run perpendicular and parallel with the average track angle of tropical cyclones in the area respectively. The opposite occurs

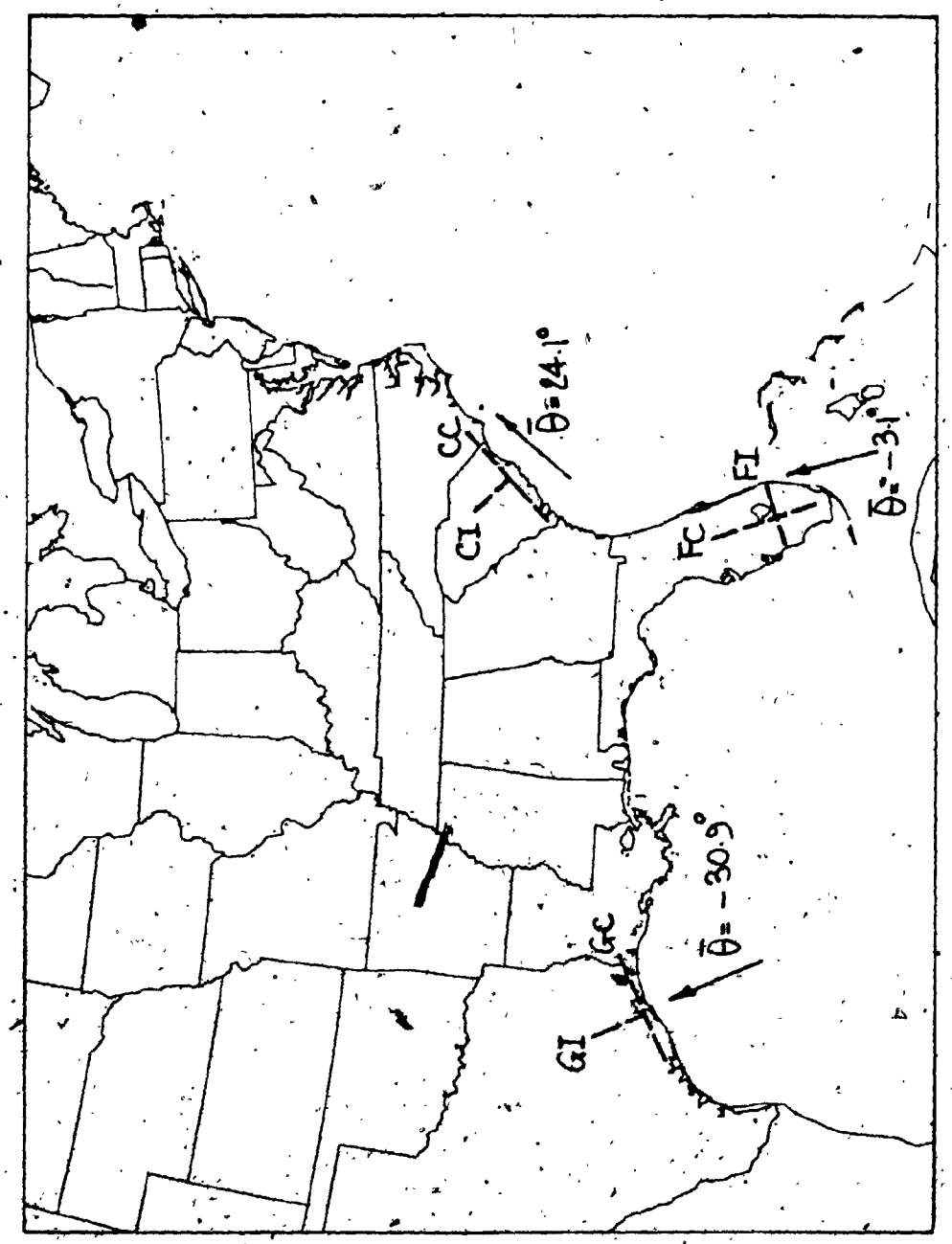

FIGURE 7.1 Location Map for Line-Like Risk Examples

for the two Charleston lines, with the coastal line (CC) aligned almost parallel with the predominant storm direction and the inland line (CI) perpendicular. The two lines located within the lower Florida peninsula are both inland.

For each of the six lines defined, the simulation procedure was run for time periods resulting in the generation of approximately 2500 tropical cyclones. As each storm was created within the simulation, wind speeds were concurrently recorded at fixed intervals along the line and the maximum value at any point recorded. This resulted in the compilation of a separate set of "line" extremes, representing the maximum wind speeds seen by the line, regardless of where along the line the particular speed was sustained. Clearly extreme-value distributions fitted to the line extremes would be expected to be more severe than those determined at any isolated point along the line.

The results for the two Galveston lines are shown in Figure 7.2. Extreme-value distributions were computed for a point on the coastline at the junction of lines GC and GI, for two GC lines of length 100 km and 200 km running along the coast and for a single GI line of length 100 km running inland from the coast. There is a marked increase in the risk (higher wind speeds for the same return period) for the two coastal lines, as compared with the inland line which exhibits only a modest increase. The increases are significant. For example, the 100-year return period extreme wind speed estimate is 48.0 m/sec for the single point distribution. This same speed has return periods of 50 and 25 years for the 100 km and 200 km GC coastal lines. Alternatively, the 100-year return period extreme for the 200 km GC coastal line (55.0 m/sec) has a return period of approximately 500 years for the single point distribution.

The extreme-value distributions for the Charleston point, coastal (CC) and inland (CI) line extremes are shown in Figure 7.3. The increase in risk is almost the same for the coastal and inland lines (note the coastal line is 200 km long, double the inland line length). The risk magnitudes do not change as much as indicated for the Galveston lines. The 100-year extreme speed for the 200 km CI coast line (54.0 m/sec) corresponds to a 200-year return period for the single point distribution. The results of the two simulations performed for the Florida peninsula lines were almost identical to the Charleston runs

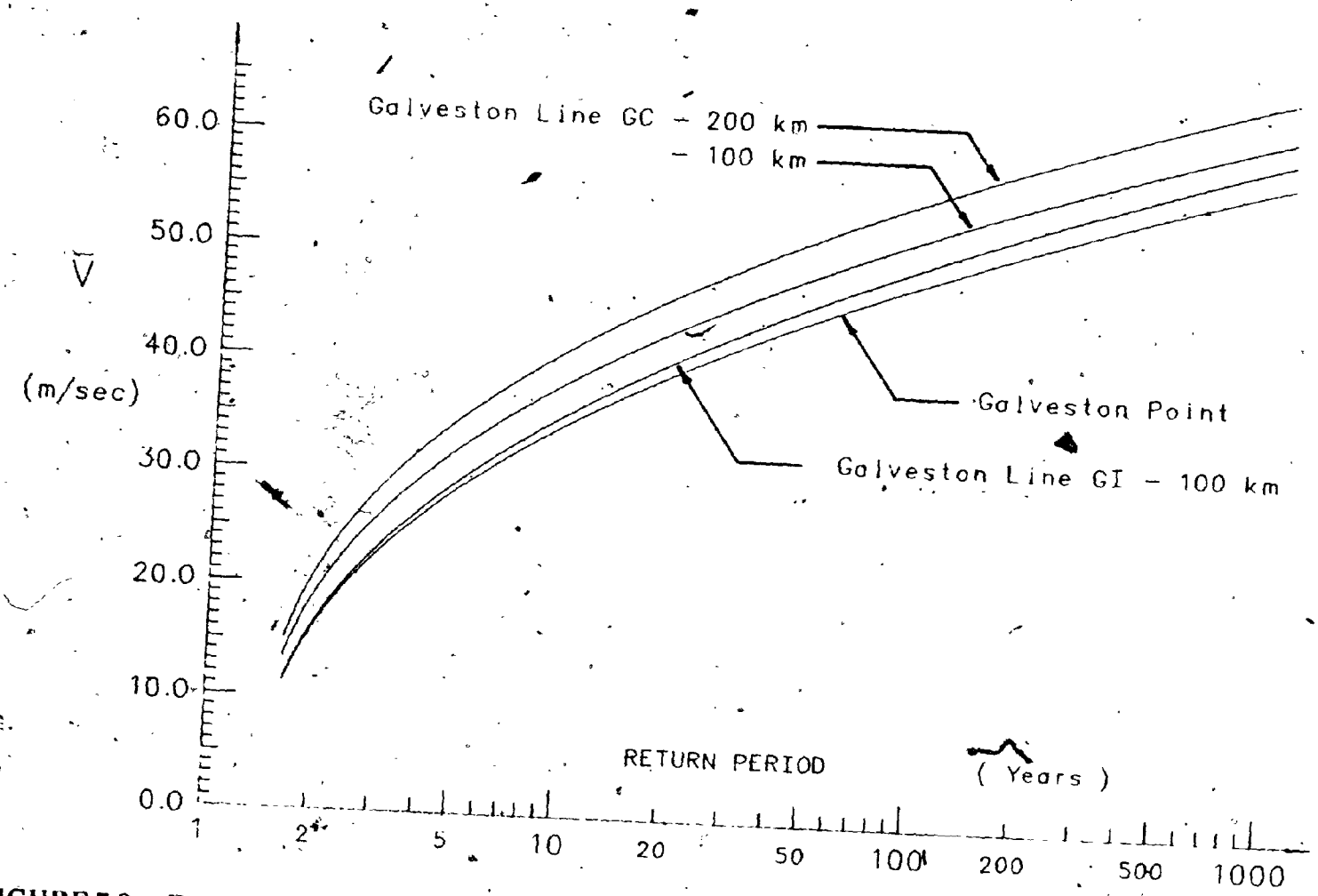

FIGURE 7.2 **Extreme-Value Distributions for Galveston Point, Coastal Lines GC (100, 200km) and Inland Line GI (100km)**

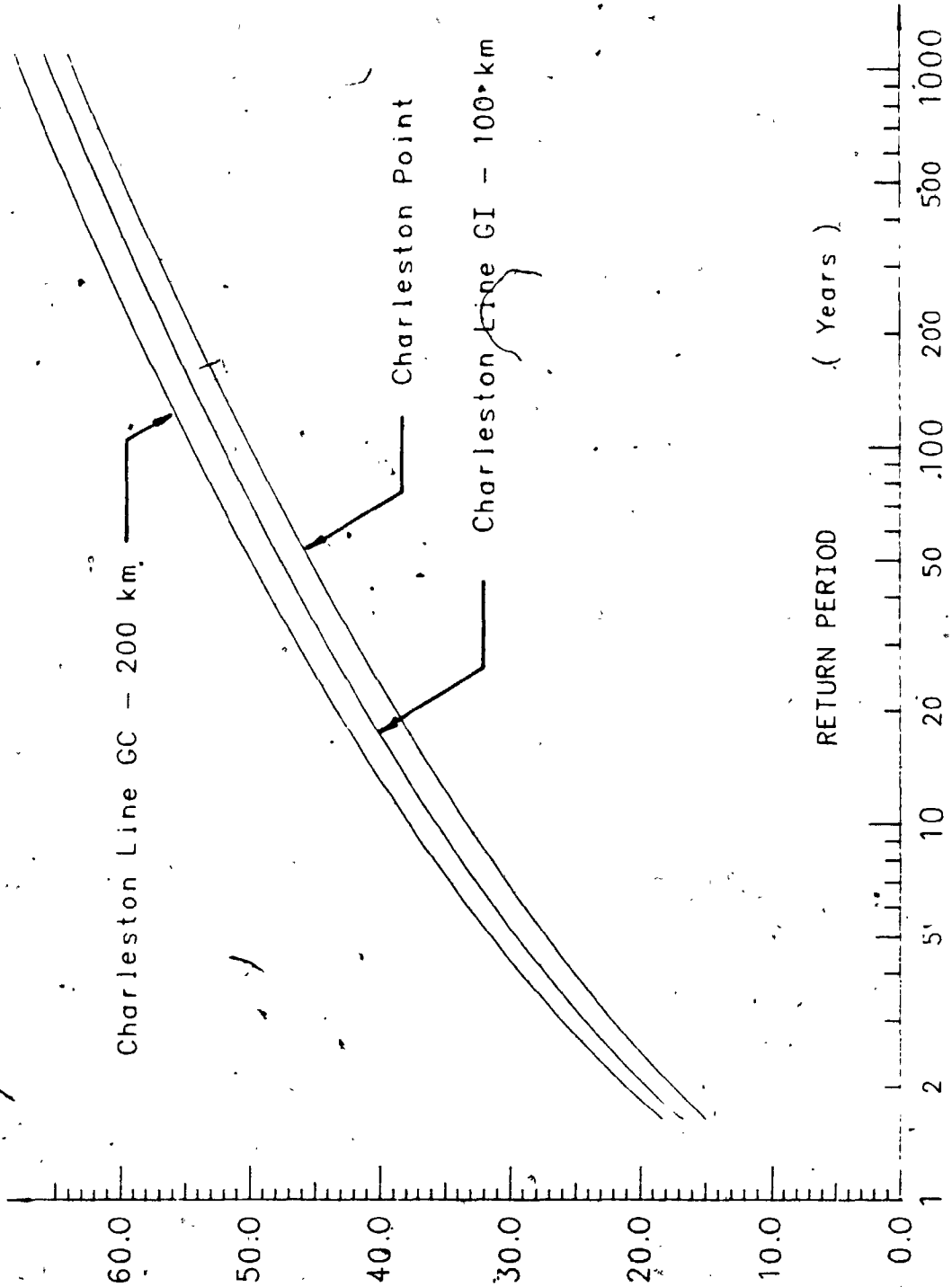

FIGURE 7.3 Extreme-Value Distributions for Charleston Point, Coastal Line CC (200km) and Inland Line CI (100km)

with similar increases in risk for the two lines running along and across the axis of the peninsula.

The differences between the line-like risk behaviour for the three locations examined can be related to the track characteristics in the area. Lines running perpendicular to the main storm track direction are likely to experience higher wind speeds over their total length. This effect coupled with the decrease in wind speeds for landfalling storms accounts for the lower risk in lines of equal length running inland in the Galveston area compared to coastal lines. Along the Atlantic coast two opposing influences tend to balance out the risk for lines located along the coast and perpendicular to the coast. Although wind speeds are generally weaker for inland locations, lines located perpendicular to the coast are also perpendicular to the mean storm direction and hence experience a greater range of storm maxima than lines located along the coast whose points will typically be at the same distance from the storm path as it moves parallel to the coast.

The three examples chosen indicate that line-like risk behaviour may be conveniently described by considering regions along the Gulf Coast separately to the Florida peninsula and Atlantic Coast. For Gulf Coast locations, a useful rule of thumb for estimating the increased risk for line-like structures is to reduce the return period associated with a given wind speed for a point structure by approximately 50% for every 100 km length for coastal lines, and 15% for every 100 km length for lines perpendicular to the coast. For Florida peninsula and Atlantic Coast regions a single reduction may be used for all lines regardless of orientation, equal to approximately 25% for every 100 km length of line.

7.2 Theoretical Approach to the Line-Like Risk Problem

The above approach is computationally demanding. As the length of any particular line being investigated increases more points must be used to record wind speeds along the line to obtain the line extremes. A more general approach to evaluating the increased risk associated with line-like structures is possible, making use of an alternative computational procedure for

evaluating the risk to isolated point structures suggested by Davenport (1984). Attention is restricted formally to the gradient balance windfield, although the results apply without any significant loss in accuracy to the windfield at other heights.

The gradient balance wind equation (E3-3) can be solved explicitly for any given group of storm parameters (Δp, $RMAX$, VT). Hence the maximum value of Vgb, denoted here as $VMAX$, can be determined if the value of $DMIN$ is known. By defining a variable, D, corresponding to distance perpendicular to the storm motion, it is possible to compute the variation of $VMAX(D)$, as shown in Figure 7.4. For any particular storm, the peak value of $VMAX(D)$ will be located near $D = RMAX$. Using the simulation procedure, a set of tropical cyclones is generated with storm parmeters (Δp_i, $RMAX_i$, VT_i ; $i=1$, N). At any fixed value of D, a set of wind maxima can then be computed, ($VMAX_i(D)$; $i=1$, N). These N maxima can be fitted by a frequency distribution, conditional upon D, whose cumulative distribution function is defined as $F^p_{VMAX/D}(VMAX, D)$. The superscripts, p and l, are used herein to differentiate between point and line-like structure parameters and functions. This is done for a complete range of D values, resulting in a set of contours of equal CDF magnitude, as shown in Figure 7.5. These are redrawn to indicate the variation with D of the exceedance probability of some particular value of wind speed, Vo, given by $F^p_{VMAX/D}(Vo, D)$, also shown in Figure 7.5.. From the historical records, it is possible to compute the number density of storm occurrence, $n_D(D)$, equal to the number of tropical cyclones per annum and unit distance crossing the D axis. The exceedance rate for the velocity level, Vo, is then given by:

$$N(>Vo) = \int_{-\infty}^{\infty} n_D(D)\, F^p_{VMAX/D}(Vo,D)\, dD \qquad E7-1$$

In section 5.8 it was shown that for most coastal locations the variation of the minimum approach distance, $DMIN$, can be reasonably approximated by the uniform distribution. Therefore, E7-1 may be rewritten:

$$N(>Vo) = \overline{n_D} \int_{-\infty}^{\infty} F^p_{VMAX/D}(Vo,D)\, dD \qquad E7-2$$

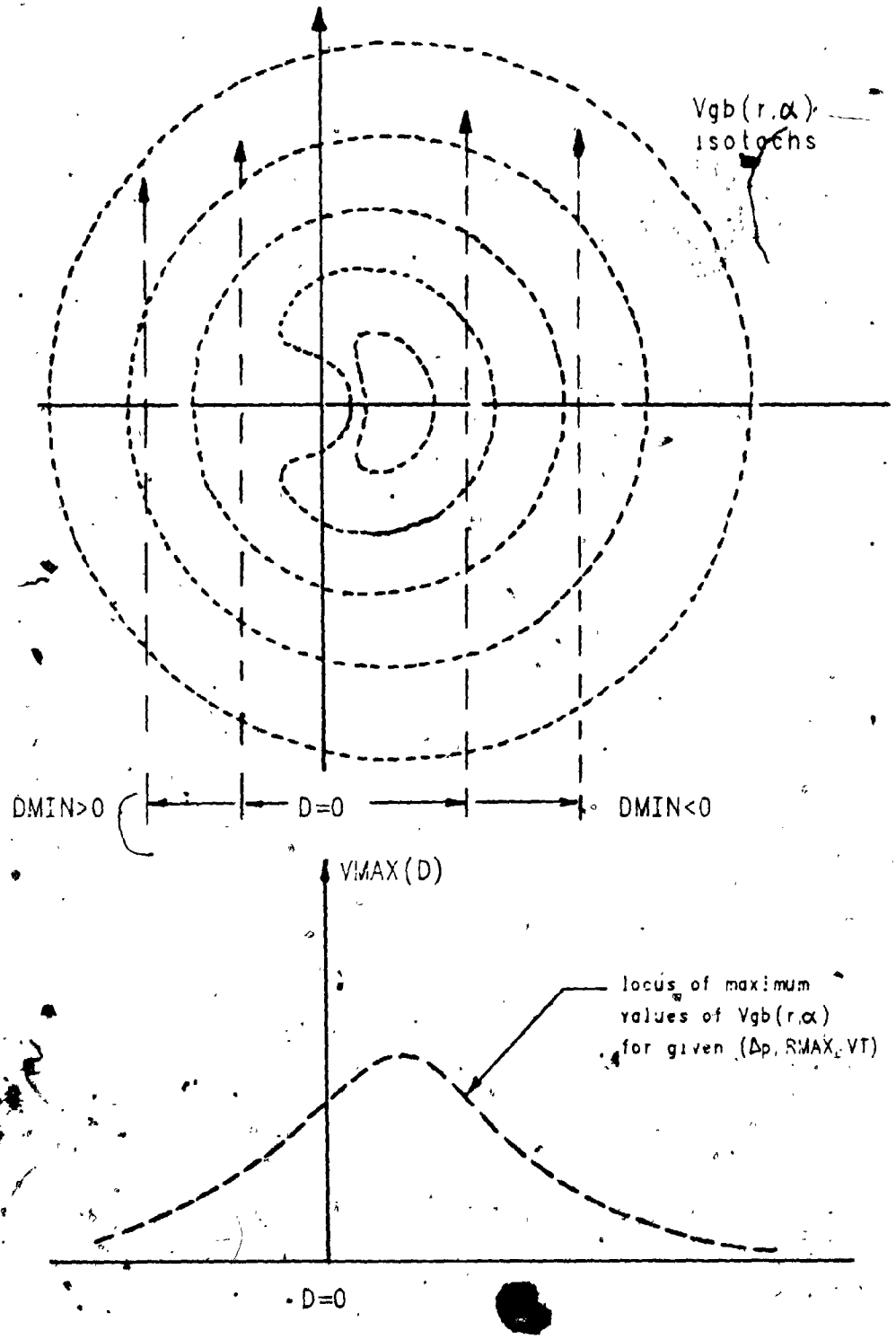

FIGURE 7.4 Gradient Balance Circulation and Variation of VMAX(D) for a Point Structure

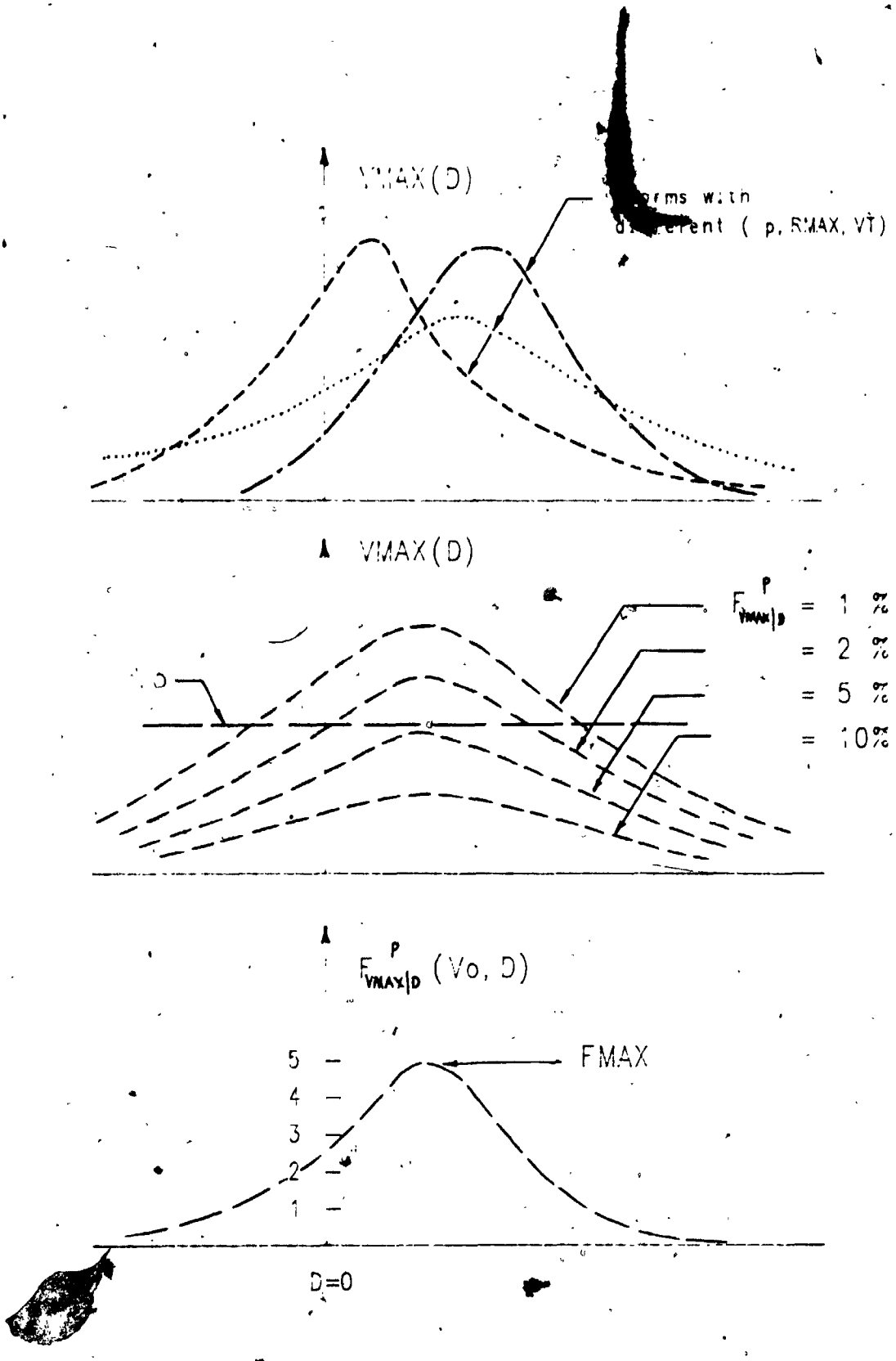

FIGURE 7.5 . Development of $F^{P}_{VMAX/D}$ (VMAX, D) Curves

$\overline{n}_D$ = average number density

For high values of *Vo*, the exceedances can be assumed to be Poisson distributed and hence the extreme-value distribution of wind speed can be obtained as :

$$F(<Vo) = \varepsilon^{-N(>Vo)} \qquad E7-3$$

The advantage of this particular approach stems from the economy in the number of storms required to establish the extreme-value distribution. This is due firstly to the reduction in computations resulting from the direct integration of the distance to track influence. Secondly, the information required to form the *CDF* exceedance functions is obtained from storms whose maximum wind speeds exceed the *Vo* value. Weaker storms generated in the simulation are not needed in the computations. Hence it is possible to specify a lower cut-off level for Δp values further decreasing the necessary computations. Disadvantages arise from the necessity of having to be able to analytically determine the maximum wind speeds for a given value of *DMIN*, once Δp, *RMAX*, *VT* etc. are known. This is possible for the gradient balance windfield, but not for the 500 metre height and surface windfields, although the approximately constant ratios between surface winds and upper-level winds minimizes the errors. A more significant problem arises from having to take into account the effects of filling, and the resulting decrease in maximum wind speeds, for locations inland from the coast.

This approach can however be used to determine the relative change in risk for line-like structures, not affected by the previous constraints. The gradient balance windfield shown in Figure 7.4 is considered again. This time a length of line, *DL*, spanning the storm centre is constructed and the resulting *VMAX(D)* computed. In this case *VMAX(D)* is the maximum value occurring anywhere along the length of the line. It can be seen that the resulting curve, shown in Figure 7.6, is simply an extension of the isolated point curve in Figure 7.4, with a constant maximum level over a length equal to *DL*. The exceedance curves, applying to the line, $F^L_{VMAX/D}(VMAX, D)$, shown in Figure 7.7, are also simple extensions of their isolated point

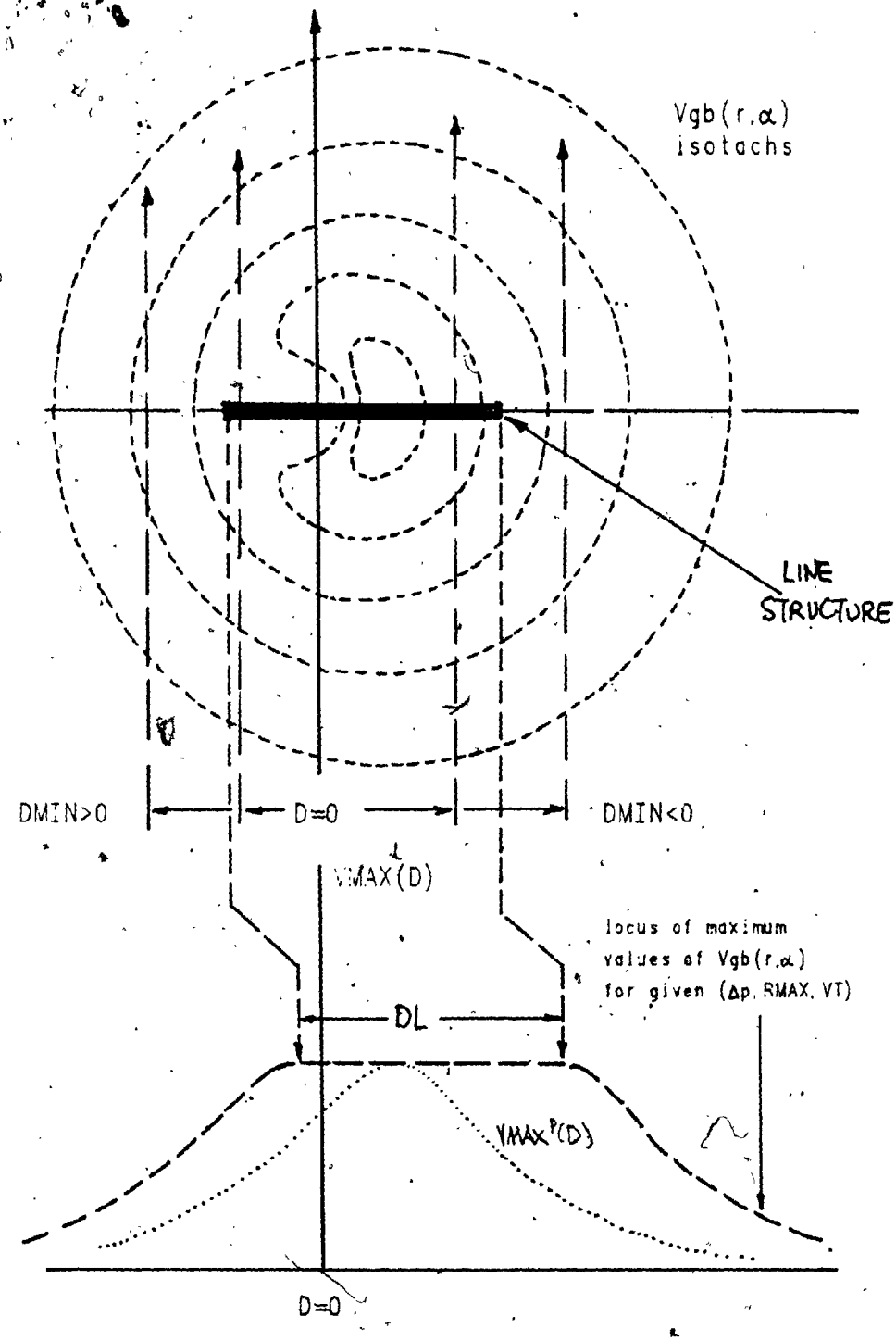

FIGURE 7.6 Gradient Balance Circulation and Variation of VMAX(D) for a Line Structure

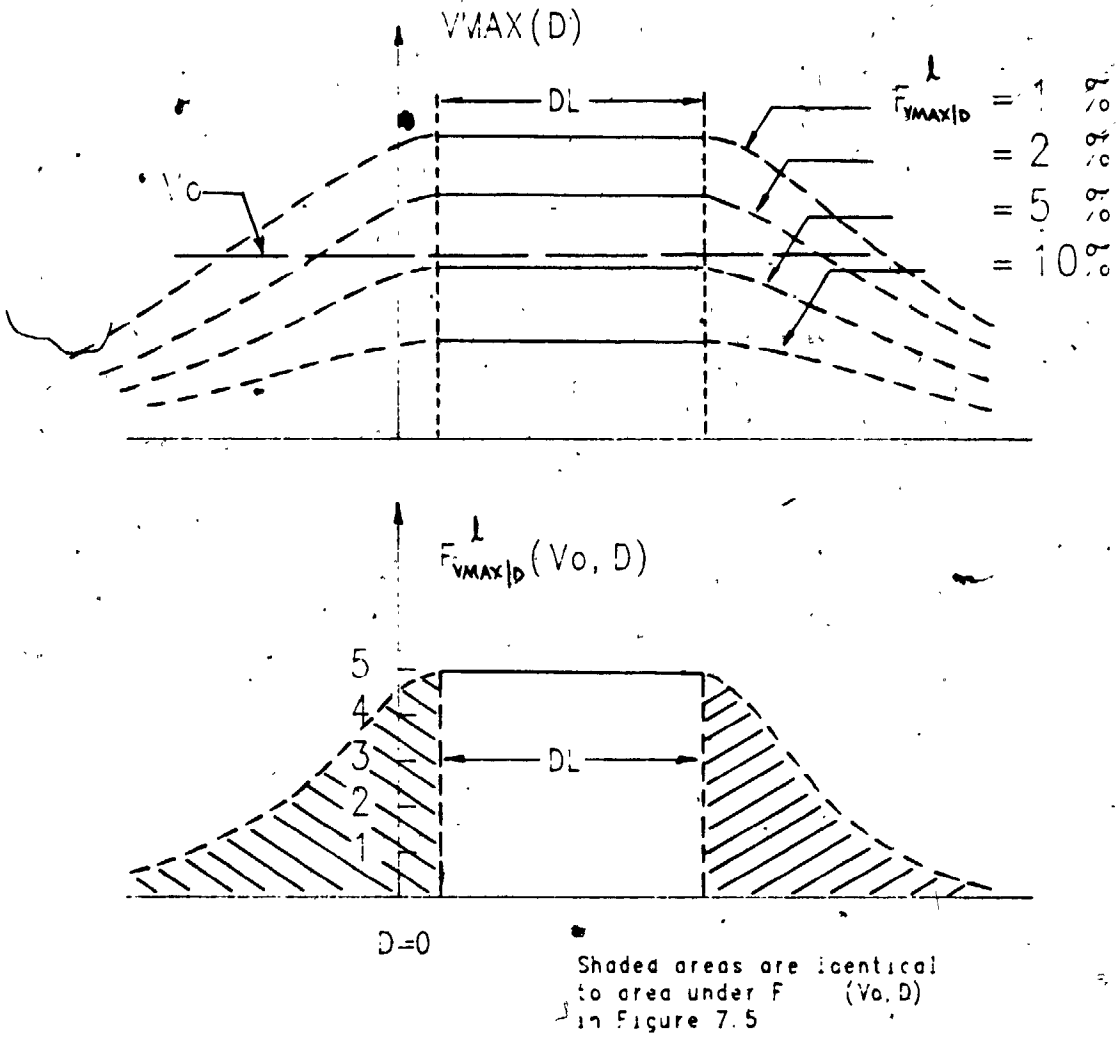

FIGURE 7.7 Development of $F_{VMAX/D}^{1}$(VMAX, D) Curves

counterpart. The influence of the line is to increase the area in the integral of E7-2, so that the line exceedance rate for a velocity Vo becomes:

$$N^L(>Vo) = N^P(>Vo) + \overline{n_D}\ FMAX\ DL \qquad E7-4$$

$FMAX$ = maximum value of $F^P{}_{VMAX/D}(Vo, D)$ (see Figure 7.5).

Thus the ratio, $\eta(Vo)$, of exceedance rate of velocity Vo for line of length DL to that of a single point is :

$$\eta(Vo) = \frac{N^L(>Vo)}{N^P(>Vo)} \qquad E7-5$$

$$= 1 + \frac{FMAX\ DL}{\int_{-\infty}^{\infty} F^P_{VMAX/D}(Vo,D)\,dD}$$

This may be somewhat more conveniently written by defining an "effective hurricane line length", D_e, such that :

$$\int_{-\infty}^{\infty} F^P_{VMAX/D}(Vo,D)\,dD = FMAX \cdot D_e(Vo) \qquad E7-6$$

The value of D_e depends upon the wind speed, Vo. The exceedance rate ratio for line-like to point structures and the resulting line-like extreme-value distribution can then be simply written as :

$$\eta(Vo) = 1 + \frac{DL}{D_e(Vo)} \qquad E7-7$$

$$F^L(<Vo) = \varepsilon^{-\eta(Vo)N^P(>Vo)} \qquad E7-8$$

This simple formulation needs to be corrected for two factors. In the above derivation it was assumed that all storms move along parallel tracks (i.e. with the same approach angle) and that the direction of these tracks is perpendicular to the direction of the line. The second factor is simply handled

by taking the distance component of the line that is perpendicular to the direction of the tracks. This modifies E7-7 so that :

$$\eta(Vo) = 1 + \sin\theta_L \frac{DL}{D_e(Vo)} \qquad E7-9$$

θ_L = angle between storm track and line

In practice the track angle is not constant, but distributed about some mean direction θ_o, typically in a Gaussian fashion, as described in section 5.7. The effect of the variation in approach angle is illustrated in Figure 7.8. When the mean storm approach angle is normal to the line, there will still be a considerable percentage of paths with values of θ_L less than 90°, decreasing the value of $\eta(Vo)$. Conversely, lines which run parallel to the mean approach angle will not experience zero increase in risk as suggested in E7-9 as many paths will exhibit values of θ_L greater than zero.

Figure 7.8 shows how the value of $\eta(Vo)$ is affected at various values of θ_L. The fractional change is expressed by a factor, ϕ_L, which depends on the magnitude of the standard deviation of the approach angle, $RMS(\theta)$, about the mean storm direction. Locations on the upper Atlantic coast exhibit "tight" approach angle distributions, $RMS(\theta)$ less than 20°, whereas $RMS(\theta)$ values are typically around 40° for much of the Gulf Coast and over 50° in the Florida peninsula region. A number of trial computations showed that the ϕ_L factor could be estimated as $RMS(\theta)/500.0$. This last correction gives the ratio of line-like to point exceedance rate as :

$$\eta(Vo) = 1 + \psi(\theta_L, \phi_L) \frac{DL}{D_e(Vo)} \qquad E7-10$$

where

$$\psi(\theta_L, \phi_L) = 3\phi_L + (1 - 4\phi_L)\sin\theta_L$$

The advantage of this approach is that only the computations for a single point are used. These are illustrated for the Galveston area in Figures 7.9 and 7.10. It can be seen that the value of D_e varies considerably over the range of velocities of interest. D_e equals 88 km at the 100-year return speed of 48.0

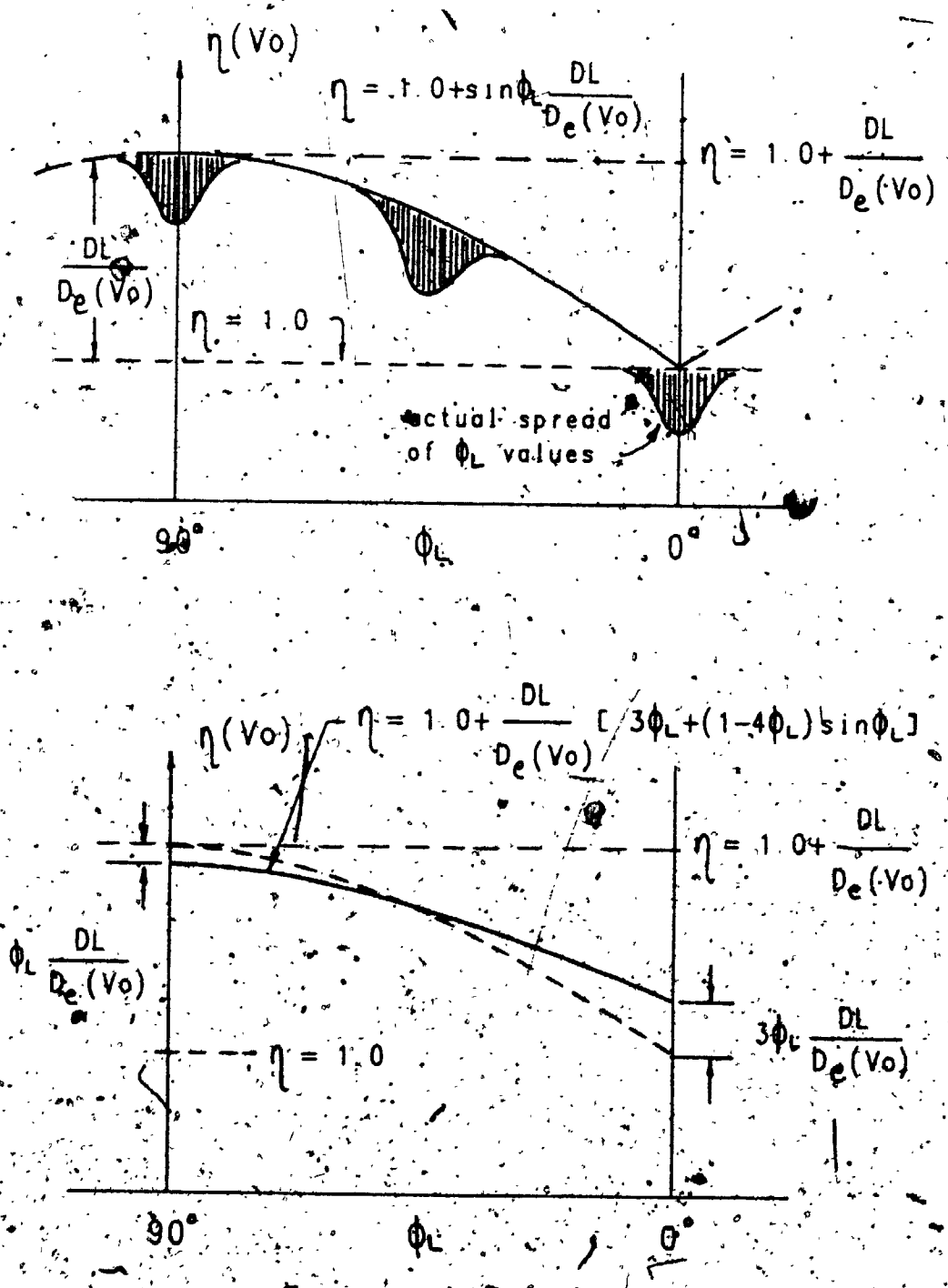

$$\phi_L = \frac{\sigma_\theta}{500.0} \qquad \sigma_\theta = \text{approach angle rms}$$

FIGURE 7.8 Effect of Distribution of Approach Angle on Line Exceedance Rate

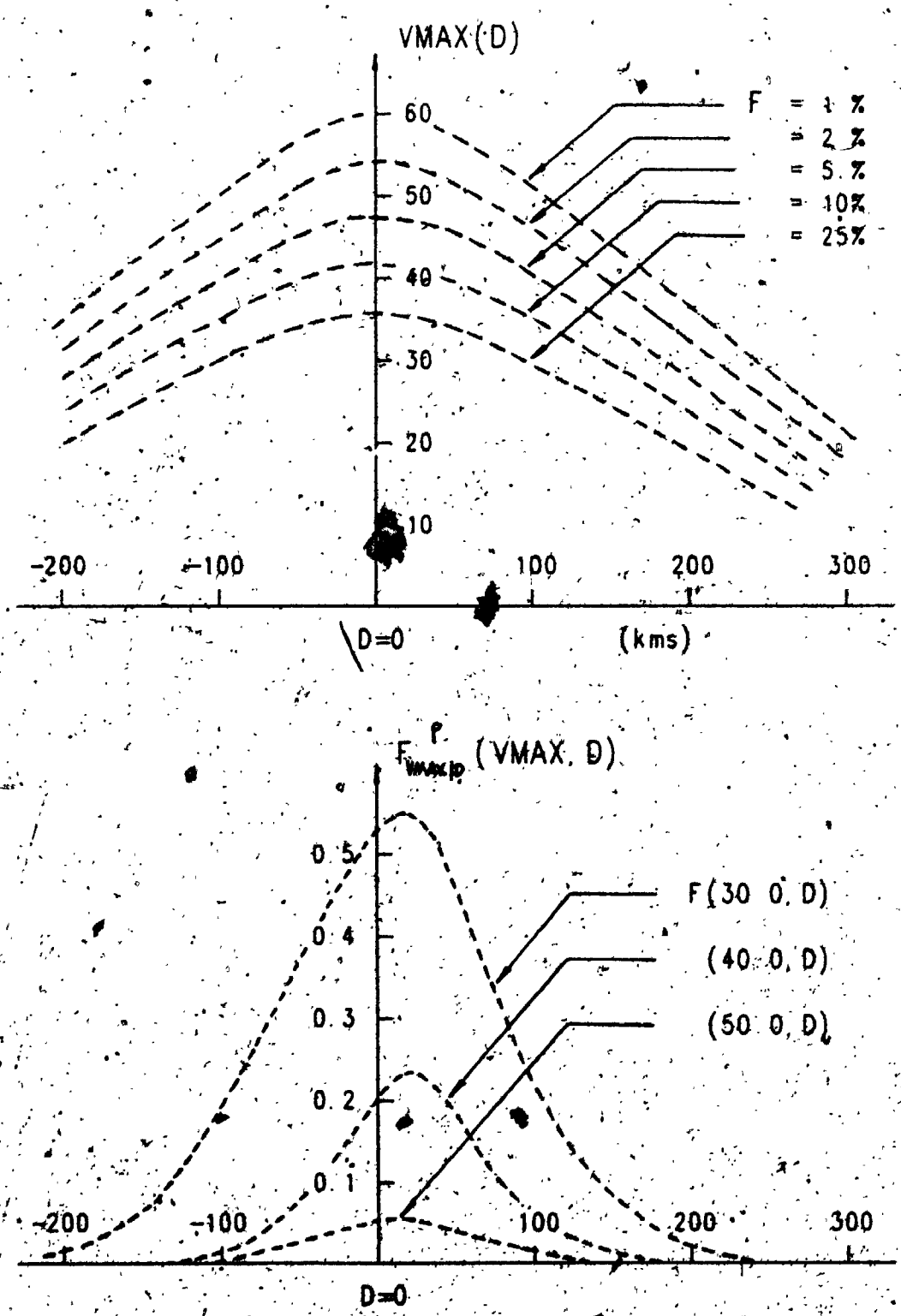

FIGURE 7.9 Exceedance Functions VMAX(D) and $F^{P}_{VMAX|D}$(VMAX,D) for the Galveston Area

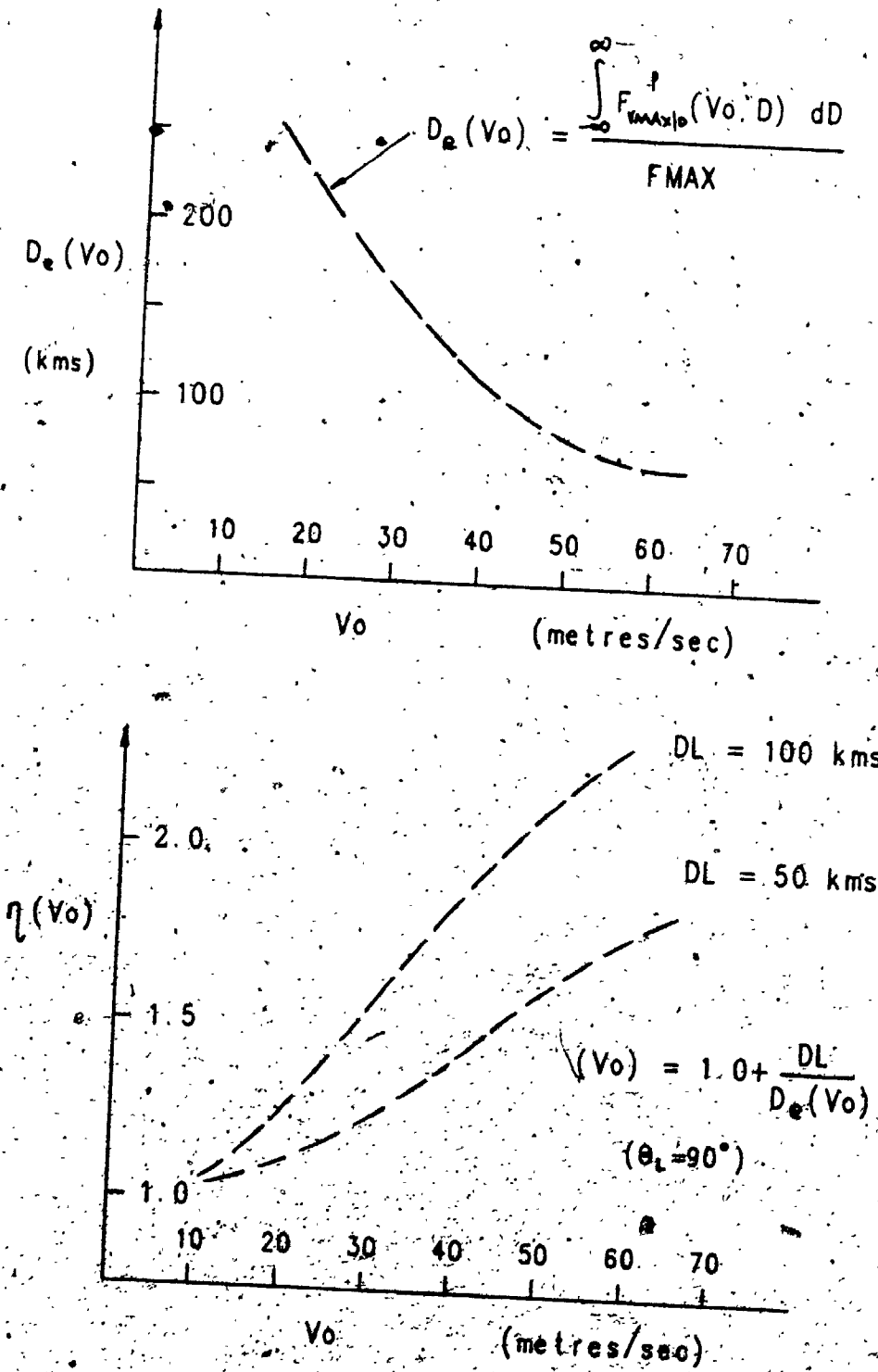

FIGURE 7.10 Effective Hurricane Line Length and Line Exceedance Rate for the Galveston Area

m/sec. In the Galveston area, the rms value of approach angle is 42.8°. Hence the value for ϕ_L is 0.086. If two lines of length 100 km are considered, one running parallel to the coast and the other inland, which coincide approximately with values of θ_L equal to 90° and 0° respectively, then the increase in exceedance rates for wind speeds in the range 45-50 m/sec are approximately 1.7-2.0 and 1.1-1.2 respectively. These figures translate into reductions of the corresponding return period of 50-60% and 10-20% respectively, which agree very well with the actual figures calculated in section 7.1.

7.3 Standard Exceedance Rate Method for Determining Response Extremes

The "wind loading chain" discussed in section 1.1 (Figure 1.4) showed the sequence involved in computing the wind-induced response of structures. Through the use of wind tunnel testing; relationships can be determined between a response, R, or external or internal pressure, p, and wind speed and direction. These usually take the form :

$$R(V,\theta) = B(\theta)\, V^{n(\theta)} \qquad E7-11$$

$$p(V,\theta) = C_p(\theta)\,\frac{1}{2}\rho V^2 \qquad E7-12$$

$B(\theta)$, $n(\theta)$, $Cp(\theta)$ = functions of wind direction only

ρ = air density

For the purposes of analysis, digitized values of $B(\theta)$, $n(\theta)$ and $Cp(\theta)$ can be Fourier-fitted as continuous functions of the azimuth angle, θ. These relationships can be used in conjunction with the wind speeds and directions within the Monte-Carlo simulation to generate a set of response extremes or peak pressures, which can then be fitted directly to determine extreme-value distributions of structural response, cladding pressures etc.

This quickly becomes computationally exhaustive, particularly in the case of peak pressure calculations. A typical wind tunnel test may involve the measurement of pressures in over 500 locations of a building facade. Since peak positive pressures and peak suctions must be considered separately this would require the storing and processing of over 1000 sets of extremes if the above direct approach were used. This problem can be avoided by making use of the parent distribution of wind speed and direction, $p(V,\theta)$. Davenport (1977) has shown that for well-behaved wind climates the exceedance rate of some response, R, is given by:

$$N(>R) = \nu \sqrt{2\pi}\, v\sigma_v \int_o^{2\pi} \sqrt{\left\{1 + \left(\frac{dV_R}{V_R d\theta}\right)^2\right\}}\, p(V_R,\theta)\, d\theta \qquad E7-13$$

where

$$V_R = \left[\frac{R}{B(\theta)}\right]^{\frac{1}{n(\theta)}}$$

ν = mean cycling rate

σ_v = wind speed standard deviation, regardless of direction

The cycling rate of the process, ν, is usually evaluated from the spectrum of the wind velocity and is of the order of 600-900 cycles/year. The relationship between the parent wind distribution, $p(V,\theta)$, and the exceedance rate of extremes is of particular interest to the simulation procedure-derived wind speeds. Since the exceedance of some velocity, Vo, is a special case of a response exceedance, i.e. $R = Vo$, E7-13 can be used to relate the parent wind distribution and extreme winds:

$$N(>Vo) = \nu \sqrt{2\pi}\, v\sigma_v \int_o^{2\pi} p(Vo,\theta)\, d\theta$$

$$= \nu \sqrt{2\pi}\, v\sigma_v\, p(Vo) \qquad E7-14$$

$p(Vo)$ = parent velocity probability distribution function, regardless of direction

This is a useful check to apply to the parent and extreme distributions obtained in the simulation procedure before using E7-13 to predict extreme-value estimates of structural responses and peak pressures. When this is done it has been found that E7-14 does not hold. In the previous chapter, the parent and extreme-value distributions obtained from the Miami simulation were shown (Figures 6.4 and 6.5). Figure 7.11 shows the value of the cycling rate required to satisfy E7-14, using the values of $p(V,\theta)$ and $N(>V)$ derived from the Miami simulation. It can be seen that the cycling rate varies significantly over the range of velocities of interest.

The derivation of E7-13 involves assumptions about the statistical characteristics of the wind. These are satisfied for non-tropical cyclone winds, which can effectively be considered as stationary in the exceedance calculations, but not for tropical cyclone winds, which clearly cannot. The derivation of the Davenport exceedance rate formula, E7-13, is now reformulated in a more general manner, showing which assumptions need to be modified in order to be applicable to simulation-generated wind speeds (and non-stationary winds in general).

7.4 Modified Exceedance Rate Method Suitable for Tropical Cyclone Winds

Figure 7.12 shows the two-dimensional variation of some process exhibiting a random path in the x-y plane. The problem to be solved concerns the out-crossing of a continuous response boundary, R, i.e. the exceedance rate of response, R, by the process. Also shown is a section of the boundary in greater detail. A local system of co-ordinates, (n,s), is defined for normal and tangential components to the boundary at some point (x_R, y_R). At this point, the velocity components of the process as it crosses the boundary are $(\dot{x},\dot{y})$ or $(\dot{n},\dot{s})$. The joint probability density function (PDF) of the process being at (x_R, y_R) with velocity components $(\dot{x},\dot{y})$ is defined as $p(x_R, y_R, \dot{x},\dot{y})$. The percentage of the time that the process will be within the boundary element $[ds,dn]$ will be $p(x_R, y_R, \dot{x},\dot{y})dsdn$. The time taken to cross the boundary is $dn/\dot{n}$. Thus the number of crossings of the boundary at (x_R, y_R) with velocity $(\dot{x},\dot{y})$ will be

$$N(>V) = \sqrt{2\pi}\,\nu\,\sigma_V \int_0^{2\pi} p(V,\theta)\,d\theta$$

$$\therefore \nu = \frac{N(>V)}{\sqrt{2\pi}\,\sigma_V\, p(V)}$$

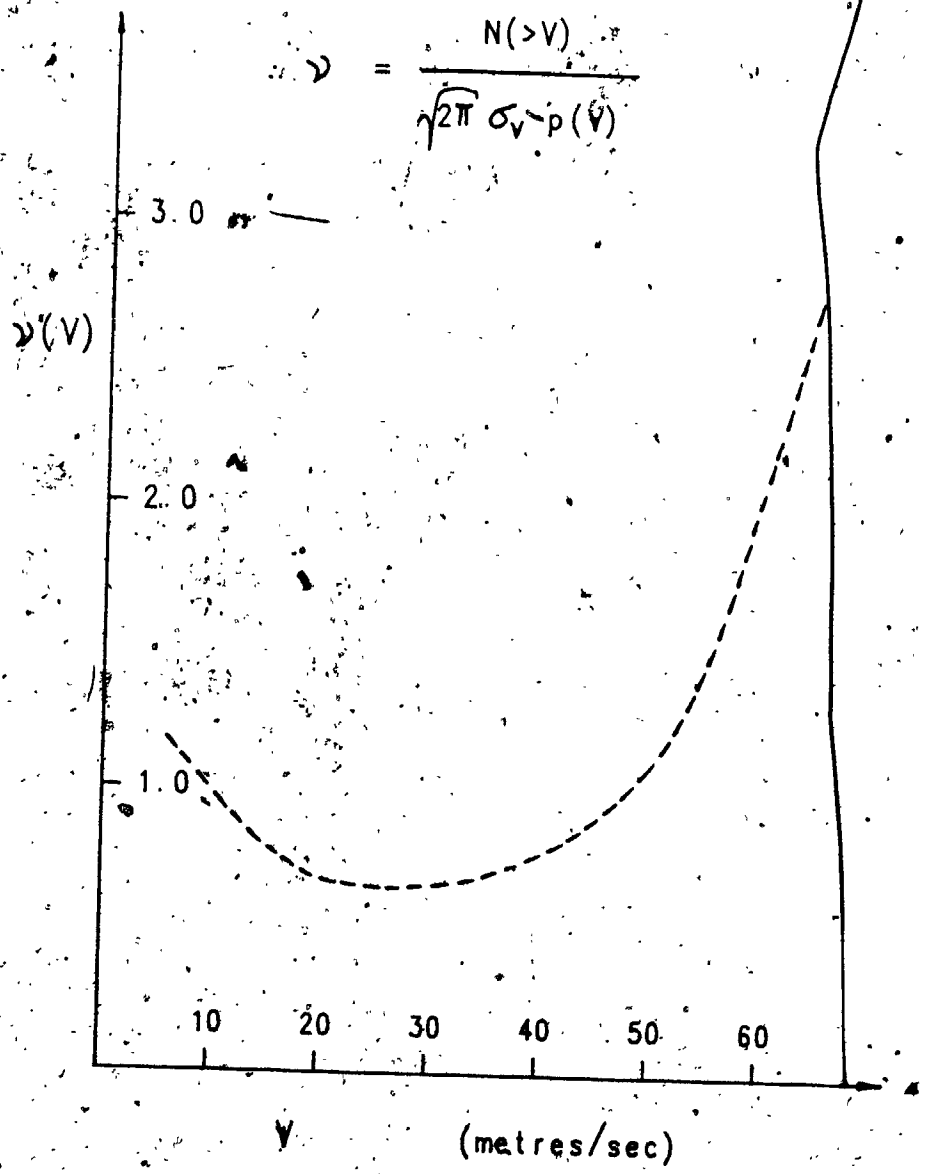

FIGURE 7.11 Simulation Derived Cycling Rate for Miami from Standard Response Exceedance Method

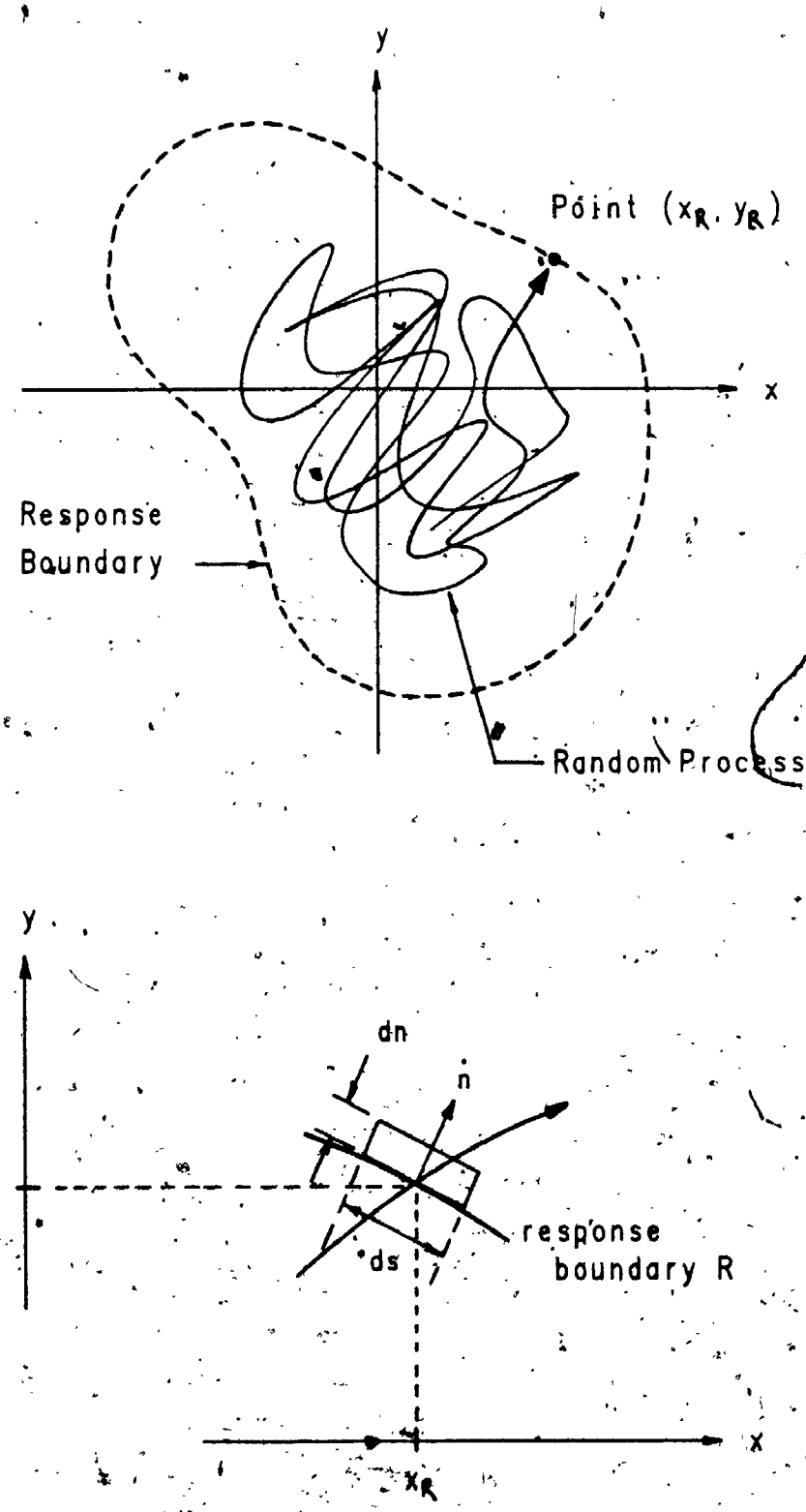

FIGURE 7.12 Random Two-Dimensional Process and Associated Response Boundary

$\dot{n}p(x_R, y_R, \dot{x},\dot{y})ds$. The total number of crossings of the boundary element can be computed by integrating over all possible values of the velocity, i.e. $\int_{-\infty}^{\infty}\int_{-\infty}^{\infty}[\ldots]d\dot{x}d\dot{y}$. This then allows the total number of crossings of the complete boundary, R, to be calculated, yielding :

$$N\pm(R) = \oint_R \left[\int_{-\infty}^{\infty}\int_{-\infty}^{\infty} \dot{n}\, p(\dot{x},\dot{y}|x_R,y_R)d\dot{x}d\dot{y}\right] p(x_R,y_R)ds \qquad E7-15$$

$p(\dot{x},\dot{y}/x_R,y_R)$ = marginal PDF of $(\dot{x},\dot{y})$ conditional upon (x_R,y_R)

$p(x_R,y_R)$ = PDF of (x_R,y_R)

The term in square brackets in E7-15 can be simplified by a change of variables from $(\dot{x},\dot{y})$ to $(\dot{n},\dot{s})$. It may then be noted that for an out-crossing to occur, $\dot{n}>0$. The total number of out-crossings of the complete boundary is then given by :

$$N+(R) = \oint_R \left[\int_{-\infty}^{\infty}\int_{-\infty}^{\infty} \dot{n}\, p(\dot{n},\dot{s}|x_R,y_R)d\dot{n}d\dot{s}\right] p(x_R,y_R)ds \qquad E7-16$$

If the process considered is the the wind velocity, then (x,y) are the east and north components of the wind vector. If the cartesian co-ordinates (x,y) are transformed to the more familiar polar co-ordinates (V,θ), then $ds = \sqrt{(dx^2+dy^2)} = \sqrt{(V^2d\theta^2 + dV^2)}$ and the crossing rate of the boundary (out-crossings considered only) is given by :

$$N(>R) = \int_0^{2\pi} M(\dot{n},\dot{s}|V_R,\theta_R)\, S(V_R,\theta)\, p(V_R,\theta)\, d\theta \qquad E7-17$$

where $M(\dot{n},\dot{s}|V_R,\theta_R) = \int_0^{\infty}\int_{-\infty}^{\infty} \dot{n}p(\dot{n},\dot{s}|V_R,\theta_R)\, d\dot{n}d\dot{s}$

and $S(V_R,\theta) = \sqrt{\left\{1+\left(\frac{dV_R}{V_R\,d\theta}\right)^2\right\}}$

This expression is exact, but difficult to compute in the case of arbitrary boundaries because of the mixing of the two co-ordinate systems $(\dot{n},\dot{s})$ and

(V,θ), involved in determining the value of $M(\dot{n},s|V_R,\theta_R)$. The reduction of the somewhat complicated expression in E7-17 to the Davenport exceedance rate formula, E7-13, involves four assumptions. These are :

(1) $\dot{n}$ and s are independent
(2) $\dot{n}$ is independent of (x_R,y_R)
(3) $\dot{n}$ has a Gaussian PDF
(4) $\dot{n}$ can be replaced by $\dot{V}$

These modify E7-17 as follows :

$$N(>R) = \int_0^{2\pi} \left| \int_0^{\infty} \dot{n}\, p(\dot{n}|V_R,\theta_R)\, d\dot{n} \right| S(V_R,\theta)\, p(V_R,\theta)\, d\theta \qquad \text{by (1)}$$

$$= \int_0^{\infty} \dot{n}\, p(\dot{n})\, d\dot{n} \int_0^{2\pi} S(V_R,\theta)\, p(V_R,\theta)\, d\theta \qquad \text{by (2)}$$

$$= \frac{\sigma_{\dot{n}}}{\sqrt{2\pi}} \int_0^{2\pi} S(V_R,\theta)\, p(V_R,\theta)\, d\theta \qquad \text{by (3)}$$

$$= \frac{\sigma_{\dot{V}}}{\sqrt{2\pi}} \int_0^{2\pi} S(V_R,\theta)\, p(V_R,\theta)\, d\theta \qquad \text{by (4)} \qquad E7-18$$

The last expression, E7-18, for the crossing exceedance rate is equivalent to E7-13, since $\nu = 1/2\pi(\sigma_{\dot{V}}/\sigma_V)$. Assumptions (1) through (3) have been found to be satisfied for non-tropical cyclone winds. Assumption (4) does not depend upon the wind climate but the shape of the response boundary, R. For tropical cyclone winds, assumption (1) is appropriate as determined from distributions of wind speed and direction generated using the simulation procedure. The assumptions which fail for tropical cyclone winds are (2) and (3). This is clearly related to the lack of stationarity in the parent wind distribution. Thus an appropriate formula for the exceedance rate of structural responses applicable to tropical cyclone winds is :

$$N(>R) = \int_0^{2\pi} \left| \int_0^{\infty} \dot{V}\, p(\dot{V}|V_R,\theta_R)\, d\dot{V} \right| S(V_R,\theta)\, p(V_R,\theta)\, d\theta \qquad E7-19$$

The process used in the development of E-19 had a continuous path in the time sense, whereas in the case of tropical cyclones the wind speed vector can only exist during the occurrence of a storm. This problem may be overcome by replacing the square bracketed term in E7-19, the average value of positive velocity components, $\dot{V}$, at a given (V_R, θ_R), by the probability that a storm occurs coupled with the conditionally dependent local V derivative. This yields the final expression necessary to evaluate extremes from simulation generated wind speeds and directions:

$$N(>R) = \lambda \int_o^{2\pi} G(V|V_R,\theta_R)\, S(V_R,\theta)\, p(V_R,\theta)\, d\theta \qquad E7-20$$

where $$G(V|V_R,\theta_R) = \int_o^{\infty} \frac{dV}{d\theta} \cdot p\left(\frac{dV}{d\theta}|V_R,\theta\right) d\left\{\frac{dV}{d\theta}\right\}$$

λ = annual tropical cyclone occurrence rate

The corresponding relation to E7-14 then becomes:

$$N(>Vo) = \lambda \int_o^{2\pi} G(V|Vo,\theta)\, p(Vo,\theta)\, d\theta \qquad E7-21$$

A typical variation of $G(V'|V,\theta)$ is illustrated in Figure 7.13. The results were derived from the extended Miami simulation run using 10,000 tropical cyclones to generate the distribution functions. The parent distribution of wind speed and direction was shown in Figure 6.4. Figure 7.13 shows that the exceedance potential is greatly enhanced when the wind direction is from the northeast and the speed in the range 25-50 m/sec.

Finally, E7-21 was used to estimate the extremes using the simulation derived $p(V,\theta)$ and $G(V'|V,\theta)$ distribution functions. These are compared to the actual extremes derived from the simulation in Figure 7.14. It can be seen that the modified exceedance equation E7-21 performs well. This then allows the use of E7-20 for the predictions of response extremes, significantly reducing the computational requirements necessary for response calculations.

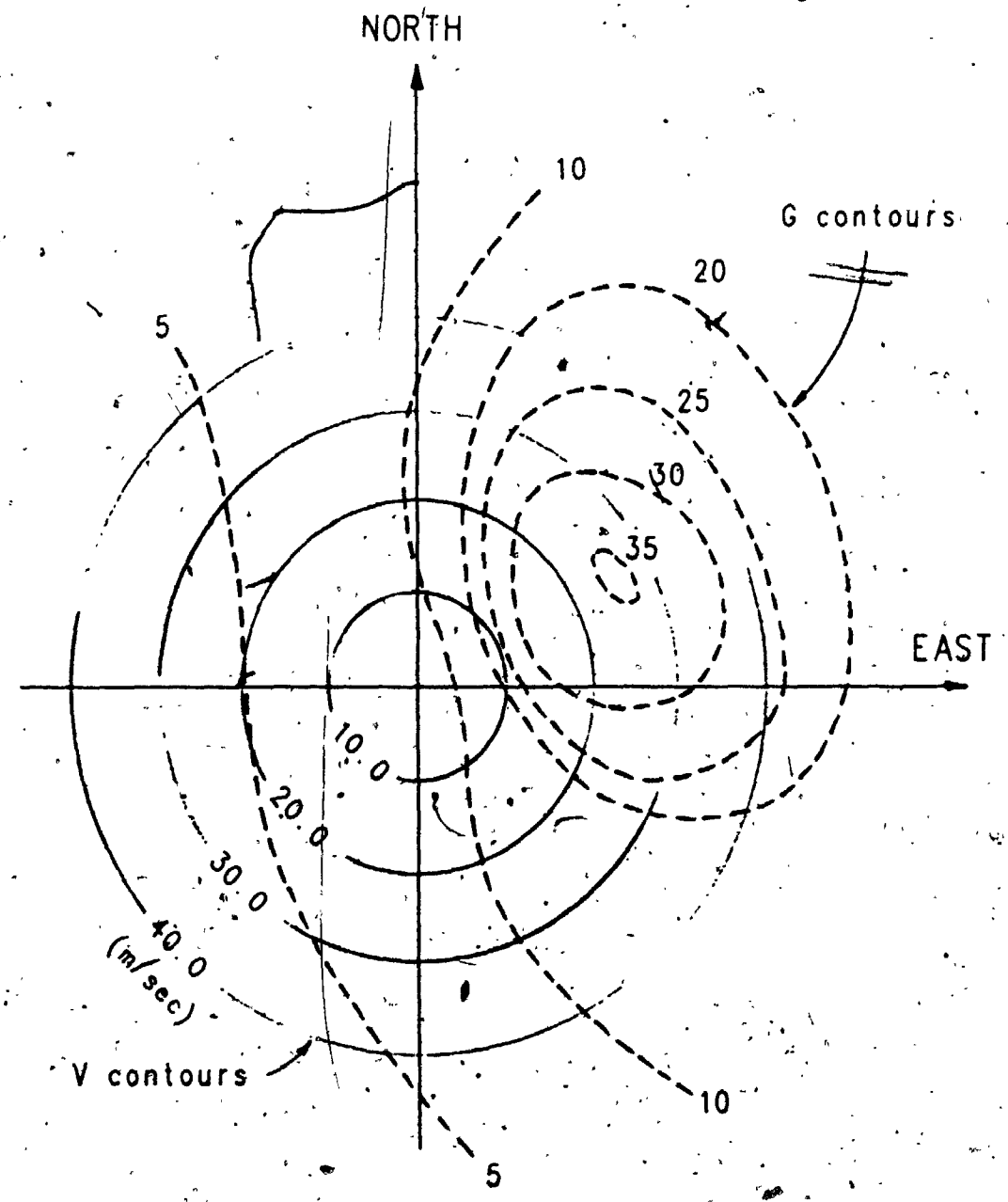

FIGURE 7.13 Miami Simulation Variation of G(V'|V; θ)

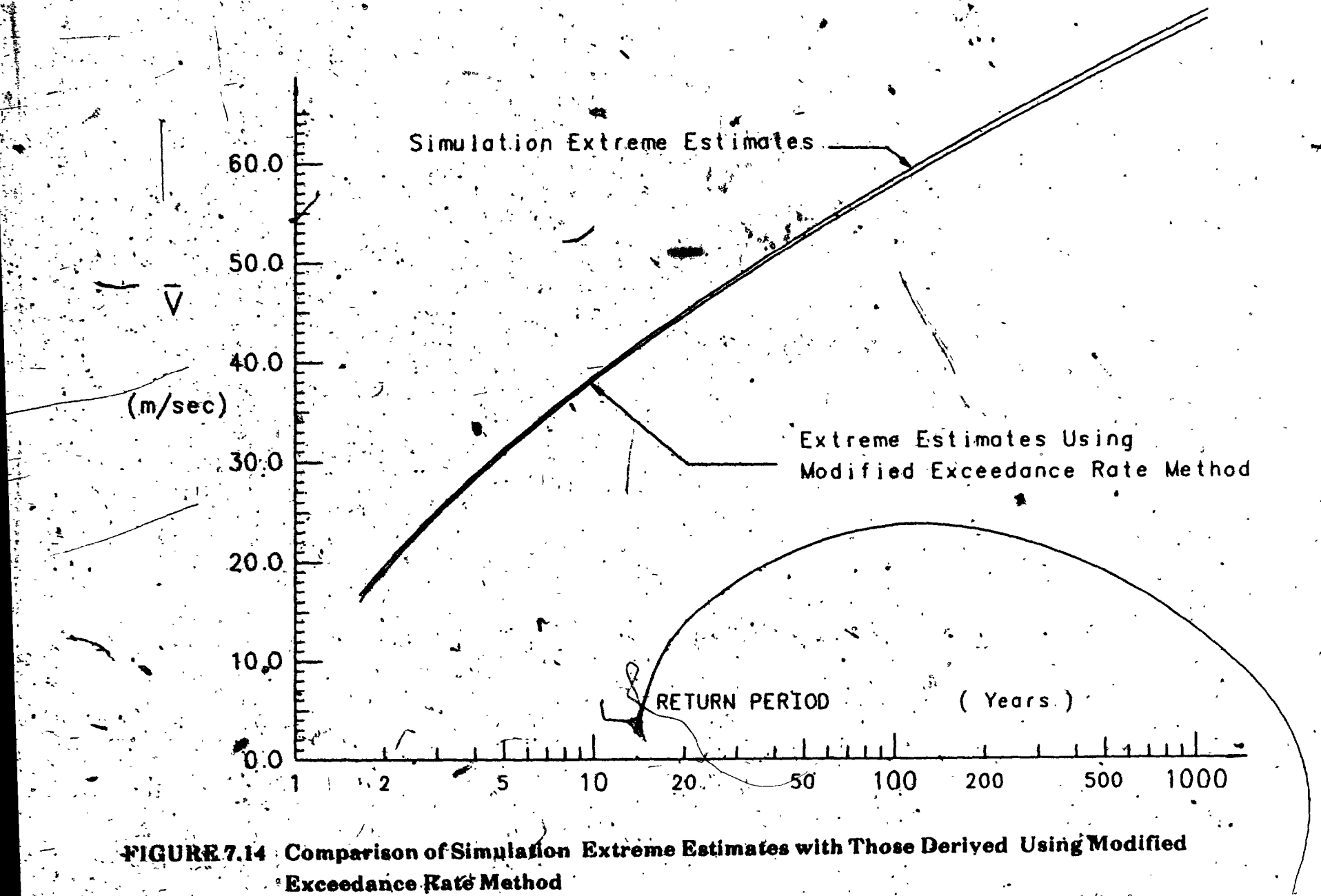

FIGURE 7.14 Comparison of Simulation Extreme Estimates with Those Derived Using Modified Exceedance Rate Method

CHAPTER 8

CONCLUSIONS AND RECOMMENDATIONS FOR FUTURE WORK

8.1 Summary

The simulation approach has emerged recently as the most reliable means available for predicting design wind speeds in tropical cyclone-prone regions. This thesis has presented a refined simulation procedure and applied it to hurricane-prone regions of the United States. Improvements have been made in the current procedure in all phases of the simulation.

The windfield model proposed is considerably more complex than those used in previous simulation procedures. Upper-level speeds have been separated into two circulations, one where the gradient balance assumption is assumed to apply and a lower level within the tropical cyclone inflow layer where surface friction affects the wind speeds and directions. The gradient balance equation incorporates a pressure profile exponent giving greater flexibility to the model when applied to different tropical cyclone regions. The circulation designated at the 500 metre height has been defined in the current procedure making use of a numerical model (Shapiro, 1983) recently developed at the Hurricane Research Division of A.O.M.L., Miami, Florida. The adaption of this numerical model to the current simulation windfield model allows realistic evaluation of the combined effects of surface friction and storm translation on the tropical cyclone circulation to be computed. The boundary layer variation of wind speed and the influences of landfall on surface speeds have been based on data gathered in recently occurring landfalling storms. A new filling model has been developed for use in the simulation procedure. This model allows for geographical variations in the decay rate of landfalling storms and takes account of the observed over-water central pressure difference drop for Atlantic seaboard storms.

The representation of tropical cyclone characteristic parameters within the simulation was reviewed and in several cases new distributions have been proposed. The choice of the Weibull distribution for the central pressure

4 4

OF/DE

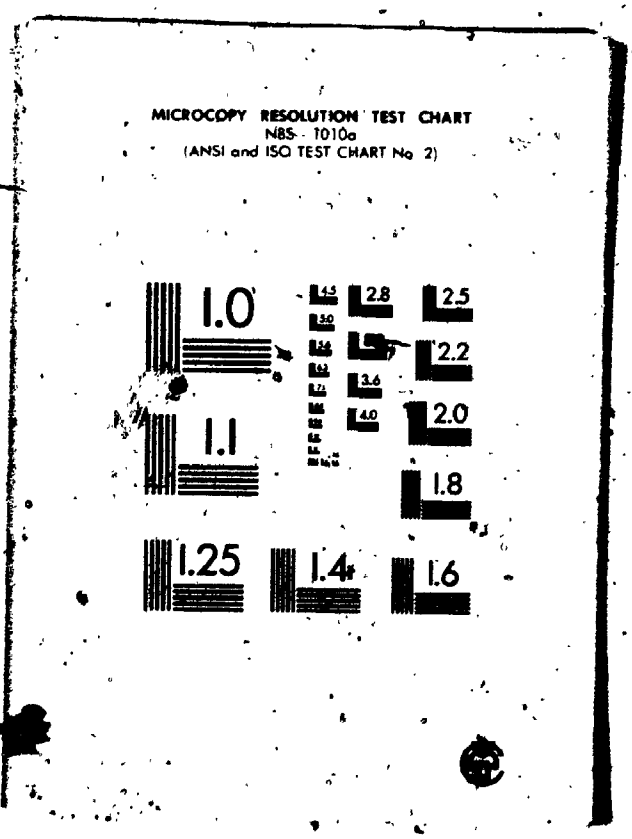
MICROCOPY RESOLUTION TEST CHART
NBS-1010a
(ANSI and ISO TEST CHART No 2)
1.0
1.1
1.25
1.4
1.6
2.8
2.5
2.2
3.6
2.0
4.0
1.8

simulation could be used. This bypassed the limitations imposed by its non-stationary characteristics.

8.2 Future Refinements to the Simulation Procedure

Improvements to the windfield model must be viewed in the light of the overall uncertainties in the simulation. For example, a more sophisticated definition of the value of air density to take into account the variation of sea surface temperature with latitude would seem unwarranted in view of the overall potential accuracy of any windfield model in predicting wind speeds and directions. On the other hand there are several areas where improvements may enhance the reliability of the model.

The gradient balance wind equation contains a pressure profile exponent which theoretical studies have suggested has a climatological variation as well as being sensitive to storm intensity. The definition of this parameter, B, is an important input to the windfield model. In the present study, the value of B was based upon data gathered in a limited number of predominantly severe tropical cyclones. The specification of B would benefit significantly from the compilation of a larger data base of concurrent maximum wind, central pressure difference and radius of maximum wind data. This would allow the variation of B with parameters such as storm intensity and latitude to be better understood.

While the average surface to upper-level wind speed ratios over water appear to be adequately accounted for, the variation of the vertical profile with wind speed should be improved when data currently being gathered using the new airborne-Doppler radar instrumentation have been analyzed. Initial studies have shown a significant variation in profiles, within and outside of rainbands and close to and far away from the eyewall. Once these are more clearly defined it may be possible to vary the boundary layer profile within the windfield model as a function of radial distance from the circulation centre or with storm intensity.

simulation could be used. This bypassed the limitations imposed by its non-stationary characteristics.

8.2 Future Refinements to the Simulation Procedure

Improvements to the windfield model must be viewed in the light of the overall uncertainties in the simulation. For example, a more sophisticated definition of the value of air density to take into account the variation of sea surface temperature with latitude would seem unwarranted in view of the overall potential accuracy of any windfield model in predicting wind speeds and directions. On the other hand there are several areas where improvements may enhance the reliability of the model.

The gradient balance wind equation contains a pressure profile exponent which theoretical studies have suggested has a climatological variation as well as being sensitive to storm intensity. The definition of this parameter, B, is an important input to the windfield model. In the present study, the value of B was based upon data gathered in a limited number of predominantly severe tropical cyclones. The specification of B would benefit significantly from the compilation of a larger data base of concurrent maximum wind, central pressure difference and radius of maximum wind data. This would allow the variation of B with parameters such as storm intensity and latitude to be better understood.

While the average surface to upper-level wind speed ratios over water appear to be adequately accounted for, the variation of the vertical profile with wind speed should be improved when data currently being gathered using the new airborne-Doppler radar instrumentation have been analyzed. Initial studies have shown a significant variation in profiles, within and outside of rainbands and close to and far away from the eyewall. Once these are more clearly defined it may be possible to vary the boundary layer profile within the windfield model as a function of radial distance from the circulation centre or with storm intensity.

At landfall, there remain significant uncertainties in the magnitude of wind speed and direction changes within the boundary layer, especially to the front and right of the storm circulation at the time of landfall, with the possibility of a low-level jet sustaining winds in the boundary layer while winds above the inflow layer are being reduced due to filling. Gust factors at the surface have shown large variability, from 1.4 in Hurricane Frederic (1979) to 1.6 in Hurricane Alicia (1983). The reduction of these uncertainties must await the documentation of future landfalling storms such as was done for Hurricanes Frederic and Alicia.

The variable least well-documented amongst the characteristic storm parameters is the radius of maximum winds. One of the assumptions made in the simulation procedure is that *RMAX* remains unchanged throughout the passage of a storm within the simulation circle. This is clearly inappropriate for locations on the Atlantic seaboard, where studies have shown that as storms move northward and generally weaken, their *RMAX* value almost always increases. The magnitude of the increase and its dependence upon latitude, storm intensity and speed have not been documented and would represent an additional realistic input to the simulation model.

The continuing assessment of the windfield model through comparisons of the type performed in Chapter 4 is of critical importance to the simulation procedure. Comparisons of this type not only yield a qualitative assessment of the reliability of the windfield model wind speeds and directions, but offer the best form of assurance to those interested in adopting the simulation approach that the windfield model is indeed capable of reproducing the salient features of the tropical cyclone circulation.

8.3 Suggested Future Work

An application of important social and economic value for the simulation which has not been addressed in the current study is the prediction of storm surge extreme levels along the coastline, often the greatest contributor to loss of life and damage to structures. Numerical programs are currently available capable of computing storm surge for single tropical cyclones. They will be

difficult to combine in a simulation-type procedure because of computational time limitations. It may be possible to incorporate such models in the same way that the Shapiro numerical model was used in the current study.

One attractive aspect of the application of the simulation approach to the prediction of storm surge is the possibility of comparing simulation predictions to actual peak storm surge data. This data is not prone to the same problems that affect wind data and hence it should be possible to calibrate a storm surge simulation procedure more fully than is possible with wind speed extremes.

A promising avenue of future research lies with the modified simulation computational approach used to develop the line-like theoretical calculations. Because of the reduction of storms generated in the simulation, this approach may be extremely useful in applications such as storm surge simulations where computer time limitations are the greatest obstacles to overcome.

REFERENCES

Chapter 1

ANTHES, R.A., "Tropical Cyclones : Their Evolution Structure and Effects", Meteorological Monographs, A.M.S, Volume 19, No. 41, February 1982.

BATTS, M.E., CORDES, M.R., RUSSELL, L.R., SHAVER, J.R. and SIMIU, E., "Hurricane Wind Speeds in the United States", National Bureau of Standards Report No.BSS-124, U.S. Department of Commerce, May 1980.

CHIN, P.C. and LEONG, H.C., "Estimation of Wind Speeds near Sea-Level During Tropical Cyclone Conditions in Hong Kong", Technical Note No. 45, Royal Observatory, Hong Kong, July 1978.

DAVENPORT, A.G., "The Dependence of Wind Loads on Meteorological Parameters", Proceedings, International Conference on Wind Effects on Buildings and Structures, Ottawa, September 1967, University of Toronto Press, 1968.

DAVENPORT, A.G., GEORGIOU, P.N., MIKITIUK, M., SURRY, D. and LYTHE, G., "The Wind Climate of Hong Kong", Proceedings, 3rd International Conference on Tall Buildings, Hong Kong and Guangzhou, December 10-15 1984.

DAVENPORT, A.G., GEORGIOU, P.N. and SURRY, D., "Hurricane Wind Speeds and Risk in the Caribbean", Report for the Pan-Caribbean Disaster Preparedness and Prevention Project, University of Western Ontario, BLWTL Report, May 1985.

FISHER, R.A. and TIPPETT, L.H.C., "Limiting Forms of the Frequency Distribution of the Largest or Smallest Member of a Sample", Proceedings, Cambridge Philosophical Society, Volume 24, Part 2, 1926.

FRIEDMAN, D.G., "Assessment of the Magnitude of the Hurricane Risk", Proceedings, 11th Technical Conference on Hurricanes and Tropical Meteorology, Miami Beach, Florida,December 13-16 1977.

GEORGIOU, P.N., DAVENPORT, A.G. and VICKERY, B.J., "Design Wind Speeds in Regions Dominated by Tropical Cyclones", 6th International Conference on Wind Engineering, Gold Coast, Australia, March 21-25 1983, Auckland, New Zealand, April 6-7 1983.

GILMAN, C.S. and MYERS, V.A., "Hurricane Winds for Design Along the New England Coast", Journal of theWaterways and Harbours Division, A.S.C.E., Volume 127, Part IV, 1962.

GOMES, L., and VICKERY, B.J., "On the Prediction of Tropical Cyclone Gust Speeds Along the Northern Australian Coast", Civil Engineering Transactions, Institute of Engineers Australia, Volume CE18, No. 2, 1976.

GOMES, L. and VICKERY, B.J., "On the Prediction of Extreme Wind Speeds from the Parent Distribution", Journal of Industrial Aerodynamics, Volume 2, pp. 21-36, 1976.

GOMES, L. and VICKERY, B.J., "Extreme Wind Speeds in Mixed Wind Climates", Journal of Industrial Aerodynamics, Volume 2, pp 331-344, 1977/1978.

GUMBEL, E.J., "Statistics of Extremes", New York Columbia University Press, 1958.

HEBERT, P.J., "The 1979 Hurricane Season", Monthly Weather Review, A.M.S., Volume 108, June 1980.

LUDLUM, D.M., "Early American Hurricanes 1492-1870", A.M.S., Boston Massachussetts, 198 pp, 1963.

MARSHALL, R.D., "Fastest-Mile Windspeeds in Hurricane Alicia", National Bureau of Standards Technical Note No. 1197, U.S. Department of Commerce, 1984.

MARTIN, G.S., "Probability Distributions for Hurricane Wind Speeds on the Australian Coast", Conference on Applications of Probability Theory to Structural Design, Melbourne, Australia, November 14 1974.

MYERS, V.A., "Storm Tide Frequencies on the South Carolina Coast", NOAA Technical Report NWS-16, U.S. Department of Commerce, June 1975.

NAISBITT, J., "Megatrends : Ten New Directions Transforming Our Lives", Warner Books, February1984.

POWELL, M.D., MARKS, F.D. and BLACK, P.G., 'The Asymmetric Structure of Alicia's Windfield at Landfall", Proceedings, A.S.C.E. Specialty Conference 'Alicia - One Year Later', Galveston, Texas, August 16-17 1984.

RUSSELL, L.R., "Probability Distributions for Hurricane Effects", Journal of the Waterways, Harbours and Coastal Engineering Division, A.S.C.E., Volume 97, No. WW1, February1971.

RUSSELL, L.R. and SCHUELLER, G.F., "Probabilistic Models for Texas Gulf Coast Hurricane Occurrences", Journal of Petroleum Technology, March 1974.

SAVAGE, R.P., BAKER, J., GOLDEN, J.H., KAREEM, A. and MANNING, B.R., "Hurricane Alicia : Galveston and Houston, Texas, August 17-18 1983", Committee on Natural Disasters, Commission on Engineering and Technical Systems, National Research Council, Report No. CETS-CND-028, 1984.

SCHWERDT, R.W., HO, F.P. and WATKINS, R.R., "Meteorological Criteria for Standard Project Hurricane and Probable Maximum Hurricane Wind Fields, Gulf and Atlantic Coasts of the United States", NOAA Technical Report NWS23, U.S. Department of Commerce, September 1979.

SHEETS, R.C., "Applied Research in Support of Project Hurricane Strike", National Hurricane and Experimental Meteorology Laboratory, E.R.L., U.S. Department of Commerce, March 1980.

SIMPSON, R.H. and LAWRENCE, M.B., "Atlantic Hurricane Frequencies Along the U.S. Coastline", NOAA Technical Memorandum NWS SR-58, U.S. Department of Commerce, 1971.

SIMPSON, R.H. and RIEHL, H., "The Hurricane and Its Impact", Louisiana State University Press, 1981.

SOUTHERN, R.L., "The Global Socio-Economic Impact of Tropical Cyclones", Australian Meteorological Magazine, 27, pp175-195, 1979.

S.F.R.P.C., "Southwest Florida : Hurricane Loss Study - 1982", Southwest Florida Regional Planning Council, Fort Myers, November 1982.

SURRY, D. and DAVENPORT, A.G., "Modelling the Wind Climate : An 'Over' View", Proceedings, Workshop on Wind Climate, Asheville, North Carolina, November 1979.

THOM, H.C.S., "New Distribution of Extreme Winds in the United States"; Journal of the Structural Division, A.S.C.E., Volume 94, Number ST7, Proceedings Paper 6038, July 1968.

TRYGGVASON, B.V., "Computer Simulation of Tropical Cyclone Wind Effects for Australia", Wind Engineering Report, 2/79, Department of Civil and Systems Engineering, James Cook University, Townsville, Australia, 1979.

TRYGGVASON, B.V., SURRY, D. and DAVENPORT, A.G., "Predicting Wind-Induced Response in Hurricane Zones", Journal of the Structural Division, A.S.C.E., Volume 102, No. ST12, December 1976.

WALKER, G.R., "Report on Cyclone Tracy" : Effects on Buildings - December 1974", Department of Housing and Construction, Melborne, Australia, March 1975.

W.M.O., "The Quantitative Evaluation of the Risk of Disaster from Tropical Cyclones", Special Environmental Report No. 8, WMO No. 455, World Meteorological Organization, Geneva, Switzerland, 1976.

Chapter 2

ANTHES, R.A., "The Response of a 3-Level Axisymmetric Hurricane Model to Artificial Redistribution of Convective Heat Release", NOAA Technical Memorandum ERL NHRL-92, U.S. Department of Commerce, 1971.

ANTHES, R.A., "Tropical Cyclones : Their Evolution, Structure and Effects", Meteorological Monographs, A.M.S., Volume 19, No. 41, February 1982.

ANTHES, R.A. and HOKE, J.E., "The Effect of Horizontal Divergence and the Latitudinal Variation of the Coriolis Parameter on the Drift of a Model Hurricane", Monthly Weather Review, A.M.S., Volume 103, pp757-763, 1975.

ANTHES, R.A. and CHANG, S.W., "Response of the Hurricane Boundary Layer to Changes of Sea Surface Temperature in a Numerical Model", Journal of the Atmospheric Sciences, A.M.S., Volume 35, July 1978.

ATKINSON, G.D. and HOLLIDAY, C.R., "Tropical Cyclone Minimum Sea Level Pressure-Maximum Sustained Wind Relationship for Western North Pacific", U.S. Fleet Weather Centre / Joint Typhoon Warning Centre, Guam, Technical Note JTWC 75-1, May 1975.

BATES, J., "Vertical Shear of the Horizontal Wind Speed in Tropical Cyclones", NOAA Technical Memorandum ERL WMPO-39, U.S. Department of Commerce, August 1977.

CARDONE, V.J., "Specification of the Windfield Distribution in the Marine Boundary Layer for Wave Forecasting", Report TR-69-1, Geophysical Science Laboratory, New York University, 1969.

CLINE, I.M., "Tropical Cyclones", Published byMacmillan, New York, 103 pp, 1926.

CHOW, S.-H., "A Study of the Windfield in the Planetary Boundary Layer of a Moving Tropical Cyclone", Master of Science Thesis in Meteorology, School of Engineering and Science, New York University, New York, December 1971.

COHEN, L.A. and SPAR, J., "Eddy Stresses in Hurricane Donna (1960) Over Long Island", 3rd Technical Conference on Hurricanes and Tropical Meteorology, Mexico, 1963.

COLON, J.A., "On the Evolution of the Wind Field During the Life Cycle of Tropical Cyclones", National Hurricane Research Project Report No. 65, U.S. Department of Commerce, November 1963.

DEARDORFF, J.W., "Parameterization of the Planetary Boundary Layer for Use in General Circulation Models", Monthly Weather Review, A.M.S., Volume 94, February 1972.

DeMARIA, M. and SCHUBERT, W.H., "Experiments With a Spectral Tropical Cyclone Model", Journal of the Atmospheric Sciences, A.M.S., Volume 41, March 1984.

DEPPERMAN, C.E., "Notes on the Origin and Structure of Philippine Typhoons", Bulletin of the American Meteorological Society, A.M.S., Volume 9, pp399-404, 1947.

DUNNAVAN, G.M., "An Evaluation of 700 mb Aircraft Reconnaissance Data for Selected Northwest Pacific Tropical Cyclones", Master of Science Thesis in Meteorology and Oceanography, Naval Postgraduate School, Monterey, California, September 1983.

ELIASSEN, A., "Slow Thermally or Frictionally Controlled Motions in a Circular Vortex", Astrophys. Norv., Volume 5, pp19-60, 1951.

FLETCHER, R., "Computation of Maximum Surface Winds in Hurricanes", Bulletin of the American Meteorological Society, Volume 36, June 1955.

FRANK, W.M. "The Structure and Energetics of the Tropical Cyclone.I : Storm Structure", Monthly Weather Review, A.M.S., Volume 105, September 1977.

FRANK, W.M., "A Composite Analysis of the Core of a Mature Hurricane", Monthly Weather Review, A.M.S., Volume 112, December 1984.

FRANK, W.M. and GRAY, W.M., "Radius and Frequency of 15 m/s (30 kt) Winds Around Tropical Cyclones", Journal of Applied Meteorology, A.M.S., Volume 19, February 1980.

GEORGE, J.E. and GRAY, W.M., "Tropical Cyclone Motion and Surrounding Parameter Relationships", Journal of Applied Meteorology, A.M.S., Volume 15, pp1252-1264, 1976.

GILMAN, C.S. and MYERS, V.A., "Hurricane Winds for Design Along the New England Coast", Journal of the Waterways and Harbours Division, A.S.C.E., Volume 127, Part IV, 1962.

GRAHAM, H.E. and HUDSON, G.M., "Surface Winds Near the Centre of Hurricanes (and Other Cyclones)", National Hurricane Research Report No. 29, U.S. Department of Commerce, September 1960.

GRAHAM, H.E. and NUNN, D.E., "Meteorological Considerations Pertinent to Standard Project Hurricane, Atlantic and Gulf Coasts of the United States", National Hurricane Research Project Report No. 33, U.S. Department of Commerce, 1959.

GRAY, W.M., "On the Balance of Forces and Radial Accelerations in Hurricanes", National Hurricane Research Project Report No. 54, U.S. Department of Commerce, May 1962.

GRAY, W.M., "Recent Advances in Tropical Cyclone Research from Rawinsonde Composite Analysis", WMO Programme on Research in Tropical Meteorology, Geneva, Switzerland, 1981.

HALL, M., "West Indies Hurricanes as Observed in Jamaica", Monthly Weather Review, A.M.S., Volume 45, pp573-588, 1917.

HAWKINS, H.F., "Vertical Wind Profiles in Hurricanes" National Hurricane Research Project Report No. 55, U.S. Department of Commerce, June 1962.

HAWKINS, H.F. and RUBSAM, D.T., "Hurricane Hilda, 1964. II : Structure and Budgets of the Hurricane on October 1, 1964", Monthly Weather Review, A.M.S., Volume 96, pp617-636, 1968.

HAWKINS, H.F. and IMBEMBO, S.M., "The Structure of a Small, Intense Hurricane-Inez 1966", Monthly Weather Review, A.M.S., Volume 114, April 1976.

HOLLAND, G.J., "An Analytical Model of the Wind and Pressure Profiles in Hurricanes", Monthly Weather Review, A.M.S., Volume 108, August 1980.

HOLLIDAY, C.R., "On the Maximum Sustained Winds Occurring in Atlantic Hurricanes", NOAA Technical Memorandum WBTH-SR-45, U.S. Department of Commerce, May 1969.

HUGHES, L.A., "On the Low-Level Wind Structure of Tropical Storms", Journal of Meteorology, A.M.S., Volume 9, December 1952.

JELESNIANSKI, C.P., "Numerical Computations of Storm Surges With Bottom Stress", Monthly Weather Review, A.M.S., Volume 95, November 1967.

JONES, R.W., "Vortex Motion in a Tropical Cyclone Model", Journal of the Atmospheric Sciences, A.M.S., Volume 34, October 1977.

JORGENSEN, D.P., "Mesoscale and Convective-Scale Characteristics of Mature Hurricanes. Part II : Inner Core Structure of Hurricane Allen (1980)", Journal of the Atmospheric Sciences, A.M.S., Volume 41, April 1984.

KASAHARA, A., "The Numerical Prediction of Hurricane Movement with the Barotropic Model" Journal of Meteorology, A.M.S., Volume 14, May 1957.

KRAFT, R.H., "The Hurricane's Central Pressure and Highest Wind", Mariners Weather Log, A.M.S., Volume 5, May 1961.

LaSEUR, N.E. and HAWKINS, H.F., "An Analysis of Hurricane Cleo (1958) Based on Data from Research Reconnaissance Aircraft", Monthly Weather Review, A.M.S., Volume 91, pp694-709, 1963.

MADALA, R.V. and PIACSEK, S.A., "Numerical Simulation of Asymmetric Hurricanes on a Beta-Plane With Vertical Shear", Tellus, Volume 27, pp453-468, 1975.

MALKIN, W., "Filling and Intensity Changes in Hurricanes Over Land", National Hurricane Research Report No.34, U.S. Department of Commerce, November 1959.

MALKUS, J.S. and RIEHL, H., "On the Dynamics and Energy Transformations in Steady-State Hurricanes", National Hurricane Research Project Report No. 31, U.S. Department of Commerce, September 1959.

McBRIDE, J.L., "Observational Analysis of Tropical Cyclone Formation. Part III : Budget Analysis", Journal of the Atmospheric Sciences, A.M.S., Volume 38, June 1981.

MERRILL, R.T., "A Comparison of Large and Small Tropical Cyclones". Monthly Weather Review, A.M.S., Volume 112, July1984.

MILLER, B.I., "On the Momentum and Energy Balance of Hurricane Helene (1958)", National Hurricane Research Project Report No. 53, U.S. Department of Commerce, April 1962.

MILLER, B.I., "On the Filling of Tropical Cyclones Over Land", National Hurricane Research Project Report No. 66, U.S. Department of Commerce, December 1963.

MILLER, B.I., "Characteristics of Hurricanes", Science, Volume 157, pp1389-1399, 1967.

MOSS, M.S., "Low-Layer Features of Two Limited-Area Hurricane Regimes", NOAA Technical Memorandum ERL 394-NHEML-1, U.S. Department of Commerce, March 1978.

MOSS, M.S., and ROSENTHAL, S.L., "On the Estimation of Planetary Boundary Variables in Mature Hurricanes", Monthly Weather Review, A.M.S., Volume 103, November 1975.

MOSS, M.S. and JONES, R.W., "A Numerical Simulation of Hurricane Landfall", NOAA Technical Memorandum ERL NHEML-3, U.S. Department of Commerce, November 1978.

MYERS, V.A., "Characteristics of United States Hurricanes Pertinent to Levee Design for Lake Okeechobee, Florida", Hydrometeorological Report No. 32, U.S. Department of Commerce, March 1954.

MYERS, V.A., "Maximum Hurricane Winds", Bulletin of the American Meteorological Society, A.M.S., Volume 38, pp227-228, 1957.

MYERS, V.A. and MALKIN, W., "Some Properties of Hurricane Wind Fields as Deduced from Trajectories", National Hurricane Research Project Report No. 49, U.S. Department of Commerce, November 1961.

NHRP, "Survey of Meteorological Factors Pertinent to Reduction of Loss of Life and Property in Hurricane Situations", National Hurricane Research Project Report No. 5, U.S. Department of Commerce, March 1957.

NHRP, "Details of the Circulation of the High Energy Core of Hurricane Carrie", National Hurricane Research Project Report No. 24, U.S. Department of Commerce, November 1958.

NOVLAN, D.J. and GRAY, W.M., "Hurricane Spawned Tornadoes", Atmospheric Science Paper No. 200, Colorado State University, May 1973.

NUNEZ, E. and GRAY, W.M., "A Comparison of West Indies Hurricanes and Pacific Typhoons", Proceedings 11th Technical Conference on Hurricanes and Tropical Meteorology, Miami Beach, Miami, December 13-16 1977.

OOYAMA, K., "Numerical Simulation of the Life Cycle of Tropical Cyclones", Contribution No. 67, Geophysical Science Laboratory, Department of Meteorology and Oceanography, New York University, 1967.

OOYAMA, K., "Numerical Simulation of the Life Cycle of Tropical Cyclones", Journal of the Atmospheric Sciences, A.M.S., Volume 26, pp3-40,1969.

POWELL, M.D., "An Evaluation of Diagnostic Marine Boundary Layer Models Applied to Hurricanes", Master of Science Thesis, Department of Meteorology, The Pennsylvania State University, May 1978.

POWELL, M.D., "Evaluations of Diagnostic Marine Boundary Layer Models Applied to Hurricanes", Proceedings, 5th International Conference on Wind Engineering, Fort Collins, Colorado, July 8-14 1979.

POWELL, M.D., "The Transition of the Hurricane Frederic Boundary-Layer Wind Field from the Open Gulf of Mexico to Landfall", Monthly Weather Review, A.M.S., Volume 110, December1982.

POWELL, M.D., Personal Communication, September 1984.

POWELL, M.D., MARKS, R.D.and BLACK,P.G., "The Asymmetric Structure of Alicia's Windfield at Landfall", A.S.C.E. Specialty Conference: 'Alicia, One Year Later', Galveston, Texas, August 16-17 1984.

POWELL, M.D. and BLACK, P.G. "Airborne Doppler Radar Observations of the Boundary Layer of Hurricane Debby (1982)", 22nd Conference on Radar Meteorology, Zurich, Switzerland, September 10-13 1984.

RIEHL, H., "Some Relations Between Wind and Thermal Structure of Steady State Hurricanes", National Hurricane Research Project Report No.63, U.S.Department of Commerce.

RIEHL, H., and MALKUS, J.S., "On the Dynamics and Energy Transformations in Steady State Hurricanes", Tellus, Volume 12, February 1961.

SCHLOEMER, R.W., "Analysis and Synthesis of Hurricane Wind Patterns Over Lake Okeechobee, Florida", NOAA Hydrometeorological Report No. 31, U.S. Department of Commerce, 1954.

SCHWERDT, R.W., HO, F.P. and WATKINS, R.R., "Meteorological Criteria for Standard Project Hurricane and Probable Maximum Hurricane Wind Fields, Gulf and Atlantic Coasts of the United States", NOAA Technical Report NWS23, U.S. Department of Commerce, September 1979.

SHAPIRO, L.J., "The Asymmetric Boundary Layer Flow Under a Translating Hurricane", Journal of the Atmospheric Sciences, A.M.S., Volume 40, No. 8, August 1983.

SHAPIRO, L.J., and WILLOUGHBY, H.E., "The Response of Balanced Hurricanes to Local Sources of Heat and Momentum", Journal of the Atmospheric Sciences, A.M.S., Volume 39, February 1982.

SHEA, D.J. and GRAY, W.M., "The Structure and Dynamics of the Hurricane's Inner Core Region", Atmospheric Science Paper No.182, Colorado State University, April 1972.

SHEETS, R.C., "On the Structure of Hurricanes as Revealed by Research Aircraft Data", Intense Atmospheric Vortices, Proceedings of the Joint Symposium (IUTAM/IUGG), Reading, United Kingdom, July14-17 1981.

SHIOTANI, M., "Turbulence Measurements at the Sea Coast During High Wind", Journal of the Meteorological Society of Japan, Volume 53, October 1975.

SINGER, I.A., NAGLE, C.M. and BROWN, R.M., "Variation of Wind With Height During the Approach and Passage of Hurricane Donna", Proceedings, 2nd Technical Conference on Hurricanes, June 27-30 1961, National Hurricane Research Project Report No. 50, U.S. Department of Commerce.

SYONO, S., "A Numerical Experiment on the Formation of Tropical Cyclones", Proceedings, International Symposium on Numerical Weather Prediction, Meteorological Society of Japan, pp405-418, 1962.

TAKAHASHI, K., "Distribution of Pressure and Wind in a Typhoon", Journal of the Meteorological Society of Japan, 2nd Series, Volume 17, November 1939.

TULEYA, R.E., and KURIHARA, Y., "A Numerical Simulation of the Landfall of Tropical Cyclones", Journal of the Atmospheric Sciences, A.M.S., Volume 35, February 1978.

TULEYA, R.E. BENDER, M.A. and KURIHARA, Y., "A Simulation of the Landfall of Tropical Cyclones Using a Movable Nested-Mesh Model", Monthly Weather Review, A.M.S., Volume 112, January 1984.

WILLOUGHBY, H.E., "Some Aspects of the Dynamics in Hurricane Anita of 1977", NOAA Technical Memorandum ERL NHEML-5, U.S. Department of Commerce, October 1979.

WILLOUGHBY, H.E., "Forced Secondary Circulations in Hurricanes", Journal of Geophysical Reserch, A.G.U., Volume 84, No. C6, June 1976.

WILLOUGHBY, H.E., CLOS, J.A. and SHOREIBAH, M.G., "Concentric Eye Walls, Secondary Wind Maxima, and the Evolution of the Hurricane Vortex", Journal of the Atmopsheric Sciences, A.M.S., Volume 39, February1982.

WILLOUGHBY, H.E., JIN, H.-L., LORD, S.J. and PIOTROWICZ, J.M., "Hurricane Structure and Evolution as Simulated by an Axisymmetric, Nonhydrostatic Numerical Model", Journal of the Atmospheric Sciences, A.M.S., Volume 41, April 1984.

WILLOUGHBY, H.E., MARKS, F.D. Jr and FEINBERG, R.J., "Stationary and Moving Convective Bands in Hurricanes", Journal of the Atmospheric Sciences, A.M.S., Volume 41, November 1984.

WILSON, K.J., "Wind Observations from an Instrumented Tower During Tropical Cyclone Karen, 1977", 12th Technical Conference on Hurricanes and Tropical Meteorology, New Orleans, Louisiana, April 1979.

YAMASAKI, M., "Numerical Simulation of Tropical Cyclone Development With the Use of Primitive Equations", Journal of the Meteorological Society of Japan, Volume 45, pp178-21, 1968a.

YAMASAKI, M., "A Tropical Cyclone Model With Parameterized Vertical Partition of Released Latent Heat", Journal of the Meteorological Society of Japan, Volume 46, pp202-214, 1968b.

Chapter 3

GOLDMAN, J.L. and USHIJIMA, T., "Decrease in Maximum Winds in Hurricanes After Landfall", A.S.C.E. National Meeting on Water Resources Engineering, Atlanta, Georgia, January 24-28, 1972.

GRAY, W.M., "Recent Advances in Tropical Cyclone Research from Rawinsonde Composite Analysis", WMO Programme of Research in Tropical Meteorology, Geneva, Switzerland, 1981.

MALKIN, W., "Filling and Intensity Changes in Hurricanes Over Land", National Hurricane Research Project Report No. 34, U.S. Department of Commerce, November 1959.

MILLER, B.I., "On the Filling of Tropical Cyclones Over Land", National Hurricane Research Project Report No. 66, U.S.Department of Commerce, December 1963.

POWELL, M.D., "The Transition of the Hurricane Frederic Boundary-Layer Wind Field from the Open Gulf of Mexico to Landfall", Monthly Weather Review, A.M.S., Volume 110, Decemeber 1982.

POWELL, M.D., MARKS, R.D.and BLACK,P.G., "The Asymmetric Structure of Alicia's Windfield at Landfall", A.S.C.E. Specialty Conference: 'Alicia, One Year Later', Galveston, Texas, August 16-17 1984.

SCHWERDT, R.W., HO, F.P.and WATKINS, R.R., "Meteorological Criteria for Standard Project Hurricane and Probable Maximum Hurricane Wind Fields, Gulf and Atlantic Coasts of the United States", NOAA Technical Report NWS23, U.S. Department of Commerce, September 1979.

SHAPIRO, L.J., "The Asymmetric Boundary Layer Flow Under a Translating Hurricane", Journal of the Atmospheric Sciences, A.M.S., Volume 40, No. 8, August 1983.

SHEA, D.J. and GRAY, W.M., "The Structure and Dynamics of the Hurricane's Inner Core Region", Atmospheric Science Paper No.182, Colorado State University, April 1972.

TULEYA, R.E., BENDER,M.A. and KURIHARA, Y., "A Simulation Study of the Landfall of Tropical Cyclones Using a Movable Nested-Mesh Model", Monthly Weather Review, A.M.S., Volume 112, January 1984.

Chapter 4

CHEN, T.V., "Comparison of Surface Winds in Hong Kong", Royal Observatory, Hong Kong, Technical Note No. 41, 1975.

CHIN, P.C. and LEONG, H.C., "Estimation of Wind Speeds near Sea-Level During Tropical Cyclone Conditions in Hong Kong", Technical Note No. 45, Royal Observatory, Hong Kong, July 1978.

ISYUMOV, N. and CHURCH, R., "A Study of the Wind-Induced Exterior Pressures and the Ground-Level Wind Environment for the Block 144 Project, Houston, Texas", University of Western Ontario, Engineering Science Research Report, BLWT-SS5-1980, 1980.

ISYUMOV, N. and CHURCH, R., "A Study of the Wind-Induced Aeroelastic Response for the Block 144 Project, Houston, Texas", University of Western Ontario, Engineering Science Research Report, BLWT-SS6-1980, 1980.

MARSHALL, R.D., "Fastest-Mile Windspeeds in Hurricane Alicia", National Bureau of Standards Technical Note No.1197, U.S. Department of Commerce, 1984.

POWELL, M.D., MARKS, R.D.and BLACK,P.G., "The Asymmetric Structure of Alicia's Windfield at Landfall", A.S.C.E. Specialty Conference: 'Alicia, One Year Later', Galveston, Texas, August 16-17 1984.

POWELL, M.D., GEORGIOU, P.N., ISYUMOV, N.I. and HALVORSEN, R.A., "Response of the Allied Bank Plaza Tower During Hurricane Alicia (1983). PART I : Reconstructed Storm History and Accelerations", Submitted to the Journal of Wind Engineering, September 1985.

REINHOLD, T.A., "Surface Winds in Hurricane Frederic (September 12 and 13, 1979). An Engineering Viewpoint", 2nd Specialty Conference on Dynamic Response of Structures, A.S.C.E., Atlanta, Georgia, January 15-16 1981.

SURRY, D., LYTHE, G., HORVATH, B. and DAVENPORT, A.G., "A Wind Tunnel Study of the Relationship Between Gradient Wind Speeds and the Anemometer Readings from Waglan Island, Hong Kong", The University of Western Ontario, Engineering Science Report, BLWT-SS17-1981.

Chapter 5

BATTS, ME.E., CORDES, M.R., RUSSELL, L.R., SHAVER, J.R. and SIMIU, E., "Hurricane Wind Speeds in the Unites States", National Bureau of Standards Report No. BSS-124, U.S. Department of Commerce, May 1980.

BELL, G.J., "Observations on the Size of the Typhoon Eye", W.M.O. Technical Conference on Typhoon Modification, No. 408, Manila, October 14-18 1974.

COLON, J.A., "On the Evolution of the Wind Field During the Life Cycle of Tropical Cyclones", National Hurricane Research Project Report No. 65, U.S. Department of Commerce, November 1963.

CRAMER, H., "Mathematical Methods of Statistics", Published by Princeton University Press, Princeton, New Jersey, 1946.

CRY, G.W., "Tropical Cyclones of the North Atlantic Ocean", Weather Bureau Technical Paper No. 55, U.S. Department of Commerce, 1965.

DEPPERMAN, C.E., "Some Characteristics of Philippine Typhoons", Bureau of Printing, Manilla, Philippines, 1939.

FISZ, M., "Probability Theory and Mathematical Statistics", 3rd. Edition, Published by John Wiley and Sons, New York, 1963.

GOMES, L. and VICKERY, B.J., "On the Prediction of Tropical Cyclone Gust Speeds Along the Northern Australian Coast", Civil Engineering Transctions, Institute of Engineers Australia, Volume CE18, No. 2, 1976.

GRAHAM, H.E. and NUNN, D.E., "Meteorological Considerations Pertinent to Standard Project Hurricane, Atlantic and Gulf Coasts of the United States", National Hurricane Research Project Report No. 33, U.S. Department of Commerce, 1959.

GRAY, W.M., "Hurricanes: Their Formation, Structure and Likely Role in the Tropical Circualtion", in 'Meteorology Over the Tropical Oceans', Edited by D.B. Shaw, Royal Meteorological Society, 1979.

GRAY, W.M., "Atlantic Seasonal Hurricane Frequency. Part I : El Nino and 30 mb Quasi-Biennial Oscillation Influences", Monthly Weather Review, A.M.S., Volume 112, September 1984.

GRAY, W.M., "Atlantic Seasonal Hurricane Frequency. Part II : Forecasting its Variability", Monthly Weather Review, A.M.S., Volume 112, September 1984.

HALD, A., "Statistical Theory With Engineering Applications", Published by John Wiley and Sons, New York, 1952.

HO., F.P., SCHWERDT, R.W. and GOODYEAR, H.V., "Some Climatological Characteristics of Hurricanes and Tropical Storms, Gulf and East Coasts of the United States", NOAA Technical Report NWS 15, U.S. Department of Commerce, May 1975.

HOPE, J.R. and NEUMANN, C.J., "Climatology of Atlantic Tropical Cyclones by 2-1/2 Degree Latitude-Longitude Boxes", ESSA Tehnical Memorandum WBTM SR-44, 1969.

JARVINEN, B.R., NEUMANN, C.J. and DAVIS, M.A.S., "A Tropical Cyclone Data Tape for the North Atlantic Basin 1886-1983 : Contents, Limitations and Uses", NOAA Technical Memorandum NWS NHC 22, U.S. Department of Commerce, March 1984.

KUO, H.L., "Dynamics of Convective Vortices and Eye Formation", in 'The Atmosphere and the Sea in Motion', Published by Rockefeller Institute Press, New York, New York, 1959.

LINDLEY, D.V., "Introduction to Probability and Statistics. Part II : Inference", Published by Cambridge University Press, Cambridge, England, 1965.

NHRP, "Survey of Meteorological Factors Pertinent to Reduction of Loss of Life and Property in Hurricane Situations", National Hurricane Research Project Report No. 5, U.S. Department of Commerce, March 1957.

NEUMANN, C.J., "Probability of Tropical Cyclone Induced Winds at the NASA Manned Spacecraft Center", 4th National Conference on Aerospace Meteorology, Las Vegas, Nevada, May 4-7 1970.

NEUMANN, C.J., CRY, G.W., CASO, E.L. and JARVINEN, B.R., "Tropical Cyclones of the North Atlantic Ocean, 1871-1977", National Weather Service, N.O.A.A., U.S. Department of Commerce, June 1978.

RUSSELL, L.R., "Probability Distributions for Hurricane Effects", Journal of the Waterways, Harbours and Coastal Engineering Division, A.S.C.E, Volume 97, No.WW1, February 1971.

SCHWERDT, R.W., HO, F.P. and WATKINS, R.R., "Meteorological Criteria for Standard Project Hurricane and Probable Maximum Hurricane Wind Fields, Gulf and Atlantic Coasts of the United States", NOAA Technical Report NWS23, U.S. Department of Commerce, September 1979.

SHAPIRO, L.J., "Hurricane Climate Fluctuations. Part I: Patterns and Cycles", Monthly Weather Review, A.M.S., Volume 110, August 1982.

SHAPIRO, L.J., "Hurricane Climate Fluctuations. Part II : Relation to Large-Scale Circulation", Monthly Weather Review, A.M.S., Volume 110, August 1982.

SHEA, D.J. and GRAY, W.M., "The Structure and Dynamics of the Hurricane's Inner Core Region", Atmospheric Science Paper No. 182, Colorado State University, April 1972.

THOM, H.C.S., "The Distribution of Annual Tropical Cyclone Frequency", Journal of Geophysical Research, Volume 65, January 1960.

TRYGGVASON, B.V., "Computer Simulation of Tropical Cyclone Wind Effects for Australia", Wind Engineering Report 2/79, Department of Civil and Systems Engineering, James Cook University, Townsville, Australia, 1979.

TRYGGVASON, B.V., SURRY, D. and DAVENPORT, A.G., "Predicting Wind-Induced Response in Hurricane Zones", Journal of the Structural Division, A.S.C.E., Volume 102, No. ST12, December 1976.

XUE, L. and NEUMANN, C.J., "Annual Frequency of Northwest Pacific Tropical Cyclones", National Hurricane Center Report, 1985.

Chapter 6

BATTS, M.E., CORDES, M.R., RUSSELL, L.R., SHAVER, J.R. and SIMIU, E., "Hurricane Wind Speeds in the Unites States", National Bureau of Standards Resport No.BSS-124, U.S. Department of Commerce, May 1980.

BELL, G.J., "Observations on the Size of the Typhoon Eye", W.M.O. Technical Conference on Typhoon Modification, No. 408, Manila, October 14-18 1974.

CHEN, T.V., "Comparison of Surface Winds in Hong Kong", Royal Observatory, Hong Kong, Technical Note No. 41, 1975.

DORMAN, C.M.L., "Tropical Cyclone Winds : Uncertainties in Monte-Carlo Simulation", Journal of Wind Engineering and Industrial Aerodynamics, Volume 12, pp 281-296, 1983.

GEORGIOU, P.N., MIKITIUK, M., SURRY, D. and DAVENPORT, A.G., "The Wind Climate for Hong Kong", The University of Western Ontario, Engineering Science Report, BLWT-SS2-1984.

GUMBEL, E.J., "Statistics of Extremes", New York Columbia University Press, 1958.

LIEBLEIN, J., "Efficient Methods of Extreme Value Methodology", National Bureau of Standards, NTIS NBSIR 74-602, 1974.

MELBOURNE, W.H., "Hong Kong Design Wind Speed Estimates and Pressure Measurements on Building on IL8392 Harbour Road and Fleming Road", Department of Mechanical Engineering, Monash University, Melbourne, Australia, 1981.

MERRILL, R.T., "A Comparison of Large and Small Tropical Cyclones", Monthly Weather Review, A.M.S., Volume 112, July 1984.

SCHWERDT, R.W., HO, F.P. and WATKINS, R.R., "Meteorological Criteria for Standard Project Hurricane and Probable Maximum Hurricane Wind Fields, Gulf and Atlantic Coasts of the United States", NOAA Technical Report NWS23, U.S. Department of Commerce, September 1979.

SURRY, D., LYTHE, G., HORVATH, B. and DAVENPORT, A.G., "A Wind Tunnel Study of the Relationship Between Gradient Wind Speeds and the Anemometer Readings from Waglan Island, Hong Kong", The University of Western Ontario, Enginering Science Report, BLWT-SS17-1981.

Chapter 7

DAVENPORT, A.G., " The Prediction of the Response of Structures to Gusty Wind", International Seminar on the Safety of Structures Under Dynamic Loading, Volume 1, Norwegian Institute of Technology, June 1977.

DAVENPORT, A.G., Personal Communication, July 1984.

Chapter 8

SHAPIRO, L.J., "The Asymmetric Boundary Layer Flow Under a Translating Hurricane", Journal of the Atmospheric Sciences, A.M.S., Volume 40, No. 8, August 1983.